

Protein Structure and Stability Modulation Due to Crowding Conditions: Molecular Insights on the Origin of the Effects of Crowding

THESIS

Submitted in partial fulfilment
of the requirements for the degree of
DOCTOR OF PHILOSOPHY

by

I SHIVKUMAR

ID No: 2017PHXF0427H

**Under the Supervision of
Late Prof. Ramakrishna Vadrevu
and**

**Under the co-supervision of
Prof. Sridev Mohapatra**



BITS Pilani
Pilani | Dubai | Goa | Hyderabad

BIRLA INSTITUTE OF TECHNOLOGY AND SCIENCE, PILANI

2024

BIRLA INSTITUTE OF TECHNOLOGY AND SCIENCE, PILANI

CERTIFICATE


This is to certify that the thesis titled “**Protein Structure and Stability Modulation due to Crowding Conditions: Molecular Insights on the Origin of the Effects of Crowding**” submitted by **I Shivkumar** ID No **2017PHXF0427H** for award of Ph.D. of the Institute embodies original work done by him under my supervision.

Signature of the Supervisor

Name in capital letters: Late. Prof. RAMAKRISHNA VADREVVU

Designation: Professor

Date: 02-05-2023



Signature of the Co-supervisor

Name in capital letters: Prof. SRIDEV MOHAPATRA

Designation: Associate Professor

Date: 02-05-2023

Acknowledgements

*I would like to express my deepest gratitude to my guide, **Late Prof. Ramakrishna Vadrevu**, for his guidance, support, and encouragement throughout my research. His expertise and insights have been invaluable in shaping my work, and I am extremely grateful for his patience and understanding. His dedication to academic and research excellence has been an inspiration to me, and I am honoured to have been a part of his lab.*

*A special thanks to **Prof. Sridev Mohapatra** for supporting me during these testing times and facilitating the entire process of my thesis submission hazard free.*

*I am grateful to **Prof. Debashree Bandyopadhyay** and **Prof. Durba Roy** for serving as my doctoral advisory committee members.*

*I am also grateful to the HOD **Prof. Dr. Nishit Gupta** and all faculty members of the Department of Biological Sciences for their support and expertise.*

*I would like to express my deepest gratitude to my **mother (I Visalakshmi)**, **father (S V Sharma)** and **brother (Tarunaditya)** for their unwavering love, support, and encouragement throughout my doctoral studies. Their patience, understanding, and sacrifice made it possible for me to focus on my research and complete this dissertation.*

*Words cannot express my gratitude to **Ms. Minali Singh** for her unwavering support and encouragement. Her love and belief in me have been a constant source of strength and motivation. Her constant presence and willingness to listen to my ideas, frustrations, and triumphs provided the emotional support I needed to persevere through challenging times. Her unending support made it possible for me to pursue my academic goals without any obstacles.*

*I am also grateful to my friends **Tarun Kumar Angala**, **Aditya Mudigonda**, **P. Sai Vineeth** and **Titus Kennedy** for their constant support and encouragement. A special thanks to **Aditya Mudigonda** for helping me through my tough time.*

*I'd like to acknowledge the technical staff (**Mr. Imtiyaz, Mr. Ramakrishna, Mr. Santhosh and Mrs. Poornima**) at BITS-Pilani, Hyderabad Campus for their help.*

*A special thanks to **Dr. Jithender Reddy**, Indian Institute of Chemical Technology (CSIR-IICT) for enabling NMR time at the NMR division in IICT and for teaching me tricks of handling NMR data.*

*I would like to acknowledge **Dr. D Krishna Rao**, Tata Institute of Fundament Research – Hyderabad (TIFR) for enabling NMR time on the 700 MHz spectrometer.*

I would like to thank Department of Science and Technology – Science and Engineering Research Board (DST-SERB) for providing research fellowship to me in the form of JRF and SRF.

*Finally, I would like to acknowledge the participants in my study, lab mates (**Pradeep, Aishwarya, and Pavan**), colleagues, without whom this research would not have been possible. Their willingness to share their experiences and insights has been instrumental in shaping my understanding of this topic.*

Abstract

Macromolecular crowding has been studied thoroughly for a wide variety of proteins. A plethora of data in the literature suggests the role of entropic excluded volume effect and enthalpic quinary interactions of different crowders on proteins. However, there is no unified theory. The crowding effect appears to be controlled either enthalpically or entropically and depends on the protein, molecular crowder properties, and crowding conditions. Using a combination of biophysical approaches, including far/near-UV circular dichroism, tryptophan fluorescence, 8-anilino-naphthalene-1-sulfonic acid (ANS) binding, and nuclear magnetic resonance (NMR), I probed the effect of macromolecular crowding using polyethylene glycol (PEG, 6,8,12 and 20 kDa), Ficoll-70 (70 kDa), and dextran 40 and 70 (40 and 70 kDa) on the structure and stability of a bacterial protein, chemotaxis protein Y (CheY), involved in signaling pathways. Combined CD and fluorescence analysis indicated that PEG moderately destabilized the structure and stability of apo CheY. Noticeable changes in the structure and stability were absent in the presence of Ficoll-70. However, interestingly, NMR chemical shift perturbations (CSPs) and line broadening revealed protein-PEG interactions in apo CheY. Further, evidence for this interaction comes from the decreased thermal stability measured for holo CheY in PEG. By combining the CSPs and decreased thermal stability in the presence of magnesium, it appears that crowding from PEG leads to subtle conformational rearrangement, distorted magnesium binding, and loss of magnesium binding-induced enhancement of the protein's thermal stability. Surprisingly, while no CSPs were observed in the presence of Ficoll-70, a decrease in thermal stability was observed for holo CheY in the presence of Ficoll. This effect of Ficoll is attributed to the selective destabilization of the holo form of the protein and disruption of the apo-holo equilibrium. Thus, based on these data, it is proposed that enthalpic contributions dominate in the case of PEG.

In contrast, with Ficoll, destabilization is a consequence of the entropic contributions of the crowder. In addition to macromolecules, small metabolites are present in high concentrations inside the cell. Hence, it is highly relevant to study the effect of certain small-molecule crowders on the structure and stability of proteins. We attempted to study certain common small molecules, such as amino acids, sugars, and polyamines and dissected the effect of these molecules on the structure and stability of CheY. Amino acids do not affect the structure and stability of the protein, whereas polyamines make the thermal denaturation of holo CheY reversible. This thesis presents a comprehensive study of the structure and stability of the apo and holo forms of CheY in the presence of macromolecular crowders, molecular crowders, and a combination of both.

Table of Contents

S. No.	Title	Page No.
1	Certificate	i
2	Acknowledgements	ii
3	Abstract	iv
4	List of Tables	vii
5	List of Figures	viii
6	List of Abbreviations/Symbols	xii
7	Chapter 1 – Introduction	1
8	Chapter 2 – Materials and Methods	31
9	Chapter 3 - Crowding by Polyethylene Glycols Destabilizes Chemotaxis Protein Y	41
10	Chapter 4 - Contrasting Effect of Carbohydrate Based Molecular and Macromolecular Crowders on Apo and Holo Forms of Bacterial Chemotaxis Protein Y: Selective Destabilization of the Conformationally Altered Holo Form	77
11	Chapter 5 - Molecular Insights on the Origin of the Effects of Crowding Using NMR Spectroscopy	110
12	Chapter 6 - Effect of Small Molecular Crowder and a Combination of Small Molecular and Macromolecular Crowders on the Structure and Stability of Chemotaxis Protein Y	135
13	Chapter 7 – Conclusions and Future Perspectives	156
14	References	164
15	Appendices	191
16	List of Publications and Presentations	194
17	Brief Biography of the Candidate	195
18	Brief Biography of the Supervisor	196
19	Brief Biography of the Co-Supervisor	197

List of Tables

Table No.	Caption	Page No.
1.1	Measured specific optical rotation values of carbohydrate based macromolecular crowders.	11
2.1	Details of chemicals and consumables used for experimentation.	31
3.1	Tryptophan lifetime decay parameters of CheY obtained from biexponential fits of signal decay in dilute buffer, 100 mg/mL and 200 mg/mL PEG. The individual lifetime components are denoted as τ_1 and τ_2 . Relative amplitudes are denoted as α_1 and α_2 . χ^2 represents the goodness of fit.	56
3.2	Thermodynamic parameters of CheY in dilute buffer and in the presence of 100 and 200 mg/mL PEG.	59
3.3	T_m values of CheY in the combined presence and absence of Mg^{2+} and PEG.	61
3.4	Thermodynamic parameters of apo-CheY derived from fitting the thermal denaturation data to a two-state folded to-unfolded model using CalFitter (Mazurenko et al., 2018).	68
3.5	T_m value of holo CheY in the presence of difference volume fractions of PEGs.	73
4.1	Thermodynamic parameters of apo CheY in the presence of Ficoll, sucrose, and combined presence of Ficoll and sucrose obtained from fitting of thermal unfolding to a two-state folded to unfolded model. (DeKoster et al., 1993; Filimonov et al., 1993). $\Delta T_m = T_m(\text{Ficoll}) - T_m(\text{dilute buffer})$ and $\Delta\Delta H^\circ = \Delta H^\circ(\text{Ficoll}) - \Delta H^\circ(\text{dilute buffer})$ s	86
4.2	The T_m values of holo CheY in the presence of Ficoll, sucrose, and combined presence of Ficoll and sucrose obtained from the fitting of thermal denaturation profiles to a two-state folded to unfolded model. (DeKoster et al., 1993; Filimonov et al., 1993) (*). It could not be determined due to a lack of unfolding baseline in the thermal denaturation range and high error from the fit. Since the thermal transitions were not reversible for the holo form, the thermodynamic parameters (ΔH° , ΔS° and ΔG°) are not reported. The concentration of $MgCl_2$ is 10 mM. $\Delta T_m = T_m(\text{Ficoll}) - T_m(\text{Dilute buffer})$.	86
5.1	Information obtained for different nuclei from various 3D experiments.	116
6.1	T_m for apo and holo CheY in the presence and absence of amino acids as crowders.	141
6.2	Thermodynamic parameters of apo CheY in the presence of polyamines	145
6.3	Thermodynamic parameters of holo CheY in the presence of polyamines. (ND* - Not determined due to the irreversible transition from native to denatured state)	151

List of Figures

Figure no.	Caption/legend	Page No.
1.1	Protein folding funnel (adapted from Stryer's biochemistry)	3
1.2	Representative transition from N to D for a protein following two-state unfolding model.	9
1.3	Graphical illustration of macromolecular crowding. <i>in-vitro</i> vs. <i>in-vivo</i> environment for a test protein.	9
1.4	(A) 2D representation of monomeric unit of Ficoll, (B) 2D representation of monomeric unit of Dextran, and (C) 2D representation of monomeric unit of PEG.	10
1.5	Schematic representation of the effects of crowding on a test protein.	14
1.6	Enthalpy versus entropy plot of the test protein with regimes indicated in different colors.	19
1.7	Classification of the effects of cosolutes on the protein folding equilibrium.	20
1.8	Cartoon representation of the crystal structure of CheY (PDB ID: 3CHY) generated using PyMol (Schrödinger, LLC, 2015).	21
1.9	Simplified scheme of protein-protein interactions during chemotactic signalling.	22
1.10	Overlapping crystal structure of apo and holo forms of CheY. (A) An angle highlighting the change in the loop configuration in holo form (boxed region) and (B) highlighting the slight change in secondary structure due to Mg ²⁺ binding in α -4 and β -5 (boxed region).	23
3.1	1% acetone peak (UV-280 nm) plotted against elution volume used for HETP calculations.	44
3.2	Size exclusion chromatogram of CheY obtained from size exclusion chromatography on Superdex™ G-75 column.	45
3.3	15 % Polyacrylamide gel showing pure protein (CheY) corresponding to ~14 kDa. (Lanes from left to right - molecular weight marker, elution fractions 1-10)	45
3.4	(A) Effect of PEG on the secondary structure of CheY. Far UV-CD spectra in the presence of dilute buffer (black) and in 100 mg/mL (red), 200 mg/mL (blue) and 300 mg/mL (green) of PEG. Inset indicates the average value at 222 nm, at each concentration of PEG, along with the standard deviation obtained from three independent measurements. (B) Effect of PEG on the tertiary structure of CheY. Near UV-CD spectra in the presence of dilute buffer (black) and varying concentrations of PEG are shown in red and blue for 100 and 200 mg/mL, respectively.	46
3.5	Normalized fluorescence intensity at 350 nm plotted against absorbance at 290 nm of PEG + CheY solution. (A) Up to 300 mg/mL PEG concentration and (B) up to 200 mg/mL PEG concentration. Insets in both the plots indicate the fitting parameters to exponential and linear equations, respectively.	50
3.6	(A) Intrinsic tryptophan fluorescence spectra of CheY. The fluorescence emission spectrum of CheY in the presence of dilute buffer (black) and varying concentrations of PEG (100 mg/mL in red and 200 mg/mL in blue). Inset indicates the average value at 342 nm at each concentration of PEG along with the standard deviation obtained from three independent measurements. (B) Extrinsic Fluorescence emission spectra of CheY. ANS fluorescence emission spectra of CheY in the presence of dilute buffer (black) and in varying concentrations of PEG (100 mg/mL = red, 200 mg/mL = blue and 300 mg/mL = green). Inset indicates the average value at each concentration of PEG along with the standard deviation obtained from three independent measurements.	51
3.7	Extrinsic Fluorescence emission spectra of CheY. ANS fluorescence emission spectra of CheY in the presence of dilute buffer (black) and in varying concentrations of PEG (100 mg/mL = red, 200 mg/mL = blue and 300 mg/mL = green) in (A) 50 μ M ANS, (B) 100 μ M ANS and (C) 150 μ M ANS.	52
3.8	Tryptophan lifetime decay of CheY in dilute buffer (black), 100 mg/mL PEG (red) and 200 mg/mL PEG (blue). The instrument response function (IRF) is represented in magenta. Inset indicates residuals of the fits.	55
3.9	Effect of PEG on the thermal stability of CheY. Thermal denaturation profiles of CheY were obtained by plotting-fraction unfolded as a function of temperature in dilute buffer (black), in 100 mg/mL (red) and 200 mg/mL PEG (blue). The continuous line represents the fit of the thermal melt for a two-state folded to unfolded model.	58

3.10	Effect of PEG on the thermal stability of CheY in the presence of magnesium. Thermal denaturation profiles of CheY in the presence of dilute buffer (black, closed circles), dilute buffer with Mg ²⁺ (black, open circles) with varying concentrations of PEG (100 mg/mL = red; 200 mg/mL = blue). The continuous line represents the fit of the thermal melt for a two-state folded (N) to unfolded (U) model. The concentration of MgCl ₂ was maintained at 10 mM.	60
3.11	Effect of PEG on the secondary structure of apo CheY. Far UV-CD spectra in the presence of dilute buffer (black) and in 100 mg/mL (red), 200 mg/mL (blue) and 300 mg/mL (green) in (A) PEG 6000, (B) PEG 8000 and (C) PEG 12000.	63
3.12	Effect of PEG on the tertiary structure of apo CheY. Near UV-CD spectra in the presence of dilute buffer (black) and in 100 mg/mL (red), and 200 mg/mL (blue) in (A) PEG 6000, (B) PEG 8000 and (C) PEG 12000	64
3.13	Intrinsic tryptophan fluorescence spectra of apo CheY. The fluorescence emission spectrum of CheY in the presence of dilute buffer (black) and varying concentrations (100 mg/mL in red and 200 mg/mL in blue) in (A) PEG 6000, (B) PEG 8000 and (C) PEG 12000.	65
3.14	Thermal denaturation profile of apo-CheY in the presence of (A) PEG 6000, (B) PEG 8000, (C) PEG 12000. The continuous line represents the fit obtained from a two-state folded to-unfolded model.	67
3.15	Classification of the effect of crowder on protein stability based on the thermodynamic footprints (ΔH° and ΔT_m) of apo CheY in the presence of various PEGs. (PH – Preferential Hydration, PB – Preferential binding, EV – Excluded volume)	69
3.16	Thermal denaturation profiles of holo CheY in the presence of (a) PEG 6000, (b) PEG 8000, and (c) PEG 12000.	72
3.17	Effect of PEG on the tertiary structure of holo CheY. Near UV-CD spectra in the presence of dilute buffer (black) and in 100 mg/mL (red), and 200 mg/mL (blue) in (A) PEG 6000, (B) PEG 8000 and (C) PEG 12000	74
4.1	Far UV-CD spectra in the presence and absence of Ficoll for (A) apo CheY and (B) holo CheY	81
4.2	Near UV-CD spectra in the presence and absence of Ficoll of (A) apo CheY and (B) holo CheY. The concentration of MgCl ₂ was maintained at 10 mM.	82
4.3	Thermal denaturation profiles of CheY in the presence of Ficoll for (A) apo form and (B) holo forms. The lines joining the data points correspond to a fit to a two-state, folded-unfolded model (DeKoster et al., 1993; Filimonov et al., 1993). The concentration of MgCl ₂ was maintained at 10 mM. Although data were recorded at 1°C interval, for the purpose of representation the data are plotted at 5°C interval.	85
4.4	Intrinsic tryptophan fluorescence quenching in the presence and absence of Ficoll. Tryptophan fluorescence emission of CheY in (A) dilute buffer (B) 100 mg/mL of Ficoll (C) 200 mg/mL of Ficoll. (D) 200 mg/mL sucrose and (E) 6 M Urea. The black and red colors denote the absence and presence of 4 mM MgCl ₂ .	88
4.5	Thermal denaturation profiles of CheY (A) Apo form (B) Holo form. In dilute buffer, in increasing concentrations of sucrose and in the combined presence of sucrose and Ficoll. The lines joining the points correspond to a fit to a two-state, folded-unfolded form of the protein. For the holo protein, the thermal transition was not reversible. The concentration of MgCl ₂ was maintained at 10 mM. Although data were recorded at 1°C interval, for the purpose of representation the data are plotted at 2°C interval.	90
4.6	Schematic representation of the variation in measured T _m of the apo and holo forms in the absence and presence of Ficoll and sucrose. The box in the dashed line denotes the measured T _m values of apo Che Y and holo CheY in 10 and 100 mM MgCl ₂ and serve as the reference points to guide the upward and downward trend of the T _m . The coloured arrows indicate the increase or decrease in the measured T _m with respect to the reference points. Open arrows represent T _m for apo CheY, and filled arrows represent T _m for holo CheY	93
4.7	Thermal denaturation profiles of holo form of CheY. In dilute buffer, in 200 mg/mL Ficoll and in the combined presence of 2 M urea and 200 mg/mL Ficoll. The lines joining the points correspond to a fit to a two-state, folded-unfolded form of the protein. The thermal transitions were not reversible. The concentration of MgCl ₂ was maintained at 10 mM. Although data were recorded at 1°C interval, for the purpose of representation the data are plotted at 2°C interval.	94

4.8	(A) Thermal denaturation profiles of holo form of CheY. In dilute buffer + 100 mM NaCl and in 100 mM NaCl + 200 mg/mL Ficoll. The lines joining the points correspond to a fit to a two-state, folded-unfolded form of the protein. The thermal transitions were not reversible. The concentration of MgCl ₂ was maintained at 10 mM. Although data were recorded at 1°C interval, for the purpose of representation the data are plotted at 2°C interval. (B) Schematic representation of the variation in measured T _m of holo forms in the absence and presence of Ficoll. The box in the dashed line denotes the measured T _m values of holo CheY in 1, 5, 10 and 100 mM MgCl ₂ and serve as the reference points to guide the upward and downward trend of the T _m . The coloured arrows indicate the increase or decrease in the measured T _m with respect to the reference points. The shaded region in green indicates stabilizing upward trend and red indicates destabilizing downward trend in T _m .	96
4.9	Far UV-CD spectra of apo CheY in the presence and absence of (A) Dextran 40000 and (B) Dextran 70000. (Attempt 1)	100
4.10	Far UV-CD spectra of apo CheY in the presence and absence of (A) Dextran 40000 and (B) Dextran 70000. (Attempt 2)	101
4.11	Far UV-CD spectra of apo CheY with 2 M urea in the presence and absence of (A) Dextran 40000 and (B) Dextran 70000. (Attempt 1)	102
4.12	Far UV-CD spectra of apo CheY with 2 M urea in the presence and absence of (A) Dextran 40000 and (B) Dextran 70000. (Attempt 2)	103
4.13	Far UV-CD spectra of apo CheY in the presence and absence of Dextran 6000	104
4.14	Thermal denaturation profiles of apo CheY. In dilute buffer and in 200 mg/mL Dextran 6000. The lines joining the points correspond to a fit to a two-state, folded-unfolded form of the protein. The thermal transition in the presence of Dextran 6000 was not reversible. Although data were recorded at 1°C interval, for the purpose of representation the data are plotted at 2°C interval.	104
4.15	Thermal denaturation profiles of apo CheY. In dilute buffer and in 200 mg/mL glucose. The lines joining the points correspond to a fit to a two-state, folded-unfolded form of the protein. Although data were recorded at 1°C interval, for the purpose of representation the data are plotted at 2°C interval.	105
4.16	Thermal denaturation profiles of holo CheY. In dilute buffer and in 200 mg/mL glucose. The lines joining the points correspond to a fit to a two-state, folded-unfolded form of the protein. The thermal transitions were not reversible. Although data were recorded at 1°C interval, for the purpose of representation the data are plotted at 2°C interval.	106
4.17	Thermal denaturation profiles of (A) apo CheY in dilute buffer and in 200 mg/mL glucose with and without Ficoll 200 mg/mL. (B) holo CheY in dilute buffer and in 200 mg/mL glucose with and without Ficoll 200 mg/mL. The lines joining the points correspond to a fit to a two-state, folded-unfolded form of the protein. Although data were recorded at 1°C interval, for the purpose of representation the data are plotted at 2°C interval.	108
5.1	Schematic representation of the coherence transfer in HN(CO)CA	112
5.2	Schematic representation of the coherence transfer in HN(CA)CO	113
5.3	Schematic representation of the coherence transfer in CBCA(CO)NH	113
5.4	Figure 5.4: Schematic representation of the coherence transfer in HNCA	114
5.5	Schematic representation of the coherence transfer in CBCANH	115
5.6	Schematic representation of the coherence transfer in HNCO	115
5.7	¹ H- ¹⁵ N TROSY-HSQC spectra of CheY in dilute buffer.	119
5.8	Strip scope of a triple resonance experiment (CBCANH) of CheY with peaks indicating C α , C β or i and i-1 residues.	120
5.9	(A) Superimposed ¹ H- ¹⁵ N TROSY-HSQC spectra of CheY in dilute buffer (grey), in the presence of 100 mg/mL PEG (red), and in the presence of 200 mg/mL PEG (blue). (B) A plot of chemical shift perturbations observed for the residues in the presence of 200 mg/mL PEG. The perturbations from individual cross peaks were obtained using the standard method. (Williamson, 2013, 2018) The horizontal line represents the cut-off considered for significant movement in chemical shifts ($\Delta\delta_{\text{PEG}} \geq 0.03$). (Crowley, Brett and Muldoon, 2008) (c) A subset of the residues from the superimposed ¹ H- ¹⁵ N TROSY-HSQC spectra of CheY obtained in the presence and absence of PEG, showing significant chemical shift perturbations. (Dilute buffer = grey; 100 mg and 200 mg/mL	123

	PEG = red and blue respectively). The x and y axes represent ^1H and ^{15}N chemical shifts in ppm, respectively.	
5.10	Chemical Shift Perturbations ($\Delta\delta_{\text{PEG}}$) in the presence of 200 mg/mL PEG, mapped onto the (A) crystal structure of CheY (B) Surface representation (C) Topology diagram (generated using TopDraw (Bond, 2003)) of CheY. Helices are represented as cylinders, beta strands as arrows, and continuous lines represent loops connecting these elements. PDB ID: 3CHY, with hydrophobic residues colored in red and hydrophilic in blue. Secondary structural elements are labelled and values within parentheses indicate the exposed surface area of the residue.	125
5.11	(A) Relative change in integrated peak intensities between dilute buffer and 200 mg/mL PEG. (B) Relative change in integrated peak intensities between dilute buffer and 200 mg/mL PEG mapped onto the crystal structure of CheY (PDB ID:3CHY), with hydrophobic residues colored in red and hydrophilic in blue.	127
5.12	(A) Superimposed ^1H - ^{15}N Heteronuclear Single Quantum Coherence (HSQC) spectra of apo CheY in buffer (blue), and in the presence of 200 mg/ml of Ficoll (red). (b) Superimposed ^1H - ^{15}N HSQC spectra of holo CheY in buffer (blue), and in the presence of 200 mg/ml of Ficoll (red). Boxed regions represent peaks showing minor CSPs.	130
5.13	(A) Relative intensity (ΔI_{Ficoll}) of cross peaks of apo CheY in the presence of Ficoll. (B) Relative intensity ($\Delta I_{\text{Ficoll} + \text{Mg}^{2+}}$) of cross peaks of holo CheY in the presence of Ficoll.	131
6.1	Far UV-CD spectra of apo CheY in the presence and absence of (A) Alanine, (B) Valine and (C)	139
6.2	Thermal denaturation profiles of (A) apo CheY in the presence of a combination of amino acids and in the combined presence of amino acids and 200 mg/mL of Ficoll 70. (B) Holo CheY in the presence of a combination of amino acids and in the combined presence of amino acids and 200 mg/mL of Ficoll 70. The lines joining the points correspond to a fit to a two-state, folded-unfolded form of the protein. Although data were recorded at 1°C interval, for the purpose of representation the data are plotted at 2°C interval.	140
6.3	UV-visible spectra of apo CheY in the presence of varying concentrations of (A) Putrescine, (B) Spermine, and (C) Spermidine	142
6.4	Far UV-CD spectra of apo CheY in (A) Putrescine, (B) Spermine, and (C) Spermidine	143
6.5	Fluorescence emission spectra of apo CheY in the presence of (A) Putrescine, (B) Spermine, and (C) Spermidine	144
6.6	Thermal denaturation profiles of apo CheY in the presence of (A) Putrescine, (B) Spermine, and (C) Spermidine. The lines joining the points correspond to a fit to a two-state, folded-unfolded form of the protein. Although data were recorded at 1°C interval, for the purpose of representation the data are plotted at 2°C interval.	147
6.7	Far UV-CD spectra of holo CheY in the presence of varying concentrations of (A) Putrescine, (B) Spermine, and (C) Spermidine	149
6.8	Fluorescence emission spectra of holo CheY in the presence of varying concentrations of (A) Putrescine, (B) Spermine, and (C) Spermidine	150
6.9	Thermal denaturation profiles of holo CheY in the presence of (A) Putrescine, (B) Spermine, and (C) Spermidine. The lines joining the points correspond to a fit to a two-state, folded-unfolded form of the protein. Although data were recorded at 1°C interval, for the purpose of representation the data are plotted at 2°C interval.	152
6.10	Thermal denaturation profiles of holo CheY in the presence of Putrescine and combined presence of putrescine and 200 mg/mL Ficoll 70. The lines joining the points correspond to a fit to a two-state, folded-unfolded form of the protein. Although data were recorded at 1°C interval, for the purpose of representation the data are plotted at 2°C interval.	153
6.11	Schematic representation of heat induced unfolding of CheY in the presence and absence of polyamines.	154

List of Abbreviations/Symbols

CheY	Chemotaxis Y protein
PEG	Polyethylene Glycol
IPTG	Isopropyl β -d-1- Thiogalactopyranoside
LB	Luria Bertani
UV	Ultraviolet
CD	Circular Dichroism
FL	Fluorescence
λ_{\max}	lambda maximum (wavelength at maximum fluorescence intensity).
ANS	8-anilinonaphthalene-1-sulfonic acid
kJ mol^{-1}	kilojoules per mole
aa	amino acid
PDB	Protein Data Bank
MgCl_2	magnesium chloride
Mg^{2+}	magnesium ion
IRF	Instrument Response Function
Ficoll	Ficoll 70 kDa
T_m	Midpoint of thermal denaturation
NMR	Nuclear magnetic resonance
mm	millimetre

nm	nanometre
^1H-^{15}N HSQC	^1H - ^{15}N Heteronuclear Single Quantum Coherence
TROSY	Transverse Correlation Spectroscopy
μM	micro molar
kDa	kilodaltons
LED	Light emitting diode

Amino Acid	3 Letter Code	1 Letter Code
Alanine	Ala	A
Arginine	Arg	R
Asparagine	Asn	N
Aspartic Acid	Asp	D
Cysteine	Cys	C
Glutamine	Gln	Q
Glutamic Acid	Glu	E
Glycine	Gly	G
Histidine	His	H
Isoleucine	Ile	I
Leucine	Leu	L
Lysine	Lys	K
Methionine	Met	M
Phenylalanine	Phe	F
Proline	Pro	P
Serine	Ser	S
Threonine	Thr	T
Tryptophan	Trp	W
Tyrosine	Tyr	Y
Valine	Val	V

Chapter 1

Introduction

1.1 Introduction

Cells are the structural and functional units of living organisms, and macromolecules are an inherent part of cellular processes, ranging from growth and metabolism to reproduction. Cells are the most complex systems that perform specific functions based on their location in the living system. The degree of complexity of the cellular organization varies across species. A common element among species is the involvement of proteins as effector molecules in all processes. The central dogma of biology describes the flow of information across biomacromolecules. The genetic information stored in deoxyribonucleic acid (DNA) is transcribed into messenger ribonucleic acid (mRNA), and eventually translated into a protein that carries out cellular processes. Cellular proteins perform various functions, including enzyme catalysis, signal transduction, etc. The ability to perform such diverse functions stems from their three-dimensional structure, which contains secondary structure elements packed against each other, giving rise to a functionally active tertiary structure. How a stretch of linear amino acids folds into a unique three-dimensional structure is fascinating. Twenty naturally occurring amino acids incorporated in a specific series give rise to a plethora of structures that have drawn the attention of many scientists to study and elaborate on their structure, function, dynamics, and structure-function relationships. Significant breakthroughs in nuclear magnetic resonance (NMR) and X-ray diffraction have allowed the accumulation of data on the structure, stability, and dynamics of proteins under *in vitro* conditions.

1.2 Protein folding

The amino acid sequence-driven folding process and the ensuing three-dimensional structure form the basis for the thermodynamic stability, dynamics, and function of proteins (Anfinsen,

1973; Creighton, 1990; Dobson, 2003). The overall structure and stability of biomolecules, in general, and proteins, in particular, result from a contribution from the protein chain entropy and solvent entropy. Together with entropic manipulations, enthalpic contributions due to interactions within the protein and intermolecular interactions between the protein and solvent sculpt the overall thermodynamic landscape.

Thermodynamically protein folding is visualized as a free-energy funnel or energy landscape. Depth represents the energy difference between the folded and unfolded states. Its breadth represents all possible unfolded conformers a polypeptide chain may assume (high entropy and free energy) (Figure 1.1). Each point in the energy landscape is a possible three-dimensional protein structure. As the protein folding process proceeds, the funnel narrows in size, implying fewer conformational states available for the protein to access. Folding is believed to follow one of the following mechanisms: i) local interactions take place first, forming secondary structures such as α -helices and β -strands, which then enable long-range interactions leading to the formation of tertiary structures, ii) the hydrophobic effect makes the amino acids far apart in sequence come closer in three-dimensional space leading to the formation of a globular structure. This formed structure is also called a molten globule. However, another accepted theory for protein folding is the nucleation-condensation model, which combines secondary structure-driven folding and hydrophobic collapse. The governing thermodynamics of the folding process are further elucidated. To understand the thermodynamics of unfolding, the protein of interest should be subjected to perturbations such as temperature change, pH change, increasing concentration of denaturants, etc. which will force the protein to leave the global minimum in its folding landscape and reach the top of the folding funnel. Depending on the number of stable thermodynamic states, a protein can significantly populate during the process of unfolding, the process can be classified into different models.

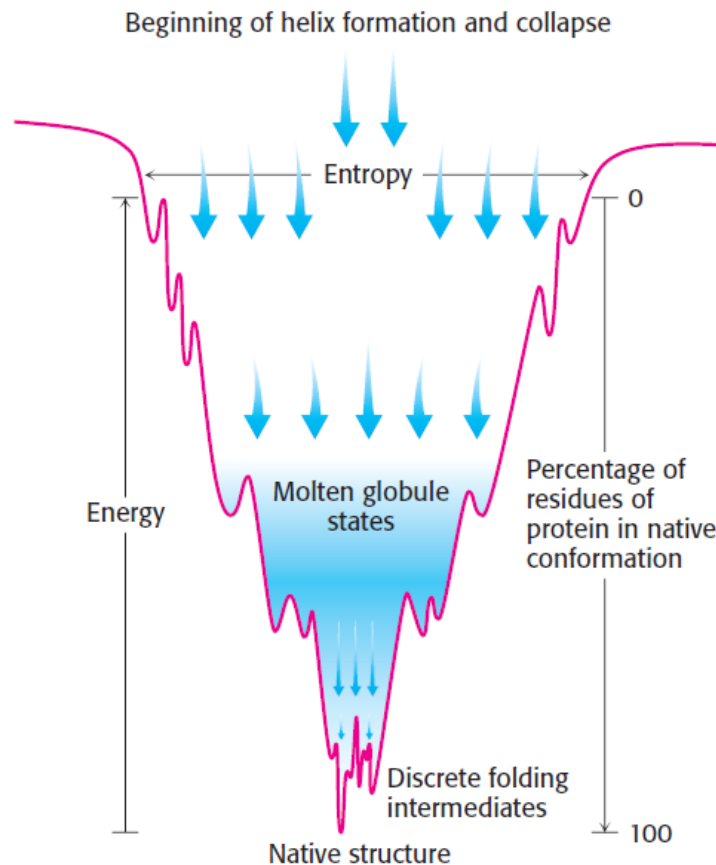


Figure 1.1: Protein folding funnel (adapted from Stryer's biochemistry)

1.3 Thermodynamics of protein folding

According to the thermodynamic hypothesis proposed by Anfinsen (Anfinsen, 1973), spontaneous folding/unfolding is governed entirely by the free energy of the folded state/native conformation. The native state would exist at the global minimum in a folding funnel compared with all the other accessible conformations (Dill, 1990).

Protein denaturation can be achieved by introducing a perturbant, chemical denaturant such as urea/guanidine hydrochloride or by subjecting the protein to various temperatures. Spectroscopic techniques such as intrinsic fluorescence spectroscopy, circular dichroism, differential scanning fluorimetry, differential scanning calorimetry, etc., can be used to monitor these reactions. Protein folding/unfolding thermodynamics can be well understood by

considering the example of a protein that unfolds following a two-state folded (Native, N) to unfolded (Denatured, D) model.

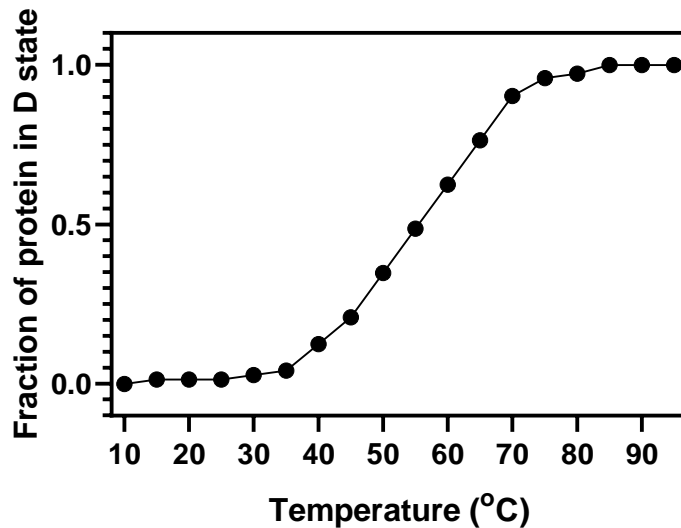
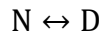


Figure 1.2: Representative transition from N to D for a protein following two-state unfolding model.

Where N and D are the only significantly populated stable thermodynamic species of the protein. In this process, the protein does not attain any significantly stable intermediate conformation while unfolding from its native state. Hence, at any given point the transition occurs as an “all or none” event i.e. either the native or the denatured conformation will be populating the energy landscape of the protein. Figure 1.2 schematically represents this event. As the protein is subjected to a perturbant, initially, the rate of the forward reaction dominates with respect to the rate of refolding. Hence, eventually with time the concentration of native state decreases and that of denatured state increases. (Shirdel and Khalifeh, 2019) At a point of time in the reaction, the rate of the forward reaction is equal to the rate of the reverse reaction, which indicates the stability of the protein and is known as the midpoint of the transition (T_m or C_m) (Shirdel and Khalifeh, 2019). At equilibrium conditions, the stability of the protein is

the ratio of the population of native state species to the population of denatured state species, with K_{eq} as the equilibrium constant depicted in the equation below.

$$K_{eq} = \frac{[D]}{[N]}$$

This equilibrium constant can be used in the following equation of standard Gibbs free energy change for the process of unfolding of a protein

$$\Delta G^\circ = -RT \ln K_{eq} = -RT \ln \frac{[D]}{[N]}$$

$$K_{eq} = \exp\left(\frac{-\Delta G^\circ}{RT}\right)$$

Where R is the universal gas constant, and T is the absolute temperature in Kelvin. Any observed spectroscopic data acquired from a two-state transition yields a sigmoidal transition, since the significant species populating will either be in the native or the denatured state which can be fitted to a Boltzmann distribution and further modified to include specific parameters for thermal and chemical denaturation. For all the spectroscopic data acquired, the observed signal is given as following

$$\text{observed signal} = f_N \cdot s_N + f_D \cdot s_D$$

Where f_X is the fractional occupation of a state X (N or D) and s_X is the signal from state X when $f_X = 1$. Expressing the f_X in terms of concentration of D and N and rearranging we get

$$f_D = \frac{[D]}{[D] + [N]} = \frac{\frac{[D]}{[N]}}{\frac{[D]}{[N]} + \frac{[N]}{[N]}} = \frac{K_{eq}}{K_{eq} + 1}$$

Similarly, we get another equation for the N state

$$f_N = \frac{[N]}{[D] + [N]} = \frac{\frac{[N]}{[N]}}{\frac{[D]}{[N]} + \frac{[N]}{[N]}} = \frac{1}{K_{eq} + 1}$$

Substituting the values for f_N and f_D in the previous equation we get,

$$\text{observed signal} = \frac{s_N + s_D \cdot K_{eq}}{1 + K_{eq}}$$

Substituting the expression of K_{eq} in the above equation,

$$\text{observed signal} = \frac{s_N + s_D \cdot e^{-\left(\frac{\Delta G^{\circ'}}{RT}\right)}}{1 + e^{-\left(\frac{\Delta G^{\circ'}}{RT}\right)}}$$

The native and the denatured baselines have a slope to it, this indicates at the intrinsic changes in the signal (within linear regime) for N and D while increasing the perturbant.

Hence the above equation can be modified as

$$\text{observed signal} = \frac{(\alpha_N + \beta_N \cdot P) + (\alpha_D + \beta_D \cdot P) e^{-\left(\frac{\Delta G^{\circ'}}{RT}\right)}}{1 + e^{-\left(\frac{\Delta G^{\circ'}}{RT}\right)}}$$

Where α_N is the N state signal at 0 K, β_N is the slope of the native baseline, α_D is the signal from D state at 0 K, and β_D is the slope of the denatured baseline, P is the degree of perturbation and R is the ideal gas constant. This equation can be written in terms of temperature as the perturbant as following

$$\text{observed signal} = \frac{(\alpha_N + \beta_N \cdot T) + (\alpha_D + \beta_D \cdot T) e^{-\left(\frac{\Delta G^{\circ'}}{RT}\right)}}{1 + e^{-\left(\frac{\Delta G^{\circ'}}{RT}\right)}}$$

Where α_N is the N state signal at 0 K, β_N is the slope of the native baseline, α_D is the signal from D state at 0 K, and β_D is the slope of the denatured baseline, T is the temperature in Kelvin (perturbant) and R is the ideal gas constant (1.987 cal.mol⁻¹.K⁻¹). The above written

equation for observed signal can be substituted with the midpoint of thermal denaturation (T_m) and the enthalpy change at the midpoint of transition (ΔH_m) to get the following

$$S(T) = \frac{S_N(T) + S_D(T) \cdot e^{\left[\frac{-\Delta H_m}{R} \left(\frac{1}{T} - \frac{1}{T_m}\right)\right]}}{1 + e^{\left[\frac{-\Delta H_m}{R} \left(\frac{1}{T} - \frac{1}{T_m}\right)\right]}}$$

Where, T_m is the midpoint of transition, ΔH_m is the denaturation enthalpy change at T_m , $S(T)$ is the optical property at temperature T (Kelvin), $S_N(T)$ and $S_D(T)$ are the optical properties of native and denatured state of the protein at temperature T (Kelvin), and R is the universal gas constant. ΔC_p was taken as zero and a linear approximation of the values near T_m were calculated (discussed further) (Mittal and Singh, 2013). To fit for thermal denaturation a rearrangement of the Gibbs Helmholtz relationship is used as following

$$\Delta G^\circ = \Delta H_m \left(1 - \frac{T}{T_m}\right) + \Delta C_p \left[T - T_m - \left(T \cdot \ln \frac{T}{T_m}\right)\right]$$

ΔC_p can be determined experimentally by calorimetry, or by measuring the denaturation curves at different pH values, or at different denaturant concentrations where T_m shows some degree of variation. The variation of ΔH_m in such experiments is dominated by the effect of ΔC_p . ΔC_p can also be estimated empirically based on the size of the protein. In the absence of an experimental value or an estimate for ΔC_p , a value of zero yields an acceptable fit and essentially correct thermodynamic parameters for most of the thermal desaturations. This is because the above equation has a parabolic form with non-zero ΔC_p . This function is closely approximated by a linear function, when setting the value of ΔC_p to zero at temperatures close to T_m (Santoro and Bolen, 1988; Jackson and Fersht, 1991; Nicholson and Scholtz, 1996).

Standard Gibbs free energy change can also be expressed as following

$$\Delta G^\circ = \Delta H^\circ - T\Delta S^\circ$$

Where ΔH° and ΔS° are the change in standard enthalpy and entropy of the system. At the operating temperature, the reactants and the product being at 1 M concentration, if protons are accepted or released as in any biological process, then this standard state must be at pH 0 (i.e. 1 M H^+ ions). Experimentally this cannot be attained. Therefore, a subscript prime (') is added to all the standard thermodynamic parameters to denote that the experimental conditions were maintained at physiological pH (~ 7.0- 8.0). Hence the thermodynamic parameters are denoted as

$$\Delta G^{\circ'} = \Delta H^{\circ'} - T\Delta S^{\circ'}$$

Where $\Delta G^{\circ'}$ is (Modified standard Gibbs free energy change), $\Delta H^{\circ'}$ (standard enthalpy change), and $\Delta S^{\circ'}$ (standard entropy change) (Sarkar, Li and Pielak, 2013; Speer *et al.*, 2022).

1.4 What is macromolecular crowding?

Laboratory/test tube/*in-vitro* conditions for elucidating structure, function, and thermodynamics vary drastically from the in-cell-like conditions. The buffers used in the experiment hardly accounted for the “crowd” inside the cell. Cellular organelles, proteins, lipids, carbohydrates, metabolites, nucleic acids, etc., heavily crowd the interior of the cell (Figure 1.3) and make it viscous. The concentration of cell interior can reach up to ~400 mg/mL (Zimmerman and Trach, 1991a; Ellis and Minton, 2003). The mere presence of these macromolecules makes the cell a highly congested environment for all the biochemical processes. This condition is termed macromolecular crowding.

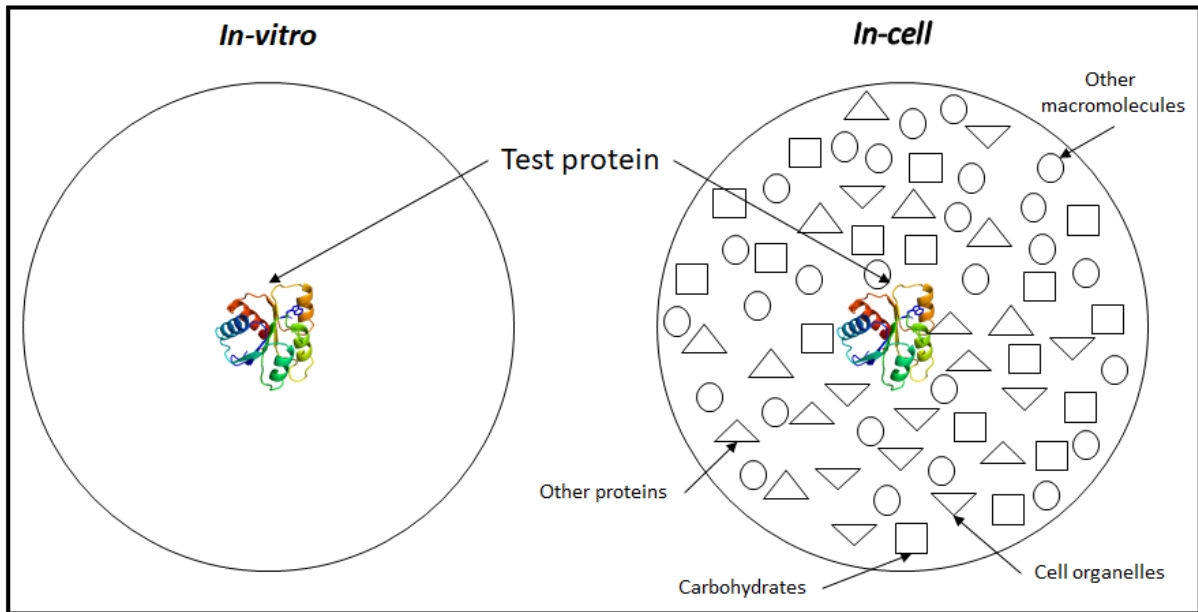


Figure 1.3: Graphical illustration of macromolecular crowding. *in-vitro* vs. *in-vivo* environment for a test protein. Nevertheless, the proteins fold to their appropriate form and perform all necessary functions accurately. Is the knowledge acquired regarding protein structure, stability, folding, and thermodynamics under *in-vitro* conditions similar to the processes occurring inside the cell? If not, what factors affect and influence these phenomena? This fundamental question has prompted researchers worldwide to study common physiological processes from a new perspective of macromolecular crowding. To achieve this, certain synthetic and natural macromolecules are used to crowd the dilute buffer environment and mimic *in-cell*-like conditions.

1.5 Macromolecular crowders

Macromolecular crowders can be classified into two categories: synthetic and natural polymers with different shapes and sizes. These crowders were used to replicate the conditions similar to that of inside the cell. Carbohydrate polymers of glucose, sucrose and other linear polymers of ethylene glycol are the most commonly used synthetic compounds to simulate the *in-cell*-like/*in-vivo* conditions in an *in-vitro* environment (Figure 1.4). Natural crowders, such as globular proteins, nucleic acids, and metabolites, are also used either in conjugation with

synthetic polymers or alone to simulate a more realistic crowding environment. Some examples of protein crowders are lysozyme, bovine serum albumin (BSA), etc.

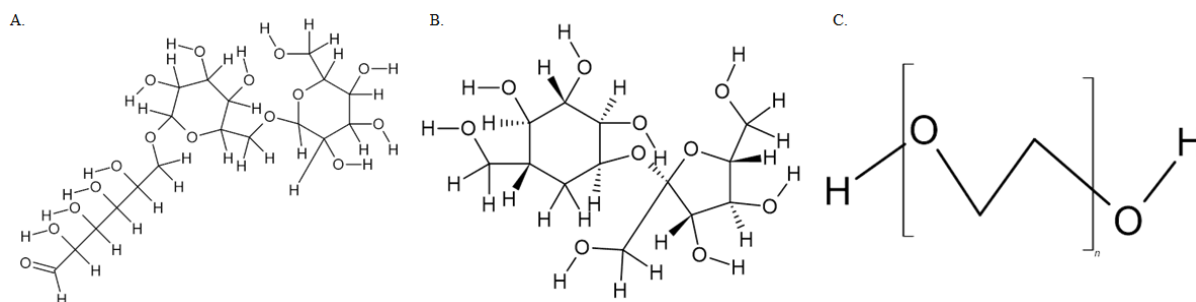


Figure 1.4: (A) 2D representation of monomeric unit of Ficoll, (B) 2D representation of monomeric unit of Dextran, and (C) 2D representation of monomeric unit of PEG.

Figure 1.4 displays the monomeric units of the synthetic polymers used as crowders. Ficoll is a high molecular weight sucrose polymer formed by copolymerization of sucrose and epichlorohydrin. These molecules are heavily branched and possess many hydroxyl groups, leading to good solubility in aqueous media. Special care should be taken while working below pH 3.0, as Ficoll rapidly hydrolyses at these pH values, especially at elevated temperatures (adapted from the material data sheet). Ficoll is synthesized mainly under two polymeric conditions, 70 kDa and 400 kDa. Ficoll 70 is assumed to be spherical, with an average molecular weight ranging from $\sim 6 \times 10^4$ to 8×10^4 . The reported Stokes radius of Ficoll 70 was ~ 5.1 nm (Harve *et al.*, 2006). Because it is a carbohydrate-based polymer, it displays optical rotation and can be quantified in solution using a polarimeter. A specific optical rotation value $[\alpha]^{20}$ of 56.5° was used to calculate the weight percentage of the solution. Similarly, Dextran is a linear polysaccharide chain of poly(D-glucose) with α 1-6 glucoside links, that spares short branches in a rod-like manner. Dextran's have the ability to polymerize in different lengths, out of which the most commonly reported sizes used for crowding are 4×10^4 and 7×10^4 Daltons. The Stoke's radius of these dextrans variants ranges approximately from 4.8 nm to 5.1 nm. Polarimeter can be used to quantify its weight percentages using the specific optical rotation values listed in Table 1.1.

Table 1.1: Measured specific optical rotation values of carbohydrate based macromolecular crowders.

S. No.	Crowder	$[\alpha]^{25}$
1	Ficoll 70,000	56.052
2	Dextran 40,000	186.972
3	Dextran 70,000	192.010

PEG is a linear polymer that is highly water soluble. PEG is used as a crowding agent because it is highly flexible and, being amphiphilic, is known to interact with polar and non-polar amino acids of proteins (Lee and Lee, 1987; Furness *et al.*, 1998; Wu *et al.*, 2014; Knowles *et al.*, 2015; Popielec *et al.*, 2020). PEG is also known to be protein-specific in terms of its effect on the structure, stability and activity (Zhang *et al.*, 2012; Wu *et al.*, 2014; Knowles *et al.*, 2015; Lai *et al.*, 2015). The general structure of PEG is a linear polymer consisting of OH-(CH₂-CH₂-O)-H]_n – H units. Depending on the length of polymerization, the physical state of PEG changes. For instance, PEG 400 is a liquid, whereas PEG 20000 is a crystalline solid (REF). Since PEG has both CH₂ and OH, it's reported to be amphiphilic in nature. PEG also can self-assemble in bulk or interfaces due to hydrophobic interactions. With the presence of a hydrophobic polar head at both ends, it is expected that PEG organises itself to form bipolar vesicles (Paik *et al.*, 2012; Parray, Hassan, *et al.*, 2020). Due to this highly organized structure of the vesicles, PEGs also possess the ability to fluoresce with a λ_{\max} value of 380 nm. Therefore, owing to these properties and the ability to increase the sample viscosity, these macromolecules are used as decoys for in-cell-like conditions.

1.6 Consequences of macromolecular crowding

The term macromolecular crowding was first coined by Minton and Wilf in 1981. They formulated a theory that the mutual exclusion of molecules is responsible for the macromolecular crowding effect on glyceraldehyde-3-phosphate dehydrogenase reaction rates. Furthermore, the presence of molecules that do not participate in the process can affect the

structure, function and dynamics of the protein (Minton, 1981). This phenomenon is termed an excluded volume, wherein the presence of other molecules constrains the space available, and the protein is forced into a cavity created by this excluded volume. It was not until 2000 that Minton formulated an elegant and simple theory to account for the importance of excluded volume on protein stability (Minton, 2000). Excluded volume theory is believed to always increase the protein's stability, as it does not allow the protein to remain in an extended form (unfolded) and forces it to be in a compact state. Consequently, either the native state is stabilized or the unfolded state is forced to exist in a compact form. Multiple studies corroborated the idea of the excluded volume effect. For instance, Stagg et al. probed the thermal unfolding of *Desulfovibrio desulfuricans* apo-flavodoxin in the presence and absence of Ficoll 70. They found that adding Ficoll increased the protein's secondary structure and thermal stability (ΔT_m of 20°C, at 400 mg/mL) (Stagg *et al.*, 2007). The tertiary structure of lysozyme showed minor rearrangements and also displayed an increased $\Delta G^\circ'$ and in the midpoint of the thermal transition (T_m) in the presence of Dextran 70 than in dilute buffer. This increase was attributed to the volume exclusion by Dextran. It was also reported that the stabilization was protein-independent, reinforcing that the effect was purely entropic in nature (Sharma, Mittal and Singh, 2015). It has been established that protein thermal stability is higher under (ΔT_m 5-20°C) *in-vivo* conditions than what is elucidated in dilute buffer environments (R. J. Ellis, 2001; Kuznetsova, Turoverov and Uversky, 2014). However, the experimentally observed increase in T_m was a maximum of 5°C except for one previously reported case. At this point, the excluded volume theory was questioned, and macromolecular crowding was speculated to be more than hard-core repulsions. Several other studies in the direction of proving the excluded volume theory continue. The first challenge to this theory that only hard-core repulsions are essential came from the Oas group, which found that the stability of monomeric λ repressor in cells is approximately the same as that measured in dilute buffer

(Ghaemmaghami and Oas, 2001). This was revisited by Miklos et al., who analyzed the effect of crowding not only from excluded volume perspective, but also from the chemical interactions between the test protein and crowder. The stability of chymotrypsin inhibitor-2 was quantified in the presence of varying molecular weights of poly(vinylpyrrolidone)s at different concentrations. The data from NMR-detected amide exchange revealed that in addition to the volume exclusion, weak non-specific chemical interaction between the protein and crowder might also stabilize the test protein (Miklos *et al.*, 2010). Moving forward, the same authors also established the destabilizing effect of these soft interactions. According to them, destabilization can arise from the competition between volume exclusion and soft interactions (Miklos *et al.*, 2011). Macromolecular crowding studies progressed towards soft interactions when Pielak's Laboratory published the dominant effect of weak non-specific interactions of Ficoll on ubiquitin via NMR amide exchange. The weak non-specific interactions completely offset the expected reduction in the entropy. The concept of balancing enthalpy and entropy stems from the research presented by this group in this study. To further dissect the effect of crowding interaction and to map the source of the effect of crowding Benton et al. performed NMR-detected amide-proton exchange experiments on chymotrypsin inhibitor 2 in the presence and absence of Ficoll and sucrose. Sucrose is a monomer of Ficoll. To establish that weak chemical interactions are also a major contributing factor in macromolecular crowding, the authors eliminated the volume exclusion effect by using the Ficoll monomer. The results obtained were contrary to all theoretical predictions. The protein was stabilized to the same extent by both Ficoll and sucrose, demonstrating the role of weak non-specific interactions. These findings clarified that crowding can manifest in two possible ways i) by volume exclusion, which is purely entropic in nature and ii) by weak non-specific chemical interactions that are enthalpic in nature. These interactions include charge-charge, dipole-dipole, nonpolar, and other interactions. Depending on the crowder-protein pair, these

interactions can stabilise or destabilise (Benton *et al.*, 2012a; Speer *et al.*, 2022). Yet another theory that exists in the field of crowding is the impact of high pressure on biological macromolecules within the crowded environment. It is a highly complex phenomenon. Increased pressure has the capability of altering thermodynamic properties of the protein, stability, interactions, etc. For instance, macromolecular crowding with dextran stabilizes Ribonuclease A against pressure-induced unfolding (Zhai and Winter, 2013). Pressure unfolding initially destabilized lysozyme and then showed stabilizing effect only at higher concentration of crowding agent. This phenomenon was explained via the counteracting forces of reduced hydration volume gain and excluded volume effect (Somkuti *et al.*, 2017). Increased pressure may also lead to phase transitions in biological macromolecules i.e. between different folded states within the energy landscape or can even unfold completely. Pressure theory is quite prominent in the intrinsically disordered proteins. Crowding and pressure can modulate the binding site of the target molecules, affecting cellular signalling and regulation.

A schematic (Figure 1.5) represents the consequences of crowding.

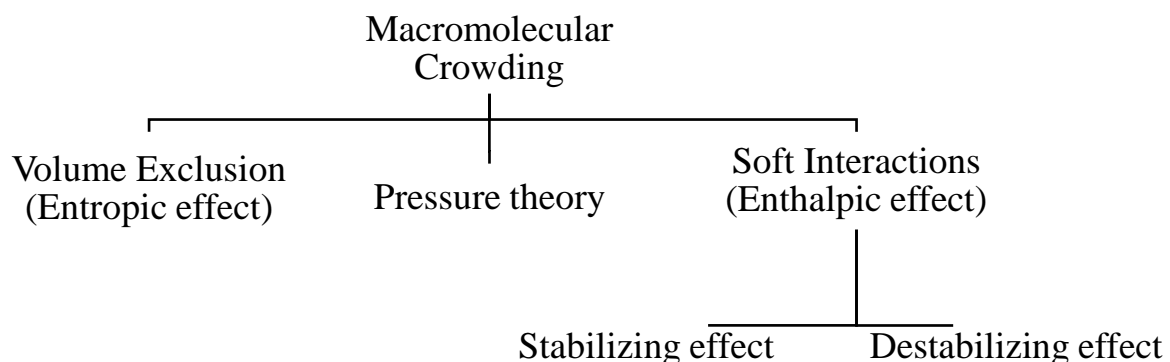


Figure 1.5: Schematic representation of the effects of crowding on a test protein.

1.7 Understanding the origin of the effect of crowding

One of the crucial gaps that needs to be addressed is the origin of the observed modulation due to crowding on the structure, stability, dynamics, and function. The commonly used crowders, Ficoll, Dextrans, and polyethylene glycols show both stabilizing and destabilizing effects depending on the test protein. Studies that can directly pinpoint (under *in-vitro* and in-cell) the origin of crowding-induced modulation are required. Investigations in this direction are beginning to provide direct clues on protein-crowder interactions at the atomic level (Kadumuri *et al.*, 2016; Adams *et al.*, 2019; Bille *et al.*, 2019; Köhn and Kovermann, 2020). One such recent interrogation by nuclear magnetic resonance (NMR) attributed crowding-induced destabilization to local unfolding arising from the interactions of the protein's long flexible loops in superoxide dismutase. Chemical shift perturbations reveal not only protein-crowder interactions but also the site of interactions (Adams *et al.*, 2019; Bille *et al.*, 2019). Another investigation that involved monitoring NMR chemical shift perturbations and hydrogen-bonding interactions concluded that stabilization due to crowding is due to a reduction in solvent accessibility for the residues in the loop regions of the protein (Köhn and Kovermann, 2019). In one of our previous investigations, a significant reduction in the NMR signals for the residues residing in the β -sheets was attributed to selective destabilization of the stable core in the presence of Ficoll (Kadumuri *et al.*, 2016).

1.8 Macromolecular crowding with proteins having complex folding mechanism

The effect of crowding, in general has been widely discussed on simple test proteins that do not display folding intermediated in their energy landscape. Most globular and intrinsically disordered proteins considered for crowding studies follow a two-state folding to unfolding model of transition. It is highly relevant to shed light on certain studies that have addressed the effects of crowding on the thermodynamically stable intermediate states of proteins. Kadumuri *et al.*, 2016 proposed and proved that Ficoll-70 destabilizes both the native and partially folded

state, as observed in circular dichroism and fluorescence studies of a 29 kDa alpha subunit of tryptophan synthase (α TS) (Kadumuri *et al.*, 2016). Similarly, myoglobin attains a molten globule like state in the presence of crowding agent Ficoll-70. The authors showed that the secondary structure of the protein remained unchanged in the presence of Ficoll. The tertiary structure is completely lost (near UV-CD), has a newly exposed hydrophobic core (ANS binding) and has an increased hydrodynamic radius (Nasreen *et al.*, 2018). Another study on apo-flavodoxin reported an increase of thermal stability by 2.9 °C in the presence of crowders, but destabilizes and aggregates the off-pathway intermediate drastically (Engel *et al.*, 2008).

1.9 Small molecule crowding:

In addition to macromolecules, cells are abundantly populated with various small molecules. Notably, these molecules span cellular organisms, plants, and animals (Somero, 1986). These compounds comprise of polyols, sugars, methylamines, amino acids, etc. Among these sugars, polyamines are the most commonly found small molecules inside cells. They can protect cells against adverse conditions such as temperature fluctuations, pH changes, dehydration, and salinity (Back, Oakenfull and Smith, 1979; Taylor *et al.*, 1995; Sola-Penna *et al.*, 1997). Osmolytes/small molecules are broadly classified into: i) bioprotective osmolytes and ii) chemical denaturants. Bioprotective osmolytes that stabilize the native state of the protein have been discussed previously. These osmolytes are preferentially excluded from the protein surface, leaving the protein preferentially hydrated. The second class of osmolytes, chemical denaturants, can directly bind to the protein backbone and destabilize them. For instance, urea can pass through the water network around a protein and directly interact with the protein. Because unfolding leads to a more exposed surface area, urea can stabilize the unfolded form and lead to the observed destabilization. This process is also accompanied by a reduction in the excess enthalpy of the protein (Canchi and García, 2013). Osmolytes/small molecules, in general, are considered to be protein stabilizers, and one of the stabilization theories is that

sugars can stabilize the native state of the protein as they are preferentially excluded from the protein surface. Hence consequently, the change in Gibbs free energy associated with the protein folding process increases (Poddar *et al.*, 2008). For instance, phosphoglycerate kinase was chemically denatured using guanidine hydrochloride (GuHCl) in the presence and absence of different sucrose concentrations. The amount of GuHCl required to unfold the protein was increased in the presence of sucrose. However, the overall ΔG° in the absence of any denaturant obtained by extrapolation showed no change. Smith *et al.* probed the thermal stability of ovalbumin, lysozyme, conalbumin, and α -chymotrypsinogen in the presence of sucrose, glucose, sorbitol and glycerol. The additions of sugars and polyols increases the thermal stability (T_m) of proteins. ΔT_m ranged from 0-18°C for conalbumin at pH 7.0 in 50% glycerol and lysozyme at pH 3.0, in the presence of 50% sorbitol, respectively. It was argued that this extent of stabilization originate from the effect of sugars and polyols on the hydrophobic interactions of the proteins (Back, Oakenfull and Smith, 1979). These studies have mainly focused on the effect of a single osmolyte on the structure and stability of proteins. However, a mixture of osmolytes coexist inside the cell. In light of this, Kishore *et al.* used glycine, alanine, DL- α -aminobutyric acid, and sorbitol individually and in combination to elucidate protein stability in a more realistic environment. The authors reported an increase in the midpoint of thermal transition (T_m) of hen egg-white lysozyme in the presence of these osmolytes. The mode of action for stabilization is proposed to be preferential exclusion. They also proved that the stabilizing effects of different osmolytes were not synergistic in nature. (Shinde *et al.*, 2020) However, the general stabilizing trend of osmolytes by preferential hydration mechanism was challenged and disproved by Song *et al.*, 2021. The authors worked with MutX, a GB3 variant protein, and four osmolytes: sorbitol, glycerol, betaine, and taurine. The protein is stabilized by glycerol and sorbitol, but slightly destabilized by betaine and taurine. This destabilization is believed to originate from the weakening of electrostatic

interactions by the zwitterionic osmolytes. The authors also performed *in-vivo* studies using *E.coli* lysates. They found that betaine and taurine further destabilized the protein under *in-vivo* conditions. In the presence of these osmolytes, quinary interactions between the protein and the environment increase, leading to the observed destabilization (Song *et al.*, 2021). Considering these factors, it is apparent that cosolutes (macromolecules and small molecules) can have diverse effects on the structure and stability of proteins. There is a need for a more carefully considered and sophisticated model to explain the molecular and thermodynamic consequences of macromolecular and molecular crowding on test proteins.

1.10 Enthalpy-entropy contribution towards crowding effect

To gain further insights into the effects of crowding on the change in the standard Gibbs free energy of protein folding, it is necessary to dissect the contributions of enthalpy and entropy towards the overall thermodynamic stability of the protein. Two groups of scientists have independently devised a quadrant-based vector system between the thermodynamic fingerprints of proteins, which helps characterize the mechanistic differences in the mode of action of a crowder on a particular protein. Harries *et al.*, measured the free energy of folding of a peptide in the presence of different cosolutes at various concentrations to determine the thermodynamic parameters of protein folding using van't Hoff's analysis. These parameters were then subtracted from the thermodynamic parameters of the native protein in dilute buffer conditions (Sukenik *et al.*, 2013). The differences in enthalpy and entropy are calculated using the following equations;

$$\Delta\Delta H^{\circ'} = \Delta H^{\circ'}_{(Dilute)} - \Delta H^{\circ'}_{(Cosolute)}$$

$$T\Delta\Delta S^{\circ'} = T\Delta S^{\circ'}_{(Dilute)} - T\Delta S^{\circ'}_{(Cosolute)}$$

The enthalpy versus entropy plots of a protein under crowded and dilute conditions ($\Delta\Delta H^{\circ'}$ and $T\Delta\Delta S^{\circ'}$) enables the classification of a system in one of the four regions of the Cartesian

plane (Politi and Harries, 2010; Sukenik *et al.*, 2013; Sapir and Harries, 2014). Figure 1.6 displays the model described above for the classification with X-axis as $\Delta\Delta H^\circ'$ and Y-axis as $T\Delta\Delta S^\circ'$ in kJ/mol. The diagonal represents the total enthalpic-entropic compensation and separates the stabilizing cosolutes that lie above the line (blue region) and destabilizing cosolutes below it (orange region).

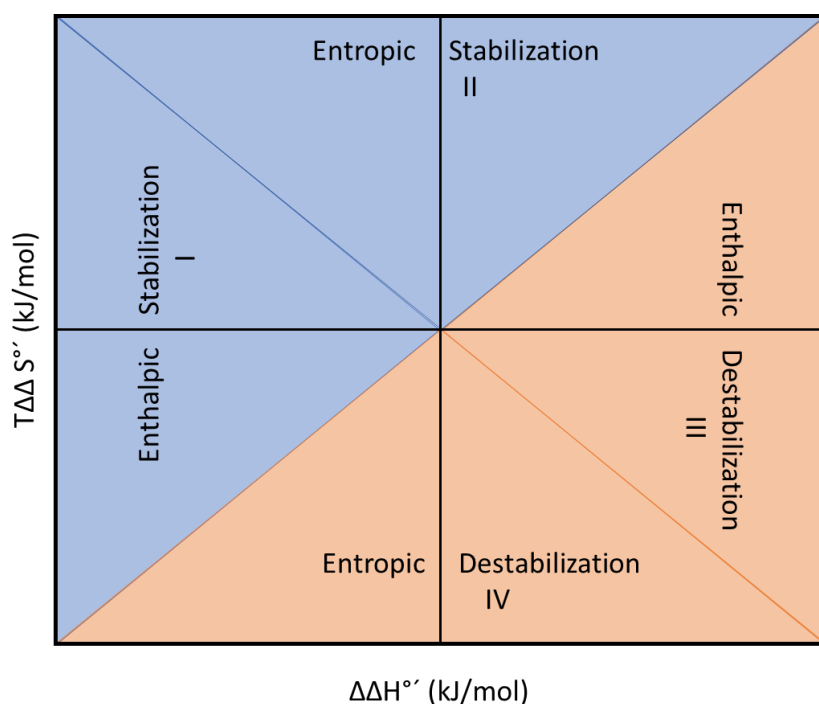


Figure 1.6: Enthalpy versus entropy plot of the test protein with regimes indicated in different colors.

The stabilizing region is further split into two: Region I represents enthalpically driven stabilization and Region II denotes entropically stabilized proteins. Similarly, the destabilizing region can be further divided into regions III and IV, representing enthalpic and entropic destabilization, respectively.

Another cartesian-based vector system devised by Senske *et al.*, (Senske *et al.*, 2014) dissects the mechanistic effects of cosolute into a different kind of characterization. These authors also plotted the difference in the thermodynamic parameters between the cosolute and dilute conditions. The difference is obtained by using the following equations:

$$\Delta\Delta H^{\circ} = \Delta H^{\circ}_{(\text{Cosolute})} - \Delta H^{\circ}_{(\text{Dilute})}$$

$$\Delta T_m = T_m(\text{Cosolute}) - T_m(\text{Dilute})$$

According to this group, a plot between ΔT_m and $\Delta\Delta H^{\circ}$ reveals the mechanistic details of the effect of cosolute (Figure 1.7). The first quadrant (ΔT_m and $\Delta\Delta H^{\circ} > 0$) corresponds to preferential hydration, the second ($\Delta T_m < 0$, $\Delta\Delta H^{\circ} > 0$) to a combination of preferential binding and hydration, the third ($\Delta T_m < 0$, $\Delta\Delta H^{\circ} < 0$) to preferential binding, and the fourth ($\Delta T_m > 0$, $\Delta\Delta H^{\circ} < 0$) to excluded-volume effects. The authors came up with this classification by testing the effect of various cosolutes on the thermodynamic stability of ubiquitin.

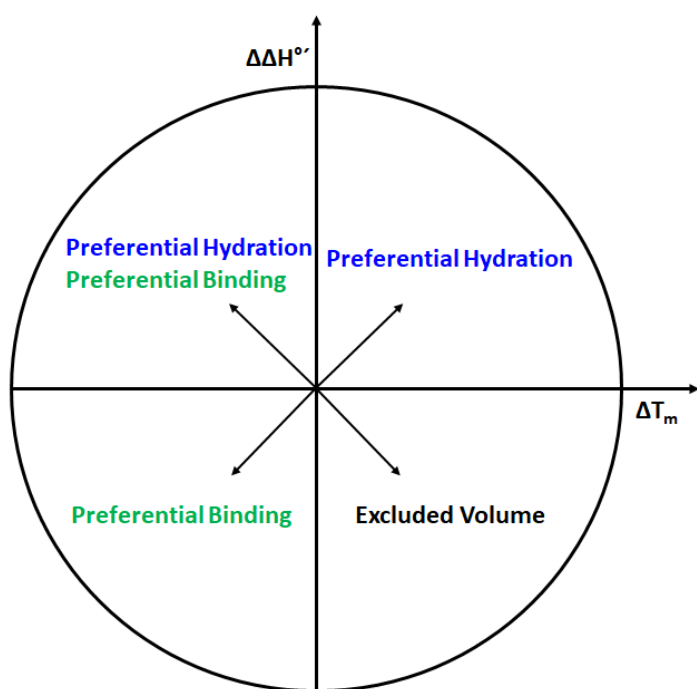


Figure 1.7: Classification of the effects of cosolutes on the protein folding equilibrium.

The quadrant-based systems discussed above will shed light on the mechanisms of action of various cosolutes and help in gaining new insights into the effects of crowding. Another situation where the contrasting effects of enthalpy and entropy cancel out the net effect of crowding is termed as enthalpy-entropy compensation. It refers to a fascinating phenomenon observed in macromolecular crowding, where the opposing effects of enthalpy and entropy

changes on a system partially cancel each other out, resulting in a smaller net effect on thermodynamic parameters like free energy. In the context of crowding, this interplay plays a crucial role in modulating the stability and interactions of biomolecules. The findings of this thesis are partially on these lines which is discussed further.

1.11 Choice of model protein

To elucidate the crowding effect, we chose a protein from the two-component signalling system of bacteria, chemotaxis protein Y (CheY). CheY is the most characterized response regulatory protein, whose structure, stability, folding, and dynamics are thoroughly probed in dilute buffer system. It is a prototype for understanding conformational switches and displays distinct populations in the metal unbound form (Bruix *et al.*, 1993; DeKoster *et al.*, 1993; Filimonov *et al.*, 1993; Moy *et al.*, 1994; Munoz *et al.*, 1994; Simonovic and Volz, 2001; Hills *et al.*, 2010). CheY is a 129 amino acid long single domain bacterial response regulatory protein. It has a single tryptophan residue at position 58 (Figure 1.8).

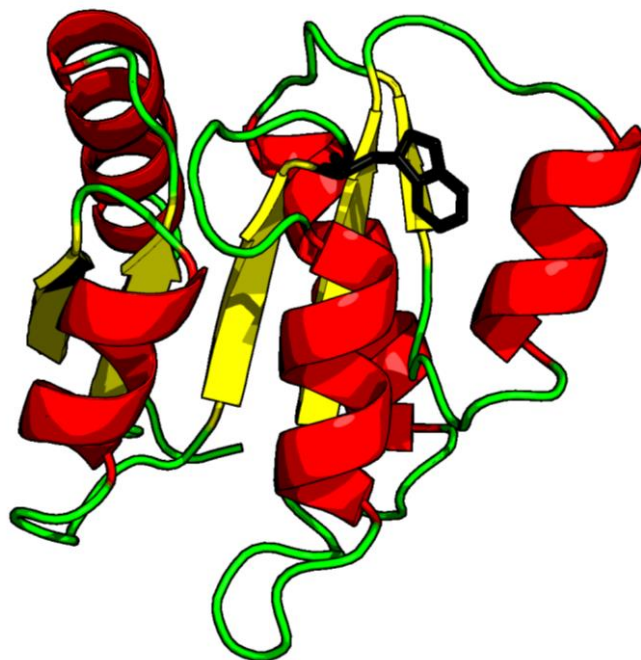


Figure 1.8: Cartoon representation of the crystal structure of CheY (PDB ID: 3CHY) generated using PyMol (Schrödinger, LLC, 2015).

This tryptophan is partially exposed, as proven by acrylamide quenching studies performed by Lukat et al. 1990 (Lukat, Stock and Stock, 1990). The protein has a net negative charge at physiological pH. The protein is composed of five α -helices and five β -sheets placed in an alternating topology.

The primary role of CheY is to convey the signals received at the cell surface to effector proteins, specifically FliM protein. Upon divalent metal ion binding, CheY initiates a cascade of events that ultimately leads to a switch in flagellar rotation from the anti-clockwise to clockwise direction. A series of proteins participate in this process, with CheY at the central stage of the entire process. Figure 1.9 shows the role of CheY in signal transduction along with all its interacting partner proteins.

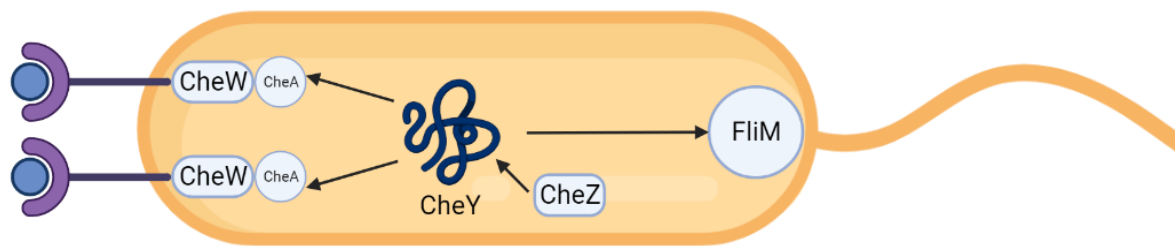


Figure 1.9: Simplified scheme of protein-protein interactions during chemotactic signalling.

The receptor binding domain of Chemotaxis protein A (CheA) receives a signal in the presence of a chemical attractant or repellent. This leads to autophosphorylation of CheA. The phosphate group is then transferred to the Asp-57 residue of the signal transduction protein CheY. An outcome of autophosphorylation is the reduced affinity of CheY for CheA. CheY binds to CheA via direct contact with amino acids on the surface of both proteins. The residues involved in the interactions are Ala-90, Lys-92, Ile-95, Ile-96, Ala-99, Gln-100, Ala-103, Ser-104, Gly-105, Tyr-106, Lys-122, Glu-125, and Lys-126 (Gouet *et al.*, 2001). Consequently, the affinity of phosphorylated-CheY (CheY-P) is very high for the flagellar motor switch component, FliM. CheY-P is released into the cytoplasm and interacts with the flagellar motor complex by binding to FliM. The N-terminal region is also involved in this interaction. This leads to a

change in flagellar rotation from an anticlockwise direction to a clockwise direction. (Djordjevic and Stock, 1998; Bren and Eisenbach, 2000). CheY-P forms large oligomeric complexes with chemotaxis protein Z (CheZ), yet another component of the bacterial chemotaxis process that is responsible for CheY dephosphorylation. The C terminal 19 amino acid region is responsible for binding interactions with CheY-P. The residues from CheY that are involved in the binding to CheZ have been identified in two clusters. One is near the active site and the other consists of parts of $\alpha 1$ and $\alpha 5$ and the loop connecting $\beta 5$ - $\alpha 5$. These residues overlap with the FliM interaction site. CheZ recognizes only free CheY-P and is not bound to FliM (Eisenbach, 1996; Bren and Eisenbach, 2000). CheY must undergo structural changes to interact with various partners in the signal transduction cascade. As discussed earlier, to bind to the incoming phosphate group from CheA, CheY first binds to a divalent metal ion, preferably Mg^{2+} . Magnesium binding is the most crucial step in signal transduction and results in a series of structural changes in CheY. Figure 1.10A and B highlight the changes that occur in the protein upon metal binding.

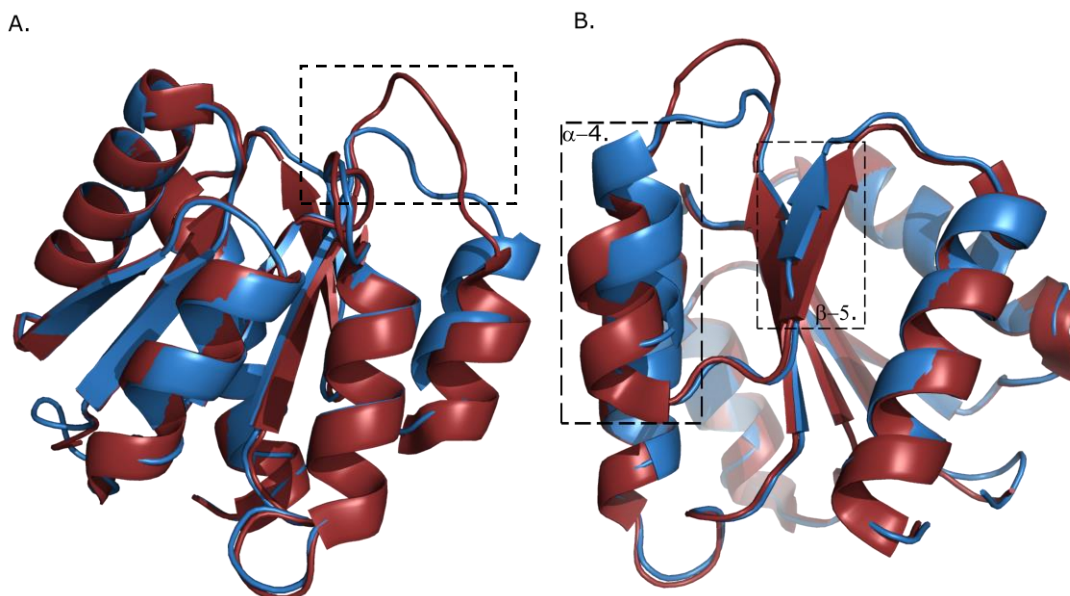


Figure 1.10: Overlapping crystal structure of apo and holo forms of CheY. (A) An angle highlighting the change in the loop configuration in holo form (boxed region) and (B) highlighting the slight change in secondary structure due to Mg^{2+} binding in α -4 and β -5 (boxed region).

CheY has a metal-binding pocket containing residues Asp-13, Asp-57, and Asn-59. Upon Mg^{2+} binding, the side chain of Asp-57 rotates to approach the metal ions, while Asp-12 and Asp-13 change their orientations. The Phe-14 aromatic ring rotates by 60° to avoid steric clashes with the water-metal clusters. Metal binding changes the salt bridging between Lys-109 – Asp-57 to Lys-109 – Asp-12, affecting the positions of the main chains of residues Val-108, Lys-109, Pro-110 and Phe-111. Asn-59 moves away from the active site by 2 \AA , forming a new hydrogen bond with Glu-93, which displaces Glu-93 by approximately 10 \AA . This shift results in the reorientation of sidechains of Trp-58, Thr-87, and Tyr-106, which is the reason for fluorescence quenching, as Trp-58 moves towards a more polar environment in the holo-state.(Stock *et al.*, 1993; Bellolell *et al.*, 1994).

As discussed above, CheY is structurally and thermodynamically the most characterized switch class of proteins, displaying distinct conformations in its apo and holo forms. Thus, CheY is an ideal test protein. Any alterations in the native state characteristics of CheY can be attributed to crowding-induced changes. Using different molecular and macromolecular crowders, we can test a wide range of crowding implications on this protein's structure, stability and function.

1.12 Gaps in research

As discussed earlier, crowding can manifest its effects in either hardcore entropic repulsions, leading to stabilization, or soft chemical non-specific interactions between the crowder and protein that can stabilize or destabilize. The comprehension of protein structure, stability, function and thermodynamics is derived from dilute buffer conditions, which do not account for cellular crowding. Several studies have been conducted on various biochemical processes in the presence of macromolecular and molecular crowders. The results obtained were highly diverse, and no simple trend could explain the diversity of these results. Hence, studying protein folding thermodynamics in crowded environments is of great importance to add to the existing knowledge and provide new insights.

Conformational changes upon the binding of metals, substrates, etc. are well-established in biological processes. These conformational changes regulate several biological processes. However, the effect of crowding on conformationally distinct forms has not been comprehensively studied. Although a few studies have highlighted the effect of crowding on conformational equilibrium, this aspect remains relatively underexplored. Studying the effect of crowding on conformationally distinct structures of the same protein will help increase the understanding of the structure-function relationship under in-cell-like conditions.

However, another gap in existing research is that the origin of the modulation of the effect of crowding remains elusive. Studies with residue-specific information in the presence and absence of crowders are scarce because of the inherent complexity of recoding such information via high-end techniques such as NMR spectroscopy, in a crowded environment. Not many proteins have a well-characterized structure, determined by NMR spectroscopy. Working with one such test protein in the presence or absence of crowders may open avenues to probe for structural changes and attribute it to crowding-induced perturbations.

In addition to macromolecules present inside the cell, small-molecule osmolytes are abundant. The effects of these osmolytes have been well studied in terms of protein structure and stability. However, combinatorial studies on the presence of macromolecular crowders and small molecules are limited. Attempts to perform studies in the combined presence of these molecules will be closer to a realistic, cell-like environment.

Understanding the complex role of crowding is important for both fundamental science and human health.

1.13 Objectives

1. To study the effects of macromolecular crowding on protein structure and stability under *in-vitro* conditions by using common synthetic crowders such as Ficoll, Dextran, and Polyethylene Glycols (PEG) in comparison with dilute buffer conditions.
2. To assess the effect of mixed macromolecular crowding on the structure and stability of proteins.
3. To gain insight into the molecular origins of the effects of macromolecular crowding.

1.14 Overview of the thesis

This thesis focuses on the following key points.

- (i) Understanding the mechanistic details of crowding on the structure and stability of a bacterial Chemotaxis protein Y (CheY) that displays distinct apo and holo forms, by using various macromolecular crowders such as poly(ethylene) glycols ranging from 6000 to 20000, Ficoll-70 kDa, Dextran 40 and 70 kDa.
- (ii) Gaining mechanistic insights into the effect of molecular and macromolecular crowding on apo protein by dissecting the thermodynamic parameters contributing to the Gibbs free energy of the protein folding process.
- (iii) Understanding the effect of osmolytes and macromolecular crowders on the conformational equilibrium between the apo and holo forms.
- (iv) Identifying the source of modulation of the effect of macromolecular crowding on the apo and holo forms of CheY via nuclear magnetic resonance (NMR) spectroscopy.

1.15 Chapter-wise summary of the thesis is given below:

Chapter 3: Poly(ethylene) glycols induced protein destabilizations of Chemotaxis protein Y

This chapter mainly focuses on the effects of different sizes of PEG on the structure, stability, and magnesium-binding ability of CheY. This study used a series of PEGs, ranging from PEG 6000 to PEG 20000. Circular dichroism, fluorescence emission spectroscopy, ANS binding emission, and tryptophan lifetime measurements indicated that the secondary and tertiary structures of the apo form of the protein are affected by PEG 20000. The thermodynamic stability was observed to decrease in a concentration-dependent manner. The observed destabilization was enthalpic in nature. A combined reduction in the T_m and ΔH° values indicated direct PEG protein interactions for PEG 20000. Similarly, all of these studies were performed in the presence of PEG 6000, 8000 and 12000. The secondary and tertiary structures did not change significantly during crowding in these PEGs. However, the thermal stability of apo CheY in the presence of all PEGs reduced in a concentration-dependent manner by an average of 1-3°C. Surprisingly, all PEGs, starting from 6000 to 20000, showed a drastic reduction in the thermal stability of holo CheY in a concentration-dependent manner. Therefore, it can be concluded that PEG-protein interactions are prominent, irrespective of the polymer size. These crowder-protein interactions with the apo form of the protein are to such an extent that the metal-binding site is either disrupted or is in a non-native form.

Chapter 4: Effect of carbohydrate-based crowders on the apo and holo form on CheY:

Selective destabilization of holo form of the protein

This chapter mainly focuses on crowding induced by carbohydrate-based polymers such as Ficoll 70000, Dextran 6000, Dextran 40000, and Dextran 70000. These are the most commonly used sugar-based polymers for mimicking in-cell-like conditions. Structural and stability studies were conducted in the presence and absence of these crowders. We report that, in the

presence of Dextran 40 and Dextran 70, the structure of CheY was perturbed in a manner that showed no specific trend in either secondary or tertiary structures. However, Dextran 6000 behaves differently from the other two Dextrans. Its effect on the secondary structure was negligible, but the thermal stability in the presence of Dextran 6000 increased drastically when compared to dilute buffer conditions. The thermal transition of apo CheY in the presence of Dextran 6000 was irreversible. This unusual behavior might be due to the aggregation/association induced in the apo form of the protein. Inconsistent results led us to not pursue crowding with Dextrans on our test protein.

Furthermore, studies on the effect of crowding on the two conformationally distinct states of the same test protein were performed. We observed a stabilizing effect of Ficoll 70 on the apo form of the protein. The effect of Ficoll 70 was opposite on the holo form of CheY. Intriguingly, macromolecular crowding by Ficoll resulted in a selective reduction in the thermal stability of the holo form. The reduced thermal stability of the holo form raises a fundamental question; is the metal-binding site intact in Ficoll? The data obtained from intrinsic tryptophan quenching indicated that metal binding ability is retained in a crowded environment. Since metal–protein interactions remain unperturbed, the alternative possibility for the exclusive reduction in the thermal stability of the holo form is Ficoll-induced modulation of the relative population of apo and holo forms of CheY.

Chapter 5: The origin of the modulation of the effect of crowding mapped onto the protein structure using NMR spectroscopy

This chapter mainly deals with obtaining molecular insights into the origin effects of the modulation of crowding on CheY. In chapter 2, it was established that there are direct PEG–protein interactions as the T_m and $\Delta H^\circ'$ values decreased simultaneously. This became the premise for further probing the study to obtain molecular insights into the effects of macromolecular crowding in the presence and absence of PEG 20000. ^1H - ^{15}N TROSY-HSQC

were recorded for CheY in the presence of varying concentrations of PEG to unravel PEG-protein interactions and their consequences on the conformation of the protein. The relative changes in NMR linewidths and chemical shift perturbations of the protein under crowding conditions in relation to their measurements in dilute buffer indicated the potential sites of interactions and/or crowding-induced changes in the conformation and dynamics. A significant number of residues exhibited small chemical shift changes in the presence of 100 mg/mL PEG. At 200 mg/mL, there was a further gradual movement in the chemical shifts for a set of residues. It is interesting to note that there is a subset of residues that are not exposed to the solvent but still display CSPs, suggesting that the origin of CSPs for these residues may not emanate from direct contact between the protein and PEG, but rather may be due to conformational changes and/or fluctuations prompted in the presence of PEG 20000. A significant number of residues with chemical shifts occur in α -helices, followed by loops/turns and β -strands. These residues reside at the terminal positions of the secondary structural elements. Along with the CSPs, the intensities of the cross-peaks also revealed a mixture of polar and non-polar residues that were affected in the presence of PEG. In conclusion, PEG distorts the apo structure around the metal-binding site, which leads to the loss of the metal-binding ability of CheY. Thus, corroborates the results obtained in Chapter 2 for the thermal stability of holo CheY.

Contrary to the effects observed for PEG, Ficoll 70 showed no significant CSPs in the ^1H - ^{15}N HSQC spectrum compared with the dilute buffer conditions. We have already established from the earlier chapter that in the presence of Ficoll, the metal binding ability is retained. We confirmed metal binding again by observing the overlap of the ^1H - ^{15}N HSQC spectrum of holo CheY in the presence of Ficoll with the holo CheY spectrum in dilute buffer. The likelihood of Ficoll-protein interactions was determined by analyzing the line broadening of backbone resonances. In the presence of Ficoll alone, a significant number of resonances demonstrated

increased linewidths in the presence of 200 mg/ml Ficoll, indicating the likelihood of protein-Ficoll interactions. In the presence of Ficoll, in holo CheY, more than a dozen residues showed further increased linewidths. The intensities of certain residues overlapped with the region that showed structural perturbation upon Mg^{2+} binding, suggesting the possibility of disruption of the apo-holo equilibrium.

Chapter 6: Molecular crowding using osmolytes and small molecules: individual and combinatorial effect of small molecules with macromolecular crowders on the structure and stability of CheY.

This chapter focuses on inducing crowding conditions using small-molecule crowders. These include amino acids, polyamines, and combinations of these with macromolecular crowders. It was found that the majority of these molecules did not affect the structure and stability of CheY. On the other hand, polyamines stabilize the apo form of the protein. The holo protein did not show any increase in thermal stability in the presence of various polyamines, but the folding process attains reversibility. This was attributed to the charge-neutralizing properties of the polyamines. An interesting finding from this chapter is the ability of polyamines to neutralize the effect of macromolecular crowding induced by Ficoll. Generally, in the presence of any crowder, the thermal stability of CheY always decreased to a point where it coincided with the apo form or was found to be between the apo and holo forms. In contrast, in the combined presence of polyamines and Ficoll, holo protein does not show any reduction in thermal stability. These findings were explained by some speculated theories in this chapter.

Chapter 2

Materials and Methods

2.1 Materials

Table 2.1: Details of chemicals and consumables used for experimentation.

S. No	Chemical/consumable	Catalogue No.	Make
1	PEG 20000	95172	Sigma
2	PEG 12000	81285	Sigma
3	PEG 8000	89510	Sigma
4	PEG 6000	81255	Sigma
5	Ficoll 70	F2878	Sigma
6	Dextran 70	31390	Sigma
7	Dextran 40	31389	Sigma
8	Potassium phosphate monobasic	191430	Sigma/MP Biomedicals
9	Potassium Phosphate Dibasic	191431	Sigma/MP Biomedicals
10	Sigma 9 (Tris)	T-1378	Sigma
11	Sodium Chloride		Sigma
12	Magnesium Chloride hexahydrate	M9272	Sigma
13	Isopropyl β -D-1-thiogalactopyranoside (IPTG)	R-0392	Sigma
14	$^{15}\text{NH}_4\text{Cl}$	NLM-467	Cambridge Isotopes
15	Glucose 13C	CLM-420	Cambridge Isotopes
16	LB broth	M1245	Himedia
17	Ampicillin sodium salt	A9518	Sigma
18	Chloramphenicol	C0378	Sigma
19	Sucrose		Sigma
20	Glucose	G8270	Sigma
21	Spermine	22310	SRL Chemical
22	Spermidines	17030	SRL Chemical
23	Putrescine	81343	SRL Chemical
24	ANS	A1028	Sigma
25	D ₂ O		Cambridge Isotopes
26	NMR tubes, 5 mm diam, precision	Z412015	Wilmad®
27	UV Cuvette	NA	Jasco
28	CD cuvette (0.2cm)	1103-4152	Jasco
29	Fluorescence cuvette	NA	Jasco

30	Snake skin dialysis membrane	88242	Thermo Fischer Scientific
31	0.22 µm syringe filters	9913-2502	Millipore
32	SDS	436143	Sigma
33	Acrylamide	MB068	SRL Chemicals
34	TEMED	T9281	Sigma
35	Ammonium persulfate	MB003	Sigma
36	Glycine	MB013	Accelra
37	HCl	NA	Himedia
38	Acetic acid	3064121118	Qualigens
39	β-Mercaptoethanol	M6250	Sigma
40	Bromophenol blue	39121	Sigma
41	Comasine brilliant blue	190682	MP Biomedicals
42	Methanol	29051100	Qualigens/Thermo Fischer

2.2. Methods

2.2.1 Protein expression and purification

Escherichia coli strain BL21DE3 RIL was transformed with a pET21 vector containing the CheY gene. Cells were grown at 37°C on LB media, and protein overexpression was achieved by inducing the cells with IPTG to a final concentration of 0.5 mM for 8-10 h (Filimonov *et al.*, 1993). Protein was purified as described (Filimonov *et al.*, 1993; Kathuria *et al.*, 2008). Purity of the protein was assessed by 15% sodium dodecyl sulphate polyacrylamide gel electrophoresis (SDS-PAGE). The approximate yield was 20 mg from one litre of bacterial culture. The protein was flash frozen using liquid nitrogen and stored at -80°C until further use.

2.2.2 Chromatography column packing and determination of packing efficiency

The slurry of the desired chromatographic resin was obtained from GE Healthcare (resin is supplied pre-swollen in a storage solution of 20 % ethanol and 0.2 M sodium acetate). It is a prerequisite to determine the exact amount of resin required for packing the column and the following equation calculates the same

Once the desired volume of resin was calculated, it was washed before loading onto the column.

The storage solution was then replaced with the desired buffer. This slurry was then slowly

poured into a column (XK 16/100). Once the slurry settles, a packing flow rate of 2 mL/min is applied, and the column is packed. The bed height was determined by visual inspection of the column. It is important to note that bubbles and cracks in resins should be avoided for efficient column functioning. The packing efficiency was determined once the column was packed. The best method for evaluating the efficiency of a packed column is to determine the height equivalent to the theoretical plate (HETP) and asymmetry factor (A_s). To determine these two parameters, a 1% solution of acetone was applied to the column and the UV signal at 280 nm was recorded. Acetone (1%) yielded a single peak at the end of one column volume. This peak was used for further determination of HETP and A_s . The following equations are used for the same:

$$\text{HETP} = \frac{L}{N}$$

$$N = 5.54 * \left[\frac{V_R}{W_h} \right]^2$$

$$h = \frac{\text{HETP}}{d_{50v}}$$

$$A_s = \frac{b}{a}$$

where L is the bed height in centimeters, N is the number of theoretical plates, V_R is the volume eluted from the start of sample application to the peak maximum, W_h is the peak width measured as the width of the recorded peak at half of the peak height, d_{50v} is the median particle size, a is the ascending part of the peak at 10% of the peak height, and b is the descending part of the peak at 10% of the peak height.

2.2.3 Determining protein concentration using UV-Vis spectroscopy

The frozen protein was thawed at room temperature and was dialyzed against 10 mM potassium phosphate pH 7.0 in a 3 kDa cut-off dialysis membrane prior to each spectroscopic measurement. After the dialysis, protein was extracted from the dialysis tubing, filtered using

a 0.22 μm syringe driven filter and subjected to UV spectroscopy in a 1 cm pathlength cuvette. UV spectra was recorded on a Jasco V-650 UV-Visible spectrophotometer, from 320 to 250 nm. Concentration was determined using a molar extinction coefficient of $8250 \text{ M}^{-1}\text{cm}^{-1}$ at 280 nm (Filimonov *et al.*, 1993).

2.2.4 Sample preparations for crowding studies

An 8 μM protein concentration was used for far UV-CD, fluorescence spectroscopy, ANS binding and thermal stability recordings in the far UV-CD region. A concentration of 70 μM was used for recording the near UV-CD spectra for CheY. For NMR studies a concentration of 700-800 μM was used to record the TROSY-HSQC and HSQC. Protein samples were dialyzed filtered and then incubated with various concentrations of crowding agents at room temperature for ~8-10 h before collecting spectrometric data. The stock solution of crowding agents (400 mg/mL; w/v) was prepared in 10 mM potassium phosphate, pH 7.0 for all the spectroscopic techniques, except NMR. For NMR studied the buffer used for both dialysis and sample preparation was 25 mM Potassium phosphate buffer pH 7.0. Mild centrifugation and vortexing ensured the complete dissolution of the crowding agents.

2.2.5 Circular dichroism (far and near UV)

2.2.5.1 Far UV-CD

Far UV circular dichroism spectra were recorded on a JASCO J-1500 CD spectrometer (Jasco, Tokyo, Japan/Easton, MD, USA) equipped with a thermoelectric cell holder (Peltier cell holder) at 25 $^{\circ}\text{C}$ in the spectral range of 260-190 nm and 260-200 nm in dilute buffer and in PEG solutions, respectively. The spectra were obtained using a 0.2 cm pathlength cell, with a bandwidth of 2.50 nm, and a scan speed of 100 nm/min. All spectra are an average of three scans, buffer corrected and converted into MRE.

2.2.5.2 Near UV-CD

Near UV-CD spectra were recorded in the spectral range of 310-250 nm with a protein concentration of 70 μ M. All spectra shown are the average of three scans and were background corrected and converted to mean residue ellipticity (MRE).

2.2.5.3 MRE calculations

The following equation was used for MRE calculations for both far and Near UV CD spectra

$$\text{MRE} = \frac{[\text{Signal (m.deg.)} * 10^6]}{[\text{Concentration } (\mu\text{M}) * \text{Pathlength (mm)} * \text{no.of peptide bonds}]}$$

2.2.6 Thermal stability using far-UV CD

Temperature-induced unfolding of CheY was performed by recording the far UV-CD spectra in the range of 260-200 nm at 1 nm interval. Spectra were collected at 1°C interval from 20 – 80 °C with a heating rate of 1°C/min. The buffer-corrected CD signal at 222 nm was converted to fraction unfolded (f_u) using the equation, $f_u = (y - y_N)/(y_D - y_N)$, where y = CD signal of the protein at 222 nm, y_N and y_D are the signals for folded and unfolded states respectively. The data were fit to a two-state, folded to unfolded equilibrium model (Filimonov *et al.*, 1993) using CalFitter (Mazurenko *et al.*, 2018) to obtain the mid-point of the temperature-induced transition (T_m) and change in enthalpy, ΔH°_m . All the thermal melts for apo and holo protein were performed in 10 mM potassium phosphate buffer. Since the solubility of MgCl_2 is limited in phosphate buffers, the thermal melt for holo CheY at 100 mM MgCl_2 concentration was performed in 50 mM Tris-Cl pH 7.4. The holo protein in the presence of Tris-Cl, pH 7.4 did not show a change in measured T_m .

2.2.6.1 Fitting the data to a two-state model using CalFitter

The normalized data from temperature 20-80°C was loaded in to the online tool. Global fit option with spectroscopic data as the option was selected. A text file containing the spectroscopic data was uploaded. In model selection panel, a model depicting N=D (Van't

Hoff's) was selected. 20 iteration (default value) was used to obtain the global fit. The following equations were used to derive all the thermodynamic parameters by CalFitter.

$$\Delta H^{\circ}(T) = \Delta H_{vh} + \Delta C_p * (T - T_m)$$

$$\Delta S^{\circ}(T) = \frac{\Delta H_{vh}}{T_m} + \Delta C_p * \ln \frac{T}{T_m}$$

$$\Delta G^{\circ}(T) = \Delta H^{\circ}(T) - T * \Delta S^{\circ}(T)$$

Where, ΔH_{vh} – Vant Hoff's enthalpy, ΔC_p – heat capacity at constant pressure, and T_m – midpoint of thermal transition, and T is the reference temperature. To obtain values such as ΔG , ΔH , and $T\Delta S$, the radio button with get bio data was clicked and reference temperature was entered into it (where ever applicable). Experimental ΔC_p value for all the crowding scenarios was not determined, instead a value of zero was used. Errors in the fitting of T_m and all other parameters are estimated by first order Tylor expression depicted below.

$$f(T_m, est) \approx f(T_m) + f'(T_m) * (T_m, est - T_m),$$

where T_m, est is the estimated T_m from the experiment, T_m is the true denaturation temperature, $f'(T_m)$ is the first derivative of $f(T_m)$ with respect to T_m evaluated at T_m . This approximation allows to estimate the error in T_m based on the measured T_m , and the slope of the denaturation profile at that temperature.

2.2.7 Fluorescence Measurements

2.2.7.1 Intrinsic tryptophan fluorescence

Intrinsic tryptophan fluorescence emission spectra were recorded on a Horiba Fluorolog spectrofluorometer in the range of 300-500 nm in a 1 cm pathlength cell. The excitation wavelength was 290 nm, and the excitation and emission bandwidths were 1.5 nm. Spectra were recorded in triplicate and averaged. Sample spectra were corrected for background by

subtracting the appropriate buffer spectra. The fluorescence intensity of the tryptophan residue was corrected for the primary inner filter effect (IFE) (Lakowicz, 2006; Fonin *et al.*, 2014, 2017; Kumar Panigrahi and Kumar Mishra, 2019). The corrected fluorescence intensity, F_{corr} was calculated using the equation, $F_{\text{corr}} = F_{\text{obs}} * 10^{(A_{\text{ex}}+A_{\text{em}})/2}$ where F_{obs} is the recorded fluorescence intensity, A_{ex} is the absorption at the excitation wavelength, and A_{em} is the absorption at emission maximum wavelength. Although measures such as using a small pathlength cuvette, ensuring linear relationship between absorbance and normalised fluorescence intensity, the inner filter effect cannot be completely eliminated (Fonin *et al.*, 2014).

2.2.7.2 ANS fluorescence

The concentration of ANS was determined by diluting it ten times in 10 mM potassium phosphate buffer at 350 nm by using the molar extinction coefficient of $5000 \text{ M}^{-1}\text{cm}^{-1}$ on a Jasco V-650 UV-Visible spectrophotometer. Samples were incubated for 30 min at a final concentration of 50, 100, 150, and 250 μM ANS. The ANS-protein samples were excited at 350 nm, and emission was recorded in the spectral range of 400 – 650 nm in a 1 cm pathlength cell, with an excitation and emission bandwidth of 1.5 nm. Spectra shown are an average of three scans.

2.2.7.3 Intrinsic tryptophan fluorescence quenching measurement

Intrinsic tryptophan fluorescence quenching studies were performed to check if CheY retained metal binding ability in Ficoll, sucrose, and 6 M urea. A 200 mM stock solution of MgCl_2 was prepared in 50 mM Tris-Cl pH 7.4, and an appropriate amount was added to achieve a final concentration of 4 mM (Lukat, Stock and Stock, 1990). Protein concentration was kept constant at 10 μM , and an emission spectrum was recorded in the range of 300 to 500 nm by exciting the protein at 295 nm. Excitation and emission slits were set to 1.5 nm. Three accumulations

were collected, and data were averaged. High concentrations of magnesium chloride precipitates in phosphate buffer; hence it precludes using the same buffer for this study.

2.2.8 Time-resolved fluorescence measurements (only in the presence of PEG 20000)

Excited state tryptophan fluorescence lifetime measurements were recorded using a time-correlated single photon counting (TCSPC) spectrofluorimeter (HORIBA DeltaFlex) by exciting the protein with a nano LED at 283 nm. Emission was recorded at 350 nm, with a bandpass of 32 nm and a polarization angle of 55°. 10000 bins were collected for determination of the instrument response function (IRF) and for sample analysis. The IRF was recorded in the presence of a scatterer, specifically, a dilute solution of ludox (34 wt.% suspension of colloidal silica) in water. The fluorescence decay data obtained from the lone tryptophan at position 58 under dilute buffer and crowded conditions were fit to a biexponential least-squares fit using EZTime software to obtain the average tryptophan lifetimes. The goodness of fit was assessed by Chi-squared values and the weighted distribution of residuals. The autocorrelation function of residuals was uniformly distributed around zero. The average lifetime, $\langle\tau\rangle$ was calculated by using the equation, $\langle\tau\rangle = \frac{\sum a_i \tau_i}{\sum a_i}$ where α_i is the relative amplitude of the individual components, and τ_i is the decay time of the individual components (Batra, Xu and Zhou, 2009; Malik *et al.*, 2012; Goswami *et al.*, 2021).

2.2.9 Protein expression for NMR experiments

Escherichia coli strain BL21DE3 RIL was transformed with a pET21 vector containing the CheY gene. Cells were grown at 37°C on M9 media with half the concentration of antibiotics, and protein overexpression was achieved by inducing the cells with IPTG to a final concentration of 0.5 mM for 8-10 h (Filimonov *et al.*, 1993). Protein was purified as described (Filimonov *et al.*, 1993; Kathuria *et al.*, 2008). Purity of the protein was assessed by 15% sodium dodecyl sulphate polyacrylamide gel electrophoresis (SDS-PAGE).

2.2.10 ¹H-¹⁵N Transverse Relaxation Optimized Heteronuclear Single Quantum Coherence (TROSY-HSQC) with PEG

¹H-¹⁵N Transverse Relaxation Optimized Heteronuclear Single Quantum Coherence (TROSY-HSQC) spectra were acquired on a Bruker Avance 700 MHz spectrometer equipped with a cryogenic probe at 25 °C and a protein concentration of ~800 μM in 25 mM potassium phosphate, pH 7.0. The chemical shift perturbations (weighted Pythagorean distance) (CSPs) for individual cross peaks in the presence of PEG ($\Delta\delta_{\text{PEG}}$) were obtained using the equation, $\Delta\delta_{\text{PEG}} = \sqrt{(\Delta\delta_{\text{N}} * 0.14)^2 + \Delta\delta_{\text{HN}}^2}$ (Williamson, 2018). Standard deviation (σ) was calculated, and a value of 2σ was used as a cut-off for significant movement of shifts (Schumann *et al.*, 2007; Williamson, 2013). The protein used in a previously published ¹H-¹⁵N-HSQC study (Bruix *et al.*, 1993) has two amino acids difference at the N-terminus compared to the native CheY sequence that is used in this work. The ¹H-¹⁵N-HSQC spectrum of our protein sample at near identical conditions to that of the published spectrum (Bruix *et al.*, 1993), shows minor changes in the pattern of cross peaks. To ascertain the assignments, a set of standard 3-D triple resonance spectra were recorded at 25 °C, pH 7.0 on a uniformly enriched ¹³C/¹⁵N CheY sample.

2.2.11 ¹H-¹⁵N-Heteronuclear Single Quantum Coherence (HSQC) with Ficoll-70

¹H-¹⁵N-Heteronuclear Single Quantum Coherence (HSQC) NMR spectra were acquired on Bruker Avance 700 MHz NMR spectrometer equipped with a cryogenic probe at 25°C at a protein concentration of ~700 μM in 25 mM potassium phosphate at pH 7.0 with and without 10mM MgCl₂. The spectra were processed using NMRPipe (Delaglio *et al.*, 1995). The backbone ¹H-¹⁵N HSQC assignments for CheY in the presence of MgCl₂ were obtained from previously published data deposited in Biological Magnetic Resonance Bank (BMRB entry 4083) The published backbone assignments (at 35°C) for CheY in dilute buffer (Bruix *et al.*,

1993), in combination with our assignments (at 25°C), confirmed from standard triple resonance NMR experiments and scalar coupling correlations of the backbone atoms were considered for the analysis in this work (Moy *et al.*, 1994). The spectrum was analysed using Computer Aided Resonance Assignment (CARA) (Keller, 2004). The ¹H-¹⁵N HSQC cross peaks were integrated using model based linear equation system in CARA, with integration widths of 0.033 ppm and 0.138 ppm on ¹H and ¹⁵N axes respectively, with a peak tolerance set to 40% (Keller, 2004). CSPs are calculated using the following equation $\Delta\delta_{Ficoll} =$

$$\sqrt{(\Delta\delta_N * 0.14)^2 + \Delta\delta_{HN}^2} \quad (\text{Williamson, 2013, 2018}).$$

2.2.12 Relative change in intensity in the presence of PEG and Ficoll

The relative change in intensity was calculated using the following equation $\Delta I = \frac{I_{Buffer} - I_{crowder}}{I_{crowder}}$ (Majumder *et al.*, 2015), where I_{Buffer} is the intensity of cross peak in dilute buffer and $I_{Ficoll\ 200\text{mg/mL}}$ is the intensity of same cross peak with Ficoll, for apo and holo forms of CheY.

Chapter 3

Crowding by Polyethylene Glycols Destabilizes Chemotaxis Protein Y

3.1 Introduction

Cell interiors are a complex mixture of macromolecules such as carbohydrates, lipids, nucleic acids, proteins etc., which can reach concentrations of ~400 mg/mL depending on the cell type and its location (Zimmerman and Trach, 1991b; Zimmerman and Minton, 1993; R. John Ellis, 2001). Small molecules from various metabolic pathways further add 50-100 mg/mL of solute to the milieu (Bennett *et al.*, 2009). As a consequence, proteins and other macromolecules may experience (i) hydrophobic and electrostatic interactions (Qi *et al.*, 2014; Cohen and Pielak, 2016) (ii) different mode of hydration on their exposed surfaces and (iii) excluded volume effects (Eggers and Valentine, 2001; Harada, Sugita and Feig, 2012; Kuznetsova *et al.*, 2015). In addition to the crowding effects resulting from other macromolecules inside the cells, the cell interiors provide hydration around the proteins that could be different from the situation a protein experiences in otherwise homogeneous buffer conditions. Thus, the experimentally-derived measurements from *in-vitro* investigations performed in dilute buffers may be less relevant than those performed under conditions that mimic intracellular interactions. For this reason, researchers have begun to address the consequence of crowding on thermodynamic and kinetic aspects of biochemical processes (Zimmerman and Harrison, 1987; Van Den Berg, Ellis and Dobson, 1999; Ellis and Minton, 2003; Sasahara, McPhie and Minton, 2003; Minh *et al.*, 2006; Dong, Qin and Zhou, 2010; Kuznetsova, Turoverov and Uversky, 2014; Horvath, Kumar and Wittung-Stafshede, 2021).

Numerous studies using macromolecules such as Ficoll, Dextran, and polyethylene glycols as crowders, mimicking cellular crowding, are providing insights into the role of both entropic and

enthalpic interactions in modulating the structure, stability, function and conformational dynamics of the proteins (Politi and Harries, 2010; Sukenik *et al.*, 2013; Sapir and Harries, 2014). The interactions due to crowding may be driven by various interatomic interactions, including charge-charge, hydrophobic, and polar contacts, which can favor either the folded or the unfolded states leading to a perturbation in their structure, stability, binding, dynamics and function (Harada, Sugita and Feig, 2012; Erlkamp, Grobelny and Winter, 2014; Nolan, Sánchez and Perillo, 2015; Xu *et al.*, 2017).

Currently, contrasting observations imply the role of both volume exclusion (entropic) and soft interactions (enthalpic) in modulating the structure, stability, and function leading to new perspectives and questions (Mikaelsson *et al.*, 2014; Senske *et al.*, 2014; Kundu *et al.*, 2015; Abriata, Spiga and Peraro, 2016a; Kadumuri *et al.*, 2016; Adams *et al.*, 2019; Bille *et al.*, 2019; Davis, Deutsch and Gruebele, 2020). The effect of crowders depends on the nature, size of the crowder and the protein itself (Guseman *et al.*, 2018; Das and Sen, 2019). Further, crowding not only can modulate conformational stability but can also affect the equilibria between the accessible conformational states (Adams *et al.*, 2019; Parray, Ahmad, *et al.*, 2020). Along similar lines, recent data indicate that crowding can induce stable non-native states (Cremades and Sancho, 2008; Tsao and Dokholyan, 2010; Kumar *et al.*, 2018; Parray *et al.*, 2019). We analyzed the effect of polyethylene glycol with an average molecular mass of 20000 on the (i) structure and (ii) thermal stability of a bacterial regulatory protein Chemotaxis Y (CheY).. Recent studies have also confirmed the important role of CheY in bacterial colonization and disease mediated by protein-protein interactions (Matilla and Krell, 2018). Detailed studies addressing the structure, stability, folding, and metal-binding induced conformational and stability changes of CheY were explored in great detail under dilute buffered solutions (Stock *et al.*, 1989; Filimonov *et al.*, 1993; Moy *et al.*, 1994; Munoz *et al.*, 1994; Cho *et al.*, 2000; Kathuria *et al.*, 2008; Hills *et al.*, 2010). However, the studies in dilute and homogeneous buffers do not resemble the

realistic cellular interior and, as a result, may not provide a comprehensive depiction of the condition experienced by proteins in a cellular environment. Therefore, in this study, we addressed the specific question of the effect of PEG on the structure, stability, and magnesium-CheY interactions.

PEG is used as a crowding agent due to its highly flexible nature and, being amphiphilic, is known to interact with polar and non-polar amino acids of proteins (Lee and Lee, 1987; Furness *et al.*, 1998; Wu *et al.*, 2014; Knowles *et al.*, 2015; Popielec *et al.*, 2020). PEG is also known to be protein specific in terms of its effect on the structure, stability and activity (Zhang *et al.*, 2012; Wu *et al.*, 2014; Knowles *et al.*, 2015; Lai *et al.*, 2015). The effect of PEG is also dependent on the length of the polymer of PEG and volume fraction used in the study (Arakawa and Timasheff, 1985; Lee and Lee, 1987; Xie and Timasheff, 1997; Wu *et al.*, 2014; Nolan, Sánchez and Perillo, 2015; Paudel *et al.*, 2018; Nolan *et al.*, 2020; Subadini *et al.*, 2021; Parray *et al.*, 2022). Another important aspect of crowding is the dependence of the effect of crowding on the volume fraction. For instance, PEG 2000 and 4000 show no effect on the secondary and tertiary structure of CRABP-I concentration < 400 mg/mL, but a moderate effect is seen at a high volume fraction (Subadini *et al.*, 2021). Similarly, the highest ribozyme activity is at different volume fractions of PEG 1000 and 35000 (Paudel *et al.*, 2018). It is becoming increasingly clear that not only the shape, size, and nature of the crowder but also the volume fraction can also be a deciding factor for the overall effect of crowding. To assess the dependency of crowding on polymer size and volume fraction, we further explored the effect of a range of PEGs (6000 to 12000) in addition to PEG 20000.

Our results provide insights into the structure, stability, and metal-binding properties under conditions that mimic cellular crowding. A surprising result relates to the effect of PEG on metal-ion binding. While macromolecular crowding due to PEG affects the structure and thermal stability of CheY, a significant decrease in thermal stability was observed for the protein in the

presence of magnesium, a trend that is opposite to magnesium-induced enhancement of stability observed in dilute buffer. PEG appears to interact with CheY in a manner that leads to subtle conformational changes. Thus, PEG prompted conformational perturbation, presumably, provides a different environment and or situation for magnesium interaction. In summary, our results highlight the dominance of enthalpic contributions between PEG and CheY, which can subtly affect the conformation and modulate the metal-protein interaction and stability, irrespective of the polymer chain length of PEG.

3.2. Results and discussion

3.2.1 HETP calculations and protein purification

The column used for purification was manually packed and evaluated for packing efficiency by using the equations listed in materials and methods. The asymmetry ratio was found to be 1.06 which falls in the accepted range of asymmetry ration defined by the resin manufactures. Similarly, HETP was also calculated and was found to be with in the accepted values as described by the resin manufacture. In order to calculate the above-mentioned values 1% acetone was passed through the column with water as the mobile phase. The peak shown in figure 3.1 is the UV 280 nm absorbance plotted against elution volume.

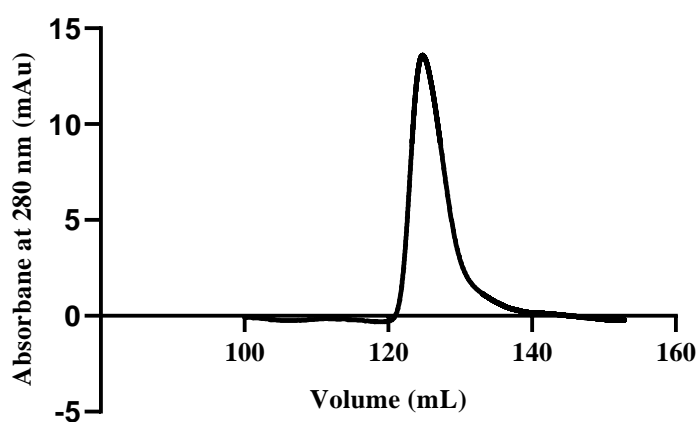


Figure 3.1: 1% acetone peak (UV-280 nm) plotted against elution volume used for HETP calculations.

CheY was purified as described earlier by (Filimonov *et al.*, 1993; Kathuria *et al.*, 2008). Figure 3.2 depicts the purification profile obtained after size exclusion chromatography. The boxed peak at ~300 mL denoted the purified monomeric CheY of ~14 kDa.

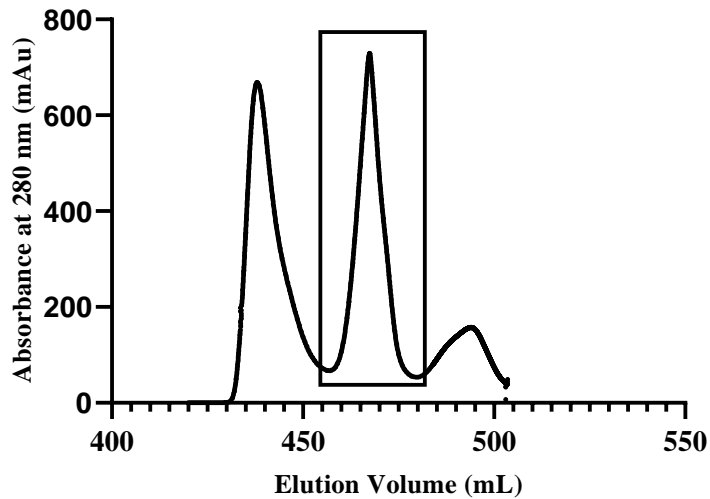


Figure 3.2: Size exclusion chromatogram of CheY obtained from size exclusion chromatography on Superdex™ G-75 column. (boxed region represents the protein of interest)

The purity of the protein was confirmed by running a 15% SDS-polyacrylamide gel. Figure 3.3 clearly indicates a single band corresponding to ~14 kDa.

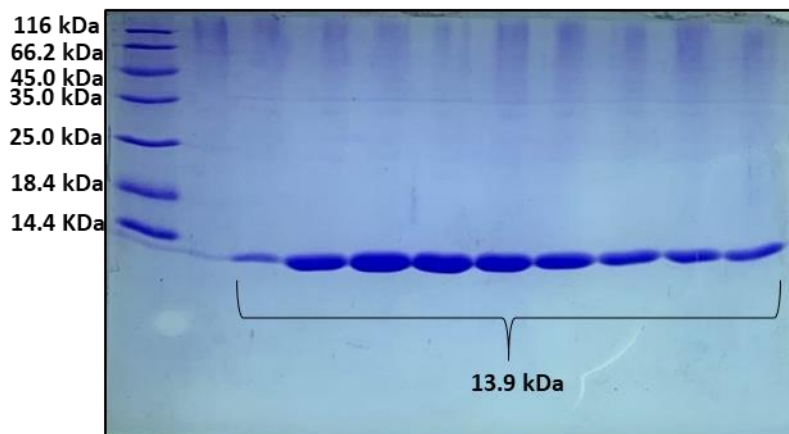


Figure 3.3: 15 % Polyacrylamide gel showing pure protein (CheY) corresponding to ~14 kDa. (Lanes from left to right - molecular weight marker, elution fractions 1-10)

3.2.2 Crowder induced changes in the secondary and tertiary structure of CheY

3.2.2.1 Far UV-CD measurements

The effect of crowding on secondary and tertiary interactions was monitored by far and near UV-CD spectroscopy as the concentration of PEG varied from 0 to 300 mg/mL. Figure 3.4A summarizes the secondary structure perturbation monitored by comparing the signal changes in the far UV-CD region of the spectra.

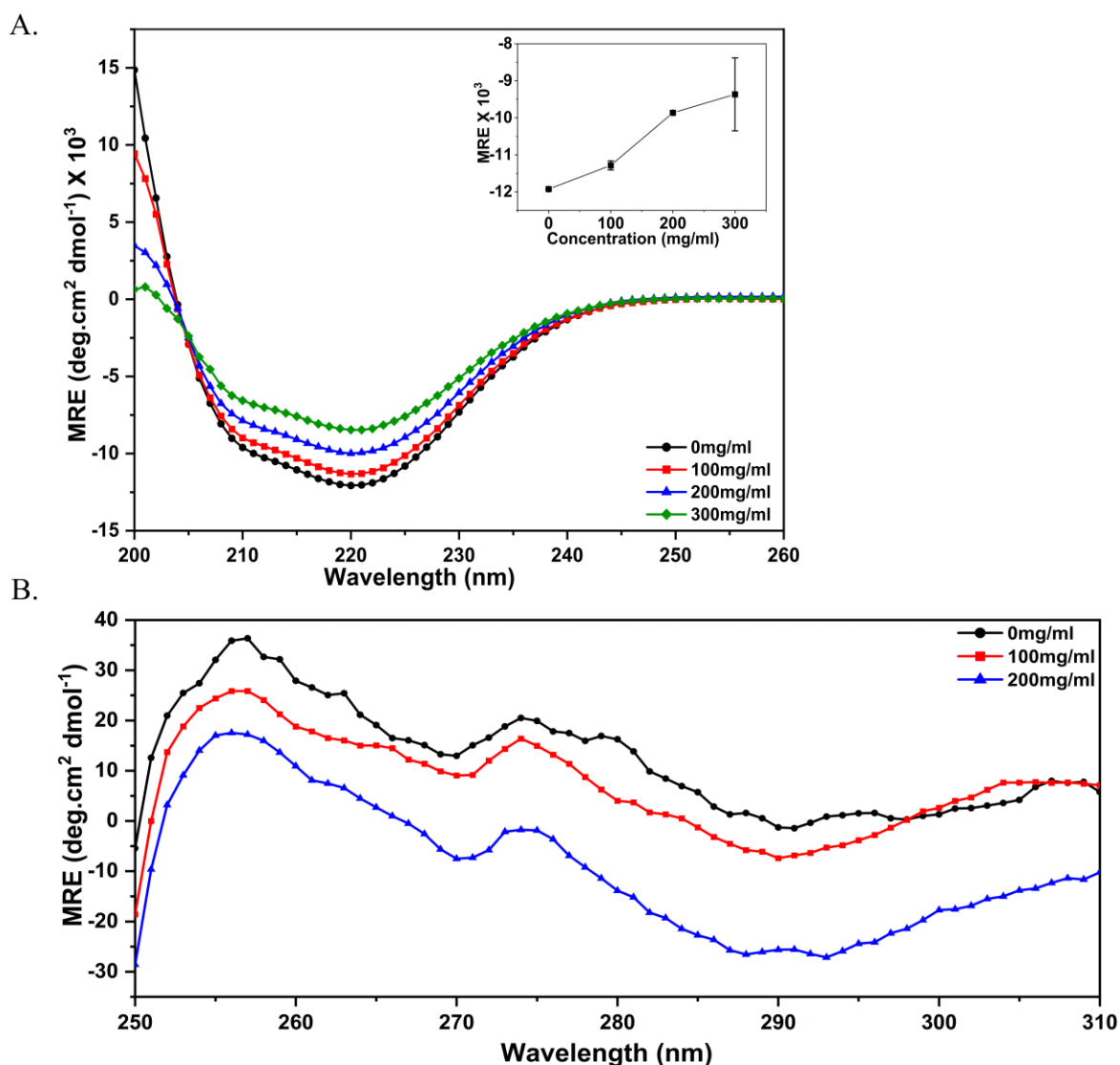


Figure 3.4: (A) Effect of PEG on the secondary structure of CheY. Far UV-CD spectra in the presence of dilute buffer (black) and in 100 mg/mL (red), 200 mg/mL (blue) and 300 mg/mL (green) of PEG. Inset indicates the average value at 222 nm, at each concentration of PEG, along with the standard deviation obtained from three independent measurements. (B) Effect of PEG on the tertiary structure of CheY. Near UV-CD spectra in the presence of dilute buffer (black) and varying concentrations of PEG are shown in red and blue for 100 and 200 mg/mL, respectively.

The far UV-CD spectrum of CheY in the absence of crowding condition resembles the spectrum reported earlier under dilute buffer conditions, with signature features at 210 and 222 nm (Filimonov *et al.*, 1993; Kathuria *et al.*, 2008), characteristic of proteins possessing both α helix and β sheet structures. A monotonic decrease in signal intensity is observed in the presence of increasing amounts of PEG, consistent with the changes to the secondary structure. Specifically, the negative signal at 222 nm is diminished by ~10% in the presence of 200 mg/mL, indicating the destabilization of the secondary structure. At concentrations >200 mg/mL PEG, the destabilization of the native state appears to be substantial, presumably leading to variable, aggregation-prone states, a possibility supported by the large error bars on 222 nm signal in the presence of 300 mg/mL PEG. In contrast, at 100 and 200 mg/mL, the spectra were highly consistent between independent runs, as reflected by the negligible error bars. In summary, the gradual decrease in the far UV-CD signal is consistent with a PEG-dependant loss of secondary structure.

3.2.2.2 Near UV-CD measurements

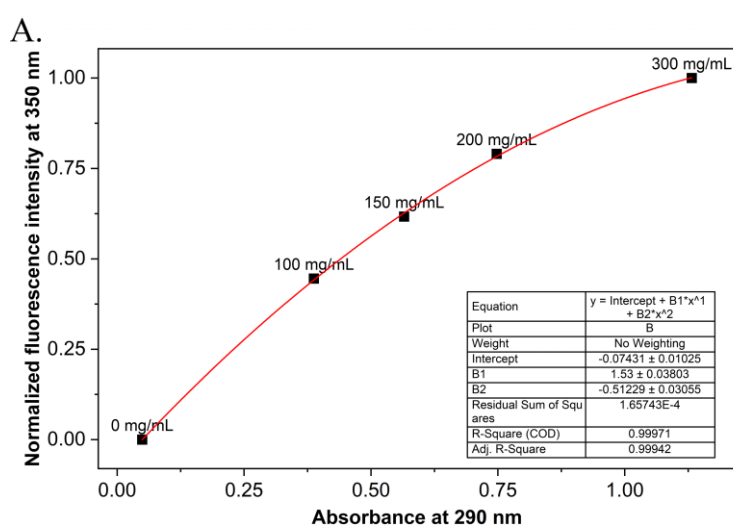
The tertiary packing interactions of aromatic amino acids were probed as a function of PEG concentration by monitoring the near UV region of the CD spectrum. Restricted motion of aromatic amino acids due to their involvement in tertiary core packing will give rise to CD signal in the near UV region (Kelly and Price, 2005). Changes in spectral features denote adjustment in the packing interactions of the aromatic amino acids. Under native buffer conditions, the near UV-CD spectrum of CheY is characterized by a distinct minimum at ~290 nm and four structural features in the 250 – 280 nm region (Figure. 3.4B) (Filimonov *et al.*, 1993). The broad minimum at ~290 nm is most probably associated with the lone tryptophan residue, while the features between 250 – 280 nm may arise from tyrosine, phenylalanine, and tryptophan residues (Filimonov *et al.*, 1993). The subtle deviations and diminution, but not complete disappearance, of the spectral features emanating from the tyrosines, phenylalanines,

and tryptophan suggest loosening of aromatic packing interactions. Major conformational rearrangement can be ruled out because there were no large spectral changes, and the signal did not completely disappear. Thus, the minor changes observed in the secondary structure appear to be echoed in the altered tertiary packing of the aromatic residues. Moreover, the subtle changes to the near UV-CD spectral features suggest that no major unfolding occurs, and only minor conformational changes occur in tertiary aromatic interactions. The decrease in the far UV-CD signal may indicate the loss of secondary structure due to local dynamics. Taken together, the changes in the far and near UV-CD signals suggest that moderate amounts of PEG cause minor perturbations in secondary structure and tertiary aromatic packing and that the highest concentration of PEG leads to significant perturbation of the native structure.

3.2.2.3 Intrinsic tryptophan fluorescence measurements

Intrinsic tryptophan fluorescence emission is a useful reporter of conformational perturbations because peak intensity and wavelength of maximum emission are highly sensitive to the microenvironment of tryptophan sidechain. Thus, further evidence for the changes in the tertiary structure suggested by the near UV-CD studies can be obtained by monitoring the changes observed in the fluorescence (FL) emission intensity and wavelength maxima in the presence of PEG. CheY has a single tryptophan located at position 58 in the loop connecting β strand 3 ($\beta 3$) and α helix 3 ($\alpha 3$); Trp58 is partially buried and contributes to the observed fluorescence emission of the protein (Filimonov *et al.*, 1993; Kathuria *et al.*, 2008). The fluorescence emission spectrum of native CheY in the presence of dilute buffer shows maximum emission intensity (λ_{\max}) at 342 nm. As the PEG concentration increases, the intensity at 342 nm decreases and the value of the λ_{\max} is shifted to longer wavelengths or redshifted. The decrease in the Trp emission intensity and the concomitant shift of the λ_{\max} to longer wavelengths (redshift) (Figure 3.6A) suggest that, in the presence of PEG, the lone Trp residue is experiencing a more polar microenvironment than in the native state, possibly due to

local unravelling of the structure around the sidechain. The reduction in intensity can also be a consequence of primary inner filter effect. This phenomenon occurs when a component of the system, other than the protein has the an overlap with the excitation maximum of the protein (Lakowicz, 2006; Kumar Panigrahi and Kumar Mishra, 2019). As a consequence of which the excitation energy is split between the protein and the other component resulting in reduced emission intensity. This effect can mislead the conclusions derived based on the intensity measurements therefore, it is of utmost relevance to correct for the primary inner filter effect while considering the emission intensity of the protein. Polyethylene glycols solutions form a vesicular organization beyond a particular concentration. These vesicles offer an electron dense region which are the inherent sites for fluorescence. It was reported earlier that PEGs of various molecular weights (400-12000) fluoresce with an excitation of ~300 nm and an emission maximum of ~380 nm (Paik *et al.*, 2012). Therefore, measure have been taken in order to minimize the effect and also a correction method mentioned in the method section was employed. Before recording the proteins spectra in PEG solution, a relationship was established between the absorbance and normalized fluorescence to limit the fluorescence measurements to a concentration that falls in the linear regime of the plot shown in Figure 3.5.



B.

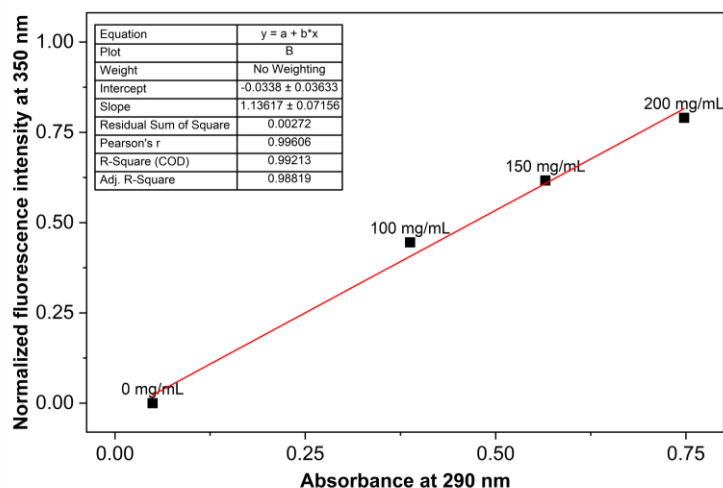


Figure 3.5: Normalized fluorescence intensity at 350 nm plotted against absorbance at 290 nm of PEG + CheY solution. (A) Up to 300 mg/mL PEG concentration and (B) up to 200 mg/mL PEG concentration. Insets in both the plots indicate the fitting parameters to exponential and linear equations, respectively.

As evident from the above plots, up to 200 mg/mL of PEG concentration the relationship between abs and FL is linear, which limits the interference from primary inner filter effect. Beyond this concentration a curvature is introduced and the relationship changes to a complex polynomial. Therefore, fluorescence measurements were limited to a maximum PEG concentration of 200 mg/mL. In addition to this, limiting the light entering via the cuvette can also decrease the interference from IFE therefore, we used a cuvette with 1 cm pathlength leading to a more reliable data collection in the crowding environment. It a well-established fact that any measures taken to decrease the IFE contribution cannot result into elimination of the contribution in the emission intensity, hence a correction factor derived the relationship established (mentioned in methods section) is used to rescale the emission intensity for appropriate conclusions from the study. Since, measures were employed to tackle the primary inner filter effect in our measurements, drawing conclusions is relevant and clearly indicate consequence of PEG induced changes to the structure of protein.

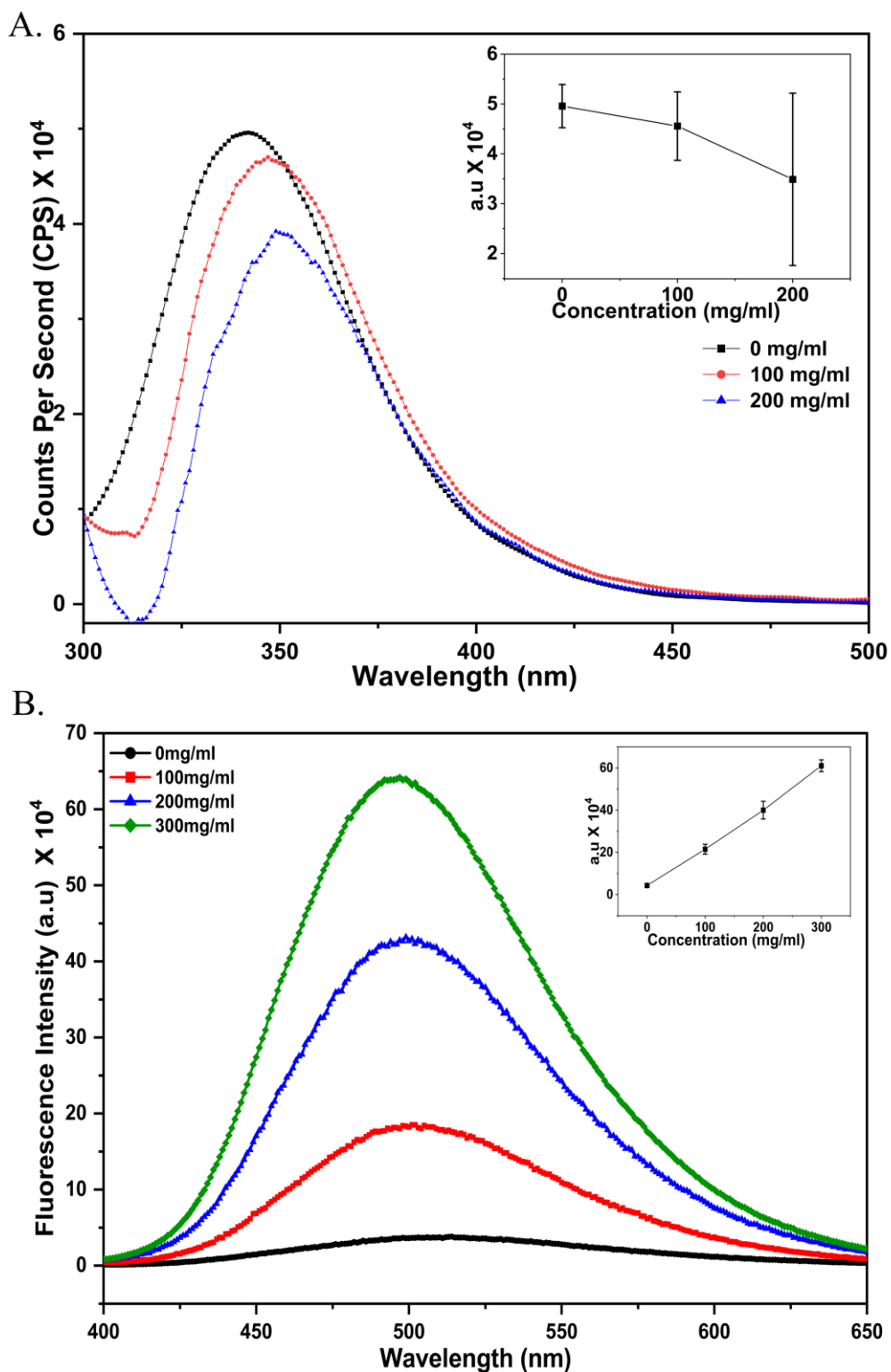


Figure 3.6: (A) Intrinsic tryptophan fluorescence spectra of CheY. The fluorescence emission spectrum of CheY in the presence of dilute buffer (black) and varying concentrations of PEG (100 mg/mL in red and 200 mg/mL in blue). Inset indicates the average value at 342 nm at each concentration of PEG along with the standard deviation obtained from three independent measurements. (B) Extrinsic Fluorescence emission spectra of CheY. ANS fluorescence emission spectra of CheY in the presence of dilute buffer (black) and in varying concentrations of PEG (100 mg/mL = red, 200 mg/mL = blue and 300 mg/mL = green). Inset indicates the average value at each concentration of PEG along with the standard deviation obtained from three independent measurements.

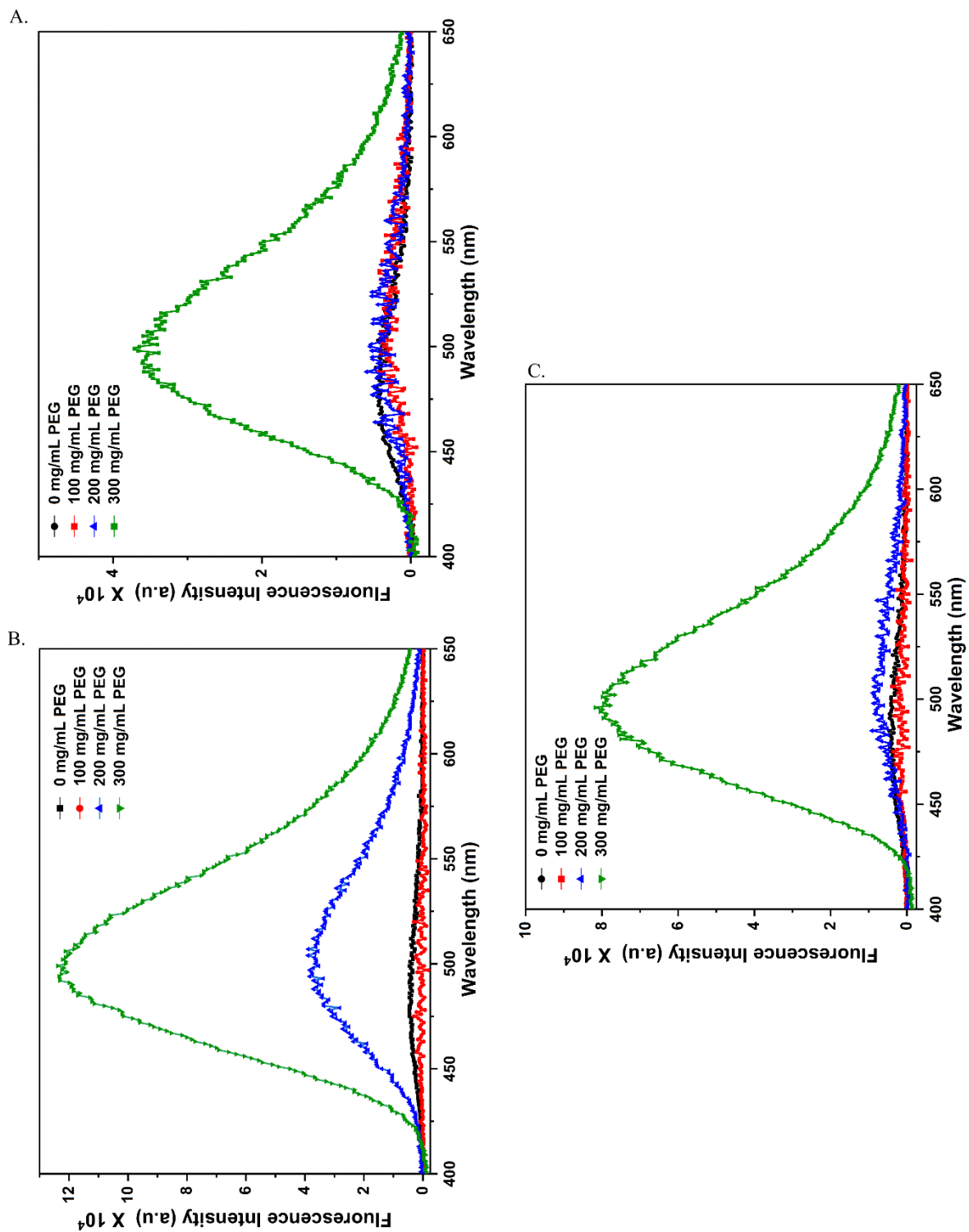


Figure 3.7: Extrinsic Fluorescence emission spectra of CheY. ANS fluorescence emission spectra of CheY in the presence of dilute buffer (black) and in varying concentrations of PEG (100 mg/mL = red, 200 mg/mL = blue and 300 mg/mL = green) in (A) 50 μ M ANS, (B) 100 μ M ANS and (C) 150 μ M ANS.

Thus, the reduction in the intensity of intrinsic fluorescence emission of tryptophan along with the changes in far and near UV-CD spectra support the notion that the presence of PEG induces structural perturbation of CheY.

3.2.2.4 ANS fluorescence emission measurements

The effect of PEG on the secondary and tertiary structure was further investigated by monitoring the changes in the fluorescence emission of 8-anilinonaphthalene-1-sulfonic acid (ANS). ANS is commonly used to detect accessible protein hydrophobic patches because its fluorescence emission intensity increases in hydrophobic environments (Engelhard and Evans, 1995; Ptitsyn, 1995). Therefore, if PEG induces partial unfolding of CheY, as suggested by changes in CD and intrinsic tryptophan fluorescence, there should be an enhancement of ANS fluorescence emission when formerly buried sidechains and backbone are exposed. Fluorescence emission spectra of ANS in the presence of increasing concentrations of PEG are shown in figure 3.6b. The steady increase in ANS emission intensity as the concentration of PEG is raised from 100 - 300 mg/mL is consistent with partial and/or local unfolding that exposes hydrophobic surface. PEG appears to be altering or loosening the native tertiary interactions in a manner that allows more access for ANS to bind to an increased accessible hydrophobic surface. In summary, a combination of far and near UV-circular dichroism, intrinsic tryptophan and extrinsic ANS fluorescence emission spectra strongly support the idea that interactions between PEG and CheY produce at least minor structural perturbation of the native structure.

Generally, the concentration of ANS is maintained between 50-100 μ M. We used a concentration of 200 μ M. In the presence of increasing amounts of PEG, ANS shows concentration dependent binding. During our experiments, we observed that, 100-150 micromolar ANS does not show significant binding to native protein and to the protein in the presence of 100 and 200 mg/ml PEG. (Figure 3.7) However, shows binding in the presence of

300 mg PEG. Therefore, to observe the binding of ANS in the presence of PEG, we have used 200 μ M ANS to detect the changes in its fluorescence. It may be interesting to note that, the ANS fluorescence does not change when bound to the native protein at all concentrations of ANS. (in the absence of PEG). In this context, it is interesting to note that ANS binds weakly to the native protein (at pH 7.0) and binds in a concentration dependent manner to a weakly populated state of the protein at pH 2.5 as previously reported by Filimonov et al. (Filimonov *et al.*, 1993).

3.2.2.5 Time-resolved fluorescence measurements

Tryptophan exhibits fascinating internal dynamics through its side chain. Different conformations of which are termed as "rotamers". These rotamers arise from rotations around the single bond connecting the indole ring to the backbone. Two main rotamers, designated "p" and "t", dominate, characterized by different orientations of the indole relative to the peptide bond. Each rotamer possesses a unique fluorescent lifetime – the average time it spends in the excited state before emitting light. Fluorescence lifetime measurements serve as a powerful tool to probe both rotamer populations and their interconversion dynamics. Analyzing these lifetimes reveals a surprising interplay between stability and dynamics. Typically, the p-rotamer (indole parallel to the backbone) holds the crown for kinetic stability, residing longer in the excited state. However, at higher temperatures, the t-rotamer (indole flipped perpendicular) can unexpectedly take the lead, showcasing a temperature-dependent shift in rotamer dominance. This intricate relationship between rotamer lifetimes and environment, influenced by factors like temperature, solvent, and surrounding protein structure, provides crucial insights into protein folding, stability, and function. For instance, changes in rotamer populations have been linked to protein-ligand interactions and enzyme catalysis. Unraveling the secrets of how rotamers dance and how their lifetimes influence biomolecular processes continues to be a captivating exploration.

Time-resolved tryptophan fluorescence studies were performed on CheY in dilute buffer and in increasing crowder concentrations of PEG. Fluorescence excited state lifetime is a sensitive parameter for analyzing environmental changes around the tryptophan residue, providing an opportunity for further insights into the effect of PEG on protein structure. The lone tryptophan 58 in CheY predominantly adopts an outward facing conformation, pointing away from the active site. It is also half exposed to the solvent with the accessible surface area of 48 \AA^2 . However, a meta active state of CheY always populates the conformational landscape of CheY. This meta active CheY is in equilibrium with apo CheY and this variation can give rise to different conformers of TRP-58 (Filimonov *et al.*, 1993; Simonovic and Volz, 2001). Figure 3.8 represents the fluorescence decay of CheY in dilute buffer, 100 mg/mL, and 200 mg/mL PEG.

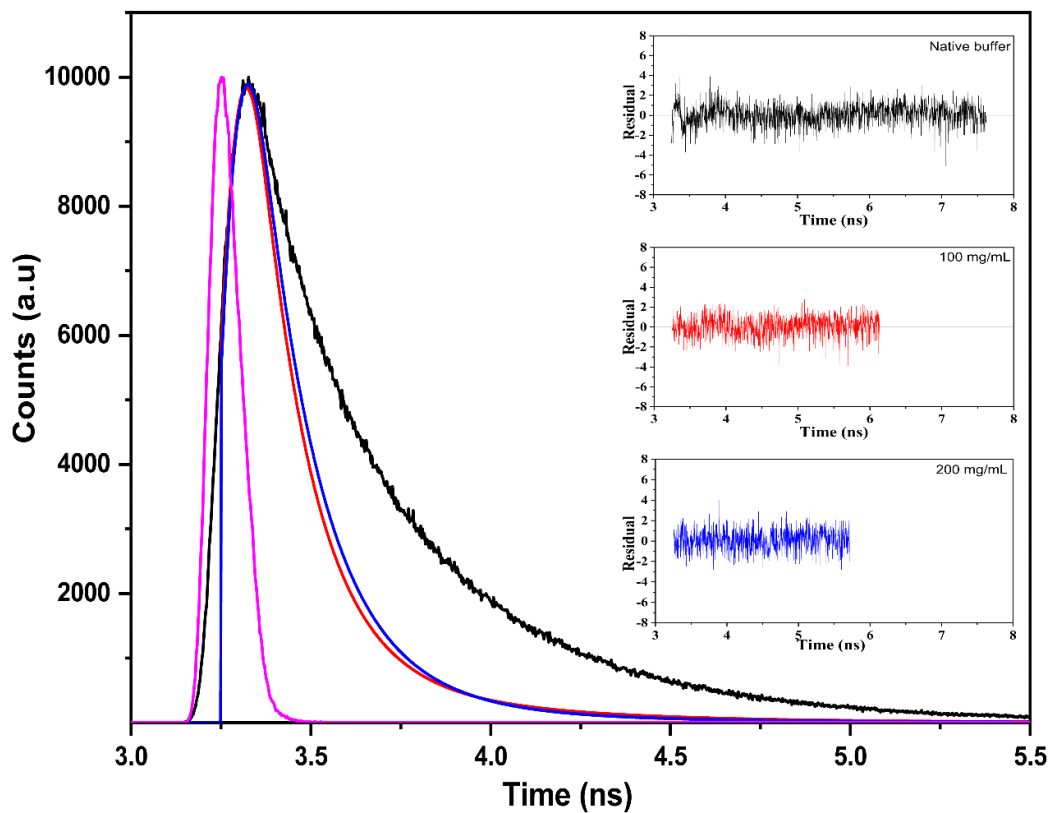


Figure 3.8: Tryptophan lifetime decay of CheY in dilute buffer (black), 100 mg/mL PEG (red) and 200 mg/mL PEG (blue). The instrument response function (IRF) is represented in magenta. Inset indicates residuals of the fits.

The lifetime decays of CheY in dilute buffer and in the presence of PEG were best fit to a biexponential model, and the derived tryptophan averaged lifetime values are listed in Table 3.1. The shorter lifetime τ_1 represents a conformation of tryptophan that is more solvent accessible. The longest lifetime τ_2 represents a relatively unquenched conformer of tryptophan (Siemiarczuk *et al.*, 2004).

Table 3.1: Tryptophan lifetime decay parameters of CheY obtained from biexponential fits of signal decay in dilute buffer, 100 mg/mL and 200 mg/mL PEG. The individual lifetime components are denoted as τ_1 and τ_2 . Relative amplitudes are denoted as α_1 and α_2 . χ^2 represents the goodness of fit.

Sample	τ_1 (ns)	α_1	τ_2 (ns)	α_2	Average Lifetime $\langle\tau\rangle$ (ns)	Chi squared (χ^2)
CheY	1.98 ± 0.11	0.42	4.99 ± 0.02	0.57	3.7 ± 0.1	1.11
CheY+100 mg/mL PEG	1.38 ± 0.02	0.92	4.50 ± 0.08	0.08	1.62 ± 0.09	1.01
CheY+200 mg/mL PEG	1.59 ± 0.02	0.95	4.35 ± 0.1	0.05	1.7 ± 0.2	1.04

The shorter lifetime, τ_1 , 1.98 ns in the dilute buffer conditions, shows a decrease to 1.38 ns and 1.59 ns in the presence of 100 and 200 mg/mL PEG, respectively. It may also be noted that the longest lifetime values τ_2 also decrease from 4.99 ns to 4.50 ns and 4.35 ns in 100 and 200 mg/mL PEG, respectively. The reductions in values indicate increased solvent exposure of tryptophan residue, indicating the shift of conformation from a stable unquenched form to the relatively solvent exposed conformer of tryptophan which is less populated in the native state. Yet another possible explanation for this decrease is the change in solvent polarity and viscosity. An increase in the polarity or change in hydrogen bonding interactions can lead to shorter lifetimes. The α values represent the percentage contribution of each lifetime component to the average lifetime value. Any changes in this value would indicate a change in conformer composition. The α_1 values for both concentrations of PEG increase dramatically

from 0.42 to 0.92 and 0.95 in 100 mg/mL and 200 mg/mL respectively, with a concomitant reduction of α_2 from 0.57 to 0.08 and 0.05. Overall, the structural perturbations revealed by CD and tryptophan fluorescence intensity are consistent with the changes observed for tryptophan lifetime measurement in the presence of PEG.

3.2.3 Thermal stability (T_m) and enthalpy (ΔH°_m) changes in the presence of PEG

The structural perturbations induced by PEG can be further probed by comparing the resistance offered by the native protein towards temperature-induced denaturation in the presence and absence of the crowder. The parameters, T_m , the midpoint of transition and enthalpy of unfolding, ΔH°_m , in the temperature-induced conversion of native to denatured (unfolded) state serve as a measure for stability (Greenfield, 2007a). Thermal denaturation parameters were determined by measuring the far UV-CD signal between 260-200 nm as a function of temperature in dilute buffer and in the presence of 100 and 200 mg/mL PEG. Figure 3.9 shows the thermal denaturation profiles represented by plotting the fraction unfolded (f_u) as a function of temperature in the absence and presence of varying concentrations of PEG.

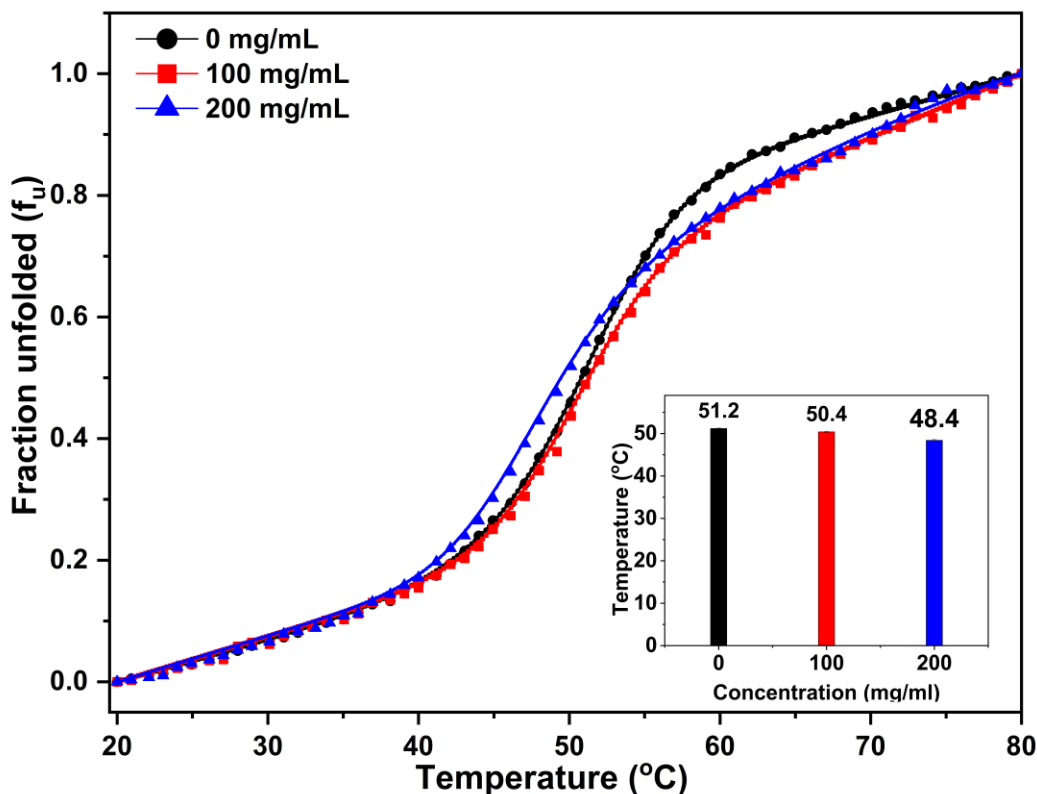


Figure 3.9: Effect of PEG on the thermal stability of CheY. Thermal denaturation profiles of CheY were obtained by plotting fraction unfolded as a function of temperature in dilute buffer (black), in 100 mg/mL (red) and 200 mg/mL PEG (blue). The continuous line represents the fit of the thermal melt for a two-state folded to unfolded model.

All transitions appear as two-state cooperative transitions and show 60-70% reversibility. The T_m value for CheY in dilute buffer obtained by fitting to a native-to-unfolded two-state model is $51.2 \pm 0.1^\circ\text{C}$. The changes of T_m , ΔH°_m , ΔG° , and ΔS° in the presence of PEG are minor (Table 2.2), decreasing uniformly as the PEG concentration increases from 0-200 mg/mL. The stability of the protein in the presence of 200 mg/mL PEG is reduced by ~ 4 kJ/mol.

Table 3.2: Thermodynamic parameters of CheY in dilute buffer and in the presence of 100 and 200 mg/mL PEG.

Crowder concentration	T_m (°C)	ΔH°_m (kJ/mol)	TΔS° (kJ/mol) at 298 K	ΔG° (kJ/mol) at 298 K
CheY	51.2 ± 0.1	260 ± 5	240 ± 4	20.5 ± 0.4
CheY + 100 mg/mL	50.4 ± 0.1	260 ± 8	240 ± 7	19.7 ± 0.6
CheY + 200 mg/mL	48.4 ± 0.2	250 ± 8	230 ± 8	16.9 ± 0.6

Thus, the conformational perturbation induced by PEG that was observed by changes in the CD and FL signals must be limited to local structure because the changes were not accompanied by a significant loss of thermal stability of the protein. The various types of spectroscopic evidence collected are consistent with local unfolding or fraying of the terminal residues of helices and strands and or loosening of the tertiary aromatic packing core in the presence of PEG. Combining the structural and thermal denaturation results, it is clear that the presence of the crowding agent PEG produces a moderate degree of non-global destabilization.

These results illustrate that PEG affected the structure and stability of CheY in a concentration dependent manner. At higher concentrations of PEG, the repulsive, destabilizing interactions seem to be more dominant, leading to a loss in the native structure and stability. The observations are not consistent with volume exclusion effects but suggest enthalpic interactions between PEG and the protein. Although PEG-protein interactions leading to perturbation of structure and stability have been observed by others (Arakawa and Timasheff, 1985; Wu *et al.*, 2014), the effect is not uniform. In some cases, an increase in either stability or activity is observed (Suthar *et al.*, 2013; Nolan, Sánchez and Perillo, 2015; Ogunmoyole, Fodeke and Adewale, 2019; Stepanenko *et al.*, 2019), but decreases are observed in other instances (Breydo *et al.*, 2015; Bhakuni and Venkatesu, 2019; Parray *et al.*, 2019).

3.2.4 Assessment of thermal stability in the combined presence of PEG and magnesium

The native state stability determined from chemical denaturation and reported by Filimonov et al. (Filimonov *et al.*, 1993), indicated that the magnesium ion (Mg^{2+}) provided a concentration-dependant enhancement in stability of 3-6 kJ/mol at 298 K. Therefore, determining the stability in the presence and absence of crowding conditions will shed light on how PEG-induced conformational changes affect the magnesium-protein interactions. Figure 3.10 shows the thermal denaturation profile of CheY in the presence of Mg^{2+} in dilute buffer and in the presence of 100 and 200 mg/mL PEG.

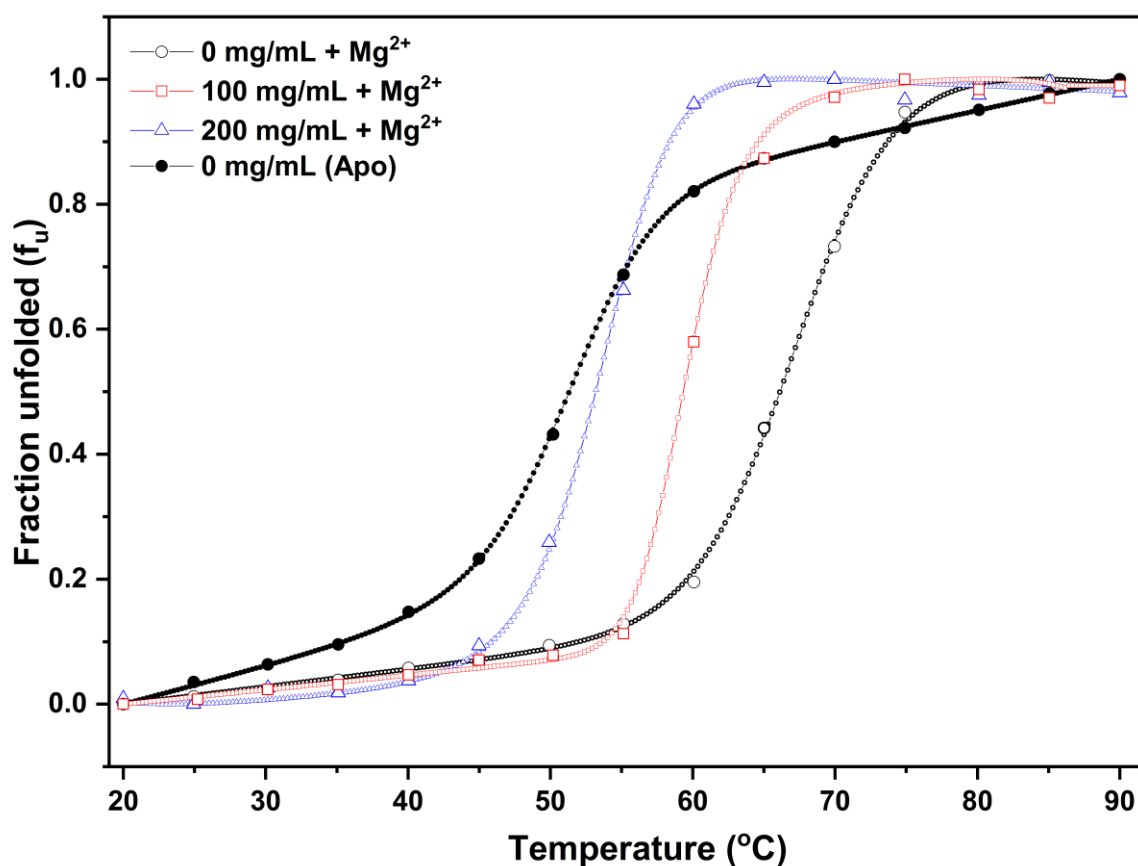


Figure 3.10: Effect of PEG on the thermal stability of CheY in the presence of magnesium. Thermal denaturation profiles of CheY in the presence of dilute buffer (black, closed circles), dilute buffer with Mg^{2+} (black, open circles) with varying concentrations of PEG (100 mg/mL = red; 200 mg/mL = blue). The continuous line represents the fit of the thermal melt for a two-state folded (N) to unfolded (U) model. The concentration of $MgCl_2$ was maintained at 10 mM.

Table 3.3: T_m values of CheY in the combined presence and absence of Mg^{2+} and PEG.

Concentration of PEG	T_m ($^{\circ}C$)	
	CheY	51.2 ± 0.1 (No Mg^{2+})
CheY + 100 mg/mL + Mg^{2+}	57.6 ± 0.2	
CheY + 200 mg/mL + Mg^{2+}	51.9 ± 0.3	

In the absence of the crowding agent, 10 mM Mg^{2+} increases the T_m of the native state by about 15°C (Table 2.3). Consistent with earlier reports, it is apparent that under dilute, uncrowded buffer conditions, Mg^{2+} binds to the metal-binding pocket, which leads to enhanced thermal stability (Filimonov *et al.*, 1993). In contrast, in the presence of 200 mg/mL PEG, a considerable decrease in thermal stability is observed, suggesting that PEG interferes with the binding of the magnesium ion to CheY. The lifetime measurements of Trp also indicate perturbation of the native structural environment of Trp58. In the native state of CheY, Asp13, Asp57, and Asn59 directly bind to the divalent magnesium ion. In fact, overall, the region-specific information from Trp lifetime fluorescence strongly supports the notion that PEG alters the native Mg^{2+} binding interactions. Thus, PEG-induced conformational change, though subtle in nature, affects the native-like metal interactions in a manner that leads to loss of stability. It should be noted that PEG-induced changes are concentration-dependent, with greater changes being observed at 200 mg/mL than at 100 mg/mL. The near overlap of the 100 mg/mL PEG near UV-CD and ANS fluorescence emission spectra with the spectra in the absence of the crowding agent supports the notion that CheY is able to tolerate moderate amounts of crowding without significant changes to the structure. From the combined analysis of the information, it can be concluded that the change indicated by (i) far UV-CD, (ii) near UV-CD and tryptophan FL emission, (iii) ANS fluorescence emission, (iv) time-resolved fluorescence, and (v) thermal denaturation profiles, PEG-induced crowding produces structural perturbations that lead to minor loss of stability in CheY. The conformational changes induced by PEG lead to locally distorted tertiary aromatic packing and altered native Mg^{2+} binding interactions contributed by

specific amino acids. The interaction of PEG with the protein surfaces leading to loss of structure and activity has been demonstrated earlier in other systems (Nolan, Sánchez and Perillo, 2015; Popielec *et al.*, 2020).

3.2.5 Effect of PEG chain length on the structure and stability of CheY

3.2.5.1 Lower molecular weight PEGs show no effect on secondary and tertiary structure of apo CheY

To check the effect of PEGs on secondary and tertiary structure, far UV-CD, near UV-CD and fluorescence emission spectra were recorded in the presence and absence of different volume fractions of lower molecular weight (LMW) PEGs (6000, 8000 and 12000). The secondary and tertiary structures of CheY in dilute buffer were similar to those reported earlier (Filimonov *et al.*, 1993; Kathuria *et al.*, 2008). A minuscule reduction is apparent up to 200 mg/mL of PEG concentration (Figure 3.11). The reproducibility in the spectral signal at concentrations >200 mg/mL was not achieved which limited the study to 200 mg/mL.

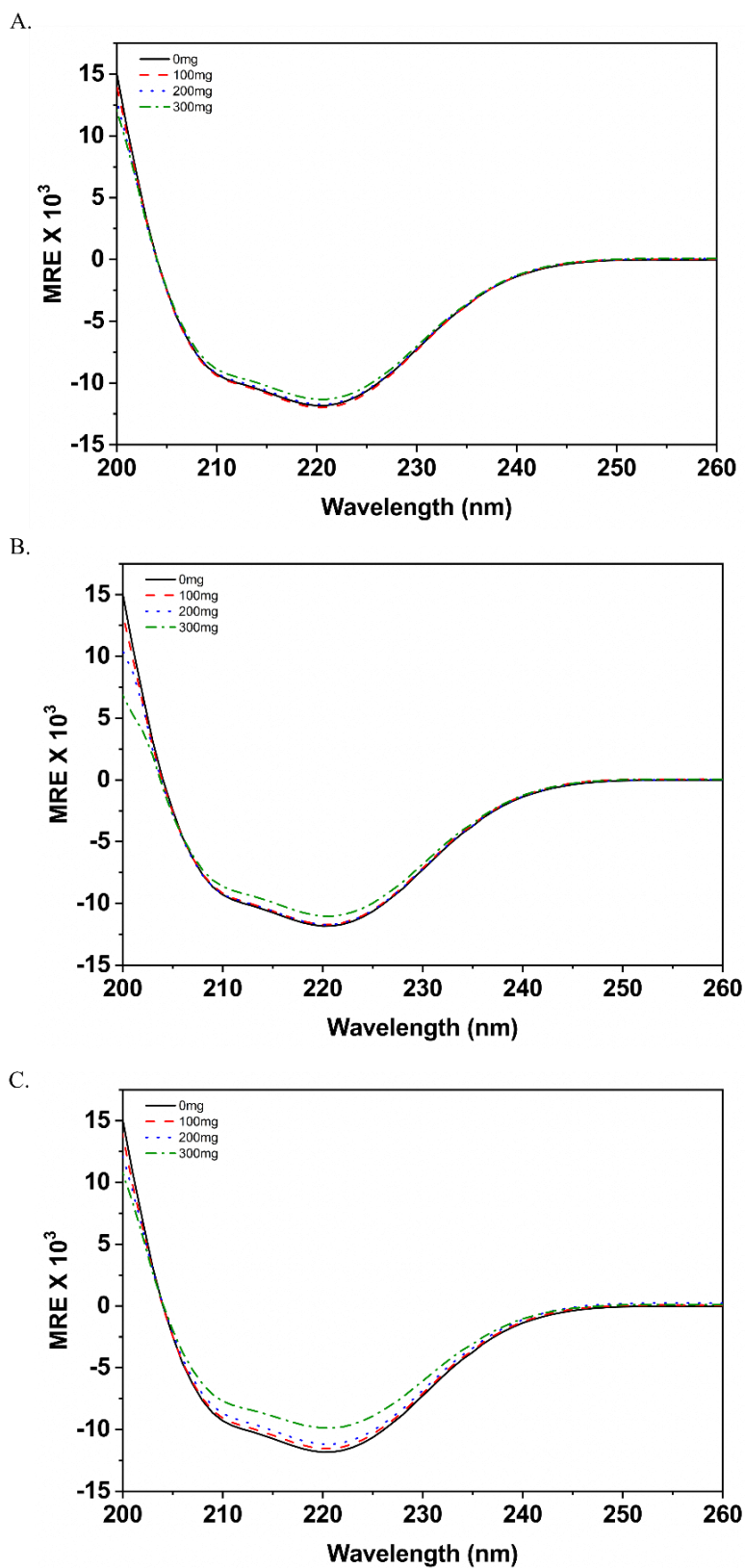


Figure 3.11: Effect of PEG on the secondary structure of apo CheY. Far UV-CD spectra in the presence of dilute buffer (black) and in 100 mg/mL (red), 200 mg/mL (blue) and 300 mg/mL (green) in (A) PEG 6000, (B) PEG 8000 and (C) PEG 12000.

Similarly, the near UV-CD of apo CheY in different volume fractions of LMW PEGs did not reflect any major changes in aromatic packing interactions (Figure 3.12). A subtle change, if any, was observed between 295-280 nm, which was attributed to the lone tryptophan residue present in CheY.

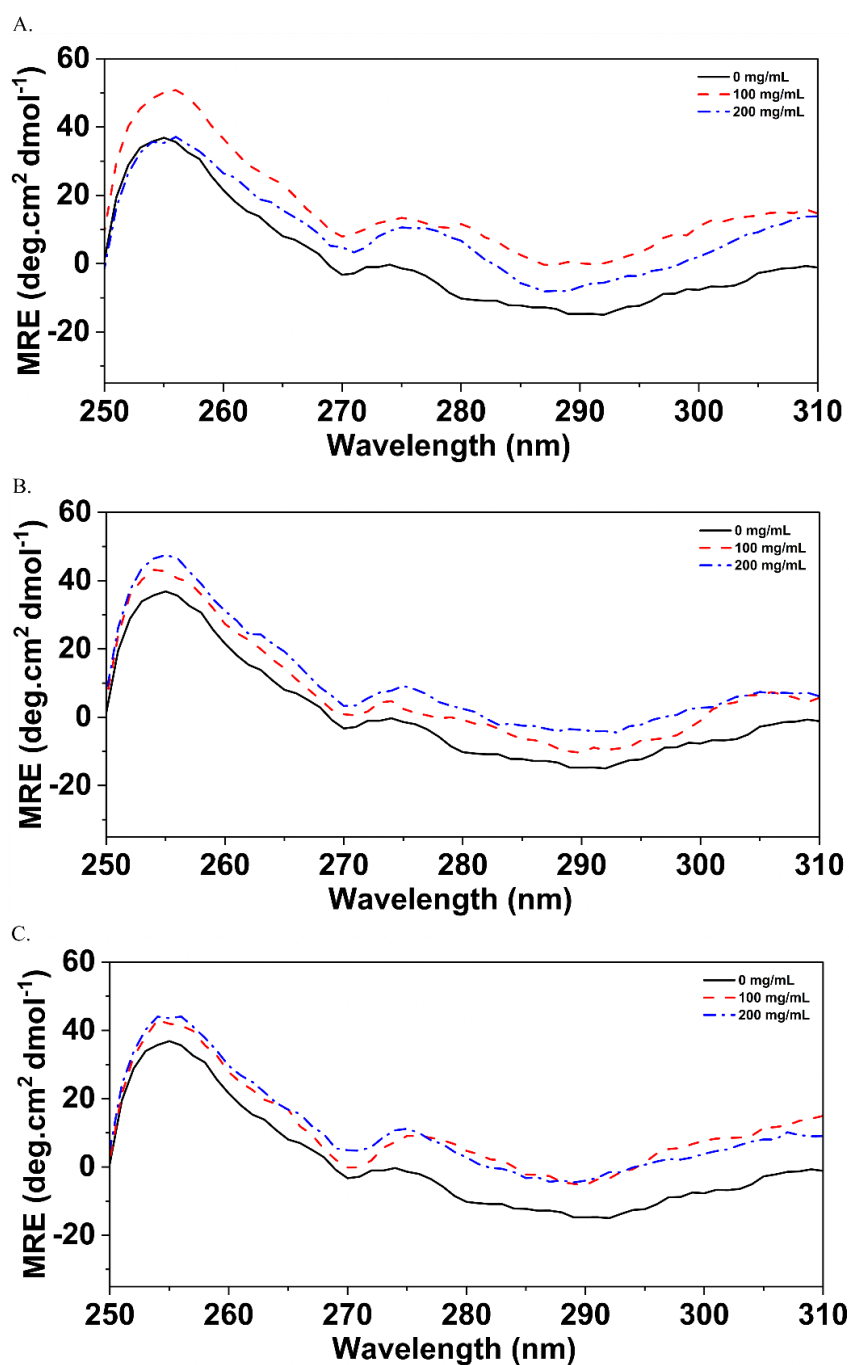


Figure 3.12: Effect of PEG on the tertiary structure of apo CheY. Near UV-CD spectra in the presence of dilute buffer (black) and in 100 mg/mL (red), and 200 mg/mL (blue) in (A) PEG 6000, (B) PEG 8000 and (C) PEG 12000

The near UV-CD results are further supported by the fluorescence emission spectra, which show negligible changes in the intensity with no shifts in the λ_{max} wavelength (Figure 3.13).

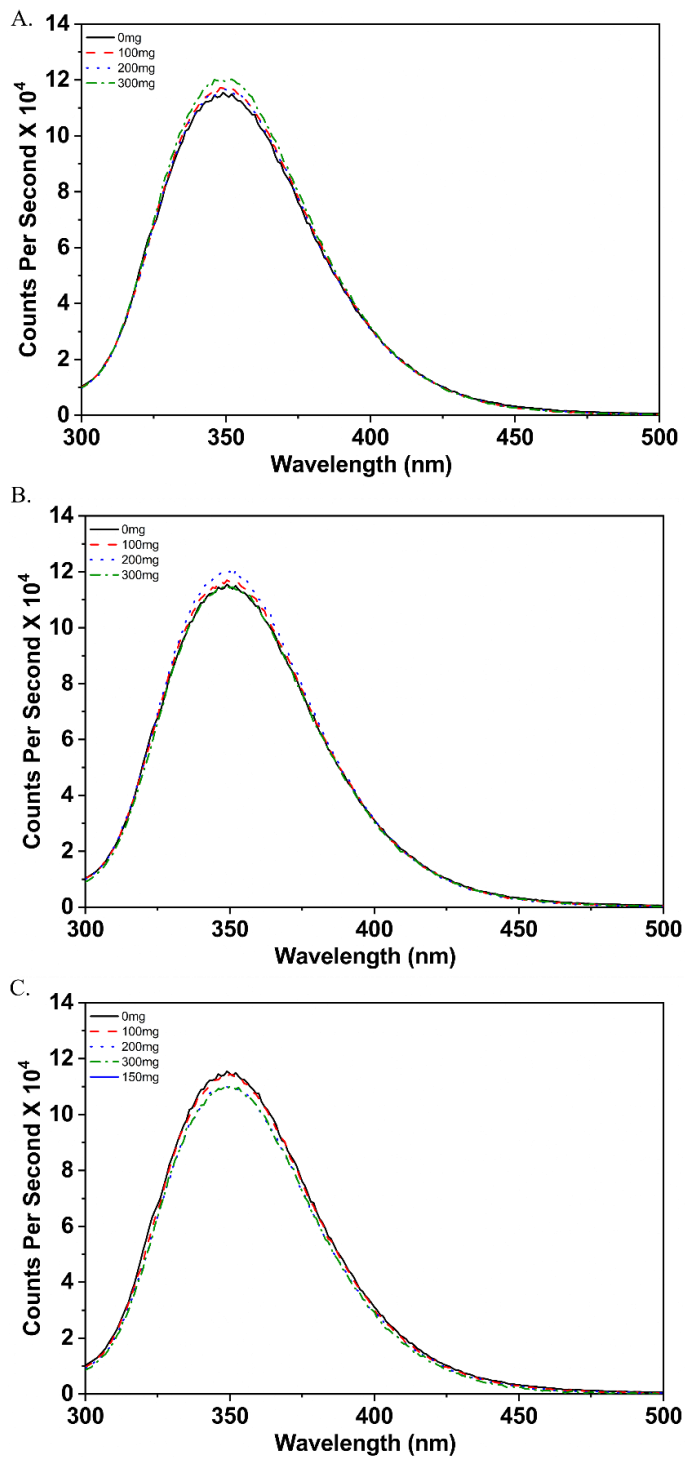


Figure 3.13: Intrinsic tryptophan fluorescence spectra of apo CheY. The fluorescence emission spectrum of CheY in the presence of dilute buffer (black) and varying concentrations (100 mg/mL in red and 200 mg/mL in blue) in (A) PEG 6000, (B) PEG 8000 and (C) PEG 12000.

This observation is unlike our previous finding with PEG 20000, where we reported a reduction in intensity and a shift in the λ_{max} value. PEGs also have the ability to not affect the secondary and tertiary structures of a protein in multiple cases. For instance, the CRABP1 protein and cytochrome c (Subadini *et al.*, 2021; Parray *et al.*, 2022) did not show a significant change in their secondary and tertiary structures in the presence of PEG. Taken together, for these protein-crowder pairs, the structure may not be drastically different from the dilute buffer conditions in the crowded scenario.

3.2.5.2 Effect of LMW PEGs on the thermal stability of apo CheY

In the absence of significant structural changes, it is important to elucidate the effect of LMW PEGs on the thermal stability of apo and holo CheY. PEGs are known to affect the thermal stability of proteins in a concentration-dependant manner (Lee and Lee, 1987). To determine the effect of LMW PEGs on apo CheY, thermal denaturation was performed in the presence and absence of different volume fractions of LMW PEGs. The midpoint of transition (T_m) was obtained for apo CheY by fitting the data to a previously reported two-state folded to unfolded model. In dilute buffer conditions, the T_m was $\sim 52^\circ\text{C}$, which was in line with a previous report (DeKoster *et al.*, 1993). In the presence of PEGs, the midpoint of transition obtained from the thermal stability curves of CheY decreased monotonously in a concentration-dependant manner from 100 to 200 mg/mL for all molecular weights of PEGs (Figure 3.14).

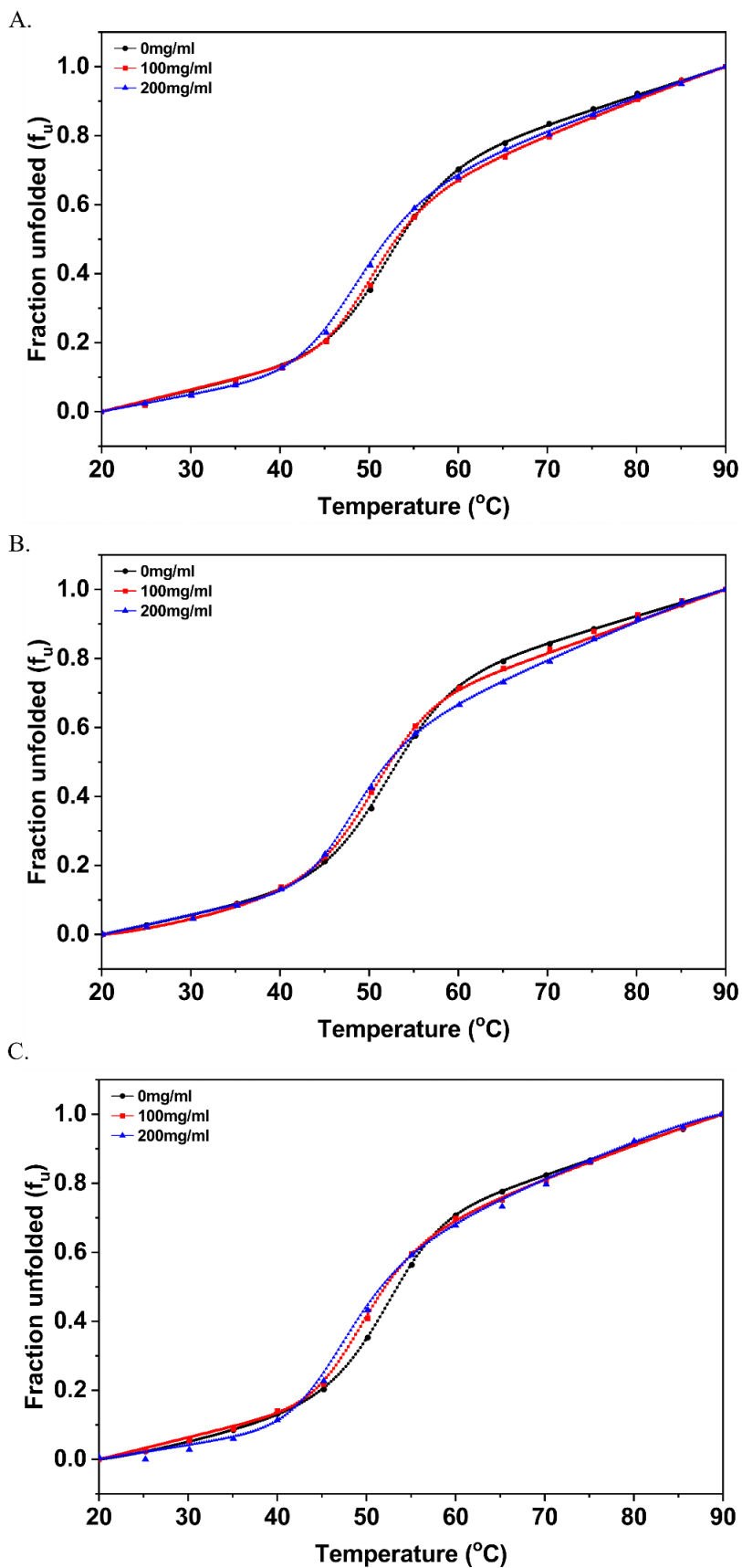


Figure 3.14: Thermal denaturation profile of apo-CheY in the presence of (A) PEG 6000, (B) PEG 8000, (C) PEG 12000. The continuous line represents the fit obtained from a two-state folded to-unfolded model.

This T_m decreases to $\sim 51^\circ\text{C}$ and $\sim 48\text{-}49^\circ\text{C}$ for 100 and 200 mg/mL concentrations of all PEGs, respectively. This reduction in T_m is in line with our previously reported data on PEG 20000, where we observed a similar extent of reduction in T_m (Irukuvajjula, Reddy and Vadrevu, 2022). A similar trend was observed by Lee et al. for four different proteins probed with different PEGs, where thermal stability reduced with the increasing hydrophobicity of the protein (Lee and Lee, 1987). Since the thermal denaturation processes were reversible, thermodynamic parameters were derived by fitting the data to a folded-to-unfolded, two-state model for protein denaturation (DeKoster *et al.*, 1993; Filimonov *et al.*, 1993; Kathuria *et al.*, 2008). Table 2.4 lists the thermodynamic parameters of protein in the presence of various PEGs. It was observed that, along with the volume fraction-based reduction of T_m , ΔG° showed a uniform yet minuscule decrease of $\sim 1\text{-}3$ kJ/mol. This is the premise to further probe the mechanistic details of individual contributions from enthalpy and entropy towards the Gibbs free energy change to decipher the effect of PEG-induced crowding on CheY.

Table 3.4: Thermodynamic parameters of apo-CheY derived from fitting the thermal denaturation data to a two-state folded to-unfolded model using CalFitter (Mazurenko et al., 2018).

Crowder concentration (mg/mL)		T_m ($^\circ\text{C}$)	ΔH° (kJ/mol)	$T\Delta S^\circ$ (kJ/mol)	ΔG° (kJ/mol)
	0	52.2 \pm 0.2	290 \pm 9	270 \pm 8	24.3 \pm 0.7
6000	100	50.5 \pm 0.4	300 \pm 15	280 \pm 14	24 \pm 1
	200	49.2 \pm 0.4	290 \pm 19	270 \pm 13	22 \pm 1
8000	100	50.2 \pm 0.3	310 \pm 11	290 \pm 11	23.9 \pm 0.8
	200	48.5 \pm 0.3	310 \pm 10	280 \pm 10	22.4 \pm 0.7
12000	100	50.1 \pm 0.4	300 \pm 17	280 \pm 16	23 \pm 1
	200	48.6 \pm 0.4	270 \pm 14	250 \pm 13	20 \pm 1

3.2.5.3 Mechanistic details and dissection of the effect of LMW PEGs on the thermodynamic stability of CheY

To dissect the effect of LMW PEGs on CheY, the thermodynamic parameters derived from the thermal denaturation curves were plotted (Senske *et al.*, 2014). Figure 3.15 shows a plot between ΔT_m and $\Delta\Delta H^{\circ'}$.

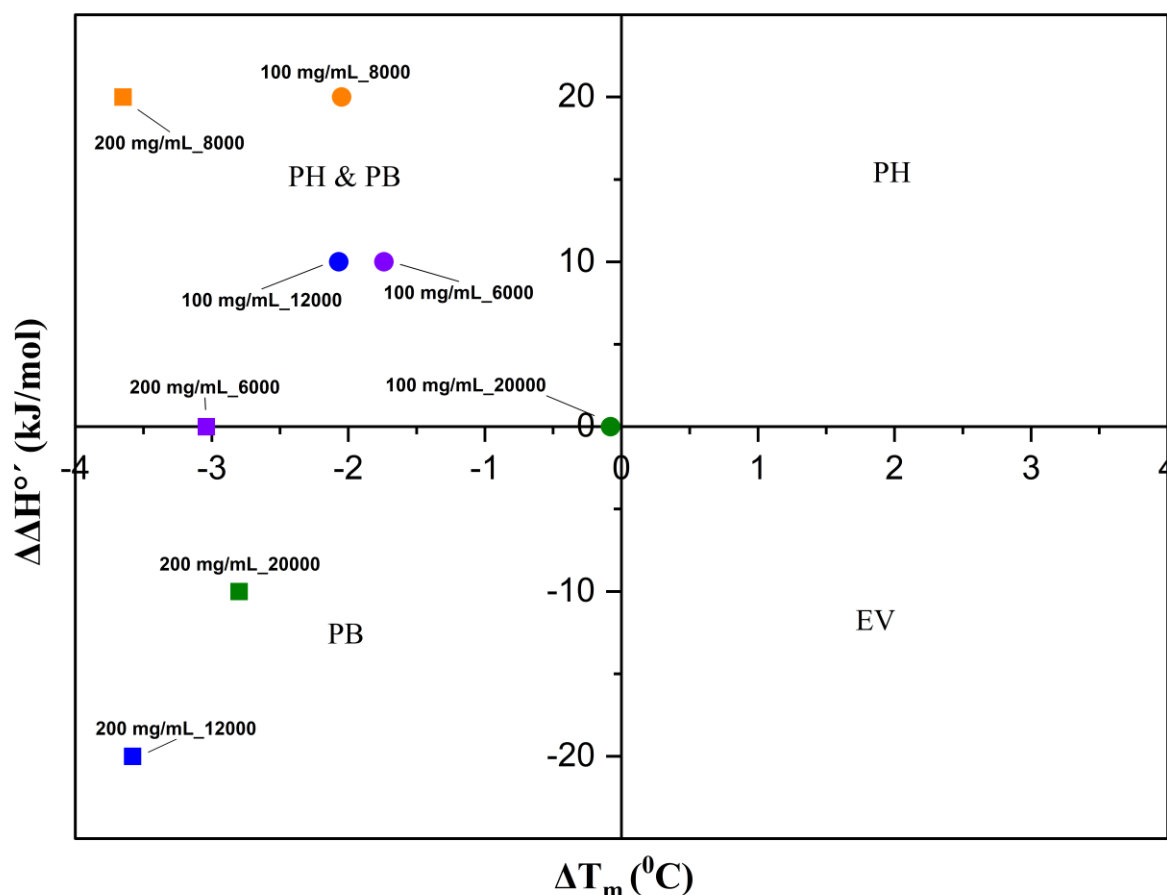


Figure 3.15: Classification of the effect of crowder on protein stability based on the thermodynamic footprints ($\Delta H^{\circ'}$ and ΔT_m) of apo CheY in the presence of various PEGs. (PH – Preferential Hydration, PB – Preferential binding, EV – Excluded volume)

A thorough analysis of the plot revealed the following: (i) PEG 6000 and PEG 8000 at 100-200 mg/mL lie in the 2nd quadrant with a positive $\Delta\Delta H^{\circ'}$ and a negative ΔT_m value. This quadrant is representative of preferential hydration and preferential binding. Cosolutes in this quadrant are capable of direct protein interactions, which reduces $\Delta H^{\circ'}$. However, at the same time, the solvent-mediated stabilization takes the $\Delta\Delta H^{\circ'}$ value to the positive regime (Senske *et al.*, 2014). Our results for PEG 6000 and 8000 are consistent with those of a previous study

in which ubiquitin interacted with PEG (Senske *et al.*, 2014). The effect of PEG 12000 at 100 mg/mL was similar to those of PEG 6000 and PEG 8000. It was able to destabilize the protein via preferential hydration and preferential binding with a positive $\Delta\Delta H^{\circ'}$. However, when the concentration of the PEG 12000 was increased to 200 mg/mL, a decrease in enthalpy along with a reduction in T_m and overall stability was observed. At this volume fraction, the data point lies in the third quadrant, which indicates preferential binding. A negative $\Delta\Delta H^{\circ'}$ along with the reduced T_m obtained for this concentration indicates that this particular PEG (12000) at 200 mg/mL volume fraction has the ability to directly interact with the protein with a higher affinity than the respective lower molecular weight PEGs (6000 and 8000). This observation can be explained with an accepted theory that with increasing size of PEG, amphiphilicity increases, which enables more contacts between the crowder and protein. In our case, PEGs up to 8000 were able to transiently establish contact with the protein; however, solvent-mediated stabilization made the excess enthalpy ($\Delta\Delta H^{\circ'}$) positive. As the PEG chain length increases to 12000 and the volume fraction is high (> 100 mg/mL), this PEG is now able to establish more contact than the lower molecular weight PEGs and also has an increased affinity. This was evidenced by the net negative $\Delta\Delta H^{\circ'}$ value in the presence of 200 mg/mL PEG 12000. This finding is in line with the previously reported work of Senske *et al.*, who classified PEGs as an intermediate between stabilizing osmolytes and chemical denaturants. Taken together, we can conclude that chemically PEG has an affinity towards CheY, but only higher-molecular-weight PEGs at a sufficiently high volume fraction can have a net negative excess enthalpy of interaction, owing to the increased affinity (Senske *et al.*, 2014). Smaller molecular weight PEGs also possess the capability of binding to CheY, but the solvent-mediated enthalpic stabilization may offset the net negative excess enthalpy and destabilize the protein. Increasing the chain length increases the amphiphilicity of PEG and hence increases the chances of contact between the crowder and the protein. In contrast, Wu *et al.*, reported that a moderate

concentration of PEG has conformational flexibility to bind to the hydrophobic patch of lysozyme and BSA and induce maximum structural changes (Wu *et al.*, 2014). We only report a moderate change in the thermal denaturation of the apo form at a higher volume fraction of the highest MW PEG used.

3.2.5.4 Effect of PEGs on the thermal stability of holo form

CheY binds to the metal ion Mg^{2+} and increases the thermodynamic stability of the protein (Filimonov *et al.*, 1993). The binding of Mg^{2+} ions increases the midpoint of the thermal transition from $\sim 52^{\circ}C$ to $\sim 68^{\circ}C$. This increase in stability is an indirect probe for metal binding that can be exploited to test the metal-binding ability of CheY in crowded environments. Hence, we performed thermal stability measurements in the presence of Mg^{2+} and different PEG polymers at increasing volume fractions. The thermal transitions were fitted to a two-state, folded-to-unfolded model (Figure 3.16). Thermal transitions in the presence of Mg^{2+} were not reversible; hence, other thermodynamic parameters could not be determined from the fit.

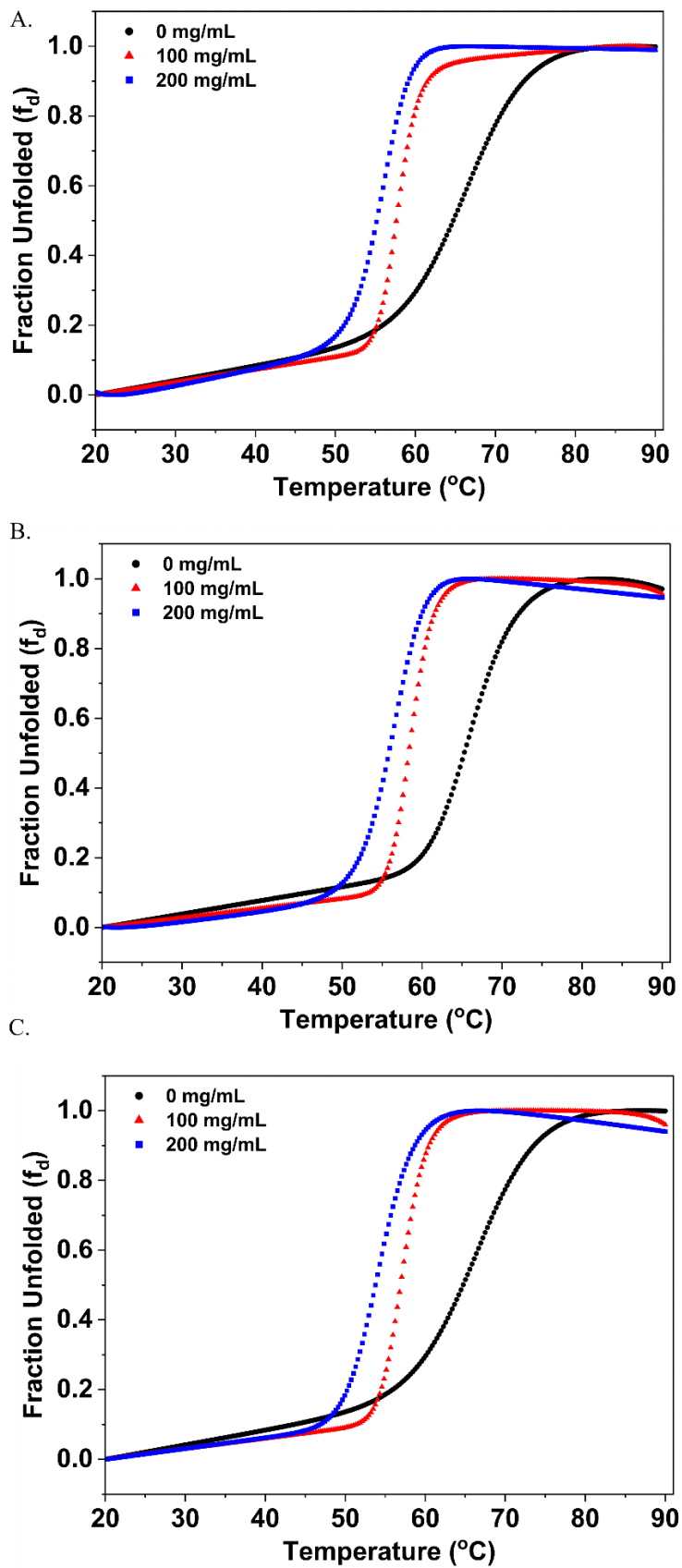


Figure 3.16: Thermal denaturation profiles of holo CheY in the presence of (a) PEG 6000, (b) PEG 8000, and (c) PEG 12000.

Table 2.5 indicates the T_m values of holo CheY in the presence of various PEG polymers.

Table 3.5: T_m value of holo CheY in the presence of difference volume fractions of PEGs.

Crowder concentration (mg/mL)		T_m (°C)
	0	67.5 ± 0.3
6000	100	59.3 ± 0.1
	200	54.7 ± 0.1
8000	100	58.5 ± 0.2
	200	56.3 ± 0.1
12000	100	57.2 ± 0.1
	200	54.4 ± 0.1

The thermal transitions revealed almost a similar T_m for all PEG polymer sizes at a particular volume fraction of 200 mg/mL. At 100 mg/mL, the T_m decreased from 68°C to ~58°C, and further increasing the concentration to 200 mg/mL reduced T_m to ~54°C. The reduced T_m closely overlap with the native apo CheY T_m of ~52°C. This observation leads to a scenario in which we can infer that the metal-protein interactions are disrupted. These results are consistent with our previous findings for PEG 20000 where we reported that the metal-binding site could have been affected. The near UV-CD recorded for holo CheY also indicated that the aromatic packing interactions were altered in a polymer length-dependent and volume fraction-dependent manner (Figure 3.17).

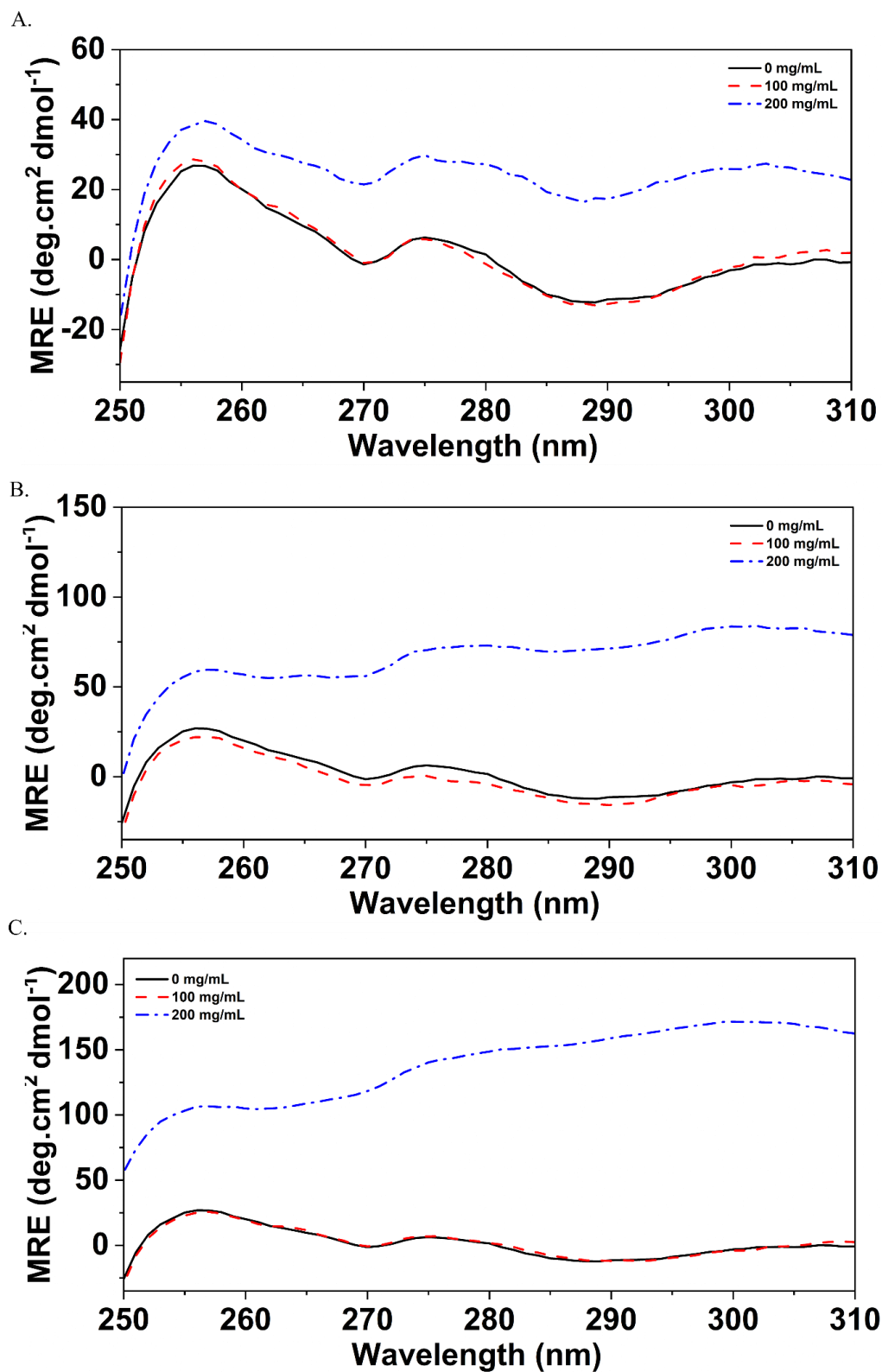


Figure 3.17: Effect of PEG on the tertiary structure of holo CheY. Near UV-CD spectra in the presence of dilute buffer (black) and in 100 mg/mL (red), and 200 mg/mL (blue) in (A) PEG 6000, (B) PEG 8000 and (C) PEG 12000

The literature also reports several cases in which the structure is unaffected, but the activity or stability is changed. The ribozyme's activity was maximum at different volume fractions of polymers of PEG; for PEG 1000 optimal activity was at 10-15% wt/vol, and for PEG 35000, optimal activity was at 5% (Paudel *et al.*, 2018). The effect of PEG 2000 on β -galactosidase was found to increase thermal stability and, at the same time, reduce its catalytic efficiency (Nolan, Sánchez and Perillo, 2015). In another instance, PEG 2000 and 4000 act as protein stabilizers by retarding unfolding kinetics. In the same study, the effect of PEGs on secondary and tertiary structures was observed only at a very high volume fraction of 400 mg/mL (Subadini *et al.*, 2021). Hence, it can be concluded that not only the size of the PEG polymer, but also the optimal concentration is crucial for elucidating the maximum effect of PEG-mediated crowding.

3.3. Conclusion

A combination of approaches suggests that PEGs interact with CheY via soft interactions, leading to local distortion and/or conformational rearrangement and affecting thermal stability in the presence of magnesium. The interactions between the crowder and apoprotein do not necessarily lead to significant changes in structure and stability. However, they can cause subtle local disorders that result in a less conformationally constrained situation. Although there may not be any changes in stability, the presence of crowders *can* affect the metal-binding interactions. CheY has a negatively charged metal-binding pocket formed by three aspartate residues (Asp 12, 13, and 57) that is stabilized by Mg^{2+} (Filimonov *et al.*, 1993). Owing to the structural perturbations induced by PEG, the metal-binding pocket may not attain a native like orientation in the presence of all PEG polymers. The overall thermodynamic stability in the presence of 200 mg/mL PEG 20000 was reduced by ~ 4 kJ/mol, accompanied by a decrease in ΔH° and ΔS° . A decrease in ΔH° suggests a direct crowder-protein interaction (Wang *et al.*, 2012; Senske *et al.*, 2014). It should also be noted that a decrease in both enthalpy and T_m

implies preferential binding of the crowder to the protein surface (Wang *et al.*, 2012; Senske *et al.*, 2014). The overall structural and functional features of proteins in dilute buffers may not be very different; however, cellular crowding conditions can lead to subtle conformational perturbations for optimized functional properties such as metal-binding, substrate binding, protein-protein interactions, etc. The present data collectively indicate that PEG interactions lead to altered native metal-binding interactions in a concentration-dependent manner. Although the structural change had only a minor effect on the stability of the apo CheY, there was a significant effect on the magnesium interaction induced stabilization. Our current results, which corroborate other examples in the literature (Sotomayor-Pérez *et al.*, 2013; Xu *et al.*, 2017), emphasize the finding that the structure, stability, and metal-binding thermodynamics may be different under conditions that mimic cellular crowding than when measured in dilute buffer solution. The physiological milieu is highly heterogeneous, and the sum total of all interactions can be different from an otherwise homopolymeric crowding outcome. As proposed earlier (Stadtmiller *et al.*, 2020), experimental conditions simulating realistic heterogeneous crowding conditions will help further decipher the nature of crowder-induced conformational and thermodynamic distortions. On this note, our results and analyses, and future studies on similar lines will not only help predict the outcome of crowding interactions based on the structure and nature of the protein surface, but also lessen the gap between experimental observations and theoretical predictions regarding the effects of crowding on proteins.

Chapter 4

Contrasting Effect of Carbohydrate Based Molecular and Macromolecular Crowders on Apo and Holo Forms of Bacterial Chemotaxis Protein Y: Selective Destabilization of the Conformationally Altered Holo Form

4.1 Introduction

Protein structure, stability, dynamics, and function are intrinsically encoded into the amino acid sequence (Anfinsen, 1973; Creighton, 1990; Dobson, 2003). The protein structure-function relationship is the hallmark of biological activity, and the function is the outcome of specific interactions between the molecules. These processes are, in turn, controlled by coordination and regulation, largely due to intermolecular interactions. Conformational changes in proteins due to intermolecular interactions serve as the control switches (Das and Sen, 2022). For instance, substrates can induce appreciable changes in the enzyme structure for optimal interactions (Müller and Schulz, 1992; Koshland, 1995; Müller *et al.*, 1996; Ådén and Wolf-Watz, 2007). Processes like the binding of metal ions, phosphorylation, etc., are also known to induce significant conformational changes within the protein (Rubin and Rosen, 1975; Johnson and Barford, 1993; Barondeau and Getzoff, 2004). The accumulated comprehension on all the aspects of proteins and biomolecules is basically derived from studies performed in dilute buffer conditions. However, in sharp contrast to the *in-vitro* test tube studies involving purified homogenous protein in dilute buffers, the interior of the cells is inherently heterogeneous by virtue of the presence of other molecules like nucleic acids, proteins, lipids, osmolytes, etc. and therefore, a far more complex environment (Fulton, 1982; Zimmerman and Trach, 1991b; Zimmerman and Minton, 1993). This “crowded” cellular environment thus enhances the chances of intermolecular encounters, and the associated crowding can affect via volume exclusion, soft interactions, a combination of both and/or change the hydration around the

molecules (Politi and Harries, 2010; Sukenik *et al.*, 2013; Sapir and Harries, 2014; Senske *et al.*, 2014; Abriata, Spiga and Peraro, 2016b; Kadumuri *et al.*, 2016; Bhakuni and Venkatesu, 2018, 2019; Irukuvajjula, Reddy and Vadrevu, 2022; Joshi and Kishore, 2022). The diverse data available on various proteins with a variety of crowders illustrate the inherent complexity of the consequences of crowding (Van Den Berg, Ellis and Dobson, 1999; Minton, 2001, 2015; R. J. Ellis, 2001; R. John Ellis, 2001; Sasahara, McPhie and Minton, 2003; Stagg *et al.*, 2007; Perham, Stagg and Wittung-Stafshede, 2007; Christiansen *et al.*, 2010; Dhar *et al.*, 2010; Zhang *et al.*, 2012; Kadumuri *et al.*, 2016; Rivas and Minton, 2018; Das and Sen, 2019; Irukuvajjula, Reddy and Vadrevu, 2022).

Most biological processes are regulated through conformational changes. Bacteria, archaea, lower eukaryotes, and plants use two-component signalling systems for signal transduction (Stock, Robinson and Goudreau, 2000). The proteins responsible for cellular signal transduction represent one of the well-characterized examples of conformational transitions and regulation of biological processes (Sada *et al.*, 2001; Ferguson, 2008; Tate and Schertler, 2009). Conformational changes are prompted by interactions with metal ions, other proteins, nucleic acids, etc. (Moy *et al.*, 1994; Masino, Martin and Bayley, 2000; Barondeau and Getzoff, 2004; Goh, Milburn and Gerstein, 2004; Tajmir-Riahi, 2006; Shinde *et al.*, 2020). Since the function, in many instances, is directly linked to changes in conformation, it is highly possible that crowding can also affect the conformationally altered states. Computational and experimental studies indicate that crowding can affect the conformational forms of the same protein differently (Dong, Qin and Zhou, 2010; Wang *et al.*, 2011; Sotomayor-Pérez *et al.*, 2013; Mittal and Singh, 2014; Xu *et al.*, 2017; Adams *et al.*, 2019). Prolyl-transfer RNA synthetase, when bound to its substrate, undergoes a significant conformational change, and it was observed that in the presence of crowding, the conformational equilibrium of the enzyme is affected (Adams *et al.*, 2019). Thus, it appears that the effect of crowding is not

just limited to the nature of the crowder and the protein but is also strongly influenced by the conformational state of the protein (Homouz *et al.*, 2009; Dong, Qin and Zhou, 2010; Sulmann *et al.*, 2014; Xu *et al.*, 2017; Nasreen *et al.*, 2018).

Chemotaxis protein Y (CheY), a 14 kDa single domain response regulator protein, is the best-characterised model protein for understanding the signal transduction process and conformational changes accompanying either metal/target binding (Djordjevic and Stock, 1998; Bren and Eisenbach, 2000; Schuster, Silversmith and Bourret, 2001; Guhaniyogi, Robinson and Stock, 2006). The apo CheY exhibits different physiologically relevant conformations in equilibrium (Djordjevic and Stock, 1998; Bren and Eisenbach, 2000; Simonovic and Volz, 2001). The signalling region of the protein, particularly, exists in two conformational states and a population shift results in a subpopulation of active conformers (Simonovic and Volz, 2001). The holo CheY, shows significantly altered conformation from the apo form (Lukat, Stock and Stock, 1990; Stock *et al.*, 1993; Bellolell *et al.*, 1994; Moy *et al.*, 1994). The structural perturbations are not limited to local changes in the vicinity of the metal binding site (Stock *et al.*, 1993; Bellolell *et al.*, 1994; Moy *et al.*, 1994), but also larger conformational changes distant from the metal binding site are observed in the presence of magnesium (Bellolell *et al.*, 1994). The conformational changes, in turn, lead to triggering a cascade of events, eventually assisting bacteria in changing the flagellar rotation from an anti-clockwise to a clockwise direction, responding to the chemical changes in its environment (Bren and Eisenbach, 2000).

. It has been experimentally shown that in the presence of magnesium, both the structure and stability are affected (Filimonov *et al.*, 1993; Bellolell *et al.*, 1994; Moy *et al.*, 1994). In the presence of increasing amounts of magnesium chloride (4-30 mM), an enhancement in standard Gibbs free energy of ~ 4 kJ/mol was observed against chemical denaturation (Filimonov *et al.*,

1993). However, the effect of macromolecular crowding on apo and holo structures and stability is unknown. This scenario prompts two key questions: (i) How does magnesium-induced change in conformation and stability respond to crowding conditions? (ii) Can sucrose also affect magnesium-induced changes in conformation and stability like Ficoll? We attempted to address these questions by investigating the effects of Ficoll-70™ with an average molecular weight of 70 kDa, a commonly used crowding mimic (hereafter referred to as Ficoll), and sucrose, the monomeric unit of Ficoll, on the thermal stability of apo and holo CheY. Here, we report that the thermal stability of CheY is affected differently for the two conformational forms in the presence of Ficoll. Interestingly, in the combined presence of magnesium and Ficoll, in contrast to the observations in (i) dilute buffer and (ii) the presence of Ficoll alone, the thermal stability of CheY is lowered. Interestingly, the selective lowering of T_m for the holo form only in the combined presence of Ficoll and sucrose, and not in sucrose alone, suggests that the observed effect is due to the macromolecular nature (entropic nature) of Ficoll and not a mere molecular crowding effect. This study emphasizes that Ficoll interacts differently with conformationally altered states and can potentially modulate the relative populations of the apo and holo forms of CheY.

4.2 Results and Discussion

4.2.1 Effect of Ficoll on the structure of the apo and holo protein

The effects of Ficoll on the secondary and tertiary structures was investigated in the far and near UV-CD regions, respectively (Figure 4.1 and 4.2). The perturbations in the secondary structure content of the apo and holo forms are not identical. A steady increase in the far UV-CD signal in the presence of Ficoll is clear for the apo form (Figure 4.1A). The secondary structure increases gradually in a concentration dependant manner, with an increase in the signal at 222 nm ~15% in the presence of 200 mg/mL Ficoll. On the contrary, the far UV-CD spectra

for holo CheY in the absence and presence of Ficoll overlapped with each other, indicating the absence of any crowding-induced secondary structure enhancement (Figure 4.1B).

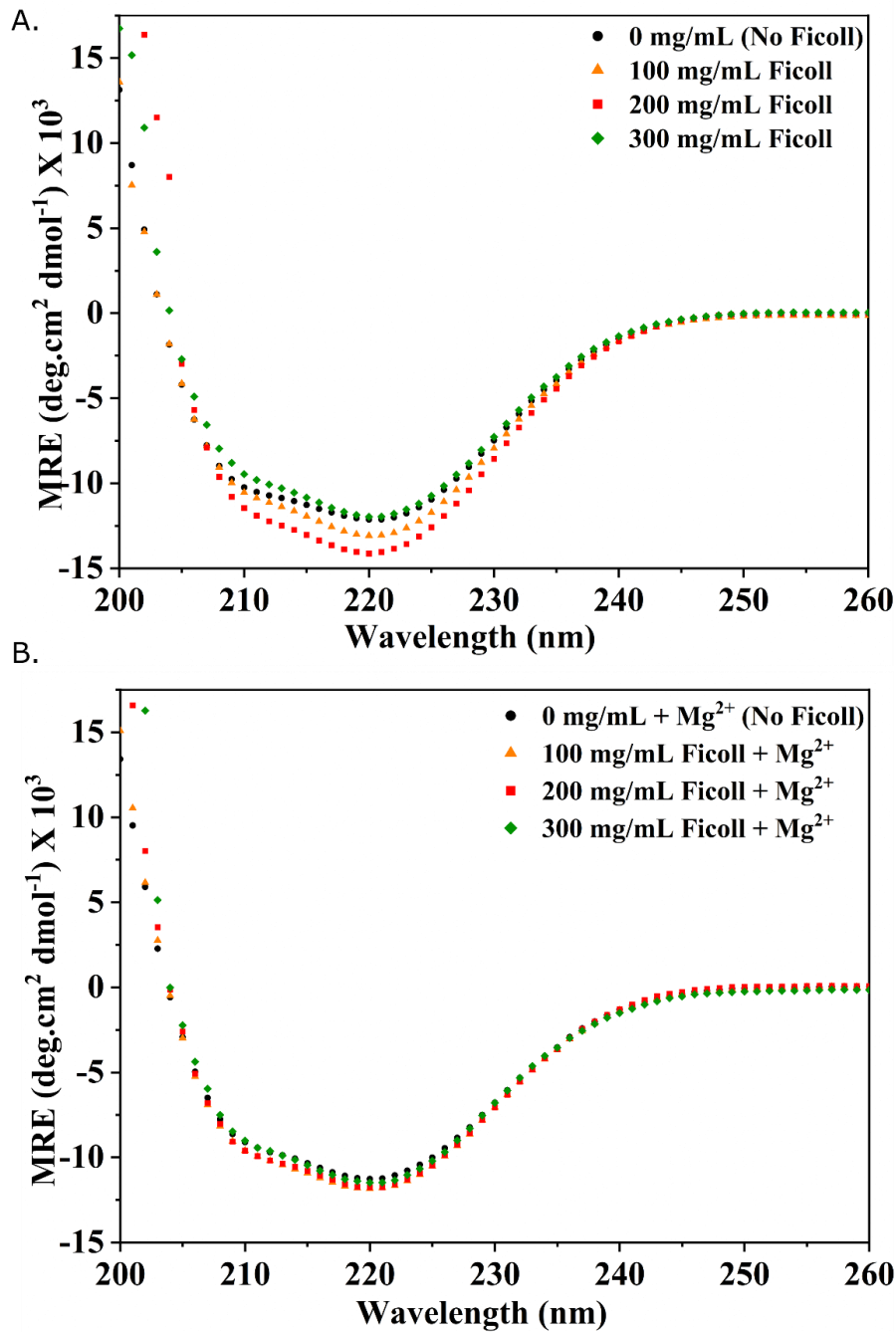


Figure 4.1: Far UV-CD spectra in the presence and absence of Ficoll for (A) apo CheY and (B) holo CheY

The CD signal for the spectra > 200 mg/mL of Ficoll, for the apo and holo forms was inconsistent and not reproducible, limiting the thermal denaturation studies to ≤ 200 mg/mL.

The near UV-CD spectra of apo CheY in the presence and absence of Ficoll are shown in Figure

4.1A. It can be observed that the spectrum in dilute buffer shows distinctive features consistent with the near UV-CD spectrum reported earlier by Filimonov et al (Filimonov *et al.*, 1993).

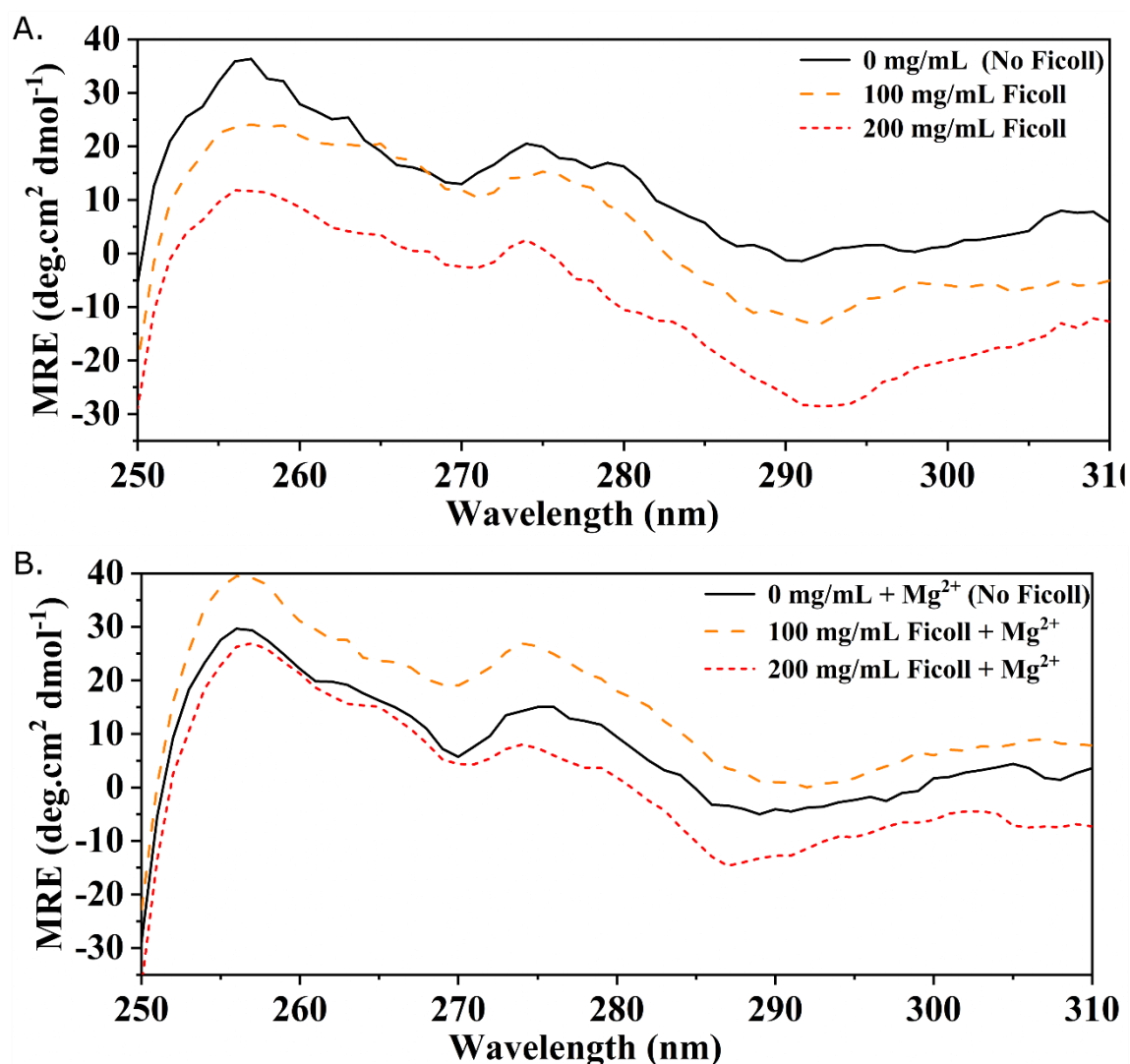


Figure 4.2: Near UV-CD spectra in the presence and absence of Ficoll of (A) apo CheY and (B) holo CheY. The concentration of $MgCl_2$ was maintained at 10 mM.

The packing of the aromatic amino acids appears to be largely unaffected, and only minor changes can be observed in the presence of Ficoll. The minor changes in the presence indicate the plausible reorientation of the native aromatic amino acid packing interactions in the presence of the crowder. Thus, the increase in the secondary structure is also reflected in the different packing of native interactions involving the aromatic residues for the apo form. Additional techniques like time resolved fluorescence and extrinsic fluorescence (8 -

anilino-naphthalene sulfonate) emission for apo CheY could not yield insights into the minor structural perturbations observed from far and near UV CD. For time resolved fluorescence, the partially exposed tryptophan residue and change in solvent polarity lead to reduction of fluorescence emission intensity. Therefore, sufficient data could not be collected and the results obtained were not significantly conclusive. ANS fluorescence for apo CheY (data not shown) does not change in crowded environment. For the holo form (Figure 4.2B) the presence of Ficoll may also induce minor reorganization of the aromatic packing interactions, similar to that of the apo form. Time resolved fluorescence studies for holo CheY are precluded due to inherent quenching of tryptophan residue in the presence of Mg^{2+} ions. ANS emission did not yield a consistent result (data not shown).

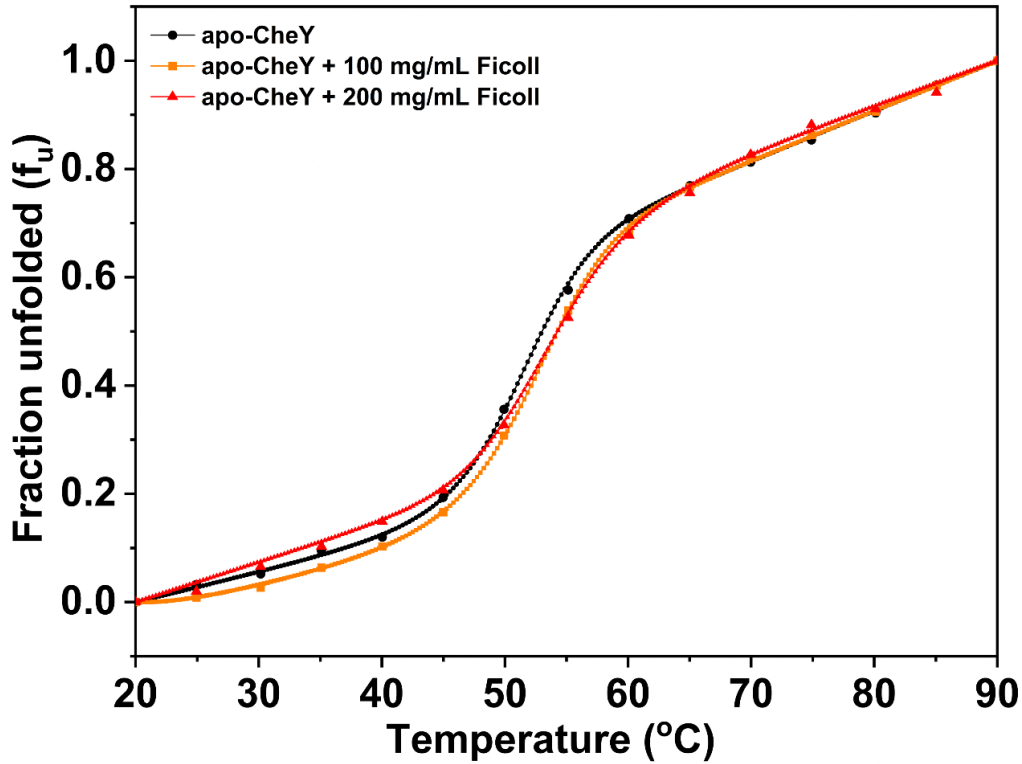
4.2.2 Macromolecular crowding affects the thermal stability of apo and holo forms differently

CheY, in its metal unbound, apo form, displays inherent structural malleability and tends to adopt multiple conformations (Simonovic and Volz, 2001). When magnesium is bound, conformational changes occur in the metal binding site's proximity and regions distant from the metal binding pocket (Bellolell *et al.*, 1994; Moy *et al.*, 1994). Thermal denaturation was performed to derive a quantitative comparison of the thermal stability of the two different conformational forms of the same test protein in the presence of the crowder. The temperature-induced unfolding in dilute buffer and in the presence of increasing amounts of Ficoll was monitored by following the change in the far UV-CD signal at 222 nm for the apo and holo protein. The mid-point of the heat-induced thermal transition (T_m) and other thermodynamic parameters obtained from a fit to a folded to unfolded, two-state equilibrium unfolding model (Greenfield, 2007b; Mazurenko *et al.*, 2018) are summarized in Table 3.1 and shown in Figure 4.3A. Although the native states of apo form in the presence and absence of Ficoll are different (slight increase in secondary structure in the presence of Ficoll) data were normalized as

reported earlier (Stagg *et al.*, 2007; Wang, He and Li, 2010). The T_m slightly increases from 52 to 54°C in the presence of 200 mg/mL Ficoll for the apo protein, accompanied by a concomitant increase in, ΔH° , $T\Delta S^\circ$, and ΔG° values suggesting a moderate Ficoll-induced stabilization. It may also be noted that the extent of Ficoll-induced stabilization increases with Ficoll concentration. The ΔT_m and $\Delta\Delta H^\circ$ show positive values (> 0), implying that the cosolute is excluded from the protein surface and or direct contact with the protein (Politi and Harries, 2010; Senske *et al.*, 2014). The apo form of CheY is known to exist in multiple conformations, and a population shift can lead to the protein accessing subpopulations in dilute buffer conditions (Moy *et al.*, 1994; Simonovic and Volz, 2001). The conformationally malleable apo form may be becoming less flexible in the presence of Ficoll. The minor changes in structure and stability suggest a moderate crowder-prompted disposition towards an increase in stability of the apo form. The relatively small increase in the intensity of the far UV-CD signal implies a reduction in local conformational flexibility and compaction of the apo form, as a significant change is not observed in the stability of the apo protein in the presence of the crowder.

Contrary to the apo situation, a striking observation is a systemic decrease in the T_m for the holo form in the presence of Ficoll (Figure 4.3B and Table 4.1). The T_m of the holo protein in dilute buffer shows a concentration dependant decrease from 68°C in dilute buffer to 62°C to 58°C in the presence of 100 and 200 mg/mL of Ficoll. Interestingly, although there is a reduction in T_m , it is still non-coincident with the T_m of the apo form. Intuitively, it is expected that the lowering of T_m for the holo form in the presence of Ficoll may result from the loss of metal-protein interaction.

A.



B.

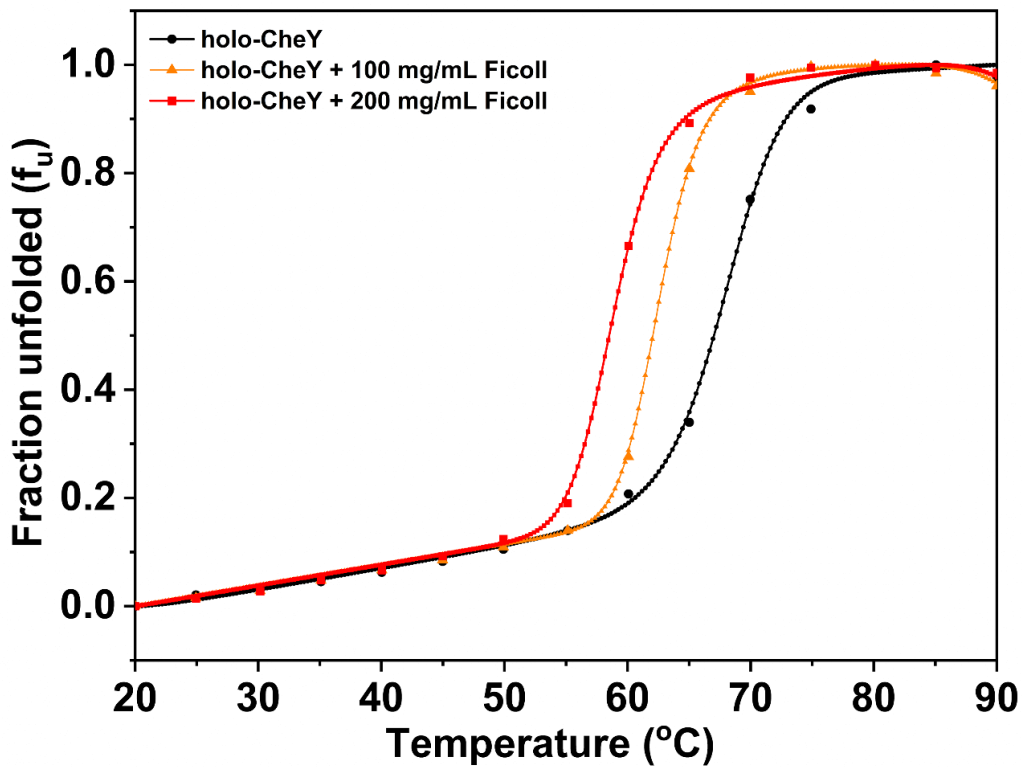


Figure 4.3: Thermal denaturation profiles of CheY in the presence of Ficoll for (A) apo form and (B) holo forms. The lines joining the data points correspond to a fit to a two-state, folded-unfolded model (DeKoster et al., 1993; Filimonov et al., 1993). The concentration of $MgCl_2$ was maintained at 10 mM. Although data were recorded at $1^\circ C$ interval, for the purpose of representation the data are plotted at $5^\circ C$ interval.

Table 4.1: Thermodynamic parameters of apo CheY in the presence of Ficoll, sucrose, and combined presence of Ficoll and sucrose obtained from fitting of thermal unfolding to a two-state folded to unfolded model. (DeKoster et al., 1993; Filimonov et al., 1993). $\Delta T_m = T_m(\text{Ficoll}) - T_m(\text{dilute buffer})$ and $\Delta\Delta H^{\circ'} = \Delta H^{\circ'}(\text{Ficoll}) - \Delta H^{\circ'}(\text{dilute buffer})$

Sample	T_m (°C)	ΔT_m (°C)	$\Delta H^{\circ'}$ (kJ/mol)	$\Delta\Delta H^{\circ'}$ (kJ/mol)	$T\Delta S^{\circ'}$ (kJ/mol)	$\Delta G^{\circ'}$ (kJ/mol)
CheY	51.1 ± 0.1	0	260 ± 3	0	240 ± 3	20.3 ± 0.2
CheY + 100 mg/mL Ficoll	51.9 ± 0.3	0.82	280 ± 9	20	260 ± 9	23.03 ± 0.7
CheY + 200 mg/mL Ficoll	53.2 ± 0.3	2.09	270 ± 9	10	250 ± 8	23.4 ± 0.7
CheY + 100 mg/mL sucrose	52.9 ± 0.5	1.85	270 ± 12	10	250 ± 11	24 +/- 1.0
CheY + 200 mg/mL sucrose	56.7 ± 0.1	5.56	312 ± 9	52	282 ± 9	30.3 ± 0.9
CheY + 200 mg/mL Sucrose + 200 mg/mL Ficoll	59.7 ± 0.4	8.93	280 ± 13	20	252 ± 12	29 +/- 1.0

Table 4.2: The T_m values of holo CheY in the presence of Ficoll, sucrose, and combined presence of Ficoll and sucrose obtained from the fitting of thermal denaturation profiles to a two-state folded to unfolded model. (DeKoster et al., 1993; Filimonov et al., 1993) (*). It could not be determined due to a lack of unfolding baseline in the thermal denaturation range and high error from the fit. Since the thermal transitions were not reversible for the holo form, the thermodynamic parameters ($\Delta H^{\circ'}$, $\Delta S^{\circ'}$ and $\Delta G^{\circ'}$) are not reported. The concentration of MgCl_2 is 10 mM. $\Delta T_m = T_m(\text{Ficoll}) - T_m(\text{Dilute buffer})$.

Sample	T_m (°C)	ΔT_m (°C)
CheY + Mg^{2+}	67.9 ± 0.3	0
CheY + Mg^{2+} + 100 mg/mL Ficoll	62.6 ± 0.1	-6
CheY + Mg^{2+} + 200 mg/mL Ficoll	58.9 ± 0.1	-9.1
CheY + Mg^{2+} + 100 mg/mL sucrose	70.5 ± 0.2	2
CheY + Mg^{2+} + 200 mg/mL sucrose	ND*	-
CheY + Mg^{2+} + 200 mg/mL Ficoll + 200 mg/mL sucrose	64.7 ± 0.1	-4.2

4.2.3 Is the metal-protein interaction retained in the presence of Ficoll?

The native structure of Che Y has a metal binding pocket comprising two negatively charged aspartates and a polar asparagine residue at positions 13, 57, and 59, respectively, wherein the magnesium ion binds. Magnesium binding leads to thermodynamic stabilization and results in

structural re-orientation not only in the vicinity of the metal binding site but also distant from the metal interaction site (Bellolell *et al.*, 1994; Moy *et al.*, 1994). As reported earlier, the lone tryptophan residue at position 58 reorients to a more polar environment, leading to significant quenching in the intrinsic fluorescence intensity. This phenomenon is specific to divalent metal ion binding and Mg^{2+} binding has physiological relevance to the process of bacterial chemotaxis (Lukat, Stock and Stock, 1990). Therefore, comparing the fluorescence quenching of tryptophan 58 in the presence and absence of Ficoll will verify if the metal-protein interaction persists in the presence of crowding conditions. If the metal binding site is distorted due to the crowding-induced effect, then the reduced thermal stability of the holo form can be attributed to the conversion to the metal unbound form. Figure 4.4 shows the quenching of tryptophan in dilute buffer and in the presence of increasing concentrations of Ficoll, sucrose and 6 M urea.

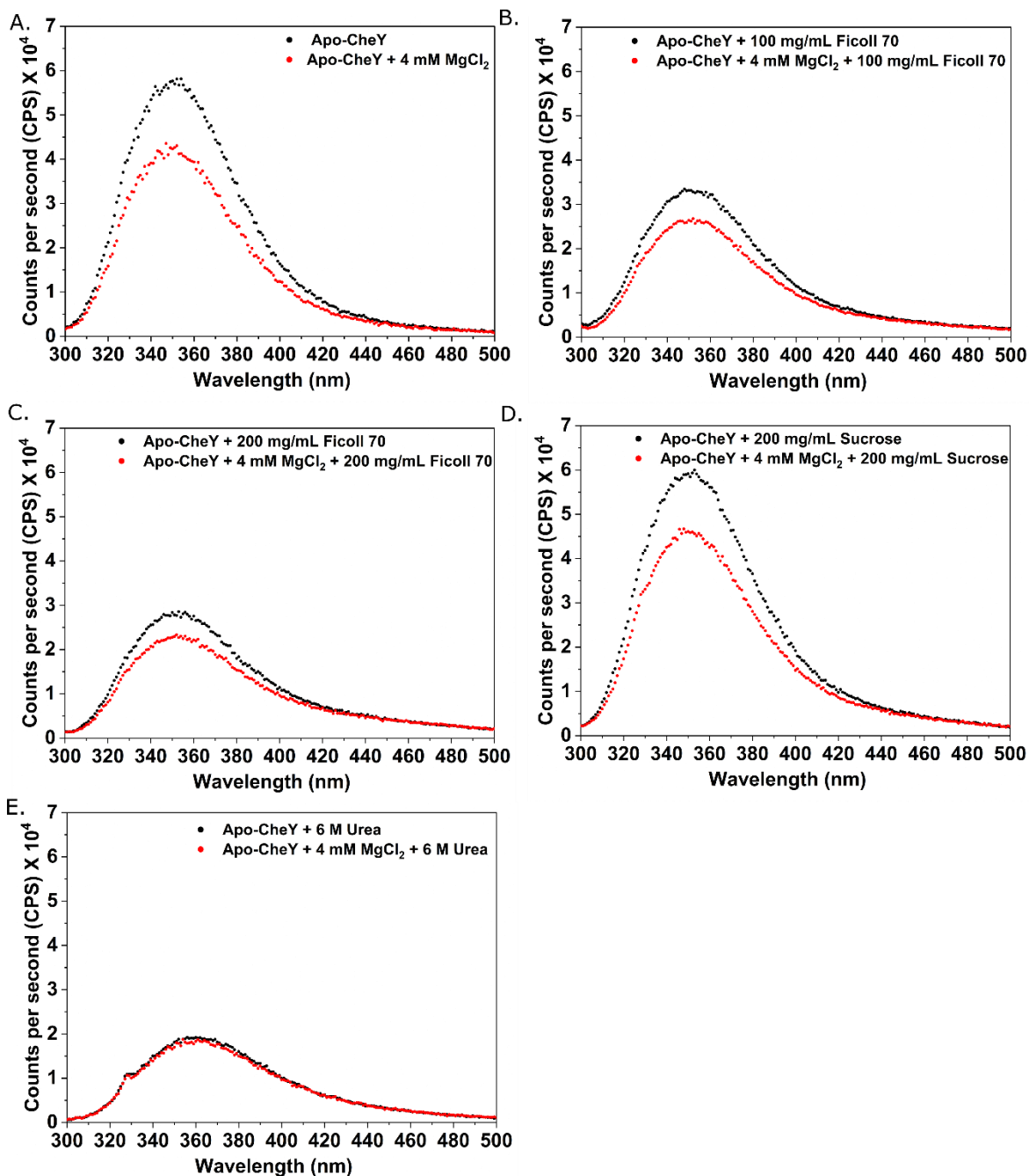


Figure 4.4: Intrinsic tryptophan fluorescence quenching in the presence and absence of Ficoll. Tryptophan fluorescence emission of CheY in (A) dilute buffer (B) 100 mg/mL of Ficoll (C) 200 mg/mL of Ficoll. (D) 200 mg/mL sucrose and (E) 6 M Urea. The black and red colors denote the absence and presence of 4 mM $MgCl_2$.

The overall trend of the reduction in the fluorescence emission in the presence of $MgCl_2$ under crowding conditions suggests that metal binding is not affected in the presence of Ficoll and sucrose (Figure 4.4 B-D). It may be noted that in the presence of 6 M urea (Figure 4.4 E), CheY is completely unfolded, and hence the metal binding pocket is disrupted and consequently, fluorescence quenching is not observed. Thus, the perturbation, if any, is not to the extent that

the metal binding pocket is completely distorted, as evidenced by the retention of tryptophan fluorescence quenching in the presence of Ficoll. Therefore, the likelihood of the observed decrease in the thermal stability in the presence of Ficoll may not be due to the loss of protein-metal interaction. Alternatively, (i) the non-coincidence of the T_m with that of the apo form may be arising due to the population of both apo and holo forms existing in conformational equilibrium, (ii) the interaction of the crowder with the holo form in a manner that leads to destabilization may be yet another possibility to result in a T_m value which is midway between the apo and holo forms.

4.2.4 Molecular crowding by sucrose increases the stability of apo and holo CheY

Is the observed stabilizing effect limited to the polymeric Ficoll, or can it be attained by sucrose, as well. Sucrose being the monomeric unit of Ficoll, was probed. The monomeric sucrose can also show a similar effect if the nature of the crowding effect is purely enthalpic (Benton *et al.*, 2012a). Similar to this result, the extent of stabilization by glucose also increases the stability in the presence of its polymer, Dextran. The effect was attributed to volume exclusion (Ghosh *et al.*, 2020). The T_m and other thermodynamic parameters, ΔH° , $T\Delta S^\circ$ and ΔG° of CheY increase in the presence of increasing amounts of sucrose (Tables 3.1 and 3.2). The combined increase of T_m and $\Delta\Delta H^\circ$ indicate preferential hydration of protein (Senske *et al.*, 2014). T_m increased with increasing sucrose concentration from 0-200 mg/mL (Figure 4.5A). In the presence of 100 mg/mL sucrose, the observed T_m is 70°C, ~3°C higher than the T_m of holo CheY measured in the absence of sucrose (Figure 4.5B). The unfolding is incomplete at ~200 mg/mL concentration of sucrose. The fits to obtain the T_m resulted in significant errors. However, the thermal profile suggests that the T_m in the presence of 200 mg/mL sucrose is at least the value that corresponds to the T_m in the presence of 100 mg/mL sucrose. Carbohydrates are known to increase protein stability. It has been proved that adding certain sugars works as protein stabilizers (Xie and Timasheff, 1997; Kim *et al.*, 2003; Poddar *et al.*, 2008). One

accepted theory for observed stabilization is that sugars stabilize the native state of the protein, as they are preferentially excluded from the protein surface.

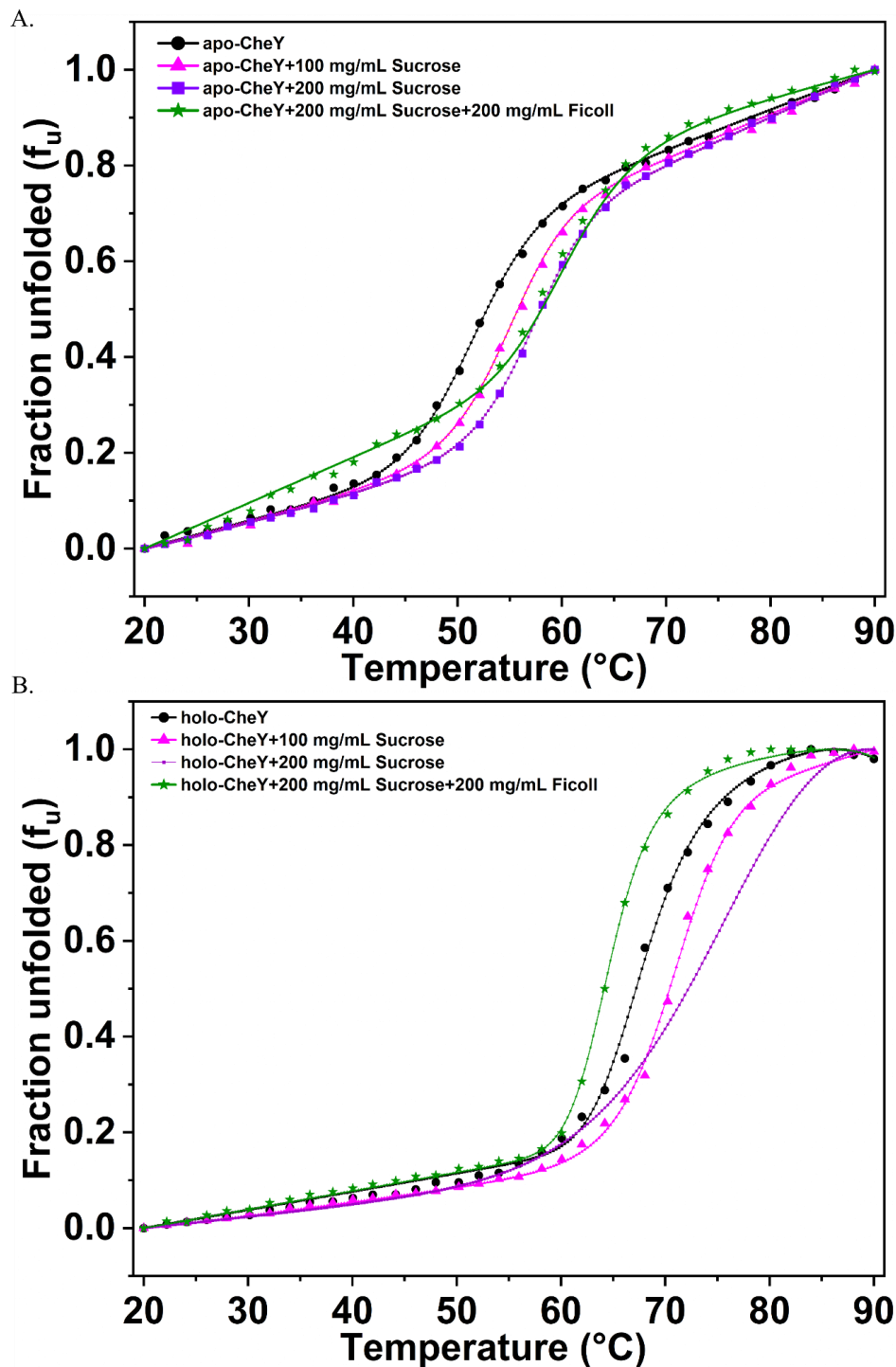


Figure 4.5: Thermal denaturation profiles of CheY (A) Apo form (B) Holo form. In dilute buffer, in increasing concentrations of sucrose and in the combined presence of sucrose and Ficoll. The lines joining the points correspond to a fit to a two-state, folded-unfolded form of the protein. For the holo protein, the thermal transition was not reversible. The concentration of $MgCl_2$ was maintained at 10 mM. Although data were recorded at $1^\circ C$ interval, for the purpose of representation the data are plotted at $2^\circ C$ interval.

Thus, in sharp contrast to the decreasing trend observed in the presence of Ficoll, the thermal stability shows an upward trend in increasing amounts of sucrose.

4.2.5 Mixed crowding by sucrose and Ficoll destabilizes holo but not the apo form

As noted earlier, a steady decrease in the T_m from 0-200 mg/mL is observed in the presence of Ficoll and an opposite, increasing trend in the presence of sucrose for holo CheY. Interestingly, when holo CheY was subjected to a thermal melt in the mixed presence of sucrose and Ficoll, a reduction in the value of T_m was observed (Figure 4.5B). The mixed crowding effect seems to be specific to the holo form as the apo protein shows a unidirectional trend towards stabilization (Figure 4.5A) suggesting that the selective decrease in the metal-binding induced thermal stability is due to macromolecular crowding (volume exclusion of Ficoll) effect and not due to molecular crowding (enthalpic effect of sucrose).

Taking together the secondary and tertiary structure of both apo and holo states largely remain unaffected in the presence of Ficoll and sucrose alone and combined; however, the thermal stability is moderately enhanced. Contrary to its effect on the apo state, Ficoll shows a differential destabilizing effect on the holo form. The crowding-induced, moderate, stabilizing effect of the apo form is ameliorated by sucrose, while the effect is opposite for the holo form in the presence of Ficoll resulting in a substantial decrease in the thermal stability. A similar effect is observed for holo myoglobin, wherein its thermal stability is reduced in the presence of Ficoll. In this instance, it should be noted that the destabilization is due to the interaction of the Ficoll with the heme-moiety (Nasreen *et al.*, 2020). For CheY, the possibility of the observed reduction in the thermal stability as a result of the loss of metal-protein interaction can be ruled out based on the retained magnesium-binding induced tryptophan quenching in the presence of Ficoll. The effect of crowder interacting with the holo form remains a certain possibility. Further, the differential effect on the holo form is dominated by the macromolecular nature of Ficoll and not its chemical nature. The observed reduction in T_m could be arising from

Ficoll influencing the relative population of the apo and holo forms because metal binds to the protein even in the presence of Ficoll.

4.2.6 Is macromolecular crowding due to Ficoll modulating the population of apo and holo forms?

In the presence of 1 mM MgCl₂, the measured T_m value was found to be 57°C, which is higher than the apo form. The T_m at 1 mM is lower than the T_m at 10 mM MgCl₂ by ~10°C. The same holds good in the presence of 5 mM MgCl₂. The T_m at 5 mM is reduced by 8°C. The MgCl₂ concentration dependence of T_m suggests that the population of apo forms may be higher at lower Mg²⁺ (Figure 4.6). It appears that the apo forms are stabilized in the presence of Ficoll. Hence, the upward trend of increasing T_m is still observed at these concentrations (Figure 4.6). The point of interest is the observation that > 5 mM MgCl₂, the trend observed for the T_m is reversed.

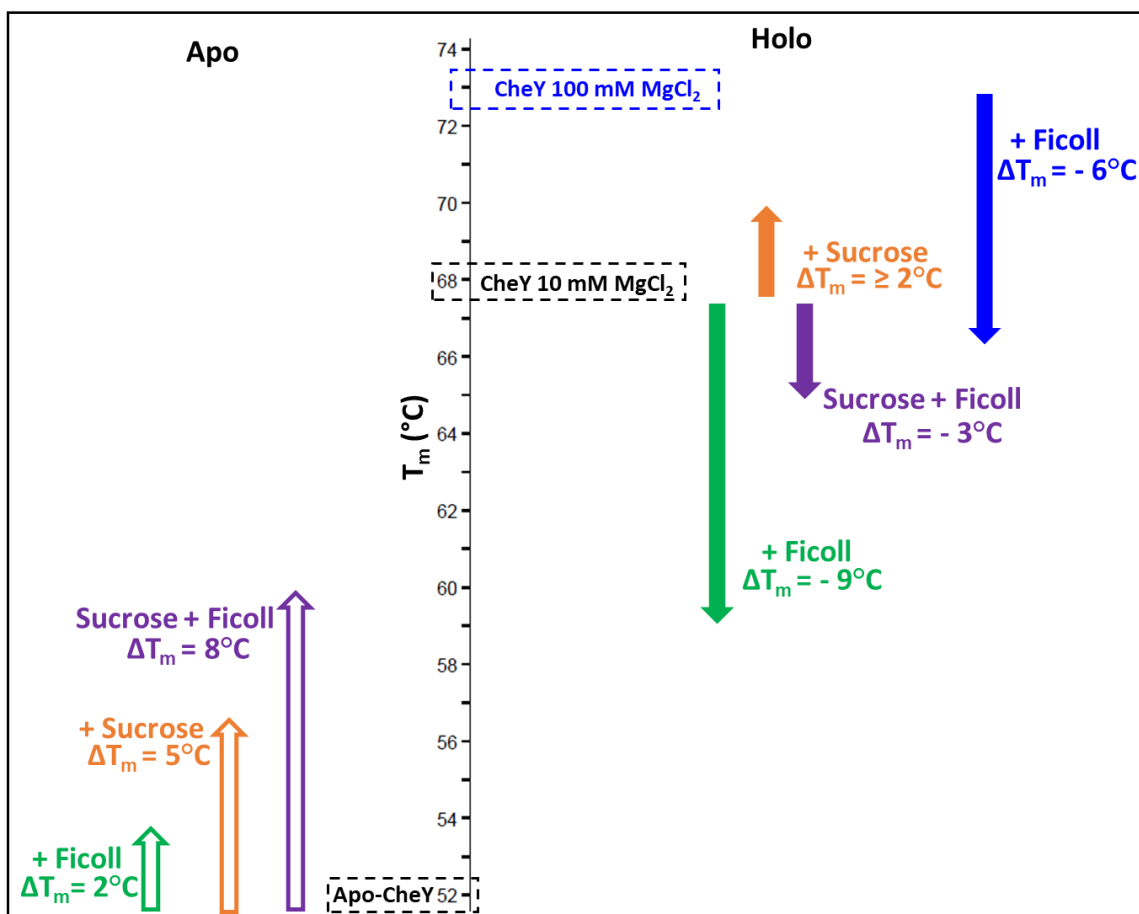


Figure 4.6: Schematic representation of the variation in measured T_m of the apo and holo forms in the absence and presence of Ficoll and sucrose. The box in the dashed line denotes the measured T_m values of apo Che Y and holo CheY in 10 and 100 mM $MgCl_2$ and serve as the reference points to guide the upward and downward trend of the T_m . The coloured arrows indicate the increase or decrease in the measured T_m with respect to the reference points. Open arrows represent T_m for apo CheY, and filled arrows represent T_m for holo CheY.

Therefore, at > 5 mM $MgCl_2$ concentration, the holo forms could dominate the conformational equilibrium. The support for this conjecture comes from NMR studies performed on CheY in the presence of $MgCl_2$ (Moy *et al.*, 1994). The appearance of backbone NMR cross peaks that were otherwise invisible in the 5 mM 1H - ^{15}N -HSQC spectrum due to conformational equilibria and exchange broadening (Moy *et al.*, 1994) appear at a higher concentration of $MgCl_2$, implying the predominance of holo forms at higher concentrations of $MgCl_2$. Based on this, we speculate that macromolecular crowding affects the population of apo and holo forms. In the absence of crowder, the metal binding converts the apo to holo form, and the predominant population is the holo form. In the presence of Ficoll, the reduced T_m strongly suggests that the predominant population is not the holo forms, and an equilibrium between apo and holo forms will exist. The crowder-concentration dependence of T_m supports the notion that the extent of population distortion differs in the presence of 100 and 200 mg/mL Ficoll. Interestingly, a T_m value of 67°C is observed in the presence of Ficoll when the magnesium concentration is increased to 100 mM $MgCl_2$. This value coincides with the T_m for CheY in the absence of Ficoll at 10 mM $MgCl_2$. This suggests that a very high concentration of $MgCl_2$ forces the equilibrium towards predominantly holo form. This is consistent with the theoretical predictions from Molecular dynamics simulations Dong *et al.*, (Dong, Qin and Zhou, 2010) based the observations from simulations on a set of 7 proteins that exist in open (apo) and closed (holo) conformation suggest that crowding can affect the populations of the open and closed conformational states (Dong, Qin and Zhou, 2010). The results also suggested that, the compact or closed state conformations will be preferred in a crowded environment if an equilibrium between conformational states exists (Dong, Qin and Zhou, 2010). Further, we performed the same thermal denaturation experiment in the presence of 2 M urea. From literature we know

that for CheY, 2 M urea does not unfold the protein as this concentration lies in the native baseline of the chemical denaturation using urea reported earlier (Filimonov *et al.*, 1993; Kathuria *et al.*, 2008). Figure 4.7 represents the thermal melts performed in the presence and absence of crowder with 2 M urea.

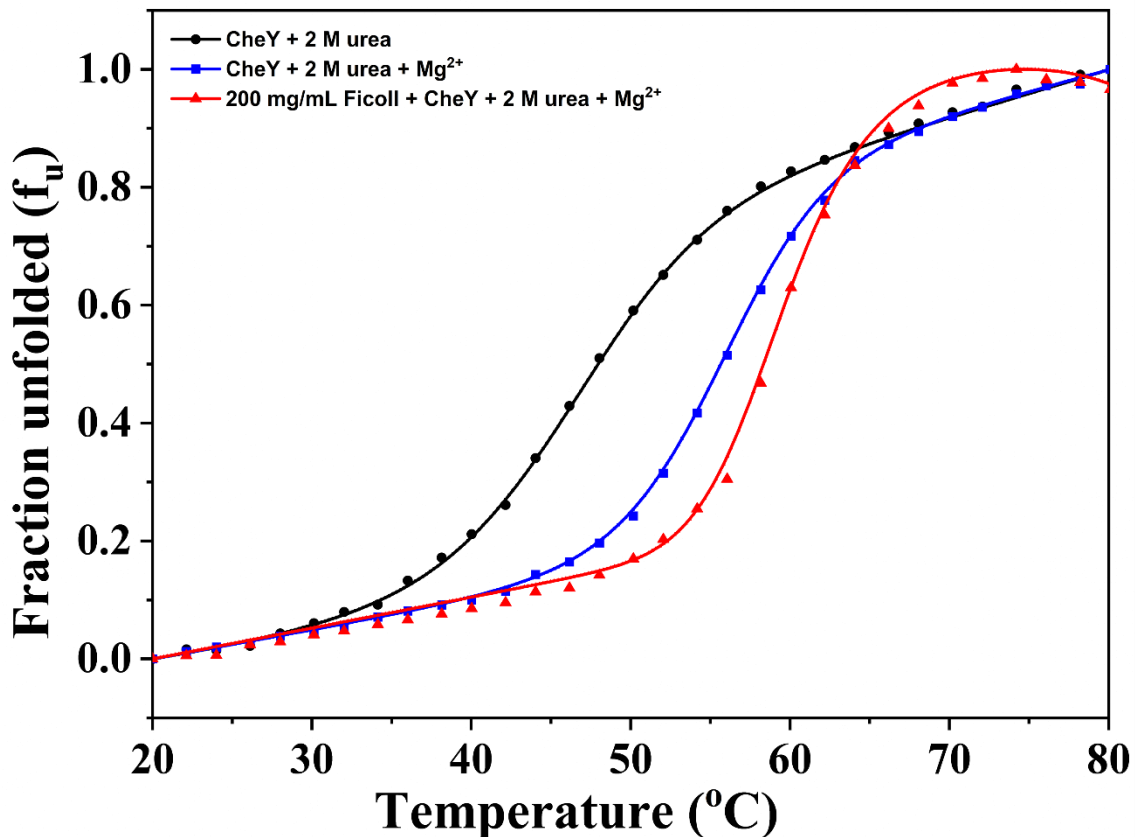


Figure 4.7: Thermal denaturation profiles of holo form of CheY. In dilute buffer, in 200 mg/mL Ficoll and in the combined presence of 2 M urea and 200 mg/mL Ficoll. The lines joining the points correspond to a fit to a two-state, folded-unfolded form of the protein. The thermal transitions were not reversible. The concentration of MgCl_2 was maintained at 10 mM. Although data were recorded at 1°C interval, for the purpose of representation the data are plotted at 2°C interval.

We report a T_m value of 46°C for apo CheY in the presence of 2 M urea which is in line with the T_m value reported earlier (Filimonov *et al.*, 1993). This T_m value increases from 46 to 56 in 10 mM MgCl_2 . The noteworthy point is that the ΔT_m obtained in the absence of 2 M urea ($\Delta T_m = 16^\circ\text{C}$) is higher than that obtained with 2 M urea. In the combined presence of 2 M urea and Ficoll, an increase in the T_m value from 55 to 59°C ($\Delta T_m = 4^\circ\text{C}$) is observed, which is greater

than the T_m of holo CheY in dilute buffer with 2 M urea. In the presence of 2 M urea the protein does not unfold and has a sub optimal metal binding ability indicated by intermediate ΔT_m value. In such a situation the population of protein species is inclined towards metal unbound state. Therefore, in the presence of 2 M urea the predominant population can be apo form. The finding of increased T_m of holo protein in crowded conditions, strengthens the view that when the population of apo forms is higher, the observed effect of crowding by Ficoll is stabilizing in nature. Thus, emphasizing selective destabilization of holo form by Ficoll. It was also highly relevant in this context to note that *E. coli* prolyl-transfer RNA synthetase, in its substrate bound form undergoes a significant conformational change and crowding effects that conformational equilibrium favouring the compact forms. The preferential exclusion of the crowders from the protein's surface altered the conformational ensemble and stabilised the protein's compact state (Adams *et al.*, 2019).

Is this reduction in T_m only a consequence of disruption of apo-holo equilibrium due to Ficoll induced crowding? Literature indicates that Ficoll 70 is heterogeneous in nature and contains a weak negative charge on about 50% of its macromolecular component (Zhu *et al.*, 2001). Since CheY displays a metal ion concentration-based increase in the thermal stability it becomes important to consider the possibility of metal ion sequestration by the charged component of Ficoll. If Ficoll sequesters metal ions from the buffer than the available concentration of magnesium would be less than expected leading to a reduction in T_m . To explore the possibility of sequestration, a set of specific experiments were designed and conducted. (i) Thermal stability in the presence of increasing concentration of Mg^{2+} ions at constant protein and Ficoll concentration, and (ii) thermal stability of holo CheY in Ficoll in the presence of high ionic strength buffer (Figure 4.8A and B represent thermal stability curves, respectively). From figure 4.8A, it was observed that the thermal stability of holo CheY in Ficoll increased up to 5 mM $MgCl_2$ concentrations.

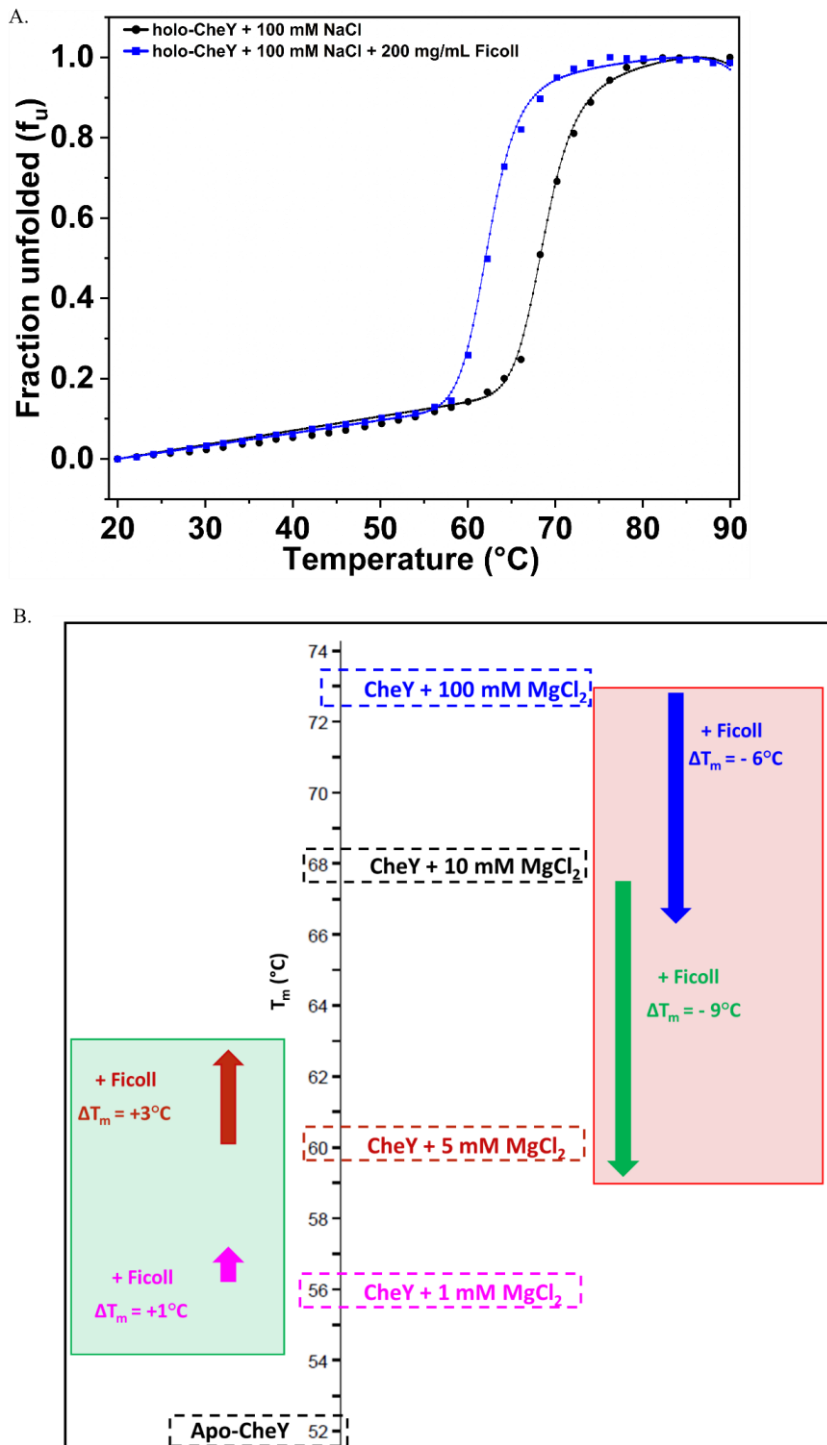


Figure 4.8: (A) Thermal denaturation profiles of holo form of CheY. In dilute buffer + 100 mM NaCl and in 100 mM NaCl + 200 mg/mL Ficoll. The lines joining the points correspond to a fit to a two-state, folded-unfolded form of the protein. The thermal transitions were not reversible. The concentration of MgCl_2 was maintained at 10 mM. Although data were recorded at 1°C interval, for the purpose of representation the data are plotted at 2°C interval. (B) Schematic representation of the variation in measured T_m of holo forms in the absence and presence of Ficoll. The box in the dashed line denotes the measured T_m values of holo CheY in 1, 5, 10 and 100 mM MgCl_2 and serve as the reference points to guide the upward and downward trend of the T_m . The coloured arrows indicate the increase or decrease in the measured T_m with respect to the reference points. The shaded region in green indicates stabilizing upward trend and red indicates destabilizing downward trend in T_m .

The reduction in the T_m was only observed for concentrations > 5 mM $MgCl_2$. If Mg^{2+} sequestration was interfering in reduction of T_m it should have been more evident at the lower concentrations of Mg^{2+} . If Ficoll sequesters Mg^{2+} ions the T_m in the presence of Ficoll in such a case should be less than the value obtained in dilute buffer at same Mg^{2+} concentrations. For example, the T_m at 5 mM $MgCl_2$ for dilute buffer is $60^\circ C$ and in the presence Ficoll is $63^\circ C$. Since we get a positive ΔT_m value for the lower concentrations the possibility of sequestration of Mg^{2+} by charged part of Ficoll can be ruled out. It should also be noted that this trend changing T_m (decrease or increase) is nonlinear with respect to Mg^{2+} concentration. Yet another interesting observation was that this experiment also reinforced the hypothesis of selective destabilization of holo part. As pointed out earlier, holo population predominates only at higher concentrations of $MgCl_2$ (Moy *et al.*, 1994), at lower concentration the majority of the population is apo form and the effect of Ficoll on the apo form is stabilization, similar to what was observed up to 5 mM. Further probing into the sequestration by Ficoll, the negative charge on Ficoll can be masked by using a buffer with high ionic strength for example like addition of high concentrations of NaCl. It has been reported earlier that addition of 100 mM NaCl neutralizes the charge on Ficoll and gave a single peak in size exclusion chromatography (Zhu *et al.*, 2001). The same strategy was employed to test the hypothesis of Mg^{2+} sequestration by Ficoll. Thermal stability of holo CheY with Ficoll was performed in the presence of 100 mM NaCl (Figure 4.8B). It was observed that the reducing trend of thermal stability for holo CheY was still observed in the presence of 100 mM NaCl. The native holo protein yielded a T_m value of $69^\circ C$, slightly higher than in the absence of 100 mM NaCl. It should be noted that increasing ionic strength has a stabilizing effect on the protein (Filimonov *et al.*, 1993). However, the T_m in the presence of 200 mg/mL Ficoll reduces to $62^\circ C$, yielding a ΔT_m value of $-7^\circ C$ which is comparable to $\Delta T_m = -9^\circ C$, obtained in the absence of 100 mM NaCl. Owing to the fact that protein is stabilized in the presence of NaCl, a $2^\circ C$ difference can be explained. The NMR

spectra of holo CheY obtained also indicates that the amount of Mg^{2+} fairly remains the same in the presence of Ficoll as the spectrum in the presence of Ficoll exactly overlays the one obtained in the absence of it. It is also highly relevant in this context to note that similar apo-holo studies on a protein Repeat in toxin (RTX) reported an increase in the secondary structure and the thermal stability of the holo protein (Sotomayor-Pérez *et al.*, 2013). Taking together, the possibility of Mg^{2+} sequestration does not seem to be the phenomenon responsible for reduction in thermal stability in the presence of Ficoll, therefore the theory of apo-holo equilibrium distortion and selective destabilization of holo protein remains the most appropriate explanation for the observed decrease in the thermal stability of CheY in the presence of Ficoll. It is well established that the conformational dynamics of proteins are the key to the function and regulation of biochemical reactions. The sampling of alternative conformational states as a consequence of metal, substrate binding, phosphorylation etc., is linked to the activity of the many proteins as indicated by the studies carried in the presence of dilute buffers. The effect on the equilibrium between the sampled states can be differently affected in the context of crowding. The crowding scenario can potentially re-sculpt the conformational and functional landscape. And in fact, the effect can be protein, conformational form and crowder dependent. Future work on the role of intracellular crowding on how the conformational states are manipulated and its consequence on binding and activity is required to derive a quantitative assessment.

4.2.7 Can the modulation of population of apo and holo forms be specific to Ficoll only?

It is evident from our experiments that Ficoll 70 can alter the apo-holo equilibrium of CheY and selectively destabilize the holo form of the protein. It is now highly relevant to check whether this phenomenon is specific to Ficoll or whether any other carbohydrate-based macromolecular crowders can also yield similar results. To test this hypothesis, Dextran – a glucose-based polymer with different molecular weights, was used to elucidate the effect of

crowding on the structure and stability of CheY. We report that both Dextran 40000 and 70000 both affected the secondary structure of CheY at a concentration of 100 mg/mL, as observed from the far UV-CD spectra recorded in the presence and absence of Dextran. However, the changes observed in the far UV-CD spectra of CheY (Figure 4.9 and 4.10) were not reproducible even at this concentration. Similarly, higher volume fractions showed no specific stabilizing or destabilizing trend. One possible explanation for the observed results is that Dextran based crowders aid in forming higher order species of the apo protein or induce an aggregation prone species of the protein in a crowded environment. A molten globule state was ruled out, as the protein still displayed a fluorescence emission spectrum with a similar λ_{max} value but has a reduced emission intensity. This reduction in intensity also limits the dynamic fluorescence measurements. The reduction in the mere intensity without any chromic shifts indicates a change in polarity of the solvent due to the addition of these polymer. Since the CD signal was not consistent in the experiments performed individually at different times, the thermodynamic stability in the presence of Dextran 40000 and 70000 was not probed further. Figure 4.9 and 3.10 display the far UV-CD spectra recorded in the presence of Dextran 40000 and 70000, respectively, at two instances to highlight the variation observed in the data.

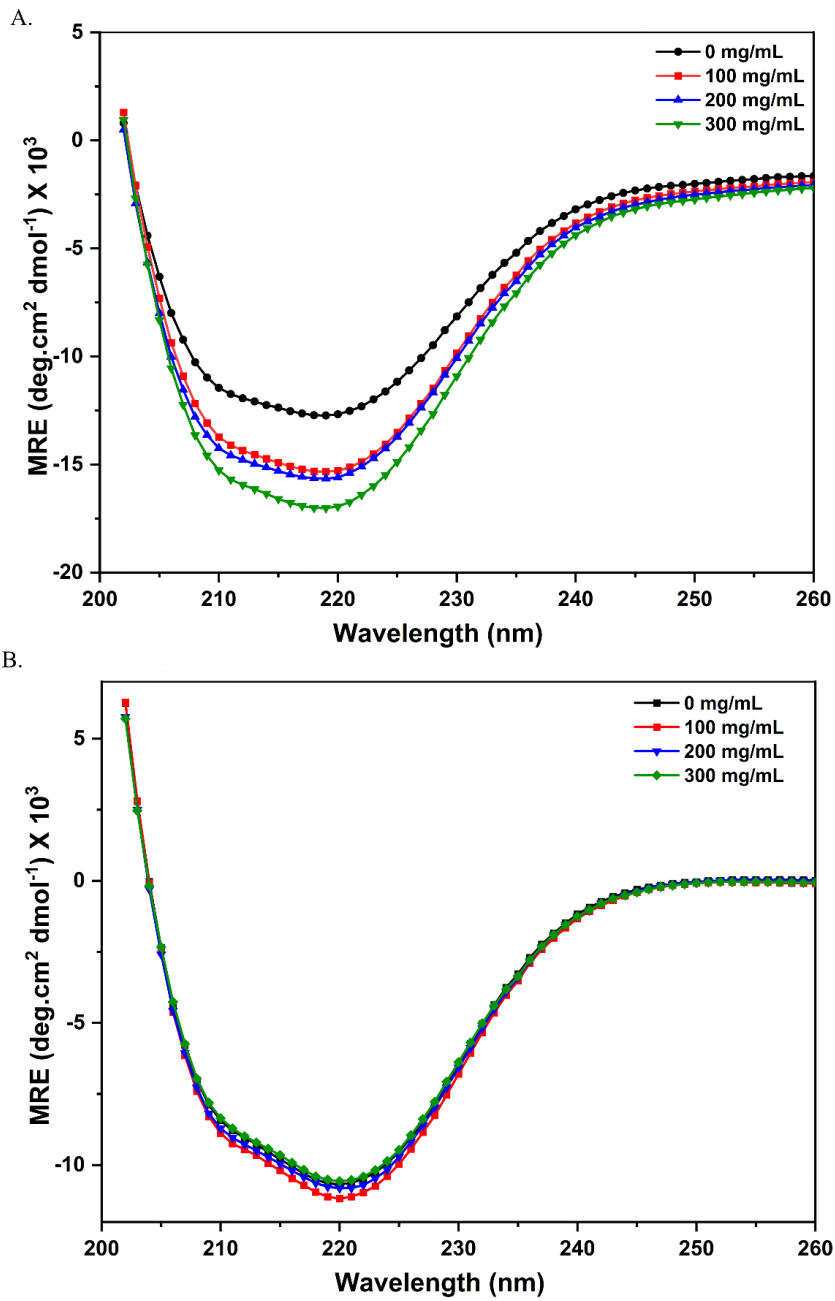


Figure 4.9: Far UV-CD spectra of apo CheY in the presence and absence of (A) Dextran 40000 and (B) Dextran 70000. (Attempt 1)

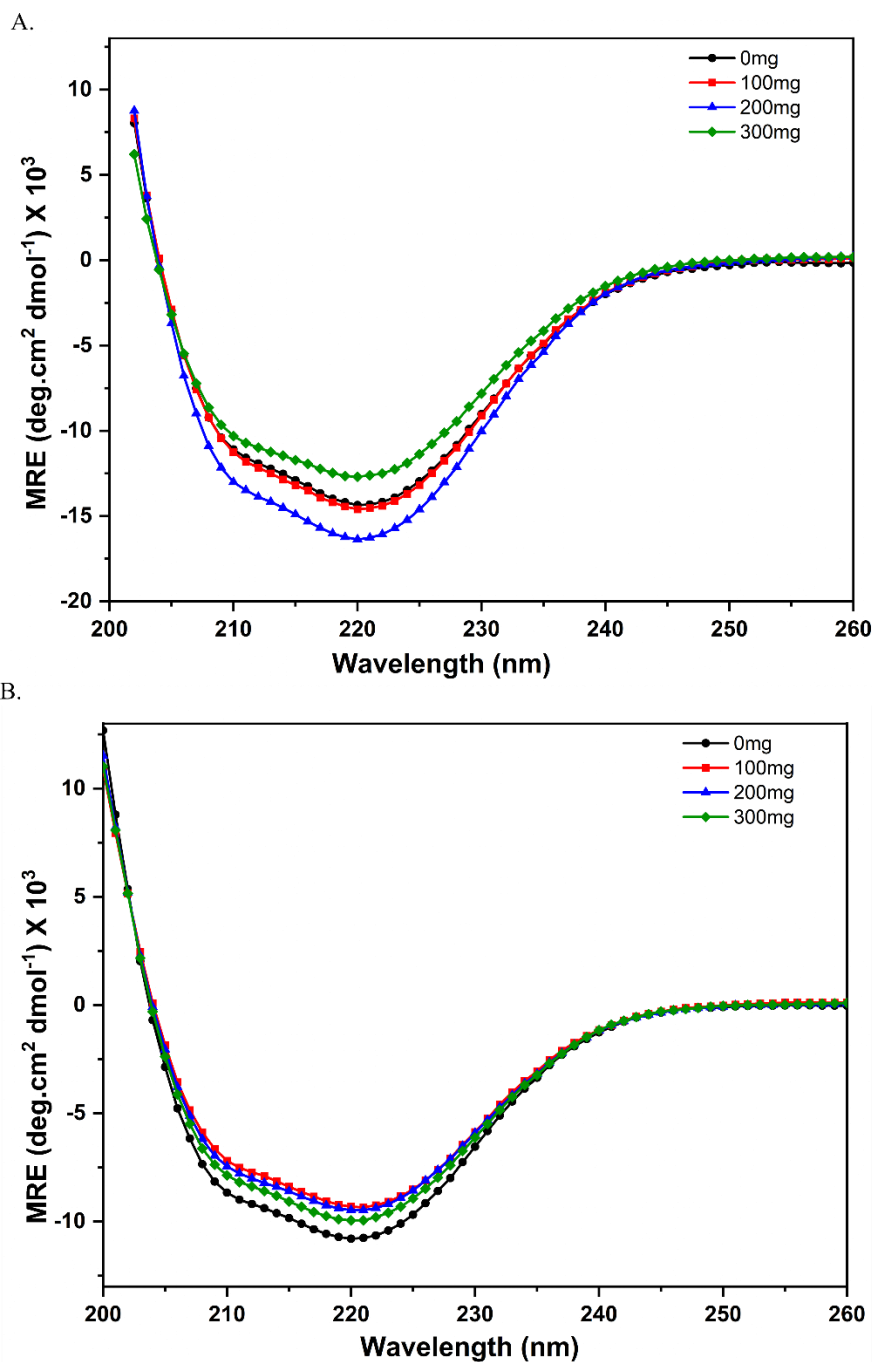


Figure 4.10: Far UV-CD spectra of apo CheY in the presence and absence of (A) Dextran 40000 and (B) Dextran 70000. (Attempt 2)

As the molten globule state was not an appropriate reason for the results obtained, we performed the same experiments with Dextran 40000 and 70000 in the presence of 2 M urea. For CheY, 2 M urea prevented protein aggregation at higher temperature. If Dextrans were able to induce this state in CheY at room temperature addition of 2 M urea should solve the inconsistency observed in the spectral signal in the far UV region. Figure 4.11 and 4.12 show

the effects of Dextran 40000 and 70000, respectively, on the secondary structure of CheY in the presence of 2 M Urea.

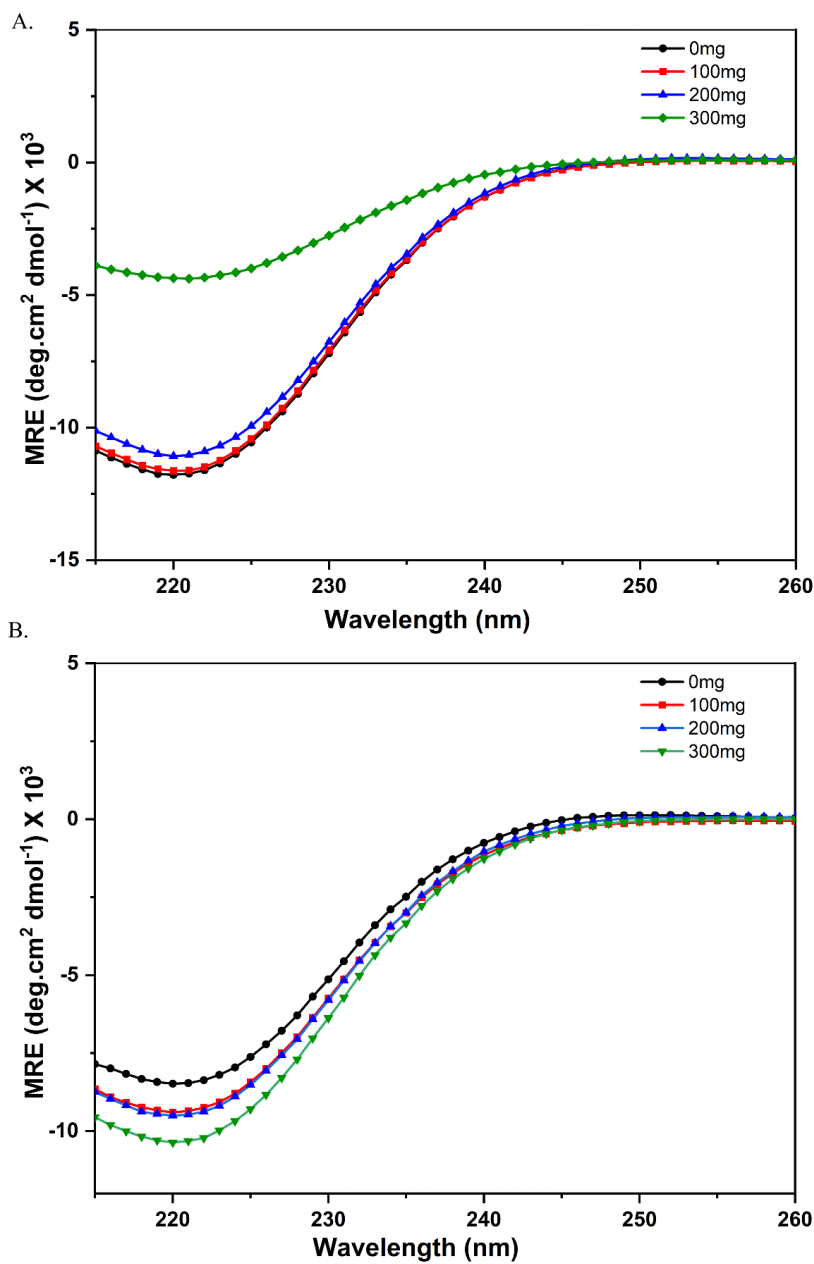


Figure 4.11: Far UV-CD spectra of apo CheY with 2 M urea in the presence and absence of (A) Dextran 40000 and (B) Dextran 70000. (Attempt 1)

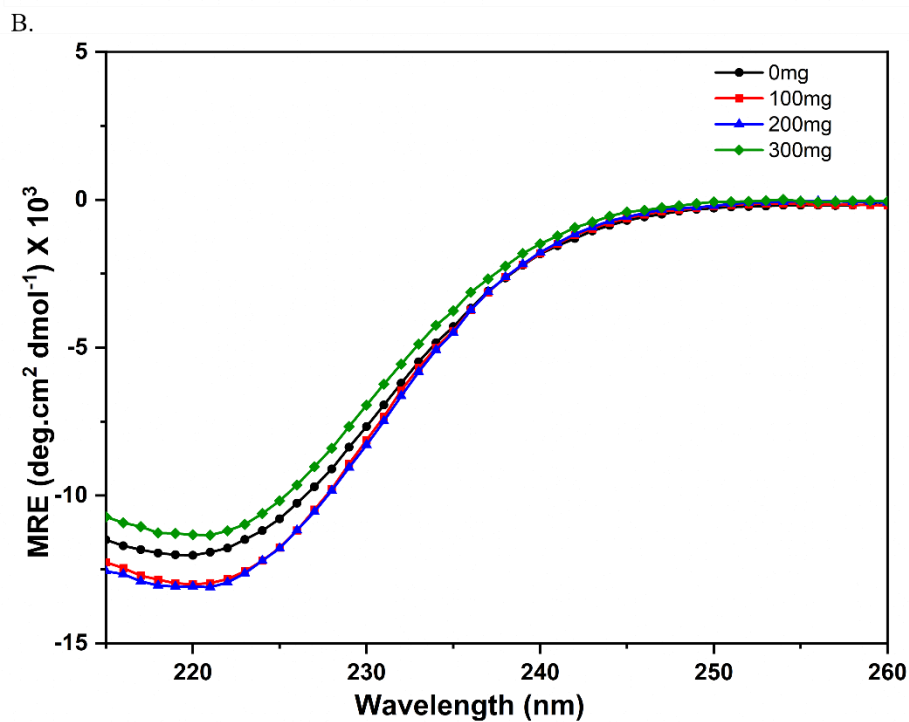
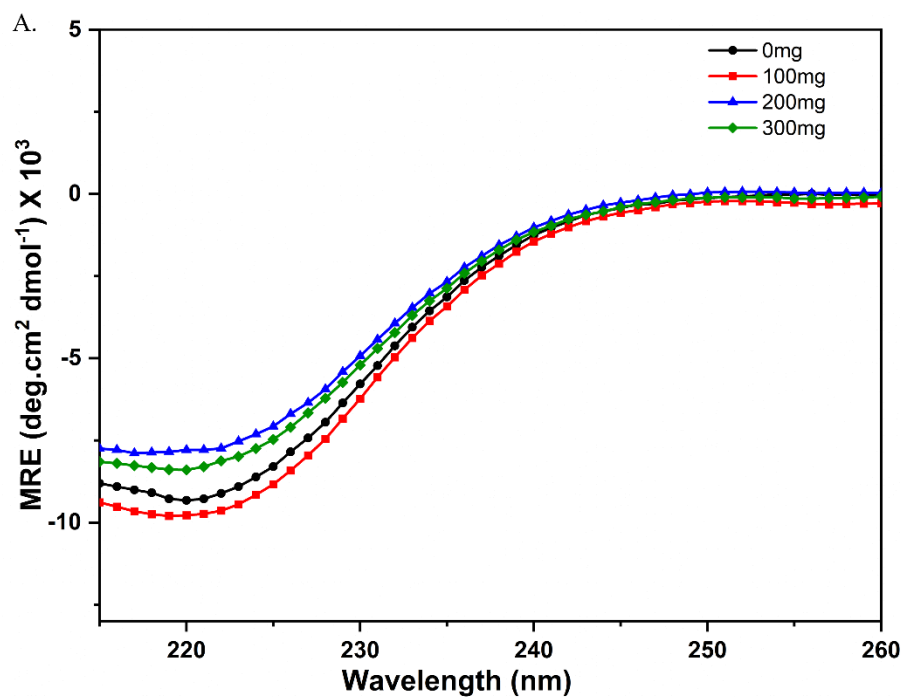


Figure 4.12: Far UV-CD spectra of apo CheY with 2 M urea in the presence and absence of (A) Dextran 40000 and (B) Dextran 70000. (Attempt 2)

Even in the presence of 2 M urea, no constant trend in the signal was observed at any volume fraction of the crowder used. Figures 4.11 and 4.12 clearly indicate that the spectra obtained from independent experiments, represented in A and B, do not reflect any trend. Hence, attempts to measure thermal stability in Dextran 40000 and Dextran 70000 were not made.

Since higher molecular weights were not a good choice for CheY, Dextran 6000 was used as another crowder for these studies. Figure 4.13 shows the far UV-CD spectra recorded in the presence and absence of Dextran 6000 for the apo protein.

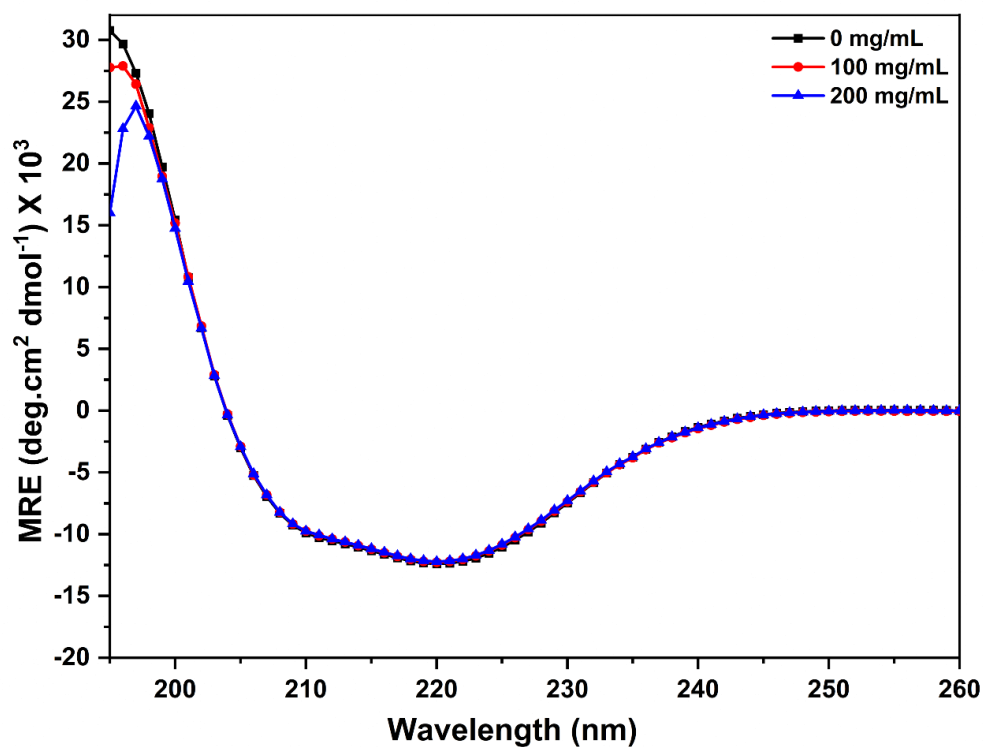


Figure 4.13: Far UV-CD spectra of apo CheY in the presence and absence of Dextran 6000

The spectra indicate a near overlap with the spectra recorded in the absence of Dextran 6000. No change in the spectral signal can be inferential of no effect on the secondary structure of apo CheY in the presence of Dextran 6000. These results were reproducible, unlike those for Dextran 40000 and 70000. This became the premise for further testing the protein for changes in thermal stability in the presence of Dextran 6000. Thermodynamic stability was measured for protein in the presence and absence of the crowder (Figure 4.14).

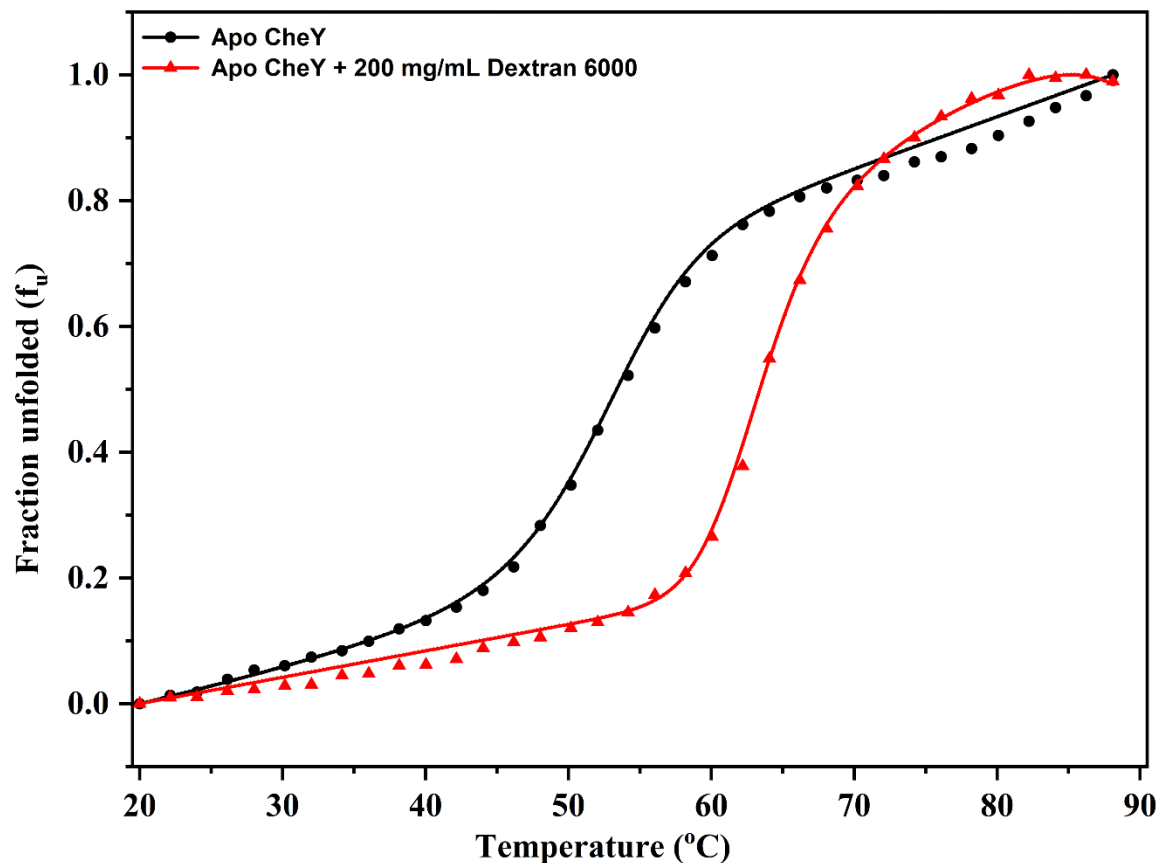


Figure 4.14: Thermal denaturation profiles of apo CheY. In dilute buffer and in 200 mg/mL Dextran 6000. The lines joining the points correspond to a fit to a two-state, folded-unfolded form of the protein. The thermal transition in the presence of Dextran 6000 was not reversible. Although data were recorded at 1°C interval, for the purpose of representation the data are plotted at 2°C interval.

Under dilute buffer conditions, the thermal stability of CheY was reversible. The thermal stability (T_m) of the apo protein increased from ~52°C to ~60°C (Figure 4.14) and the two-state folding to unfolding process was irreversible. The protein samples in Dextran 6000 show visible aggregates after the temperature ramping from 20-90°C is performed, unlike any other carbohydrate based crowder tested with CheY (Stepanenko *et al.*, 2019). This precluded any further studies using Dextrans as crowdors. However, this leads to an interesting question. Whether the observed effect of Dextran was due to the polymeric or chemical nature? To gain insights, glucose was used as molecular crowder to elucidate the effect on structure and stability of CheY. The apo protein showed an increase in the thermal stability from 52°C to ~56°C (Figure 4.15).

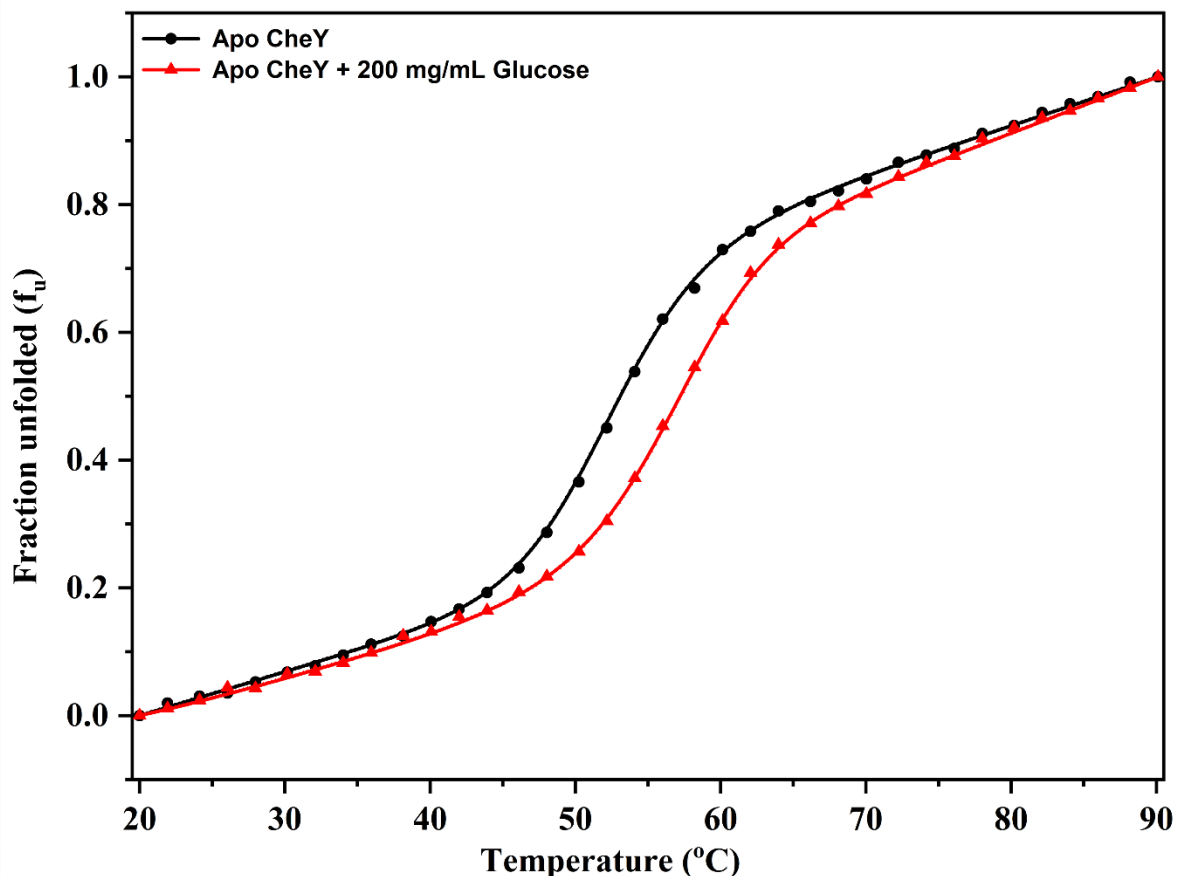


Figure 4.15: Thermal denaturation profiles of apo CheY. In dilute buffer and in 200 mg/mL glucose. The lines joining the points correspond to a fit to a two-state, folded-unfolded form of the protein. Although data were recorded at 1°C interval, for the purpose of representation the data are plotted at 2°C interval.

Similar to dilute buffer conditions, the unfolding mechanism follows a two-state model and the denaturation was reversible. The increase in the thermal denaturation temperature and other thermodynamic parameters indicate preferential hydration mode of stabilization. At the molecular level, stabilization can be explained as an optimization of hydrogen bonds as a consequence of Ficoll-induced distortion in the hydrogen bond network of hydration water of protein (Poddar *et al.*, 2008; Senske *et al.*, 2014). These results are similar to those observed for CheY in the presence of sucrose. Similarly, the effect of glucose on the holo form of CheY was also tested. The midpoint of the thermal denaturation increased from 67°C to ~73°C (Figure 4.16).

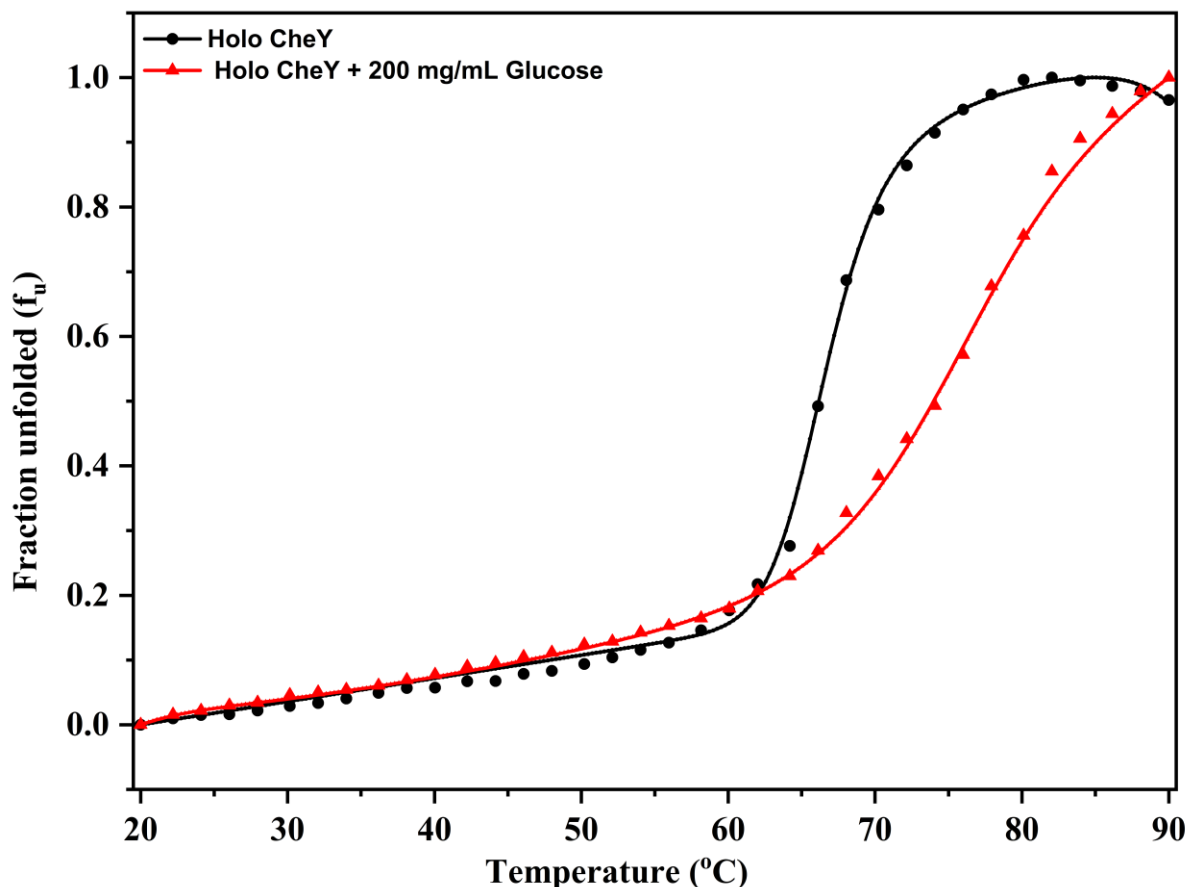


Figure 4.16: Thermal denaturation profiles of holo CheY. In dilute buffer and in 200 mg/mL glucose. The lines joining the points correspond to a fit to a two-state, folded-unfolded form of the protein. The thermal transitions were not reversible. Although data were recorded at 1°C interval, for the purpose of representation the data are plotted at 2°C interval.

The unfolding process was incomplete as we do not obtain a complete unfolding baseline. Hence an increase in T_m can be reported and the increased T_m in the presence of 200 mg/mL of glucose would be at least 73°C. These results were similar to those obtained for holo CheY in the presence of sucrose. Thermal denaturation was also performed in the presence of Ficoll and glucose on both the apo and holo forms of CheY (Figure 4.17).

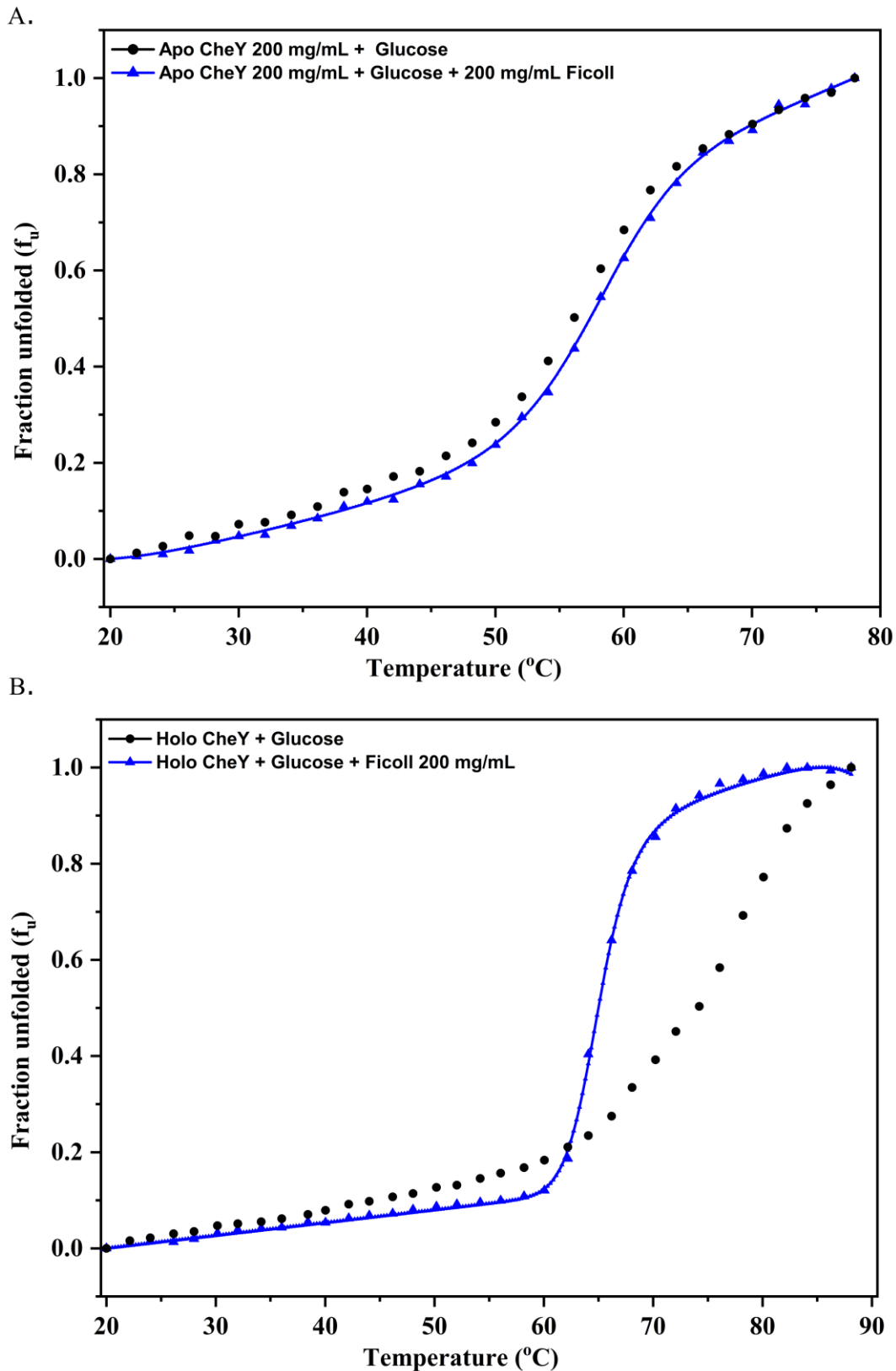


Figure 4.17: Thermal denaturation profiles of (A) apo CheY in dilute buffer and in 200 mg/mL glucose with and without Ficoll 200 mg/mL. (B) holo CheY in dilute buffer and in 200 mg/mL glucose with and without Ficoll 200 mg/mL. The lines joining the points correspond to a fit to a two-state, folded-unfolded form of the protein. Although data were recorded at 1°C interval, for the purpose of representation the data are plotted at 2°C interval.

The reduction in thermal stability was similar to in the value obtained in the combined presence of Ficoll and glucose. However, such a combination was not possible with Dextran, as the results were inconsistent, as discussed above.

4.3 Conclusion

This study led to the following conclusions: the effect of macromolecular crowding (Ficoll), molecular crowding (sucrose) and a mixture of both on the apo form of CheY remains the same. The apo form of CheY was slightly stabilized, as evidenced by the positive ΔT_m and $\Delta\Delta H^\circ$ values. A similar stabilization was observed for holo CheY in the presence of sucrose and glucose alone. However, the trend was reversed in the presence of Ficoll, in the combined presence of Ficoll, and sucrose and in the combined presence of glucose and Ficoll. This observation strongly suggests that the destabilizing effect is macromolecular (Ficoll) in nature (Das and Sen, 2020; Hishida *et al.*, 2022). We also conclude that Dextran may not be suitable crowders for CheY. The inconsistency in the data, along with a miniscule change in thermal stability, supports our statement. Dextran 6000 shows a change in mechanism of thermal denaturation for the apo form of CheY and makes it irreversible, precluding further studies on it. Since metal binding is retained in the presence of Ficoll, as indicated by intrinsic tryptophan fluorescence quenching study, and Mg^{2+} sequestration by Ficoll was systematically ruled out, the observed reduction in thermal stability can only imply that macromolecular and not molecular crowding modulates the population of apo and holo forms of CheY.

Chapter 5

Molecular Insights on the Origin of the Effects of Crowding Using NMR Spectroscopy

5.1 Introduction

5.1.1 NMR Spectroscopy based protein back bone assignments

Among the available spectroscopic techniques nuclear magnetic resonance spectroscopy is the most powerful technique for analyzing protein structure, function, and dynamics. Assignment of resonances in an NMR spectrum is the most crucial step in understanding the structure, function, and dynamics of proteins. In the early 1900s, determination of protein structure using NMR was only performed using a one-dimensional technique. It was not until the late 1970s that two-dimensional pulse sequence like correlated spectroscopy (COSY) and nuclear Overhauser effect spectroscopy (NOESY) were introduced, which increased the resolution of NMR-based structure assignment (Aue, Bartholdi and Ernst, 1976; Jeener *et al.*, 1979). A systematic method was developed for the assignment of 2D NMR spectra based on the amino acid sequence of the protein. This is known as the sequential assignment method (Billeter, Braun and Wüthrich, 1982; Wüthrich *et al.*, 1982; Wüthrich, 1986). The development of techniques such as ^{15}N uniform labelling has led to a further increase in the resolution of this sequence-based assignment method (Marion *et al.*, 1989; Messerle *et al.*, 1989). Development of double labelling in the late 1990s, gave rise to new strategies for backbone assignments based solely on through bond scalar couplings; this again increased the sensitivity of the sequence-based method and also the molecular weight limit suitable for the process (Ikura, Kay and Bax, 1990; Kay *et al.*, 1990). The current strategy of protein NMR assignments is now completely based on the triple resonance techniques that solely relies on through-bond ^1J and ^2J spin-spin coupling. The ultimate goal of obtaining the secondary structure information and torsion angles can be achieved through double labelled and triple resonance experiments.

5.1.2 ^1H - ^{15}N Heteronuclear Single Quantum Coherence spectroscopy (^1H - ^{15}N HSQC) : As fingerprint of the protein

The Majority of triple resonance experiments used in sequential assignment contain a ^1H - ^{15}N HSQC element (Bodenhausen and Ruben, 1980; Akke, Carr and Palmer, 1994). Each cross-peak in the HSQC spectrum arises from a bond between the ^1H - ^{15}N coupling (~ 90 Hz). The HSQC becomes a ‘fingerprint’ of the protein as all amino acids, except proline, give rise to a peak in the spectrum. This pulse sequence also gives rise to peaks for some sidechain nitrogens of Asn, Arg, Gln, His, Lys and Trp. If the number of peaks exceeds the expected number, it can possibly imply impurities or protein degradation. Degradation of the protein usually generates new peaks in the range of ~ 7.7 - 8.2 and 127 - 130 ppm.

5.1.3 Triple resonance assignment method

This method demands for a $>95\%$ pure and double labelled ($^{15}\text{N}/^{13}\text{C}$) protein. This method completely relies on ^1J and ^2J coupling to extract information about the self and adjacent amino acids. The triple resonance spectrum generally correlates ^1H - ^{15}N with one or more ^{13}C chemical shifts. The naming convention of these triple-resonance experiments follows a certain nomenclature. For instance, an experiment like 3D-HNCO correlates the backbone pair with the carbonyl carbon of the preceding residue. Any experiment in which if an atom is placed in parenthesis means that the chemical shift for that particular atom will not be determined, but it will be used to transfer the coherence. For example, HN(CO)CA, the backbone ^1H - ^{15}N , is correlated with the $^{13}\text{C}\alpha$ of the preceding residue; the chemical shift of $^{13}\text{C}\alpha$ is measured, but that of ^{13}CO is not. For sensitivity, triple-resonance experiments are initiated with a ^1H pulse. The signal is detected during the acquisition period. ^{15}N and ^{13}C are measured in indirect dimension. Triple-resonance experiments are mainly of two categories: i) out-and-back and ii) straight through. In the out-and-back type of experiments, the proton spin that is initially excited is the one that is detected. For instance, in HNCO, the sequence starts with ^1H , transfers to ^{15}N ,

and then to ^{13}CO . ^{13}CO is frequency labelled as t_1 , followed by a transfer back to ^{15}N , which is labelled t_2 , followed by a last transfer back to ^1H , which is labelled t_3 . Therefore, the resulting 3D-HNCO has ^1H information in F_3 , ^{15}N in F_2 , and ^{13}CO in F_1 . The straight-through experiments sequence starts with ^1H - ^{13}C HSQC, in which either ^{13}C or ^1H information is available in F_1 . The spin system information is obtained from the $C\alpha$ and $C\beta$ values. Visualization of this 3D dataset is usually performed by plotting the 2D ^1H - ^{13}C planes for a particular ^{15}N ppm value. The triple resonance spectra for a particular ^{15}N value contains only one or two peaks per residue; these peaks correlate ^1H and ^{15}N to one or more ^{13}C chemical shifts. A detailed description of the standard set of triple resonance experiments are provided below.

4.1.3.1 HN(CO)CA

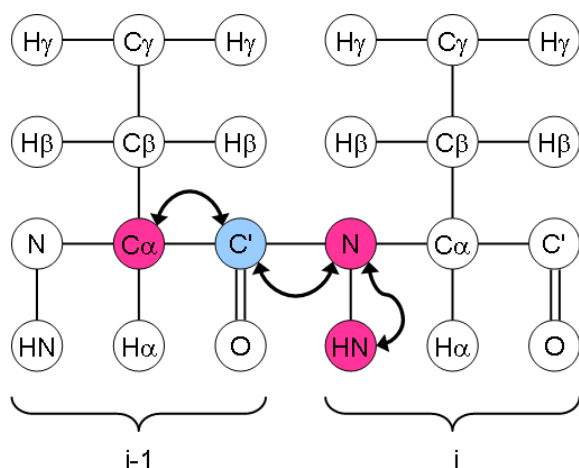


Figure 5.1: Schematic representation of the coherence transfer in HN(CO)CA

The magnetization is passed from ^1H to ^{15}N , and then to ^{13}CO . From here on, it is transferred to $^{13}\text{C}\alpha$, and a chemical shift is evolved for detection. The magnetization is transferred back to ^{15}N and then to ^1H via ^{13}CO . Chemical shifts are only evolved for ^1H , ^{15}N , and $^{13}\text{C}\alpha$. This spectrum contains information of $^{13}\text{C}\alpha$ of the preceding residue (Figure 5.1) (Kay et al., 1990; Bax and Ikura, 1991).

4.1.3.2 HN(CA)CO

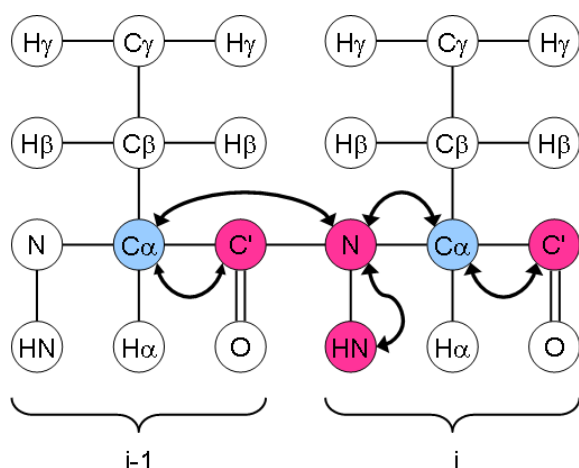


Figure 5.2: Schematic representation of the coherence transfer in HN(CA)CO

The magnetization is transferred from ^1H to ^{15}N and then to ^{13}C through the N-C α J-coupling. From there it is further transferred to ^{13}CO via the J-coupling between $^{13}\text{C}\alpha$ - ^{13}CO . For the detection of chemical shifts, the transfer happens back via the same route and shifts are evolved for ^1H , ^{15}N and ^{13}CO omitting $^{13}\text{C}\alpha$. Since ^{15}N is coupled with both the $^{13}\text{C}\alpha$ of its own and the preceding residues, the transfer happens simultaneously. Hence, for each NH group, two carbonyl peaks corresponding to self (i) and the preceding residue (i-1) are observed. Since, the coupling between the self-residue is stronger than the preceding residue the ^{13}CO peaks for i^{th} residue is intense than the i-1 residue (Figure 5.2) (Clubb, Thanabal and Wagner, 1992).

4.1.3.3 CBCA(CO)HN

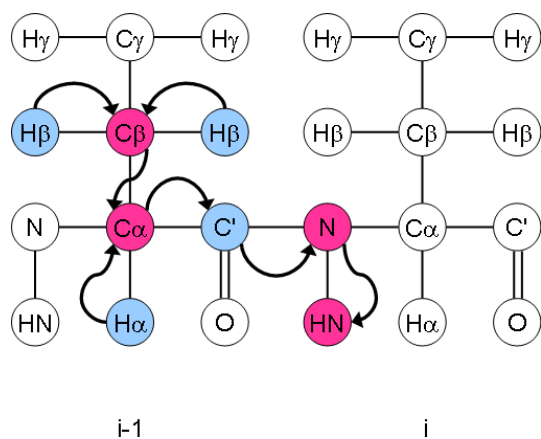


Figure 5.3: Schematic representation of the coherence transfer in CBCA(CO)HN

The magnetization is transferred from $^1\text{H}\alpha$ and $^1\text{H}\beta$ to $^{13}\text{C}\alpha$ and $^{13}\text{C}\beta$, respectively. Then from $^{13}\text{C}\beta$ to $^{13}\text{C}\alpha$. From here on, it is transferred to ^{13}CO and then to ^{15}N and then to ^1H for detection. Chemical shifts are evolved for ^1H , ^{15}N , $^{13}\text{C}\alpha$, and $^{13}\text{C}\beta$. The spectrum contains information about the $^{13}\text{C}\alpha$ and $^{13}\text{C}\beta$ of the $(i-1)^{\text{th}}$ residue (Figure 5.3) (Grzesiek and Bax, 1992b).

4.1.3.4 HNCA

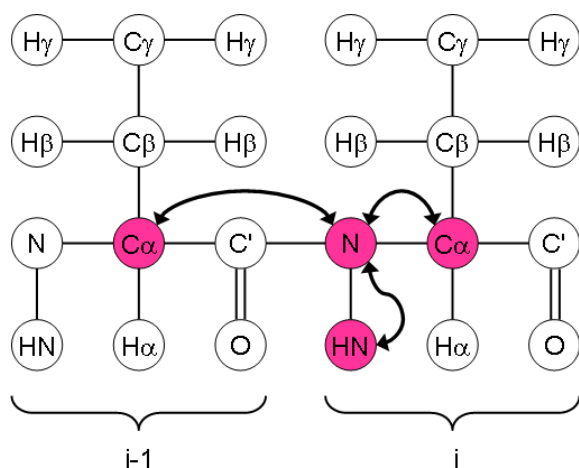


Figure 5.4: Schematic representation of the coherence transfer in HNCA

The magnetization is transferred from ^1H to ^{15}N and then to $^{13}\text{C}\alpha$ via the N-C α J-coupling. The chemical shifts are evolved for ^1H , ^{15}N , and $^{13}\text{C}\alpha$. Since ^{15}N is coupled with both the $^{13}\text{C}\alpha$ of i and $i-1$ residue, both the transfers occur simultaneously. For each NH peak the spectrum will contain information about $^{13}\text{C}\alpha$ of i^{th} and $i-1$ residue. Since the coupling between N-C α of i^{th} residue is stronger than the $i-1$ residue. This peak appears stronger in intensity on the spectrum when compared to the $i-1$ peak (Figure 5.4) (Kay *et al.*, 1990; Farmer *et al.*, 1992; Grzesiek and Bax, 1992b).

4.1.3.5 CBCANH

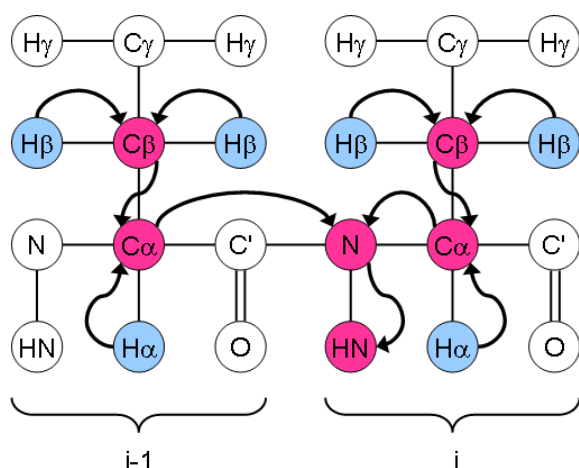


Figure 5.5: Schematic representation of the coherence transfer in CBCANH

The magnetization is transferred from $^1\text{H}\alpha$ and $^1\text{H}\beta$ to $^{13}\text{C}\alpha$ and $^{13}\text{C}\beta$, respectively. From here it is then transferred to ^{15}N and then to ^1H for detection. Magnetisation to $^{15}\text{N}_i$ comes from both $^{13}\text{C}\alpha_i$ and $^{13}\text{C}\alpha_{i-1}$. Therefore, for each NH peak the spectrum contains two C α and two C β peaks. The spectrum yields information about the $^{13}\text{C}\alpha$ i and $i-1$, $^{13}\text{C}\beta$ i and $i-1$ in one dimension along with ^{15}N and ^1H in the other two dimensions (Figure 5.5) (Grzesiek and Bax, 1992a, 1992c).

4.1.3.6 HNC0

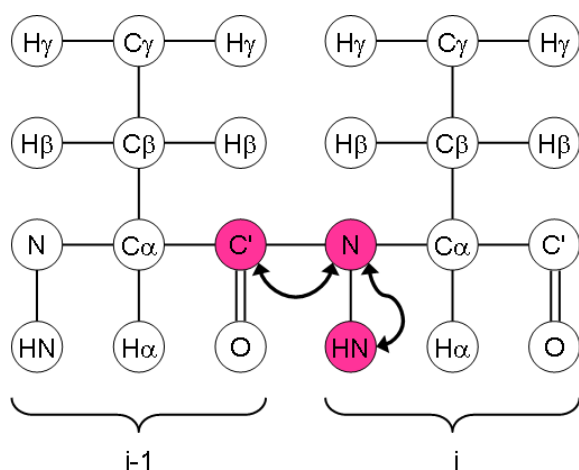


Figure 5.6: Schematic representation of the coherence transfer in HNC0

Magnetisation is passed from ^1H to ^{15}N and then selectively to the ^{13}CO via the ^{15}N - ^{13}CO J-coupling. Magnetisation is then passed back via same path for detection. The chemical shift is evolved on all three nuclei resulting in a three-dimensional spectrum. The HNC0 can be a

useful triple resonance experiment for backbone assignment in conjunction with the HN(CA)CO (Figure 5.6) (Kay et al., 1990; Grzesiek and Bax, 1992c; Muhandiram and Kay, 1994). Table 4.1 summarizes the triple resonance experiment and the corresponding nuclei's information that is obtained from the experiment.

Table 5.1: Information obtained for different nuclei from various 3D experiments.

S. No	Experiment	¹ H	¹⁵ N	CO	C α	C β
1	2D ¹ H- ¹⁵ N HSQC	i	i			
2	3D HNCO	i	i	i-1		
3	3D HN(CA)CO	i	i	i-1		
4	3D HN(CO)CA	i	i		i-1	
5	3D HNCA	i	i		i, i-1	
6	3D CBCA(CO)NH	i	i		i-1	i-1
7	3D CBCANH	i	i		i,i-1	i,i-1

5.1.4 Utilizing NMR in crowded environment

One of the crucial gaps that need to be addressed is the origin of the observed modulation due to crowding on structure, stability, dynamics, and function. The commonly used crowders, Ficoll, Dextran, and polyethylene glycols show both stabilizing and destabilizing effect depending on the protein in question. Studies that can directly pinpoint (under *in-vitro* and *in-cell*) the origin of crowding induced modulation are required. Investigation in this direction is beginning to provide direct clues on protein-crowder interactions at atomic level (Kadumuri *et al.*, 2016; Adams *et al.*, 2019; Bille *et al.*, 2019; Köhn and Kovermann, 2020). One such recent interrogation by nuclear magnetic resonance (NMR) attributed crowding induced

destabilization due to local unfolding arising from the interactions of protein's long flexible loops in superoxide dismutase. The chemical shift perturbations revealed not only protein-crowder interactions but also the site of interactions (Adams *et al.*, 2019; Bille *et al.*, 2019). In another investigation that involved monitoring NMR chemical shift perturbations and hydrogen-bonding interactions concluded that the stabilization due to crowding is due to a reduction in solvent accessibility for the residues in the loop regions of the protein (Köhn and Kovermann, 2019). In one of our previous investigations, significant reduction in the NMR signals for the residues resident in the β sheets was attributed to selective destabilization of the stable core in the presence of Ficoll (Kadumuri *et al.*, 2016). Since, crowders are highly viscous such recordings are not always possible and a lot of optimization is reacquired to obtain a good quality spectrum. In spite of the given inherent complexity of using NMR in the presence of crowders a number of studies have been published over the last decade which enabled researchers to identify the source of modulation of the effect of crowding. Benton *et al.*, proved that the extent of stabilization of chymotrypsin inhibitor-2 by sucrose and Ficoll is same by measuring the ΔG° and ΔH° of via NMR. (Benton *et al.*, 2012b). In another instance, the loop region of the protein cytochrome *c* (*cty c*) was found to show the maximum chemical shifts perturbations in the presence of 300 mg/mL PEGs. Indicating at the fact that the modulation in the stability was arising from the loop region of *cyt c* (Crowley, Brett and Muldoon, 2008).

However, data accumulated is scarce and that creates room for such similar studies with other proteins leading to an increased understanding of the effect of crowding. This chapter is an attempt to identify the source of crowding induced modulation on the apo and holo form of CheY in the presence of PEG and Ficoll. We report that the apo CheY in the presence of PEG interacts with both the hydrophobic and hydrophilic residue of CheY and perturbs the structure to such an extent that metal binding interactions are precluded. In the case of Ficoll 70, no

visible chemical shifts are reported for apo CheY leading to a belief that the protein crowder interactions can be transient in nature. However, a change in the relative signal intensity implies crowder-protein interactions. For holo CheY, certain residues display chemical shifts perturbation and additional to the residues that show line broadening in apo form certain residues show further increase in line broadening. This was interpreted as an implication towards apo holo equilibrium in the presence of Ficoll.

5.2 Results and discussion

5.2.1 Backbone assignments of CheY

Approximately 80% of the assignments were confirmed by sequentially linking the backbone assignments using the standard NMR assignment procedure from the combined information obtained from the 3-D triple resonance NMR experiments, including HNCA, HN(CO)CA, CBCA(CO)NH, and HNCACB. In addition to the backbone sequential assignment, characteristic $C\alpha$ and $C\beta$ chemical shifts were used to determine the sequence specific resonance assignments and were cross checked with those of the published spectrum (Bruix *et al.*, 1993). The published spectrum has a different amino acid sequence at the N-terminal region; hence, an exact overlap was not expected with the available data. Figure 5.7 displays the ^1H - ^{15}N TROSY-HSQC spectrum of apo CheY with the assignments labelled on it.

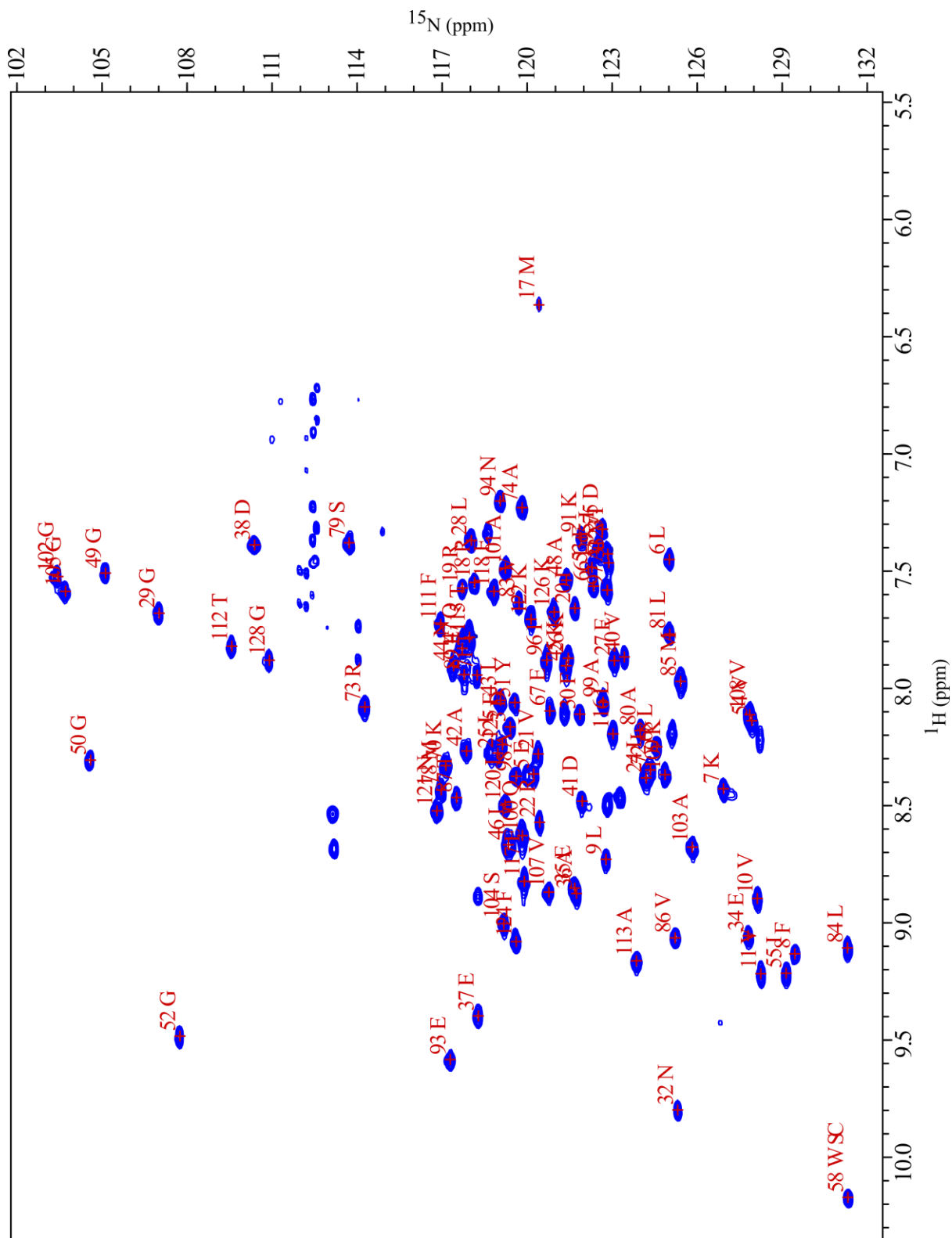


Figure 5.7: ^1H - ^{15}N TROSY-HSQC spectra of CheY in dilute buffer.

Sequence based method was used to identify the spin systems in the protein. Figure 5.8 displays a strip scope (2-D spectra of the triple resonance experiment CBCANH).

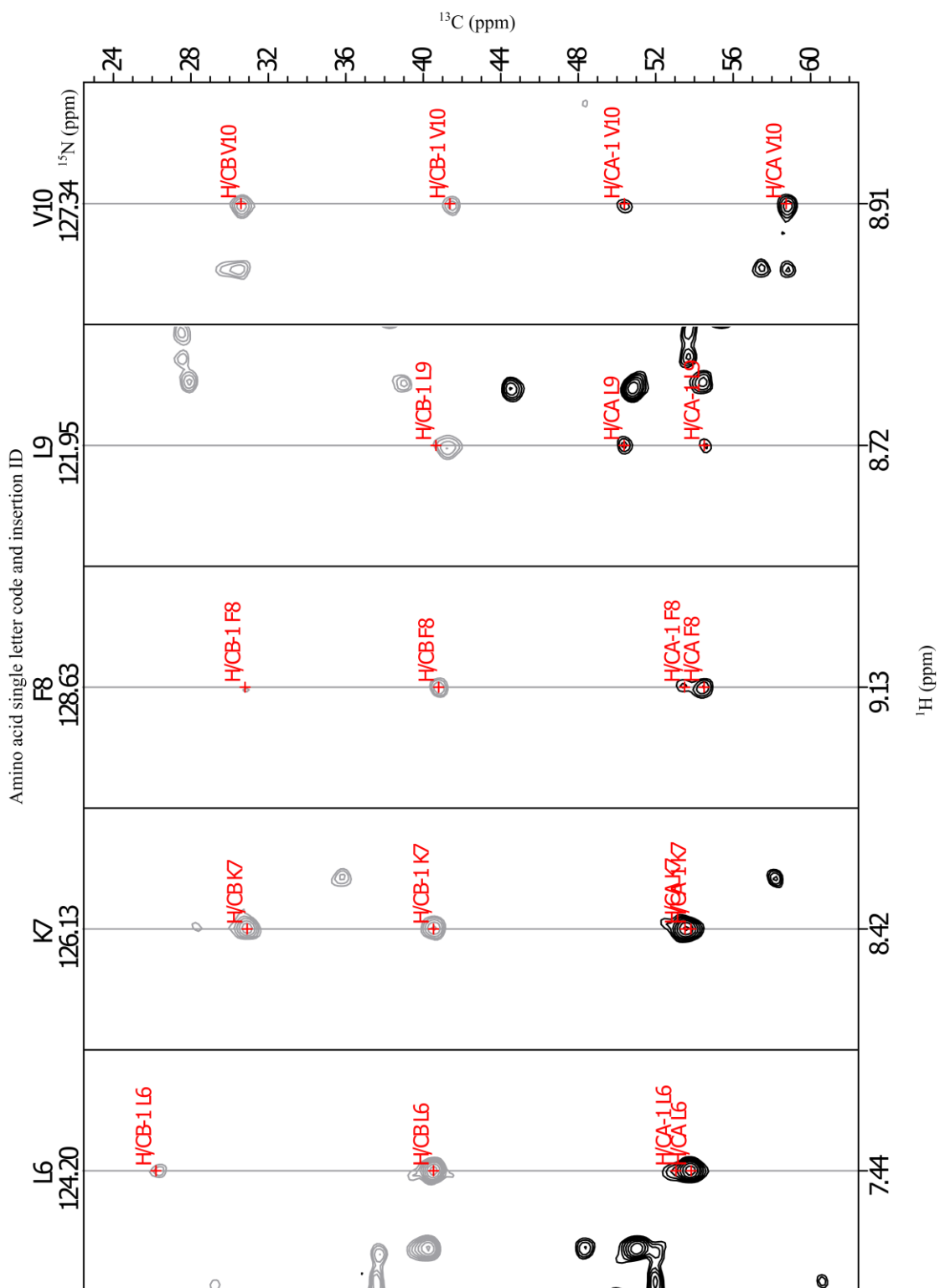
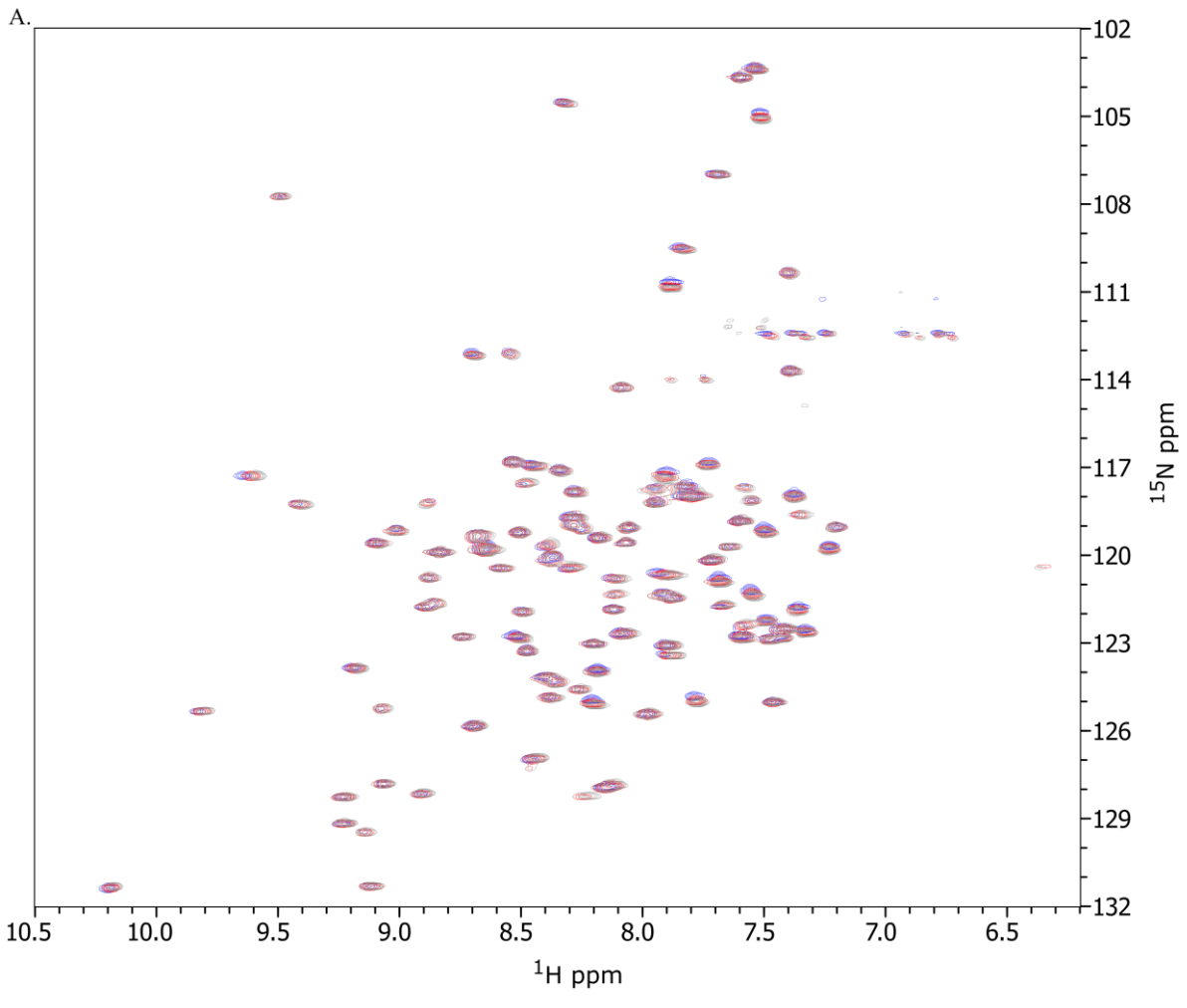


Figure 5.8: Strip scope of a triple resonance experiment (CBCANH) of CheY with peaks indicating $\text{C}\alpha$, $\text{C}\beta$ or $i-1$ residues.

It can be clearly seen from the figure 5.8 that the information on $C\alpha$ and $C\beta$ for the preceding residue (i-1) is available in the strip of the current residue (i). Since, the assignments for CheY were confirmed from the triple resonance sequential method (Appendix Table 1), we further moved to record the fingerprint spectrum of CheY in the presence and absence of crowding agents.

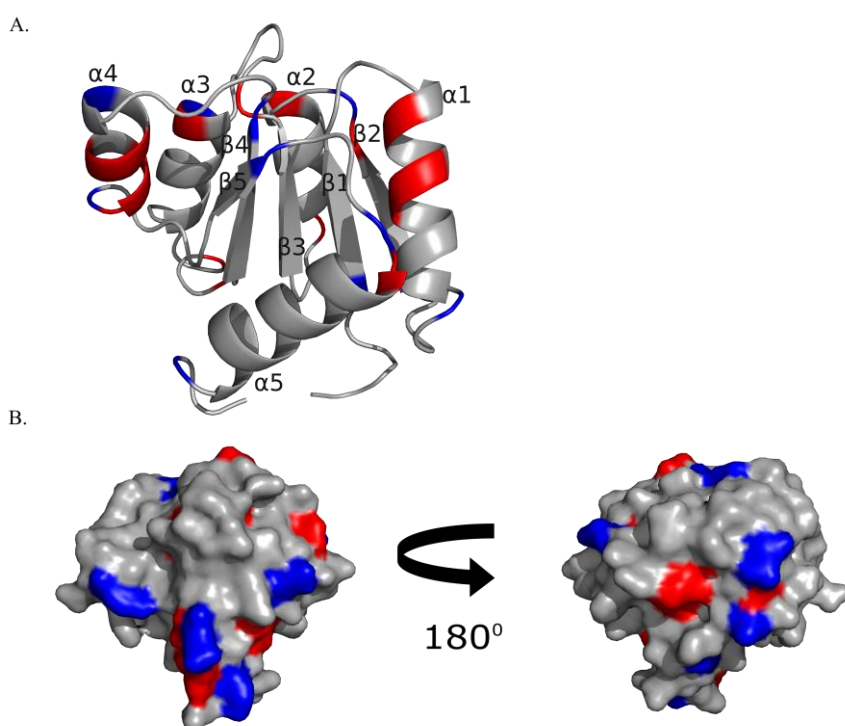
5.2.2 NMR Mapping of the protein crowder interactions in the presence of PEG

Nuclear magnetic resonance (NMR) spectroscopy can provide atomic-level insights into the molecular basis of the observed modulation of structure, stability and dynamics in a crowded scenario (Crowley, Brett and Muldoon, 2008; Monteitha and Pielak, 2014; Smith *et al.*, 2015; Kadumuri *et al.*, 2016; Diniz *et al.*, 2017; Xu *et al.*, 2017; Köhn and Kovermann, 2020). The comparative changes in NMR line-widths and chemical shift perturbations of the protein under crowding conditions in relation to their measurements in dilute buffers will indicate the potential sites of interactions and or crowding induced changes in the conformation and dynamics (Smith *et al.*, 2015; Kadumuri *et al.*, 2016; Diniz *et al.*, 2017). ^1H - ^{15}N TROSY-HSQC titration experiments were performed in increasing concentrations of PEG 20000 to unravel the PEG-protein interactions and its consequence on the conformation of the protein. The superimposed ^1H - ^{15}N TROSY-HSQC spectra of CheY in the presence of increasing amounts of PEG 20000 are shown in Figure 5.9A. A significant number of residues exhibit small chemical shift changes in the presence of 100 mg/mL PEG 20000.



obtained using the standard method. (Williamson, 2013, 2018) The horizontal line represents the cut-off considered for significant movement in chemical shifts ($\Delta\delta_{\text{PEG}} \geq 0.03$). (Crowley, Brett and Muldoon, 2008) (c) A subset of the residues from the superimposed ^1H - ^{15}N TROSY-HSQC spectra of CheY obtained in the presence and absence of PEG, showing significant chemical shift perturbations. (Dilute buffer = grey; 100 mg and 200 mg/mL PEG = red and blue respectively). The x and y axes represent ^1H and ^{15}N chemical shifts in ppm, respectively.

However, the stepwise addition of PEG 20000 to 200 mg/mL leads to a further gradual movement in the chemical shifts for a set of residues, (Figure 5.9B and C) including K7 (β 1), M17 (α 1), I20 (α 1), E27 (α 1), N32 (residue preceding β 2), A36 (β 2), E37 (loop preceding α 2), V40 (α 2), A48 (α 2), G49 (loop preceding β 3) G50 (loop preceding β 3), W58 (side chain (SC)) (β 3), M78 (loop preceding β 4), L81 (β 4), T87 (β 4), E93 (α 4), I95 (α 4), I96 (α 4), A98 (α 4), A99 (α 4), Q100 (α 4), V108 (β 5), T112 (α 5), A113 (α 5), 126K (α 5) and G128 (α 5). It is interesting to note that there is a subset of residues that are not exposed to the solvent but still display CSPs. For instance, residues A98 and A113 show CSPs even though they are buried in the protein core, (Figure 5.9C) suggesting that the origin of CSPs for these residues may not emanate from direct contacts between the protein and PEG 20000 but rather maybe from the conformational changes and or fluctuations prompted by the presence of PEG 20000. Furthermore, mapping residue CSPs onto the native structure of CheY reveals two interesting observations (Figure 5.10).



C.

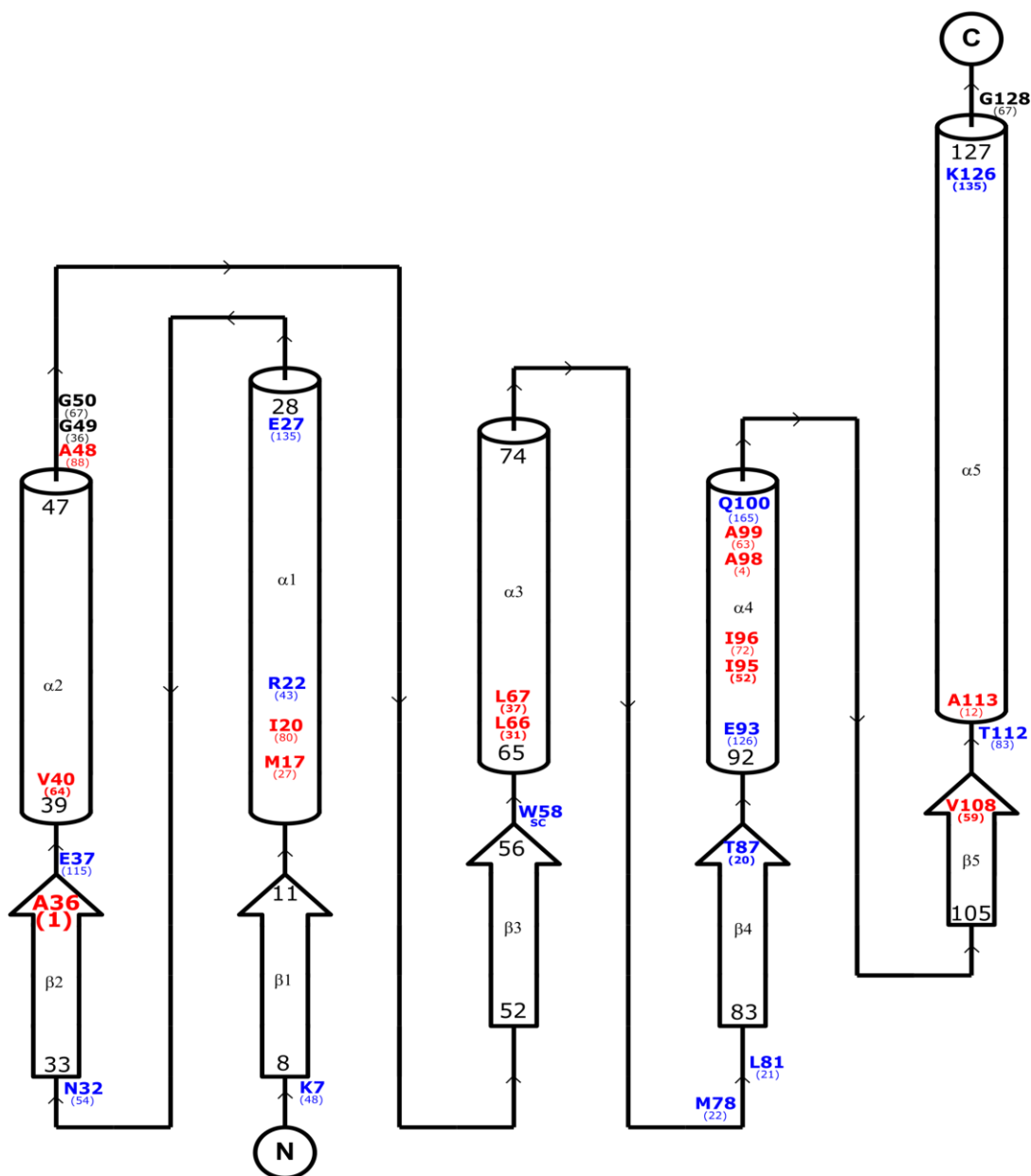


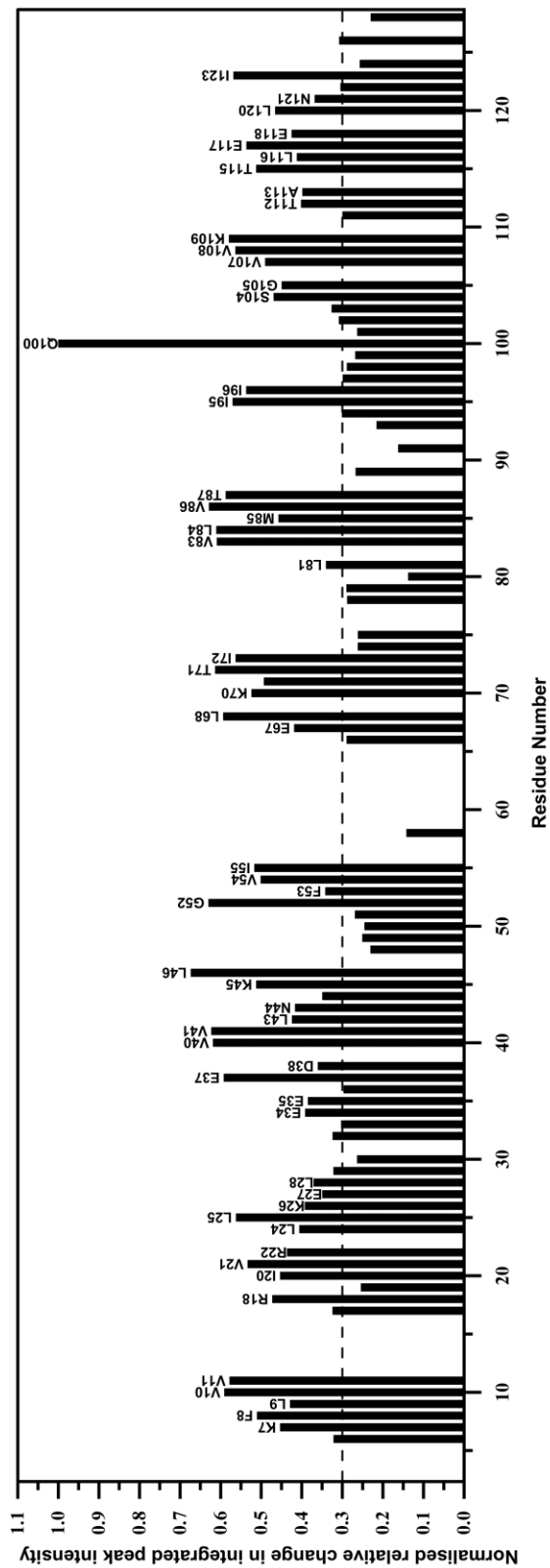
Figure 5.10: Chemical Shift Perturbations ($\Delta\delta_{\text{PEG}}$) in the presence of 200 mg/mL PEG, mapped onto the (A) crystal structure of CheY (B) Surface representation (C) Topology diagram (generated using TopDraw (Bond, 2003)) of CheY. Helices are represented as cylinders, beta strands as arrows, and continuous lines represent loops connecting these elements. PDB ID: 3CHY, with hydrophobic residues colored in red and hydrophilic in blue. Secondary structural elements are labelled and values within parentheses indicate the exposed surface area of the residue.

First, a significant number of residues with chemical shifts occur in α helices, followed by loop/turns and β strands. Second, these residues reside at the terminal positions of the above secondary structural elements (Figure 5.10). For instance, K7 corresponds to the residue

immediately preceding $\beta 1$, and V108 is the C terminal residue of $\beta 5$. V40 is the second residue of $\alpha 2$, L66 and E67, E93, and A113 are located at the N termini of $\alpha 3$, $\alpha 4$ and $\alpha 5$, respectively. α helix 1 ($\alpha 1$) and $\alpha 4$ seem to experience the effect of the crowder more than other structural elements because the changes in chemical shifts extend through the entire helix, with residues E93 and I96 in $\alpha 4$ showing the most change. The residues from the loop and turn regions that display CSPs are in close proximity to the terminal residues of α helices and β strands.

Complementing the information obtained from CSPs, analysis of the intensities of the ^1H - ^{15}N TROSY-HSQC cross peaks revealed significant loss of signal for a subset of residues that are both polar and non-polar in nature (Figure 5.11A and B).

A.



B.

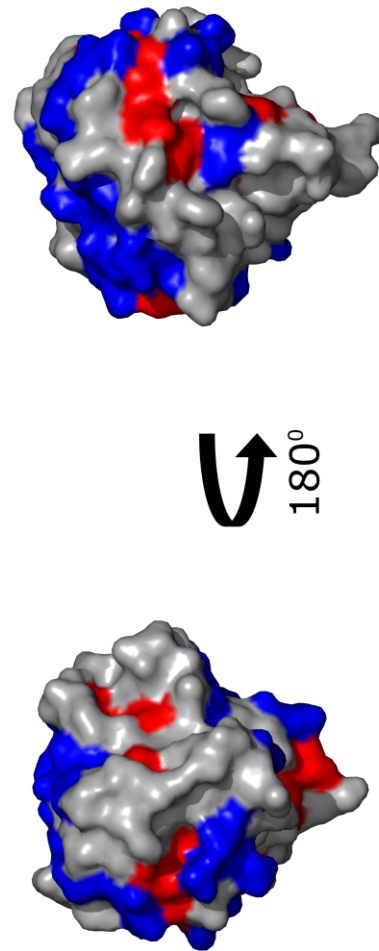


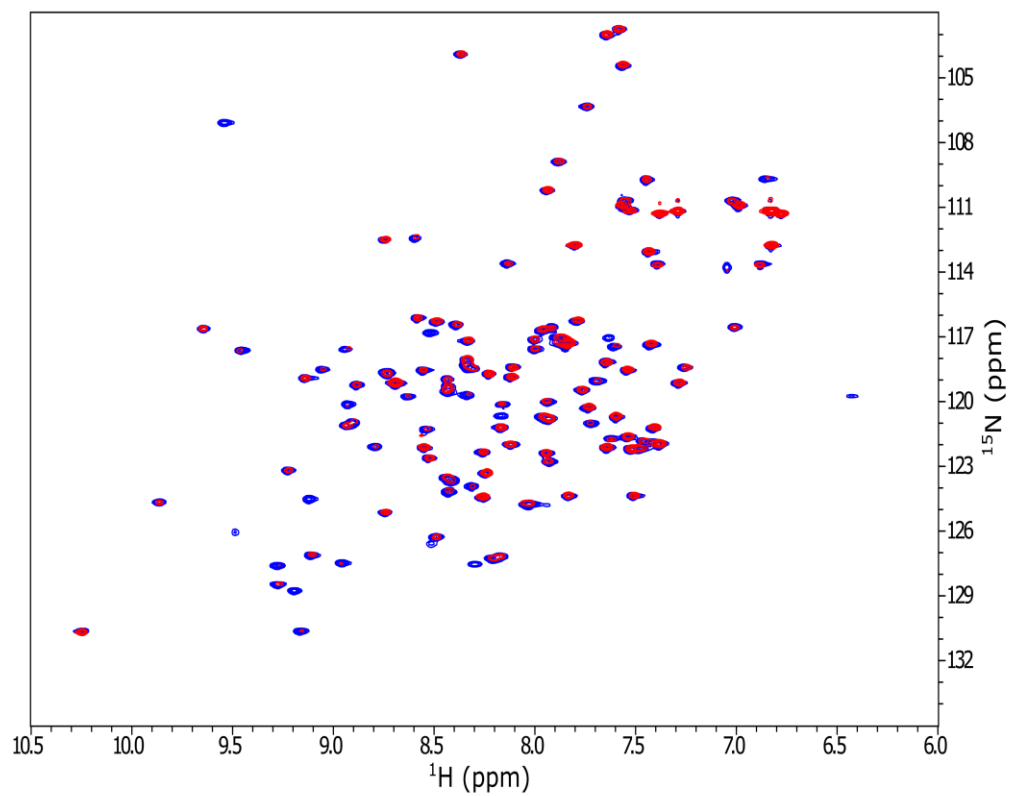
Figure 5.11: (A) Relative change in integrated peak intensities between dilute buffer and 200 mg/mL PEG. (B) Relative change in integrated peak intensities between dilute buffer and 200 mg/mL PEG mapped onto the crystal structure of CheY (PDB ID:3CHY), with hydrophobic residues colored in red and hydrophilic in blue.

In fact, the reduction in cross peak intensities is higher for specific residues such as V10, V11 in β 1, L25 in β 2, E37 in the loop preceding α 2, V40, D41 in α 2, G52 in the loop preceding β 3, L68, T71 in α 3, V83, L84, T87 in β 4, I95, I96, Q100 in α 4, V108, K109 in β 5 and E117, I123 in α 5. In the absence of any visible protein aggregation in the NMR samples, the changes in the NMR parameters clearly indicate PEG-prompted structural perturbation. In fact, the combination of CSPs and non-uniform loss in signal intensities suggest that the observed changes reflect the crowder-protein interactions and ensuing conformational perturbation are probably not caused by enhanced solution viscosity from the crowder (Cino, Karttunen and Choy, 2012). The observation of CSPs in conjunction with change in signal intensities in the presence of PEG can result from local or global unfolding or from the fluctuating ensemble of conformations sampled in the presence of PEG 20000. Similar observations for other proteins have been attributed to weak protein-crowder interactions (Crowley, Brett and Muldoon, 2008; Kadumuri *et al.*, 2016; Diniz *et al.*, 2017). Overall, the NMR analysis combined with CD and FL data (Chapter 2) clearly indicate that PEG 20000 interacts with the residues accessible at the surface, inducing conformational fluctuations. This observation strongly supports the role of attractive interactions between the protein and PEG 20000. Both polar and hydrophobic interactions can contribute to the transient non-specific weak contacts. The complex interplay of these interactions can play a vital role in the modulation of the structural and thermodynamic processes such as metal-binding under crowding conditions. CheY as a part of the signal transduction complex, is involved in protein-protein interactions with Chemotaxis A (CheA), one of the proteins involved in the bacterial chemotactic signalling pathway. The residues A90, K92, I95, I96, A99, Q100, A103, S104, G105, and Y106, are in close proximity to α 4 and K122, E125 and K126 in α 5 correspond to the set of residues that make contacts with CheA. It is intriguing to note that CSPs of surface exposed residues of CheY map well to those that interact with CheA.

5.2.3 Molecular insights of the effect of Ficoll on apo and holo forms of CheY

In order to examine the interaction and or the extent of interaction of the protein with the crowder, ^1H - ^{15}N - HSQC NMR was performed in the presence of 0, and 200 mg/mL Ficoll. The superimposed ^1H - ^{15}N - HSQC spectra of CheY in the presence of 0, and 200 mg/mL Ficoll are shown in Figure 5.12A.

A.



B.

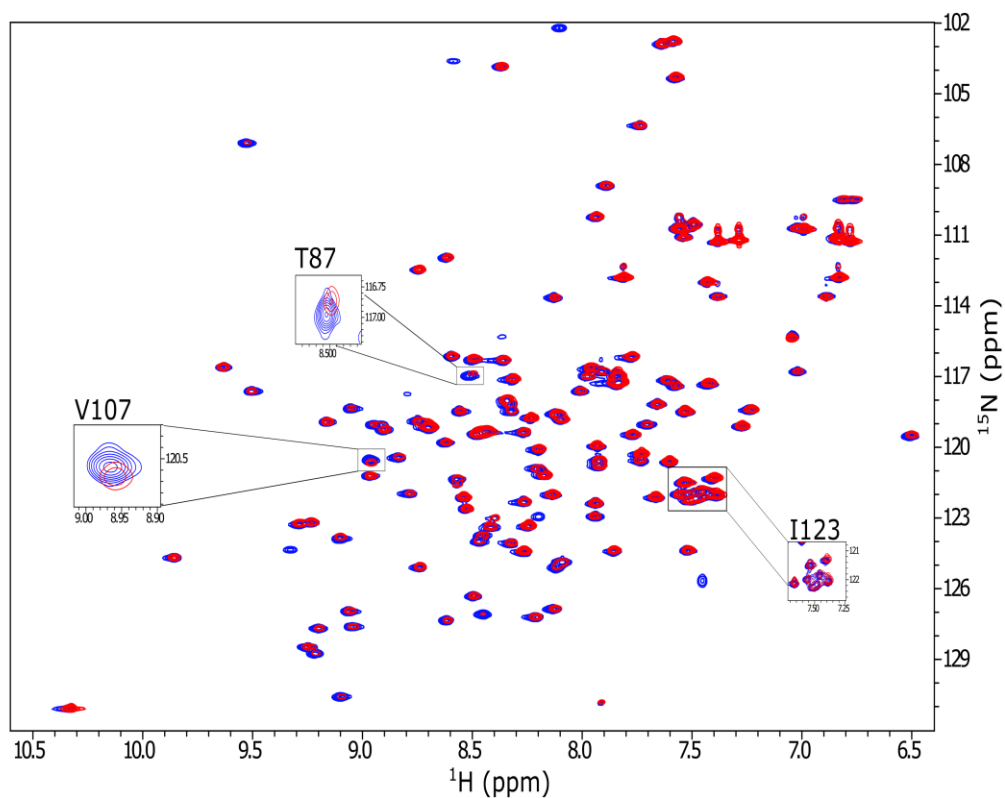


Figure 5.12: (A) Superimposed ^1H - ^{15}N Heteronuclear Single Quantum Coherence (HSQC) spectra of apo CheY in buffer (blue), and in the presence of 200 mg/ml of Ficoll (red). (b) Superimposed ^1H - ^{15}N HSQC spectra of holo CheY in buffer (blue), and in the presence of 200 mg/ml of Ficoll (red). Boxed regions represent peaks showing minor CSPs.

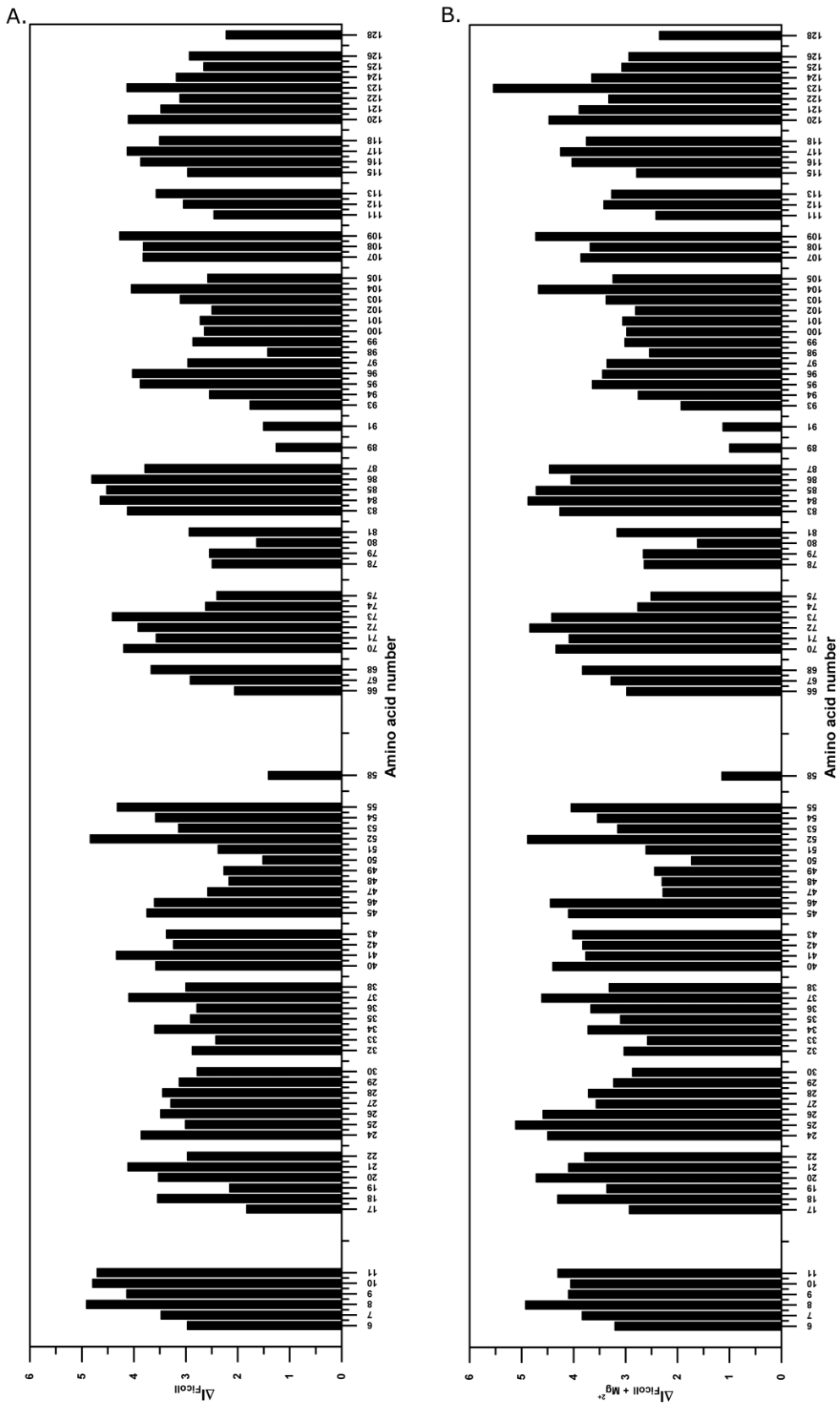


Figure 5.13: (A) Relative intensity (ΔI_{Ficoll}) of cross peaks of apo CheY in the presence of Ficoll. (B) Relative intensity ($\Delta I_{\text{Ficoll} + \text{Mg}^{2+}}$) of cross peaks of holo CheY in the presence of Ficoll.

No significant chemical shift perturbations (CSPs) are apparent in the presence of Ficoll. Ficoll being relatively larger (70 kDa) than the protein (13.9 kDa), the possibility of very weak interactions between Ficoll and protein could be non-specific and randomly occurring at different locations. Therefore, differently contributing interactions could lead to no net CSPs (Abriata, Spiga and Peraro, 2016b). However, on the other hand, a comparison of the ^1H - ^{15}N -HSQC spectra of holo CheY and holo CheY in Ficoll (Figure 5.12B) shows minor chemical shift changes for T87, V107, I123. Interestingly, the backbone conformation for the residues A88, E89, V108, K109, P110, F111, occurring in β strands 4 and 5 and residues towards the N terminus of the α -helix 4 beginning at position 92 show significant deviations in the magnesium bound CheY (Bellsollell *et al.*, 1994). The likelihood of Ficoll-protein interactions can be seen by analysing the line broadening of the backbone resonances (Majumder *et al.*, 2015; Abriata, Spiga and Peraro, 2016b; Kadumuri *et al.*, 2016; Diniz *et al.*, 2017; He, Kang and Song, 2020; Irukuvajjula, Reddy and Vadrevu, 2022). In the presence of Ficoll alone, a significant number of resonances demonstrated increased line widths in the presence of 200 mg/mL Ficoll, indicating the likelihood of protein-Ficoll interactions (Figure 5.13A). Residues G50, E89, K91, and A98, which fall in the loops, are less affected, presumably due to the slower tumbling as a result of increased viscosity by Ficoll. In the combined presence of Ficoll + magnesium (holo CheY) more than a dozen residues shows further increased line widths (L6, R19, R22, N32, E35, A36, E67, L81, A97, A99, A101, G105, and E125) (Figure 5.12B). Intensities of certain residues like L81, A97, A99, A101, and G105 overlap with the region that shows structural perturbation upon Mg^{2+} binding, hinting towards the possibility of apo-holo equilibrium. The superimposition of ^1H - ^{15}N - HSQC spectrum holo CheY and Ficoll with the spectrum of holo CheY in dilute buffer rules out the possibility of disruption of any metal binding interactions.

5.3 Conclusions

The following conclusions can be drawn from the NMR based study of CheY in the presence of PEG 20000 and Ficoll 70.

- i) A significant number of residues with chemical shifts occur in α helices, followed by loop/turns and β strands.
- ii) These residues reside at the terminal positions of the above secondary structural elements. For instance, K7 corresponds to the residue immediately preceding β 1, and V108 is the C terminal residue of β 5. V40 is the second residue of α 2, L66 and E67, E93, and A113 are located at the N termini of α 3, α 4 and α 5, respectively.
- iii) α helix 1 (α 1) and α 4 seem to experience the effect of the crowder more than other structural elements because the changes in chemical shifts extend through the entire helix, with residues E93 and I96 in α 4 showing the most change.
- iv) The backbone amide chemical shift perturbations, together with the reduction in the intensity for a subset of residues observed from 2-D TROSY-HSQC NMR analysis, indicate that PEG interacts with both hydrophilic and hydrophobic residues of CheY.
- v) The observation of CSPs in conjunction with change in signal intensities in the presence of PEG can result from local or global unfolding or from the fluctuating ensemble of conformations sampled in the presence of PEG.
- vi) No net CSPs are reported for apo CheY in the presence of Ficoll 70. Additionally, residues show line broadening. This was explained by considering the comparatively bigger size of Ficoll than the protein, due to which the crowder-protein interactions if any are limited to transient interactions.
- vii) For holo CheY in the presence of Ficoll certain CSPs were reported and additional set of residues show further line broadening. These residues also coincide with the set of

residues that show changes upon metal binding. Therefore, the CSPs along with the intensity changes imply that CheY populates multiple conformers and the apo holo equilibrium is disrupted in the presence of Ficoll.

Chapter 6

Effects of Small Molecular Crowder and a Combination of Small Molecular and Macromolecular Crowders on the Structure and Stability of Chemotaxis Protein Y

6.1 Introduction

Cellular interior is heavily crowded with various compounds, organelles, ions, salts, metabolites, etc. This complex nature affects the protein's structure, stability, and function *in-vivo*. Macromolecular crowding is a way to mimic cellular interiors by using various synthetic and natural molecules that occupy the same area and barely possess the ability to interact with the test protein. The literature reports the use of macromolecules like PEGs, Ficoll, Dextrans, etc., as crowders and elucidate the effect on structure, stability, and function of the test protein. However, these molecules alone cannot capture the essence of the complex nature of the cell. In addition to macromolecules, cells are abundantly populated with various osmolytes and small molecules. Notably, these molecules span across cellular organisms, plants, and animals (Somero, 1986). These compounds comprise polyols, sugars, methylamines, amino acids, etc. Among these sugars, polyamines and amino acids are the most commonly found small molecules inside cells. They can protect cells against adverse conditions such as temperature fluctuations, pH changes, dehydrations, salinity, etc (Back, Oakenfull and Smith, 1979; Taylor *et al.*, 1995; Sola-Penna *et al.*, 1997). Osmolytes/small molecules, in general, are considered to be protein stabilizers, and one of the stabilization theories is that sugars can stabilize the native state of the protein as they are preferentially excluded from the protein surface. Hence consequently, the Gibbs free energy change associated with the protein folding process increases (Poddar *et al.*, 2008). For instance, phosphoglycerate kinase was chemically denatured using guanidine hydrochloride (GuHCl) in the presence and absence of different

concentrations of sucrose. The amount of GuHCl required to unfold the protein increased in the presence of sucrose. However, the overall ΔG° in the absence of any denaturant obtained by extrapolation showed no change. Smith et al., probed the thermal stability of ovalbumin, lysozyme, conalbumin, and α -chymotrypsinogen in the presence of sucrose, glucose, sorbitol, and glycerol. The additions of sugars and polyols increased the T_m of the proteins. ΔT_m ranged from 0-18°C for conalbumin at pH 7.0 in 50% glycerol, and lysozyme at pH 3.0, in the presence of 50% sorbitol. It was argued that this extent of stabilization originated from the effect of sugars and polyols on the hydrophobic interactions of the proteins (Back, Oakenfull and Smith, 1979). These studies have mainly focused on the effect of a single osmolyte/small molecule on the structure and stability of proteins. However, a mixture of osmolytes/small molecules coexist inside the cell. In light of this, Shinde et al., used glycine, alanine, DL- α -aminobutyric acid, and sorbitol individually and in combination to elucidate protein stability in a more realistic environment. The authors reported an increase in the thermal transition temperature of hen egg-white lysozyme in the presence of these osmolytes. The mode of action for stabilization is proposed to be preferential exclusion. They also proved that the stabilizing effects of different osmolytes were not synergistic (Shinde *et al.*, 2020). However, the general stabilizing trend of osmolytes by preferential hydration mechanism was challenged and disproved by Yao et al. The authors worked with MutX, a GB3 variant protein and four osmolytes; sorbitol, glycerol, betaine, and taurine. The protein is stabilized by glycerol and sorbitol, but slightly destabilized by betaine and taurine. This destabilization is believed to originate from the weakening of electrostatic interactions by the zwitterionic osmolytes. The authors also performed *in-vivo* studies with *E.coli* cell lysates. They found that betaine and taurine further destabilized the protein under *in-vivo* conditions. In the presence of these osmolytes, quinary interactions between the protein and the environment increase, leading to the observed destabilization. Considering these factors, it is apparent that cosolutes can display

diverse effects on the structure and stability of proteins. There is a need for a more carefully considered and sophisticated model to explain the molecular and thermodynamic consequences of small molecule induced crowding on test proteins. As stated earlier, polyamines are also an abundant component of the cell's interior. Some commonly found polyamines are putrescine, spermine, spermidine, cadaverine, etc. These polyamines are organic nitrogen-containing compounds of low molecular weight. These molecules are aliphatic in nature and participate in a variety of cellular processes such as cell growth, cell differentiation, etc. (Kalač and Krausová, 2005; Weiger and Hermann, 2014; Chanphai, Thomas and Tajmir-Riahi, 2016; Michael, 2016). These polyamines are also important additives to a reaction mixture that prevent the heat-induced association and inactivation of various proteins, for instance, no aggregates were observed in the presence of spermine and spermidine for lysozyme after heat treatment and the residual activity was also ~ 50% (Kudou *et al.*, 2003; Okanojo *et al.*, 2005). Putrescine plays a crucial role in a microorganism's metabolic pathways; for example, it is found in fungi, gram-negative bacteria, etc. It is present in high concentrations in various other species. In plants, putrescine agglomeration may occur at high concentrations and under different stress conditions; this plays an important role in preventing ageing (Verma and Mishra, 2005). Studies reported in the literature focus on the individual effect of polyamines on the test protein's structure, stability and function. Some examples reported below shed light on the possible effects of polyamines on various proteins. It was reported that lysozyme's activity decreases in a concentration-dependent manner in putrescine, implicating the affinity of putrescine for the catalytic site of lysozyme. The secondary and tertiary structures were also found to be altered (Ashrafi *et al.*, 2022). Momeni *et al.*, reported increased thermal stability of bovine pancreatic trypsin with increasing spermine concentrations. Trypsin activity has also been reported to increase in its presence (Momeni *et al.*, 2016). Moreover, studies with a combination of small molecules and macromolecular crowders are not thoroughly reported

throughout the literature. To the best of our knowledge, this chapter is the first attempt at mixed macromolecular crowding using cellular metabolites polyamines, and macromolecules. We report the structure and stability of CheY (apo and holo forms, wherever appropriate) in the presence of amino acids, a combination of amino acids and macromolecular crowders, polyamines, and a combination of polyamines and macromolecular crowders. Amino acids, a combination of amino acids and amino acids + crowders, did not show any drastic differences in the secondary structure of the protein. However, for amino acids + crowder (Ficoll), the effect of Ficoll on the thermal stability of holo CheY was still observed as a reduction in T_m value. Polyamines stabilize the apo form of the protein by a minimal amount. The thermal denaturation curves that were reported to be irreversible for the holo form were found to be reversible. Interestingly, the effect of Ficoll on the thermal stability of holo CheY was counteracted by the presence of either putrescine or spermidine. The same effect was not observed for polyamines and PEG 20000.

6.2 Results and discussions

6.2.1 Effect of amino acids and combination of amino acids on the structure of CheY

As discussed earlier, amino acids are a significant part of the cytosol, and thus illustrating the effect of certain amino acids on structure and stability of CheY becomes essential. The effects of alanine and valine on the structure and stability of the apo and holo forms of CheY, were tested. The secondary structure content of the protein remained unaffected, as observed from the far UV-CD measured in the presence of the highest soluble concentration of the respective amino acids (Figure 6.1). The combination of amino acids further increases the complexity of crowding. The effect on the secondary structure remained the same as that observed in the presence of individual amino acids.

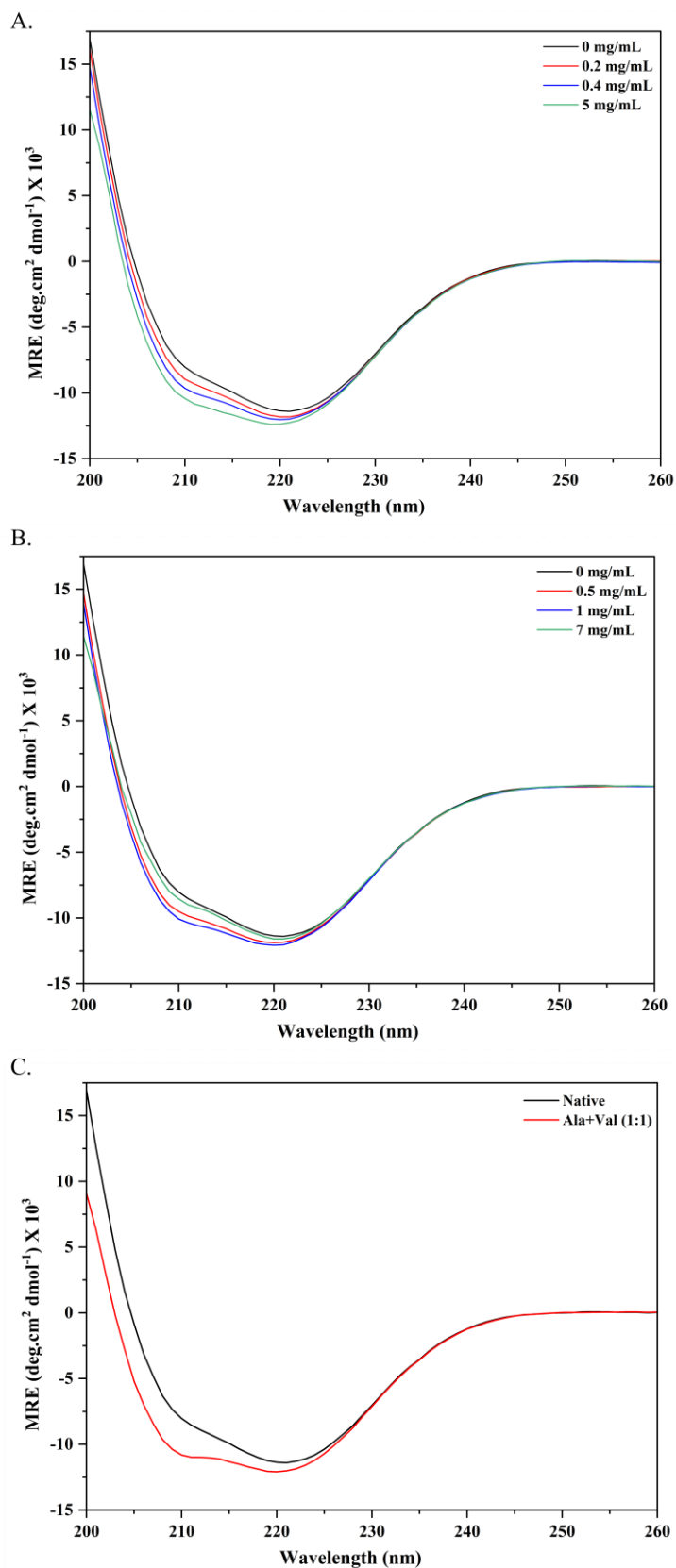


Figure 6.1: Far UV-CD spectra of apo CheY in the presence and absence of (A) Alanine, (B) Valine and (C) equimolar combination of alanine and valine.

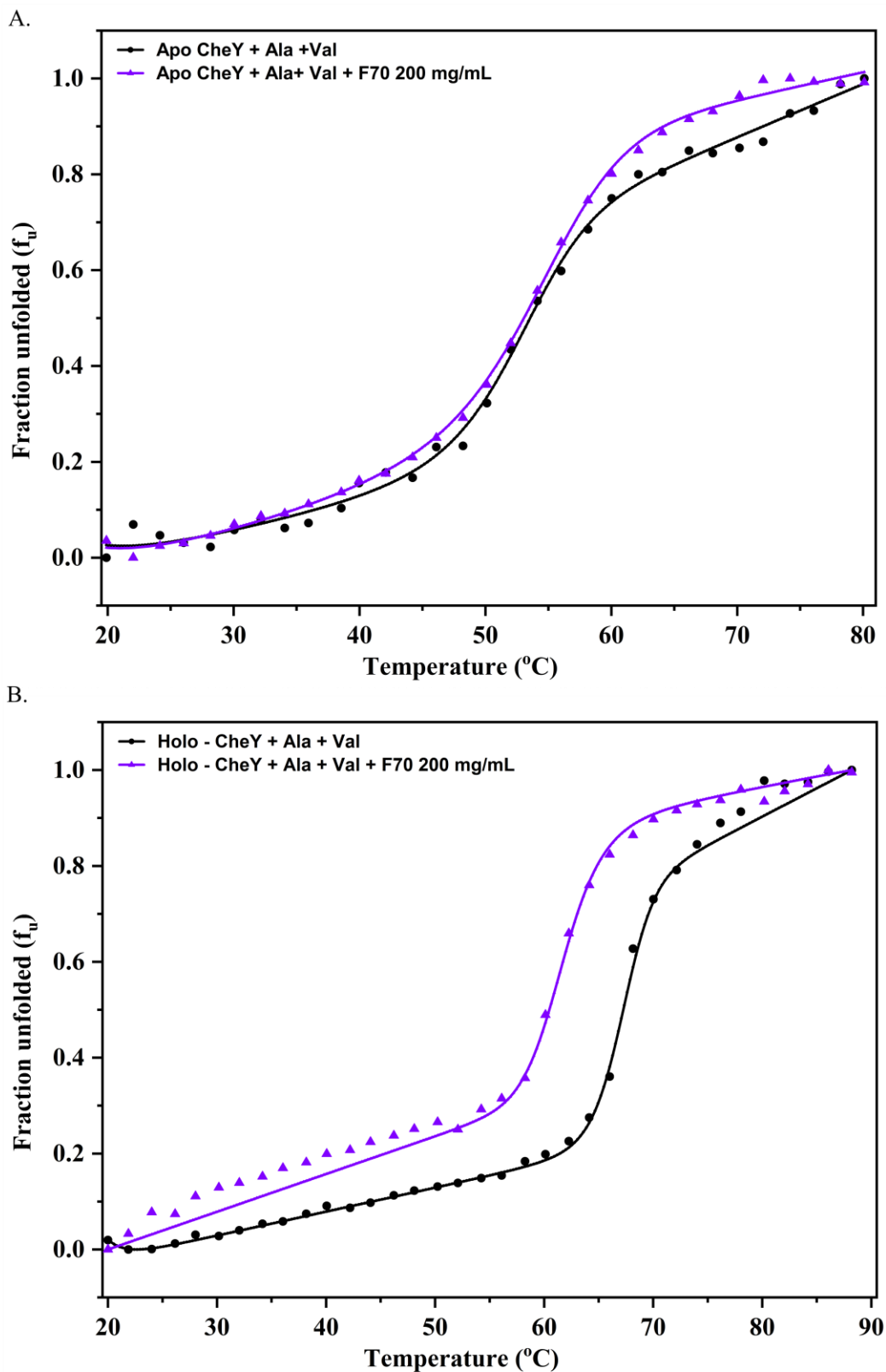


Figure 6.2: Thermal denaturation profiles of (A) apo CheY in the presence of a combination of amino acids and in the combined presence of amino acids and 200 mg/mL of Ficoll 70. (B) Holo CheY in the presence of a combination of amino acids and in the combined presence of amino acids and 200 mg/mL of Ficoll 70. The lines joining the points correspond to a fit to a two-state, folded-unfolded form of the protein. Although data were recorded at 1°C interval, for the purpose of representation the data are plotted at 2°C interval.

Earlier in this thesis, it was highlighted that thermal stability is independent of structural changes. Based on this premise, the apo and holo forms of CheY were thermally denatured using a combination of amino acids (Figure 6.2). For the apo and holo forms of the protein, the midpoint of the thermal denaturation remained unchanged. Table 5.1 lists the T_m values obtained under different conditions.

Table 6.1: T_m for apo and holo CheY in the presence and absence of amino acids as crowders.

Sample	T_m (°C)	ΔT_m (°C)
Apo CheY	52	NA
Apo CheY + Ala + Val	52.2	0.2
Apo CheY + Ala + Val + Ficoll 70	54	2
Holo CheY	68	NA
Holo CheY + Ala + Val	67	1
Holo CheY + Ala + Val + Ficoll 70	62	-6

To assess the combinatorial effect of macromolecular crowding with amino acids, Ficoll-70 was introduced into the reaction mixture and a thermal denaturation experiment was performed. It is a known fact that Ficoll-70 destabilizes the holo form of CheY (Chapter 3). This attempt to illustrate the combined effect of Ficoll and amino acids better mimicked the in-cell-like condition. No change in the midpoint of the transition for holo CheY was reported in the combined presence. This led to the conclusion that the effect exerted by macromolecular crowding, i.e. entropic destabilization, is still the major acting force, and amino acids cannot alter this predominant effect (Table 5.1).

6.2.2 Effect of polyamines on structure and stability of apo and holo CheY

Apo CheY

UV spectra was also recorded for CheY in the presence and absence of putrescine, spermine, and spermidine (Figure 6.3). The UV-visible spectrum aids in assessing the feasibility of recording far UV-CD spectra, fluorescence emission spectra and monitoring protein aggregation in the presence of these polyamines. The UV spectra of apo CheY in the presence and absence of polyamines did not show major changes. The spectra closely overlapped with

the dilute buffer spectrum of apo CheY. It can also be seen that polyamines do not interfere with the far UV-CD range (260-200 nm) as they do not display any additional absorbance (Kelly, Jess and Price, 2005). Moreover, the absorbance in the region beyond 350 nm did not show any change, which is indicative of the fact that CheY does not aggregate in the presence of polyamines.

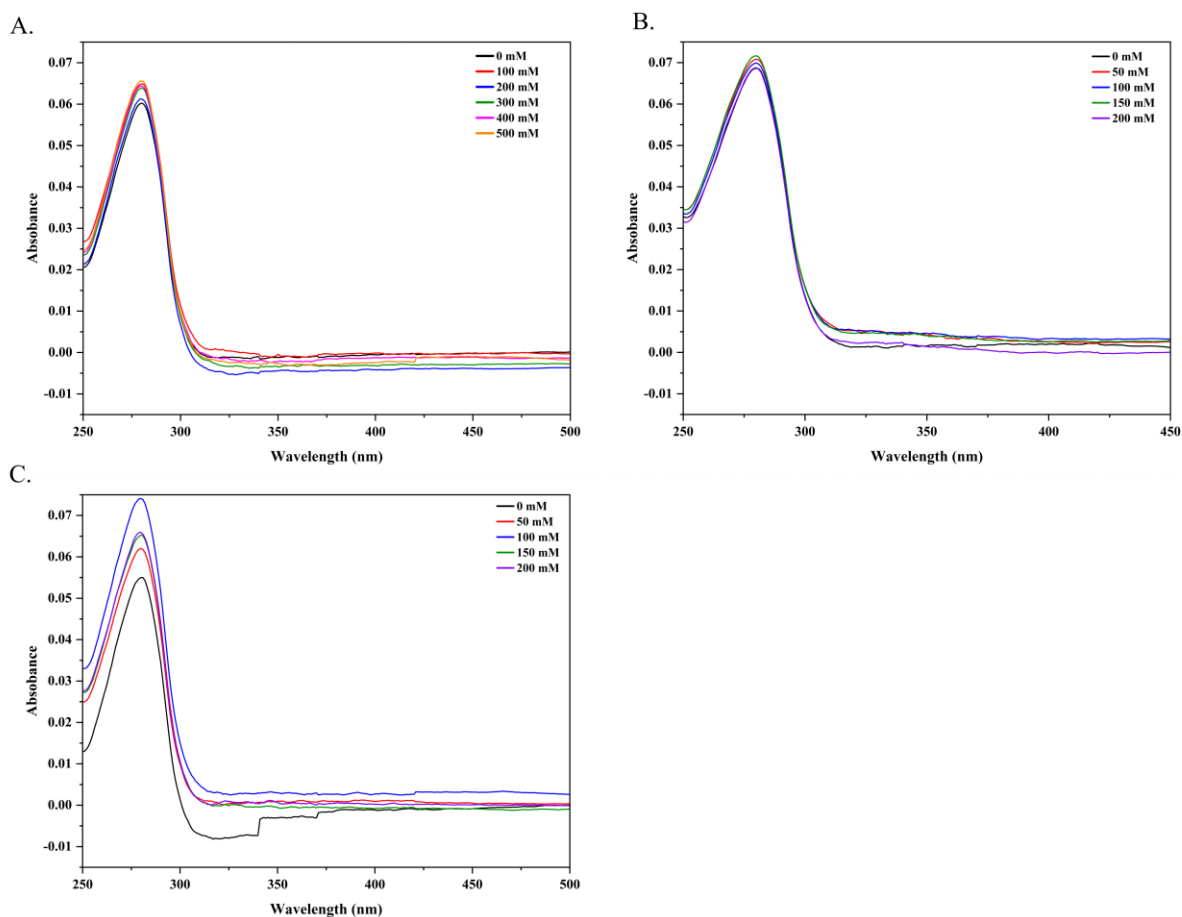


Figure 6.3: UV-visible spectra of apo CheY in the presence of varying concentrations of (A) Putrescine, (B) Spermine, and (C) Spermidine

Additionally, it can also be noted from the spectra that even in the presence of polyamines, the absorbance is fairly constant at 290 and 350 nm, which are the excitation and emission wavelengths, respectively, for the fluorescence emission spectrum. Therefore, no correction for inner-filter effect (primary or secondary) is required.

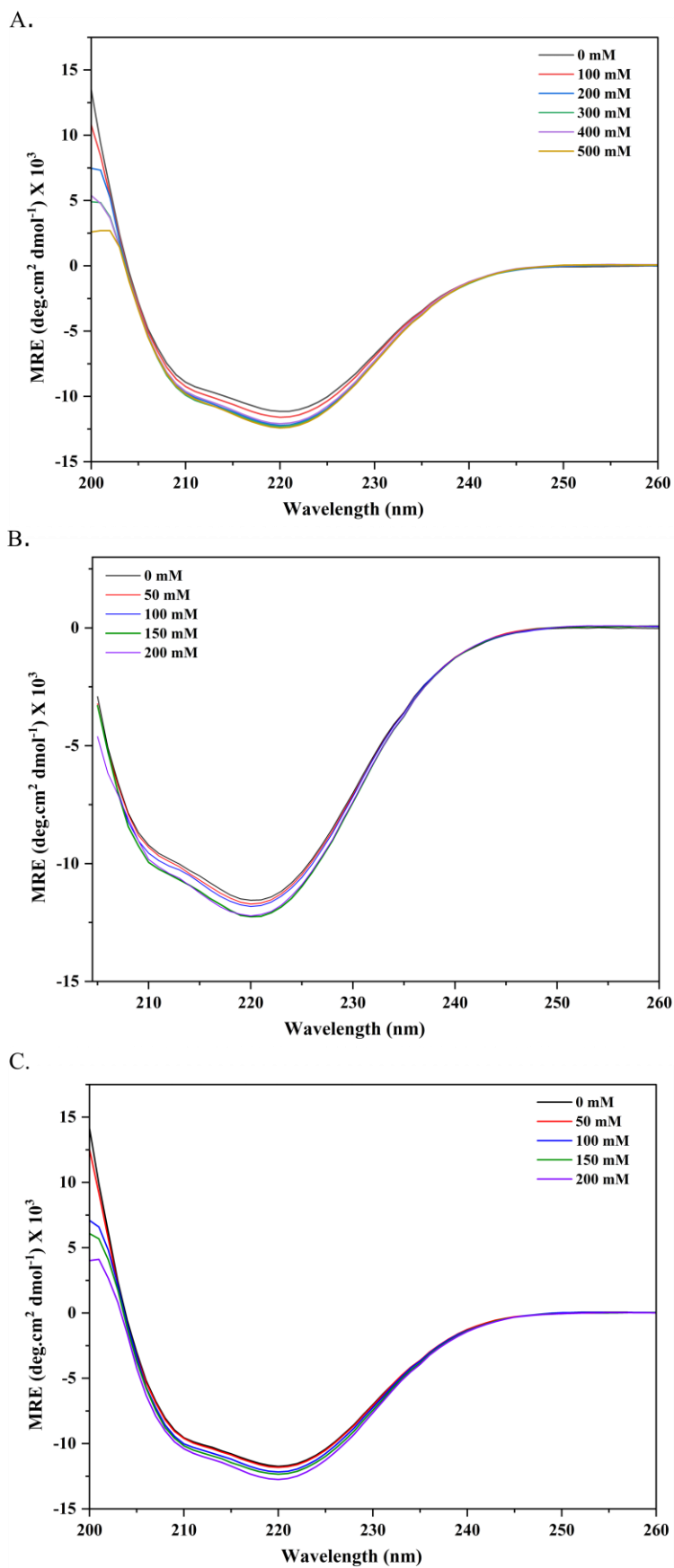


Figure 6.4: Far UV-CD spectra of apo CheY in (A) Putrescine, (B) Spermine, and (C) Spermidine

Far UV-CD spectra (Figure 6.4) of CheY in the presence and absence of all three polyamines showed no significant changes in shape and signal. A minor increase in the signal was observed at the highest concentration of polyamines. This implied that the secondary structure was not affected by these polyamines.

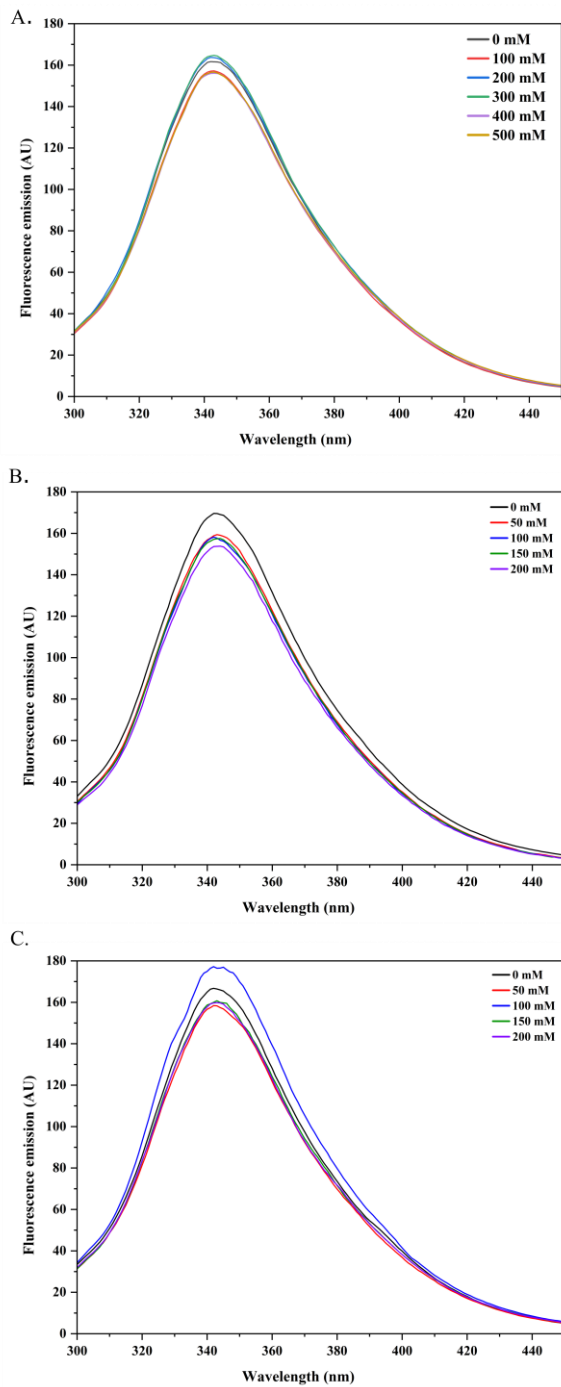


Figure 6.5: Fluorescence emission spectra of apo CheY in the presence of (A) Putrescine, (B) Spermine, and (C) Spermidine

The fluorescence emission spectra (Figure 6.5) also do not reflect drastic changes in the tertiary packing environment of CheY in the presence of all three polyamines. A minor reduction in intensity was observed, which can be attributed to the change in solvent polarity upon addition of the polyamines. The absence of any chromic shift ruled out the possibility of aggregation or unfolding.

Thermodynamic stability determines the resistance of a protein to denaturation by an external agent. It is known from the previous chapters that the structure and stability of CheY can be independent of each other. Since the structure of CheY was not affected much, as observed in the CD and FL studies, thermal denaturation was performed in the presence and absence of these three polyamines to assess their effect on thermodynamic stability. The thermal denaturation profiles were fitted to a two-state folded to unfolded model (Figure 6.6), and the thermodynamic parameters (Table 5.2) were derived using CalFitter (Mazurenko *et al.*, 2018).

Table 6.2: Thermodynamic parameters of apo CheY in the presence of polyamines

	Sample	T_m (°C)	ΔT_m	ΔH^{o'} (kJ/mol)	ΔΔH^{o'} '	TΔS^{o'} (kJ/mol)	ΔG^{o'} (kJ/mol)
1	Apo CheY	52.48 ± 0.37	NA	260 ± 10	-	240 ± 10	21.49 ± 0.84
2	Apo CheY + Putrescine (500 mM)	56.18 ± 0.37	3.70	280 ± 11	+20	250 ± 10	26.18 ± 0.98
3	Apo CheY + Spermine (100 mM)	54.77 ± 0.44	2.29	280 ± 12	+20	250 ± 11	24.86 ± 1.01
4	Apo CheY + Spermidine (200 mM)	54.77 ± 0.44	2.29	270 ± 13	+10	250 ± 12	24.55 ± 1.12

It can be seen that the overall thermodynamic stability (ΔG^{o'}) increases by an approximate value of 2-6 kJ/mol. This increase in ΔG^{o'} is mainly attributed to the increase in the ΔH^{o'}. An increase in ΔT_m and ΔΔH^{o'} indicated a preferential hydration model of stabilization in the presence of these polyamines (Senske *et al.*, 2014). The surface of CheY is negative, with a net

charge of - 4 at physiological pH. Polyamines are known to directly bind to the negative pockets of proteins; the increase in the ΔH° indicates the same in the case of CheY. Therefore, it can be concluded that polyamines bind to the surface of the protein at negative pockets and induce an increase in the stability of CheY without changing the folding-unfolding mechanism (two-state and reversible).

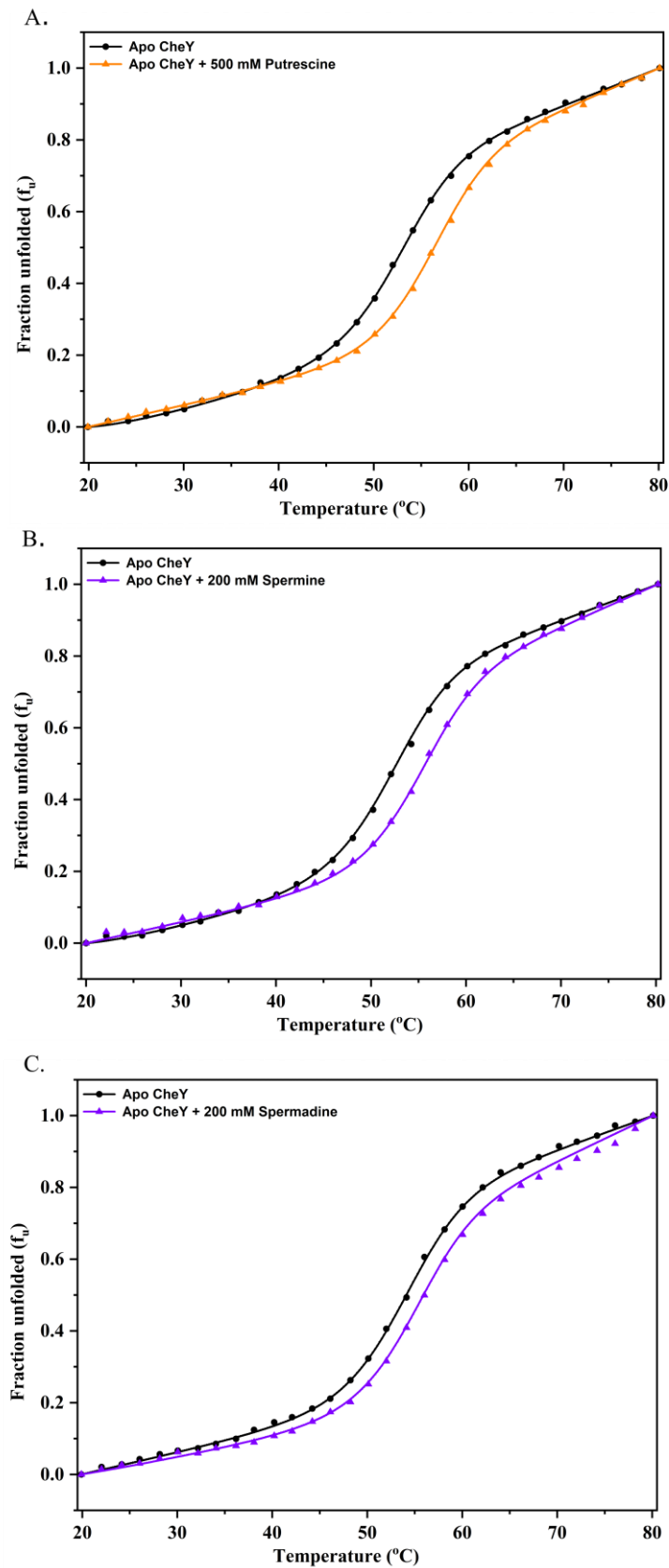


Figure 6.6: Thermal denaturation profiles of apo CheY in the presence of (A) Putrescine, (B) Spermine, and (C) Spermidine. The lines joining the points correspond to a fit to a two-state, folded-unfolded form of the protein. Although data were recorded at 1°C interval, for the purpose of representation the data are plotted at 2°C interval.

Holo CheY

Far UV-CD spectra (Figure 6.7) of holo CheY in the presence and absence of all three polyamines showed no significant changes in shape and signal. At best a miniscule increase in the signal was observed at the highest concentration of the polyamines. Therefore, it implies that the secondary structure was not affected by these polyamines. In figure 6.7B the measurement of far UV-CD was stopped at 205 nm owing to the high voltage in the region beyond 205 nm. Spermine was obtained as a tetrahydrochloride salt. Additionally, the experiments were performed in Tris-Cl buffer, which increased the effective chloride concentration of solution to a greater extent than that of the other two polyamine solutions. Therefore, measurements were limited to 205 nm in the presence of spermine.

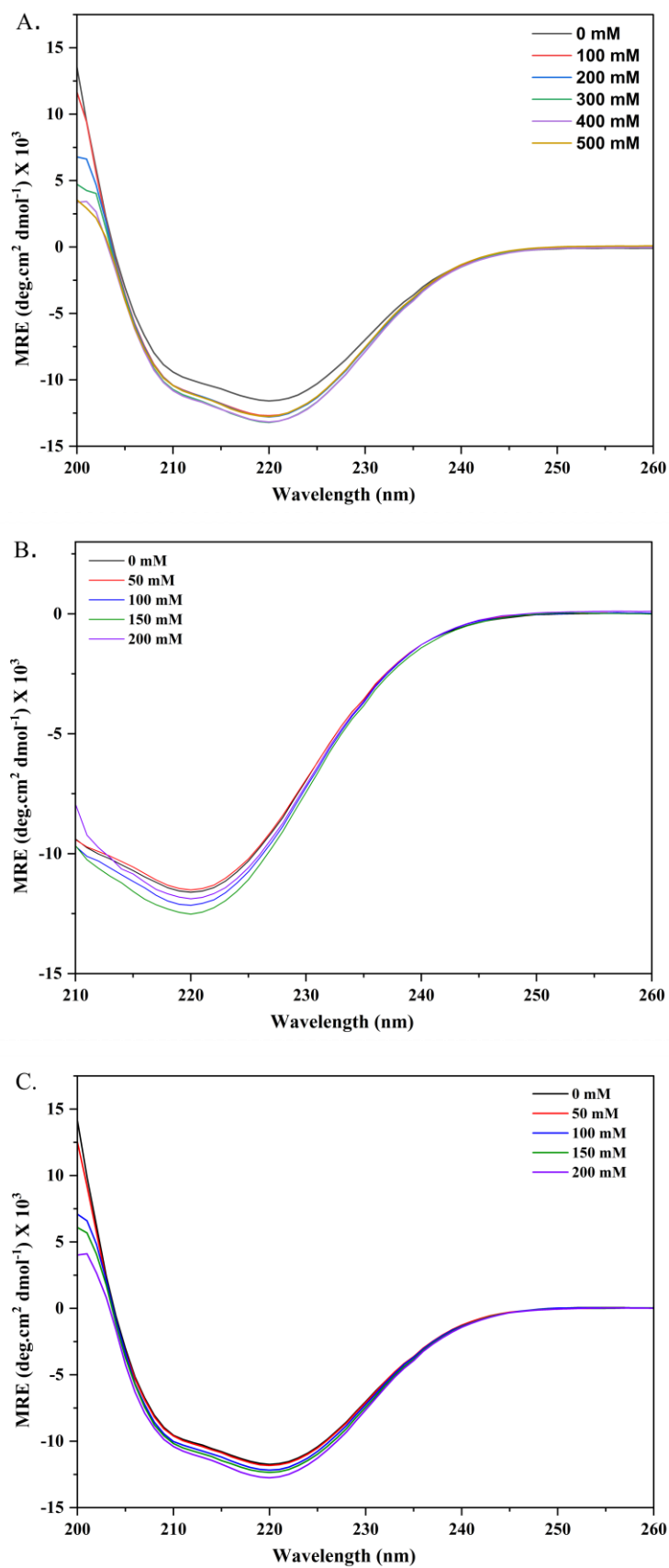


Figure 6.7: Far UV-CD spectra of holo CheY in the presence of varying concentrations of (A) Putrescine, (B) Spermine, and (C) Spermidine

The tertiary structure of holo CheY also displayed no change in the tertiary packing of CheY.

Figure 6.8 clearly indicates the quenching between apo and holo CheY, but no further change in the intensity or chromic shift in polyamines rules out aggregation and unfolding.

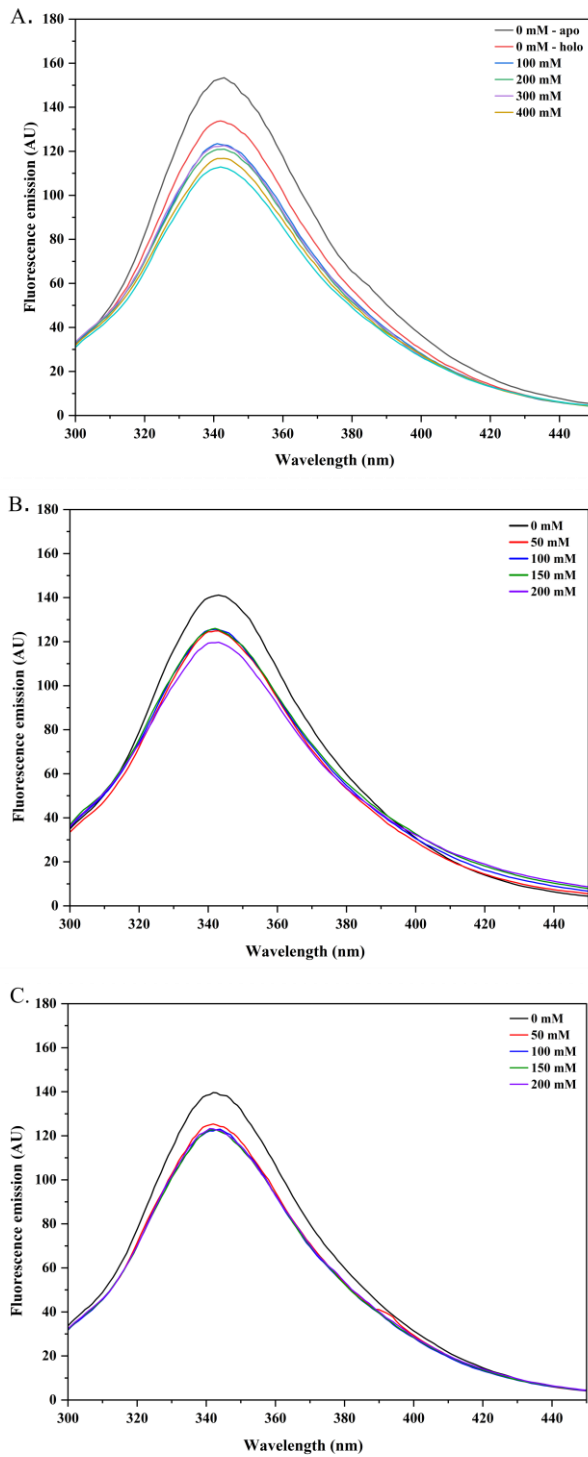


Figure 6.8: Fluorescence emission spectra of holo CheY in the presence of varying concentrations of (A) Putrescine, (B) Spermine, and (C) Spermidine

For holo CheY, thermal denaturation was irreversible. At higher temperatures holo CheY is prone to aggregation and is stuck in an energy well in the denatured state. The same thermal transition in the presence of all three polyamines (putrescine, spermine, and spermidine) was reversible (Figure 6.9), indicating that the energy landscape of the protein is altered due to interactions between polyamines and holo CheY. Table 5.3 gives the thermodynamic properties of the holo form of CheY under various conditions.

Table 6.3: Thermodynamic parameters of holo CheY in the presence of polyamines. (ND* - Not determined due to the irreversible transition from native to denatured state)

	Polyamine	T_m (°C)	ΔT_m	ΔH^{o'} (kJ/mol)	TΔS^{o'} (kJ/mol)	ΔG^{o'} (kJ/mol)
1	Holo CheY	64.23 ± 0.23	NA	ND*	ND*	ND*
2	Putrescine (500 mM)	65.5 ± 0.39	1.27	290 ± 22	251.70± 9.69	34.14 ± 1.24
3	Spermine (200 mM)	64.49± 0.56	0.27	280 ± 31	246.25± 13.30	33.56 ± 1.44
4	Spermidine (200 mM)	63.55 ± 0.42	-1.32	290 ± 27	259.87± 11.66	32.65 ± 1.67

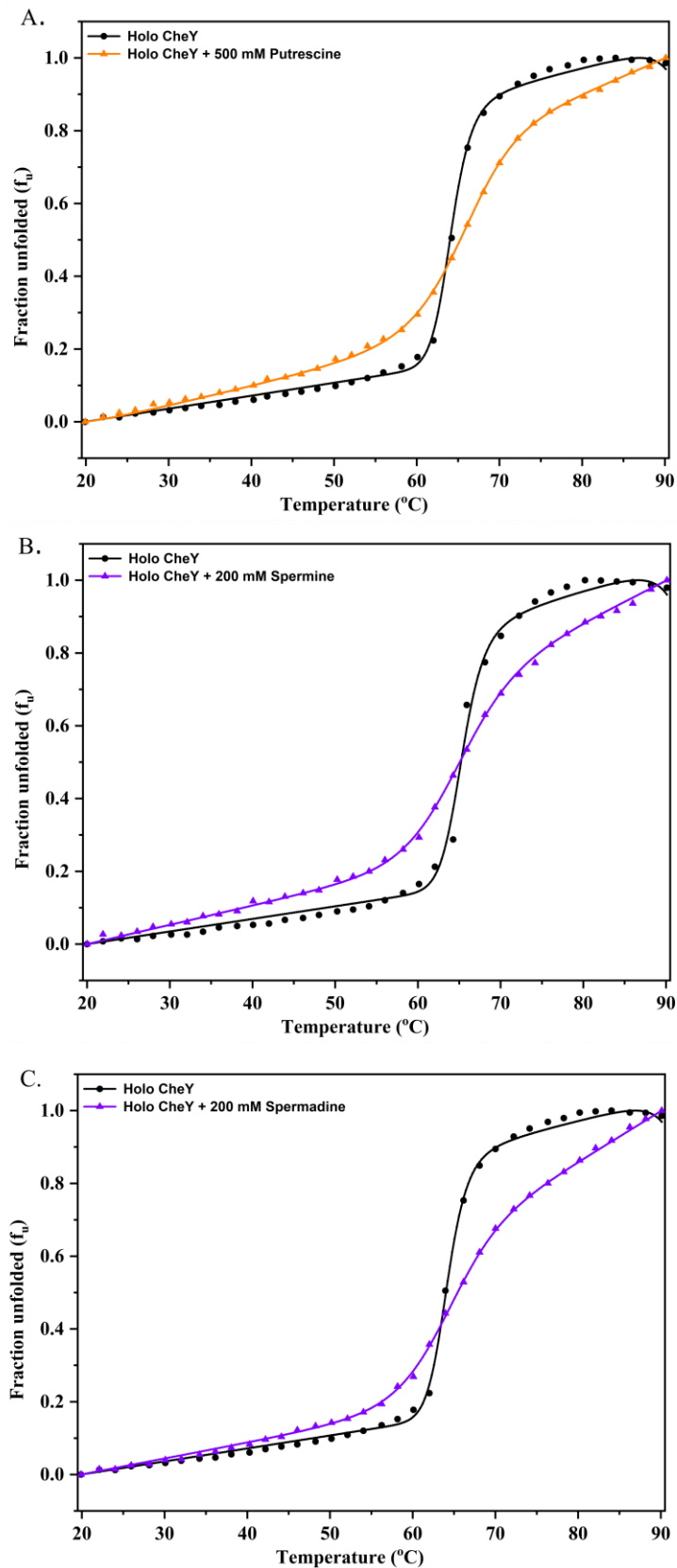


Figure 6.9: Thermal denaturation profiles of holo CheY in the presence of (A) Putrescine, (B) Spermine, and (C) Spermidine. The lines joining the points correspond to a fit to a two-state, folded-unfolded form of the protein. Although data were recorded at 1°C interval, for the purpose of representation the data are plotted at 2°C interval.

Polyamines are polycationic at physiological pH values (Groppa and Benavides, 2008). Hence, are known interact with the surface of protein and provide the additional stability, decrease aggregation tendency, etc. (Kudou *et al.*, 2003; Powroznik *et al.*, 2004). CheY, which is negatively charged (Filimonov *et al.*, 1993), offers an excellent binding surface for these small molecules. These electrostatic interactions can be one of the strong reasons that i) prevents protein aggregation, ii) makes the thermal transitions reversible, and hence alters the energy landscape of the protein (Kudou *et al.*, 2003; Powroznik *et al.*, 2004; Rezaei-Ghaleh *et al.*, 2007; Ziaee *et al.*, 2021).

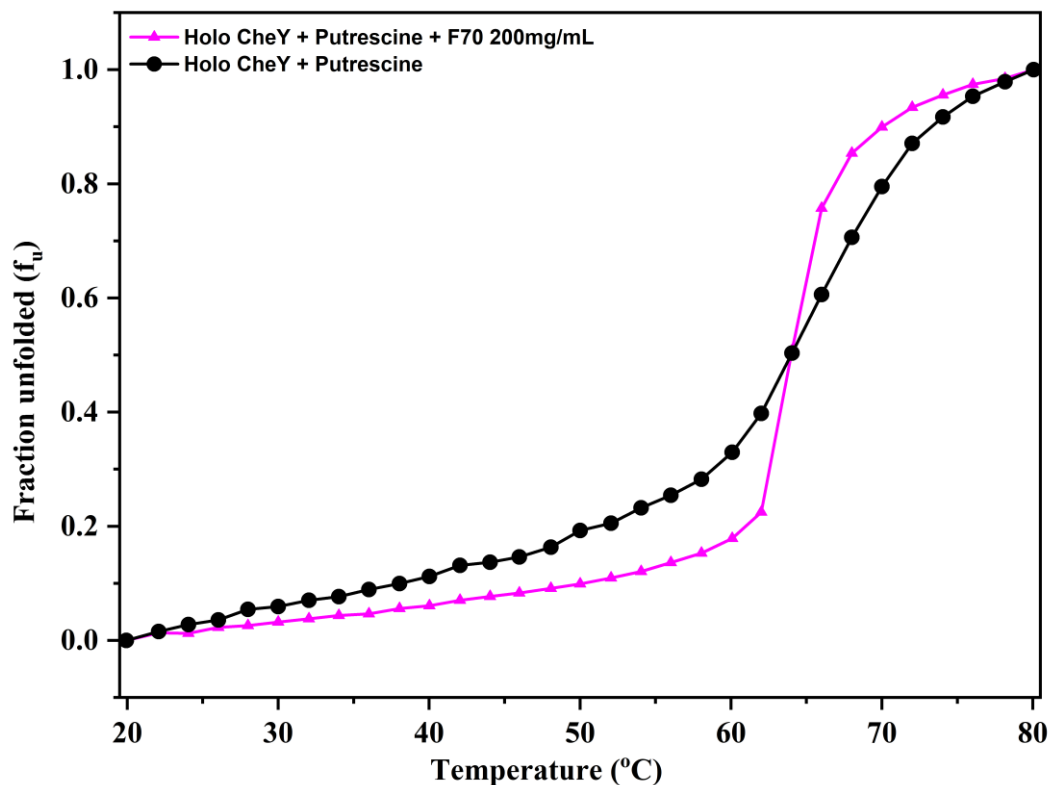


Figure 6.10: Thermal denaturation profiles of holo CheY in the presence of Putrescine and combined presence of putrescine and 200 mg/mL Ficoll 70. The lines joining the points correspond to a fit to a two-state, folded-unfolded form of the protein. Although data were recorded at 1°C interval, for the purpose of representation the data are plotted at 2°C interval.

Interestingly, when Ficoll-70 at a concentration of 200 mg/mL was introduced into the reaction, the midpoint of the thermal transition did not change, in contrast to the case in the absence of polyamines (Figure 6.10). From Chapter 4, it is clear that the presence of Ficoll affects the apo-holo equilibrium and selectively destabilizes the holo form of CheY. This selective

destabilization was overcome in the presence of spermine and putrescine. This could be explained as the apo to holo equilibrium is not affected by Ficoll anymore due to the presence of these polyamines, the hypothesis holds a good possibility of occurrence. Further advanced studies in the direction of pinpointing the source of modulation are needed to better understand the ensuing effects of combined polyamines and crowders. These findings for holo CheY in polyamines and in the combined presence of Ficoll and polyamines suggests that the energy landscape of the holo protein was modified. The following illustration (Figure 6.11) may explain this hypothesis.

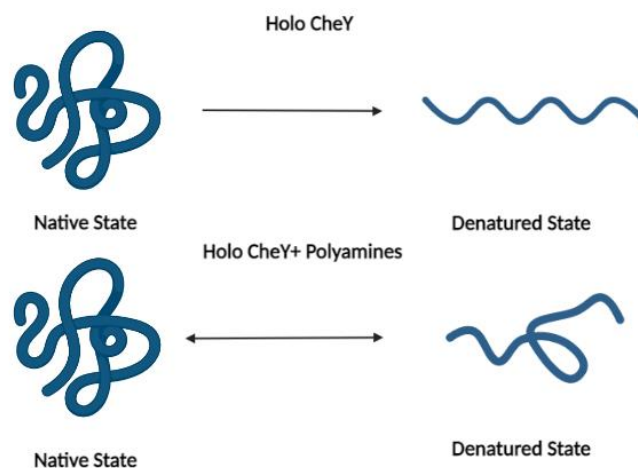


Figure 6.11: Schematic representation of heat induced unfolding of CheY in the presence and absence of polyamines.

6.3 Conclusions

The following conclusions were drawn from the systematic study performed in this chapter (i) Amino acids do not affect either the apo or the holo form of the protein, (ii) In the combined presence of a combination of amino acids and Ficoll-70, apo CheY's stability is slightly increased, similar to the increase in Ficoll alone, (iii) In the combined presence of a combination of amino acids and Ficoll-70, the stability of holo CheY's decreases to the same extent that of in Ficoll alone, indicating at the fact that the predominant macromolecular force of destabilization is still entropic in nature, (iv) The stability of apo CheY increases in the presence of polyamines, (v) In the combined presence of polyamines and Ficoll the thermal

stability of apo protein still shows an increase, (vi) For holo CheY, the presence of polyamines makes the thermal denaturation process reversible, (vii) In the combined presence of polyamines and Ficoll, the thermal stability of holo CheY did not reduce, i.e. the macromolecular forces responsible for the destabilization of holo CheY are no longer active in the presence of polyamines. These conclusions open avenues for a detailed study using various spectroscopic techniques, particularly NMR. Currently, one can only speculate the source of modulation, and targeted NMR studies to map the energy landscape of holo CheY, first in the presence of polyamines and then in the combined presence of polyamines, would certainly help in understanding the ensuing observations in a comprehensive manner.

Chapter 7

Conclusions and Future Perspectives

7.1 Conclusions

In summary, this thesis presents the effects of macromolecular crowding on the structure, stability, and function of Chemotaxis protein Y. This study elaborately describes the mechanistic details of the effects induced by crowding agents of different sizes, shapes and chemical natures. The main focus of this thesis is to highlight the fact that the same protein can display an array of effects when exposed to various crowding agents. Another important finding of this thesis is that, using NMR spectroscopy the source of modulation of the effect on the structure, stability, and function was identified and reported. Such studies are scarce in this field owing to the various limitations discussed later in this section.

Crowding with PEG 20000 suggests that PEG 20000 reduces the secondary structure by about 10-15%. Changes in the secondary structure were also reflected in the tertiary packing interactions. The intrinsic tryptophan fluorescence emission showed a red shift and a reduction in emission intensity, which corroborates the far and near UV-CD results. These changes were also reflected in the fluorescence lifetimes recorded in the presence of PEG 20000. The population with a longer lifetime was converted into the population with a short lifetime. In addition to this, ANS fluorescence showed a concentration-dependent increase in the intensity, suggesting exposure of new hydrophobic surface in the presence of PEG. The thermodynamic stability reduced slightly in a concentration-dependent manner. To gain further insight into the thermodynamic mechanism of this destabilization, we plotted the thermodynamic parameters obtained from the thermal denaturation fits. We found that the destabilization was enthalpic in nature. A combined reduction in T_m and $\Delta H^\circ'$ values indicated direct PEG-protein interactions. Similarly, all of these studies were performed in the presence of different PEG polymer lengths.

The secondary and tertiary structures did not change significantly in the presence of LMW PEGs. Intrinsic tryptophan fluorescence also showed no significant change. Hence, further ANS and lifetimes were not probed for these LMW PEGs. However, the thermal stability of apo CheY in the presence of all PEGs reduced in a concentration-dependent manner by an average of 1-3°C. Surprisingly, all PEGs starting from 6000 to 20000 showed a drastic reduction in thermal stability in a concentration-dependent manner. Hence, we concluded that in the presence of all PEGs, the apo form of CheY is affected to such an extent that the metal-binding site is either disrupted or is in its non-native form as the metal-induced increase in thermal stability was not observed.

Chapter 3 mainly focuses on crowding induced by carbohydrate-based polymers such as Ficoll 70000, Dextran 6000, Dextran 40000, and Dextran 70000. These are the most commonly used sugar-based polymers for mimicking in-cell-like conditions. We report that, in the presence of Dextran 40000 and Dextran 70000, the structure of CheY was perturbed in a manner that showed no specific trend in either secondary or tertiary structures. Fluorescence emission does not provide any insight into this phenomenon. A steady concentration-based reduction in the intensity at the emission maximum was reported due to the solvent's change in polarity after the addition of Dextran. However, Dextran 6000 behaves differently from the other two Dextrans. Its effect on the secondary structure was negligible, but the thermal stability in the presence of Dextran 6000 increased drastically when compared to dilute buffer conditions. This unusual behaviour might be due to the aggregation/association induced in the apo form of the protein. Unusual and inconsistent results led us not to avoid crowding with Dextrans on our test protein.

Furthermore, we studied the effect of crowding on the conformationally distinct states of CheY. We observed a stabilizing effect of Ficoll 70 on the apo form of the protein. The effect of Ficoll 70 was opposite for the holo form of CheY. Intriguingly, macromolecular crowding by Ficoll

resulted in a selective reduction in the thermal stability of the holo form. The reduced thermal stability of the holo form raises a fundamental question: is the metal-binding site intact in Ficoll? The data obtained from intrinsic tryptophan quenching indicated that metal binding is retained in a crowded environment. Since metal–protein interaction remain unperturbed, the alternative possibility for the exclusive reduction in the thermal stability of the holo form is Ficoll-induced modulation of the relative population of apo and holo forms of CheY. Chapter 4 focuses on obtaining molecular insights into the origin of the effects of the modulation of crowding on the test protein CheY. In Chapter 2, it was established that there are direct PEG–protein interactions as the T_m and ΔH° values decreased simultaneously. This became the premise for further probing the study to obtain molecular insights into the effects of macromolecular crowding in the presence and absence of PEG 20000. ^1H - ^{15}N TROSY-HSQC were recorded for CheY in the presence of varying concentrations of PEG 20000 to unravel PEG–protein interactions and their consequences on the conformation of the protein. The relative changes in NMR linewidths and chemical shift perturbations of the protein under crowding conditions in relation to their measurements in dilute buffers indicated the potential sites of interactions and/or crowding-induced changes in the conformation and dynamics. A significant number of residues show small chemical shift changes in the presence of 100 mg/mL PEG 20000. At 200 mg/mL, further gradual movement in the chemical shifts for a set of residues, including K7 (β 1), M17 (α 1), I20 (α 1), E27 (α 1), N32 (residue preceding β 2), A36 (β 2), E37 (loop preceding α 2), V40 (α 2), A48 (α 2), G49 (loop preceding β 3) G50 (loop preceding β 3), W58 (side chain (SC)) (β 3), M78 (loop preceding β 4), L81 (β 4), T87 (β 4), E93 (α 4), I95 (α 4), I96 (α 4), A98 (α 4), A99 (α 4), Q100 (α 4), V108 (β 5), T112 (α 5), A113 (α 5), I26K (α 5) and G128 (α 5). It is interesting to note that there is a subset of residues that is not exposed to the solvent, but still display CSPs, i.e. A98 and A113, suggesting that the origin of CSPs for these residues may not emanate from direct contacts between the protein and PEG

20000, but rather maybe from the conformational changes and or fluctuations prompted by the presence of PEG 20000. A significant number of residues with chemical shifts occur in α -helices, followed by loops/turns and β strands. These residues reside at the terminal positions of the secondary structural elements. Along with the CSPs, the intensity of the cross peaks also revealed a mixture of polar and non-polar residues getting affected in the presence of PEG 20000. In conclusion, PEG 20000 distorts the apo structure around the metal binding site, which leads to the loss of the metal-binding ability of CheY. This corroborates the results obtained in Chapter 2 for the thermal stability of holo CheY. Contrary to the effects observed for PEG 20000, Ficoll 70 showed no significant CSPs in the ^1H - ^{15}N – HSQC spectrum compared with dilute buffer conditions. We have already established from Chapter 3 that, in the presence of Ficoll, the metal binding ability is retained. We confirmed metal binding again by observing a perfect overlap of the ^1H - ^{15}N – HSQC spectrum of holo CheY in the presence and absence of Ficoll. The likelihood of Ficoll-protein interactions can be determined by analyzing the line broadening of the backbone resonances. In the presence of Ficoll alone, a significant number of resonances demonstrated increased linewidths at 200 mg/mL, indicating the likelihood of protein-Ficoll interactions. Residues G50, E89, K91, and A98, which fall in the loops, are less affected, presumably arising from the slower tumbling due to the viscosity effect of Ficoll. In the presence of Ficoll, in holo CheY, more than a dozen residues show further increased linewidths (L6, R19, R22, N32, E35, A36, E67, L81, A97, A99, A101, G105, and E125). The intensities of certain residues such as L81, A97, A99, A101, and G105 overlap with the region that shows structural perturbation upon Mg^{2+} binding, suggesting the possibility of an apo-holo equilibrium. Furthermore, all monomeric units such as glucose, sucrose, and a combination of these for mixed macromolecular crowding effect, also report results similar to those obtained previously.

The interiors of the cell are not just filled with molecules that are huge and take up space, but also have a very high concentration of metabolites, polyamines, etc. Therefore, we selected certain molecules such as amino acids and polyamine and elucidated the effect of these molecules on the structure and stability of CheY. Amino acids did not affect the structure or stability of the apo and holo forms of CheY. On the other hand, polyamines have a stabilizing effect on the apo form of CheY. Interestingly, thermal stability, which is an irreversible process for holo CheY, is reversible in the presence of polyamines. Polyamines prevent protein aggregation by binding to the exposed charged surface of proteins. CheY is net negatively charged, and polyamines are heavily positively charged at physiological pH and hence have the potential to bind to CheY. This binding leads to increased protein solubility at higher temperatures; thus, the thermal denaturation process is reversible. Furthermore, we studied the combined effects of amino acids + crowders and polyamines + crowders. Surprisingly, the thermal stability of the holo protein, which reduces drastically in the presence of crowders, remains the same as that of the native holo protein in the presence of spermine and putrescine. This effect was specifically observed in the presence of Ficoll and polyamines. Polyamines somehow have the capability of counteracting the macromolecular crowding effect induced by ficoll.

Taken together, this thesis claims the following: i) PEG-protein interactions are very high in the apo form, which disrupts the metal binding region and hence the ensuing increase in stability is not observed; ii) it is the macromolecular nature (volume exclusion) of Ficoll that disrupts the apo-holo equilibrium and selectively destabilizes the holo form of CheY; iii) monomers like glucose and sucrose alone and in combination with macromolecular crowders stabilize the apo form, whereas the holo form is destabilized; iv) polyamines alter the energy landscape of the holo form of the protein; and v) polyamines counteract the effect of Ficoll-induced macromolecular crowding effect on the holo form of protein. This thesis also precisely

dissects the effects of crowding and elucidates the mechanisms of destabilization and stabilization observed for a particular pair of protein and crowder. It is now extremely clear that cellular functions need to be studied in a complex in-cell-like conditions to better understand the changes that occur in the structure to accommodate the crowded environment inside the cell. This thesis sheds light on the fact that the same test protein can behave differently when the nature, shape, and size of the crowder vary. For all biological processes, the structure of a protein determines its function. Hence, its structure, function, and dynamics should be elucidated in a crowded environment.

7.2 Specific Contributions

This thesis highlights the following -

- Improved the understanding of protein structure-function relationship under in-cell like conditions.
- A particular protein behaves differently with the change in the nature and volume fraction of the crowder.
- The source of modulation of the effect of PEG 20000 mediated crowding originated from both hydrophobic and hydrophilic residues in the protein.
- Residues buried in the interiors of the protein structure also displayed CSPs, indicating towards PEG mediated changes in the local environment of the protein.
- PEG destabilized the protein via enthalpic contributions from PEG-protein interactions
- Ficoll selectively destabilized the holo form of the protein.
- Crowding with Ficoll disrupted the apo-holo equilibrium of the protein.
- The major destabilizing force acting in the presence of Ficoll is entropic in nature.
- Small molecular crowding with amino acids and in combination of amino acids and Ficoll had similar effect as in the absence of amino acids.

- Polyamines altered the energy landscape of the protein.
- Polyamines counteracted the effect of selective destabilization of holo form induced by Ficoll.

7.3 Limitations

Owing to the highly viscous nature of macromolecular crowders, spectroscopic measurements are difficult. In addition, certain small molecules such as amino acids, ionic liquids, etc. interfere with optical spectroscopy techniques, which limits the studies to be performed using only high-end spectroscopic techniques such as NMR. Most of the cases protein concentration for NMR experiment also stands out as a limitation for crowding studies.

Apart from the experimental limitations, it's reported in literature and this thesis also emphasizes that the effect of macromolecule crowding is much more complex than what we try to demonstrate with single, or a mixture of molecular and macromolecular crowders. Therefore, even after careful consideration, effects of crowding cannot be explained completely.

7.4 Future Scope of Work

To the best of our knowledge, this field is progressing in the direction of single-molecule spectroscopy to specifically study the effects of crowding at fundamental levels. Certain groups in India and abroad have made significant progress over the last three years in the field of single-molecule spectroscopy in crowded environments. This will increase our understanding of the protein structure and function relationships.

In-cell NMR spectroscopy and dynamics studies with NMR can yield insights into the mechanistic details of crowding. In light of this statement, to keep up with the trend in NMR spectroscopy and crowding, we have attempted to record an in-cell NMR ^1H - ^{15}N – HSQC spectrum that showed some promising results. Further optimization is required at all levels of

experimentation. For instance, the need for a clone with very high protein expression is the first basic need, and selectively labelling only our protein of interest to reduce noise from the bacterial proteome is another challenge, etc. Such experiments will open avenues for studying protein in their native environment inside the cell.

Data should be collected with as many proteins and crowders as possible to create a database that can be further used as a reference for careful design and considerations needed for all protein structure, function, and dynamics studies.

References

Abriata, L. A., Spiga, E. and Peraro, M. D. (2016a) ‘Molecular Effects of Concentrated Solutes on Protein Hydration, Dynamics, and Electrostatics’, *Biophysical Journal*, 111(4), pp. 743–755. doi: 10.1016/j.bpj.2016.07.011.

Abriata, L. A., Spiga, E. and Peraro, M. D. (2016b) ‘Molecular Effects of Concentrated Solutes on Protein Hydration, Dynamics, and Electrostatics’, *Biophysical Journal*, 111(4), pp. 743–755. doi: 10.1016/j.bpj.2016.07.011.

Adams, L. M. *et al.* (2019) ‘Crowder-Induced Conformational Ensemble Shift in Escherichia coli Prolyl-tRNA Synthetase’, *Biophysical Journal*, 117(7), pp. 1269–1284. doi: 10.1016/j.bpj.2019.08.033.

Ådén, J. and Wolf-Watz, M. (2007) ‘NMR identification of transient complexes critical to adenylate kinase catalysis’, *Journal of the American Chemical Society*, 129(45), pp. 14003–14012. doi: 10.1021/ja075055g.

Akke, M., Carr, P. A. and Palmer, A. G. (1994) ‘Heteronuclear-Correlation NMR Spectroscopy with Simultaneous Isotope Filtration, Quadrature Detection, and Sensitivity Enhancement Using z Rotations’, *Journal of Magnetic Resonance, Series B*, 104(3), pp. 298–302. doi: <https://doi.org/10.1006/jmrb.1994.1090>.

Anfinsen, C. B. (1973) ‘Principles that govern the folding of protein chains’, *Science*, 181(4096), pp. 223–230. doi: 10.1126/science.181.4096.223.

Arakawa, T. and Timasheff, S. N. (1985) ‘Mechanism of Polyethylene glycol) Interaction with Proteins’, *Biochemistry*, 24(24), pp. 6756–6762. doi: 10.1021/bi00345a005.

Ashrafi, N. *et al.* (2022) ‘The effect of putrescine on the lysozyme activity and structure: Spectroscopic approaches and molecular dynamic simulation’, *Colloids and Surfaces B:*

Biointerfaces, 213(July 2021), p. 112402. doi: 10.1016/j.colsurfb.2022.112402.

Aue, W. P., Bartholdi, E. and Ernst, R. R. (1976) 'Two-dimensional spectroscopy. Application to nuclear magnetic resonance', *The Journal of Chemical Physics*, 64(5), pp. 2229–2246. doi: 10.1063/1.432450.

Back, J. F., Oakenfull, D. and Smith, M. B. (1979) 'Increased Thermal Stability of Proteins in the Presence of Sugars and Polyols', *Biochemistry*, 18(23), pp. 5191–5196. doi: 10.1021/bi00590a025.

Barondeau, D. P. and Getzoff, E. D. (2004) 'Structural insights into protein-metal ion partnerships', *Current Opinion in Structural Biology*, 14(6), pp. 765–774. doi: 10.1016/j.sbi.2004.10.012.

Batra, J., Xu, K. and Zhou, H. X. (2009) 'Nonadditive effects of mixed crowding on protein stability', *Proteins: Structure, Function and Bioinformatics*, 77(1), pp. 133–138. doi: 10.1002/prot.22425.

Bax, A. and Ikura, M. (1991) 'An efficient 3D NMR technique for correlating the proton and ¹⁵N backbone amide resonances with the α -carbon of the preceding residue in uniformly ¹⁵N/¹³C enriched proteins', *Journal of Biomolecular NMR*, 1(1), pp. 99–104. doi: 10.1007/BF01874573.

Bellsolell, L. *et al.* (1994) 'Magnesium binding to the bacterial chemotaxis protein cheY results in large conformational changes involving its functional surface', *Journal of Molecular Biology*, 238(4), pp. 489–495. doi: 10.1006/jmbi.1994.1308.

Bennett, B. D. *et al.* (2009) 'Absolute metabolite concentrations and implied enzyme active site occupancy in *Escherichia coli*', *Nature Chemical Biology*. 2009/06/28, 5(8), pp. 593–599. doi: 10.1038/nchembio.186.

Benton, L. A. *et al.* (2012a) ‘Unexpected effects of macromolecular crowding on protein stability’, *Biochemistry*, 51(49), pp. 9773–9775. doi: 10.1021/bi300909q.

Benton, L. A. *et al.* (2012b) ‘Unexpected effects of macromolecular crowding on protein stability’, *Biochemistry*, 51(49), pp. 9773–9775. doi: 10.1021/bi300909q.

Van Den Berg, B., Ellis, R. J. and Dobson, C. M. (1999) ‘Effects of macromolecular crowding on protein folding and aggregation’, *EMBO Journal*, 18(24), pp. 6927–6933. doi: 10.1093/emboj/18.24.6927.

Bhakuni, K. and Venkatesu, P. (2018) ‘Crowded milieu tuning the stability and activity of stem bromelain’, *International Journal of Biological Macromolecules*, 109, pp. 114–123. doi: 10.1016/j.ijbiomac.2017.12.060.

Bhakuni, K. and Venkatesu, P. (2019) ‘Does macromolecular crowding compatible with enzyme stem bromelain structure and stability?’, *International Journal of Biological Macromolecules*, 131, pp. 527–535. doi: 10.1016/j.ijbiomac.2019.03.090.

Bille, A. *et al.* (2019) ‘Stability and Local Unfolding of SOD1 in the Presence of Protein Crowders’, *Journal of Physical Chemistry B*, 123(9), pp. 1920–1930. doi: 10.1021/acs.jpcc.8b10774.

Billeter, M., Braun, W. and Wüthrich, K. (1982) ‘Sequential resonance assignments in protein ¹H nuclear magnetic resonance spectra: Computation of sterically allowed proton-proton distances and statistical analysis of proton-proton distances in single crystal protein conformations’, *Journal of Molecular Biology*, 155(3), pp. 321–346. doi: [https://doi.org/10.1016/0022-2836\(82\)90008-0](https://doi.org/10.1016/0022-2836(82)90008-0).

Bodenhausen, G. and Ruben, D. J. (1980) ‘Natural abundance nitrogen-15 NMR by enhanced heteronuclear spectroscopy’, *Chemical Physics Letters*, 69(1), pp. 185–189. doi:

[https://doi.org/10.1016/0009-2614\(80\)80041-8](https://doi.org/10.1016/0009-2614(80)80041-8).

Bond, C. S. (2003) 'TopDraw: A sketchpad for protein structure topology cartoons', *Bioinformatics*, 19(2), pp. 311–312. doi: 10.1093/bioinformatics/19.2.311.

Bren, A. and Eisenbach, M. (2000) 'How signals are heard during bacterial chemotaxis: Protein-protein interactions in sensory signal propagation', *Journal of Bacteriology*, 182(24), pp. 6865–6873. doi: 10.1128/JB.182.24.6865-6873.2000.

Breydo, L. *et al.* (2015) 'Effects of polymer hydrophobicity on protein structure and aggregation kinetics in crowded milieu', *Biochemistry*, 54(19), pp. 2957–2966. doi: 10.1021/acs.biochem.5b00116.

Bruix, M. *et al.* (1993) '1H- and 15N-NMR assignment and solution structure of the chemotactic Escherichia coli Che Y protein.', *European journal of biochemistry*, 215(3), pp. 573–85. doi: 10.1111/j.1432-1033.1993.tb18068.x.

Canchi, D. R. and García, A. E. (2013) 'Cosolvent effects on protein stability', *Annual Review of Physical Chemistry*, 64, pp. 273–293. doi: 10.1146/annurev-physchem-040412-110156.

Chanphai, P., Thomas, T. J. and Tajmir-Riahi, H. A. (2016) 'Conjugation of biogenic and synthetic polyamines with serum proteins: A comprehensive review', *International Journal of Biological Macromolecules*, 92, pp. 515–522. doi: <https://doi.org/10.1016/j.ijbiomac.2016.07.049>.

Cho, H. S. *et al.* (2000) 'NMR structure of activated CheY', *Journal of Molecular Biology*, 297(3), pp. 543–551. doi: 10.1006/jmbi.2000.3595.

Christiansen, A. *et al.* (2010) 'Factors defining effects of macromolecular crowding on protein stability: An in vitro/in silico case study using cytochrome c', *Biochemistry*, 49(31), pp. 6519–6530. doi: 10.1021/bi100578x.

Cino, E. A., Karttunen, M. and Choy, W. Y. (2012) 'Effects of Molecular Crowding on the Dynamics of Intrinsically Disordered Proteins', *PLoS ONE*. Edited by Y. K. Levy, 7(11), p. e49876. doi: 10.1371/journal.pone.0049876.

Clubb, R. T., Thanabal, V. and Wagner, G. (1992) 'A constant-time three-dimensional triple-resonance pulse scheme to correlate intraresidue ^1HN , ^{15}N , and ^{13}C chemical shifts in ^{15}N - ^{13}C -labelled proteins', *Journal of Magnetic Resonance (1969)*, 97(1), pp. 213–217. doi: [https://doi.org/10.1016/0022-2364\(92\)90252-3](https://doi.org/10.1016/0022-2364(92)90252-3).

Cohen, R. D. and Pielak, G. J. (2016) 'Electrostatic Contributions to Protein Quinary Structure', *Journal of the American Chemical Society*, 138(40), pp. 13139–13142. doi: 10.1021/jacs.6b07323.

Creighton, T. E. (1990) 'Protein folding', *Biochemical Journal*, 270(1), pp. 1–16. doi: 10.1042/bj2700001.

Cremades, N. and Sancho, J. (2008) 'Molten globule and native state ensemble of *Helicobacter pylori* flavodoxin: Can crowding, osmolytes or cofactors stabilize the native conformation relative to the molten globule?', *Biophysical Journal*, 95(4), pp. 1913–1927. doi: 10.1529/biophysj.108.130153.

Crowley, P. B., Brett, K. and Muldoon, J. (2008) 'NMR spectroscopy reveals cytochrome c-poly(ethylene glycol) interactions', *ChemBioChem*, 9(5), pp. 685–688. doi: 10.1002/cbic.200700603.

Das, N. and Sen, P. (2019) 'Size-dependent macromolecular crowding effect on the thermodynamics of protein unfolding revealed at the single molecular level', *International Journal of Biological Macromolecules*, 141, pp. 843–854. doi: 10.1016/j.ijbiomac.2019.09.029.

Das, N. and Sen, P. (2020) ‘Shape-Dependent Macromolecular Crowding on the Thermodynamics and Microsecond Conformational Dynamics of Protein Unfolding Revealed at the Single-Molecule Level’, *The Journal of Physical Chemistry B*, 124(28), pp. 5858–5871. doi: 10.1021/acs.jpcc.0c03897.

Das, N. and Sen, P. (2022) ‘Macromolecular crowding: how shape and interaction affect the structure, function, conformational dynamics and relative domain movement of a multi-domain protein’, *Physical Chemistry Chemical Physics*, 24(23), pp. 14242–14256. doi: 10.1039/D1CP04842B.

Davis, C. M., Deutsch, J. and Gruebele, M. (2020) ‘An in vitro mimic of in-cell solvation for protein folding studies’, *Protein Science*, 29(4), pp. 1060–1068. doi: 10.1002/pro.3833.

DeKoster, G. T. *et al.* (1993) ‘Urea and Guanidine-HCl Yield Different Unfolding Free Energies for CheY: Which Denaturant Provides the Most Reliable Free Energy Values?’, in Angeletti, R. H. B. T.-T. in P. C. I. V (ed.) *Techniques in Protein Chemistry IV*. Academic Press, pp. 533–540. doi: 10.1016/b978-0-12-058757-5.50063-9.

Delaglio, F. *et al.* (1995) ‘NMRPipe: A multidimensional spectral processing system based on UNIX pipes’, *Journal of Biomolecular NMR*, 6(3), pp. 277–293. doi: 10.1007/BF00197809.

Dhar, A. *et al.* (2010) ‘Structure, function, and folding of phosphoglycerate kinase are strongly perturbed by macromolecular crowding’, *Proceedings of the National Academy of Sciences of the United States of America*, 107(41), pp. 17586–17591. doi: 10.1073/pnas.1006760107.

Dill, K. A. (1990) ‘Dominant forces in protein folding’, *Biochemistry*, 29(31), pp. 7133–7155. doi: 10.1021/bi00483a001.

Diniz, A. *et al.* (2017) ‘Protein-Glycan Quinary Interactions in Crowding Environment Unveiled by NMR Spectroscopy’, *Chemistry - A European Journal*, 23(53), pp. 13213–13220.

doi: 10.1002/chem.201702800.

Djordjevic, S. and Stock, A. M. (1998) 'Structural analysis of bacterial chemotaxis proteins: Components of a dynamic signaling system', *Journal of Structural Biology*, 124(2–3), pp. 189–200. doi: 10.1006/jsbi.1998.4034.

Dobson, C. M. (2003) 'Protein folding and misfolding.', *Nature*, 426(6968), pp. 884–90. doi: 10.1038/nature02261.

Dong, H., Qin, S. and Zhou, H. X. (2010) 'Effects of macromolecular crowding on protein conformational changes', *PLoS Computational Biology*. Edited by M. P. Jacobson, 6(7), p. 29. doi: 10.1371/journal.pcbi.1000833.

Eggers, D. K. and Valentine, J. S. (2001) 'Crowding and Hydration effects on protein conformation: A study with sol-gel encapsulated proteins', *Journal of Molecular Biology*, 314(4), pp. 911–922. doi: 10.1006/jmbi.2001.5166.

Eisenbach, M. (1996) 'Control of bacterial chemotaxis', *Molecular Microbiology*, 20(5), pp. 903–910. doi: 10.1111/j.1365-2958.1996.tb02531.x.

Ellis, R. J. (2001) 'Macromolecular crowding: An important but neglected aspect of the intracellular environment', *Current Opinion in Structural Biology*. Elsevier Current Trends, pp. 114–119. doi: 10.1016/S0959-440X(00)00172-X.

Ellis, R. John (2001) 'Macromolecular crowding: Obvious but underappreciated', *Trends in Biochemical Sciences*, 26(10), pp. 597–604. doi: 10.1016/S0968-0004(01)01938-7.

Ellis, R. J. and Minton, A. P. (2003) 'Join the crowd', *Nature*. England, pp. 27–28. doi: 10.1038/425027a.

Engel, R. *et al.* (2008) 'Macromolecular crowding compacts unfolded apoflavodoxin and causes severe aggregation of the off-pathway intermediate during apoflavodoxin folding',

Journal of Biological Chemistry, 283(41), pp. 27383–27394. doi: 10.1074/jbc.M802393200.

Engelhard, M. and Evans, P. A. (1995) ‘Kinetics of interaction of partially folded proteins with a hydrophobic dye: Evidence that molten globule character is maximal in early folding intermediates’, *Protein Science*, 4(8), pp. 1553–1562. doi: 10.1002/pro.5560040813.

Erlkamp, M., Grobelny, S. and Winter, R. (2014) ‘Crowding effects on the temperature and pressure dependent structure, stability and folding kinetics of Staphylococcal Nuclease’, *Physical Chemistry Chemical Physics*, 16(13), pp. 5965–5976. doi: 10.1039/c3cp55040k.

Farmer, B. T. *et al.* (1992) ‘A refocused and optimized HNCA: Increased sensitivity and resolution in large macromolecules’, *Journal of Biomolecular NMR*, 2(2), pp. 195–202. doi: 10.1007/BF01875530.

Ferguson, K. M. (2008) ‘Structure-based view of epidermal growth factor receptor regulation’, *Annual Review of Biophysics*, pp. 353–373. doi: 10.1146/annurev.biophys.37.032807.125829.

Filimonov, V. V. *et al.* (1993) ‘Thermodynamic Analysis of the Chemotactic Protein from *Escherichia coli*, CheY’, *Biochemistry*, 32(47), pp. 12906–12921. doi: 10.1021/bi00210a045.

Fonin, A. V. *et al.* (2014) ‘Fluorescence of dyes in solutions with high absorbance. Inner filter effect correction’, *PLoS ONE*. Edited by E. A. Permyakov, 9(7), p. e103878. doi: 10.1371/journal.pone.0103878.

Fonin, A. V. *et al.* (2017) ‘Structure and conformational properties of D-glucose/D-galactose-binding protein in crowded milieu’, *Molecules*, 22(2), p. 244. doi: 10.3390/molecules22020244.

Fulton, A. B. (1982) ‘How crowded is the cytoplasm?’, *Cell*, 30(2), pp. 345–347. doi: 10.1016/0092-8674(82)90231-8.

Furness, E. L. *et al.* (1998) ‘A hydrophobic interaction site for lysozyme binding to

polyethylene glycol and model contact lens polymers', *Biomaterials*, 19(15), pp. 1361–1369. doi: 10.1016/S0142-9612(98)00007-6.

Ghaemmaghami, S. and Oas, T. G. (2001) 'Quantitative protein stability measurement in vivo.', *Nature structural biology*, 8(10), pp. 879–82. doi: 10.1038/nsb1001-879.

Ghosh, S. *et al.* (2020) 'Molecular and macromolecular crowding-induced stabilization of proteins: Effect of dextran and its building block alone and their mixtures on stability and structure of lysozyme', *International Journal of Biological Macromolecules*, 150, pp. 1238–1248. doi: 10.1016/j.ijbiomac.2019.10.135.

Goh, C.-S., Milburn, D. and Gerstein, M. (2004) 'Conformational changes associated with protein–protein interactions', *Current Opinion in Structural Biology*, 14(1), pp. 104–109. doi: 10.1016/j.sbi.2004.01.005.

Goswami, S. *et al.* (2021) 'Role of Conformational Change and Glucose Binding Sites in the Enhanced Glucose Tolerance of *Agrobacterium tumefaciens* 5A GH1 β -Glucosidase Mutants', *Journal of Physical Chemistry B*, 125(33), pp. 9402–9416. doi: 10.1021/acs.jpcc.1c02150.

Gouet, P. *et al.* (2001) 'Further insight into the mechanism of function of the response regulator CheY from crystallographic studies of the CheY-CheA124-257 complex', *Acta Crystallographica Section D: Biological Crystallography*, 57(1), pp. 44–51. doi: 10.1107/S090744490001492X.

Greenfield, N. J. (2007a) 'Using circular dichroism collected as a function of temperature to determine the thermodynamics of protein unfolding and binding interactions', *Nature Protocols*, 1(6), pp. 2527–2535. doi: 10.1038/nprot.2006.204.

Greenfield, N. J. (2007b) 'Using circular dichroism spectra to estimate protein secondary structure', *Nature Protocols*, 1(6), pp. 2876–2890. doi: 10.1038/nprot.2006.202.

Groppa, M. D. and Benavides, M. P. (2008) 'Polyamines and abiotic stress: Recent advances', *Amino Acids*, 34(1), pp. 35–45. doi: 10.1007/s00726-007-0501-8.

Grzesiek, S. and Bax, A. (1992a) 'An efficient experiment for sequential backbone assignment of medium-sized isotopically enriched proteins', *Journal of Magnetic Resonance (1969)*, 99(1), pp. 201–207. doi: [https://doi.org/10.1016/0022-2364\(92\)90169-8](https://doi.org/10.1016/0022-2364(92)90169-8).

Grzesiek, S. and Bax, A. (1992b) 'Correlating backbone amide and side chain resonances in larger proteins by multiple relayed triple resonance NMR', *Journal of the American Chemical Society*, 114(16), pp. 6291–6293. doi: 10.1021/ja00042a003.

Grzesiek, S. and Bax, A. (1992c) 'Improved 3D triple-resonance NMR techniques applied to a 31 kDa protein', *Journal of Magnetic Resonance (1969)*, 96(2), pp. 432–440. doi: [https://doi.org/10.1016/0022-2364\(92\)90099-S](https://doi.org/10.1016/0022-2364(92)90099-S).

Guhaniyogi, J., Robinson, V. L. and Stock, A. M. (2006) 'Crystal Structures of Beryllium Fluoride-free and Beryllium Fluoride-bound CheY in Complex with the Conserved C-terminal Peptide of CheZ Reveal Dual Binding Modes Specific to CheY Conformation', *Journal of Molecular Biology*, 359(3), pp. 624–645. doi: 10.1016/j.jmb.2006.03.050.

Guseman, A. J. *et al.* (2018) 'Protein shape modulates crowding effects', *Proceedings of the National Academy of Sciences of the United States of America*. 2018/10/09, 115(43), pp. 10965–10970. doi: 10.1073/pnas.1810054115.

Harada, R., Sugita, Y. and Feig, M. (2012) 'Protein crowding affects hydration structure and dynamics', *Journal of the American Chemical Society*, 134(10), pp. 4842–4849. doi: 10.1021/ja211115q.

Harve, K. S. *et al.* (2006) 'Macromolecular Crowding in Biological Systems: Dynamic Light Scattering (Dls) To Quantify the Excluded Volume Effect (Eve)', *Biophysical Reviews and*

Letters, 01(03), pp. 317–325. doi: 10.1142/s1793048006000215.

He, Y., Kang, J. and Song, J. (2020) ‘ATP antagonizes the crowding-induced destabilization of the human eye-lens protein γ S-crystallin: ATP antagonizes the destabilization of γ S-crystallin’, *Biochemical and Biophysical Research Communications*, 526(4), pp. 1112–1117. doi: 10.1016/j.bbrc.2020.04.014.

Hills, R. D. *et al.* (2010) ‘Topological Frustration in $\beta\alpha$ -Repeat Proteins: Sequence Diversity Modulates the Conserved Folding Mechanisms of $\alpha/\beta/\alpha$ Sandwich Proteins’, *Journal of Molecular Biology*. 2010/03/11, 398(2), pp. 332–350. doi: 10.1016/j.jmb.2010.03.001.

Hishida, M. *et al.* (2022) ‘Effect of Osmolytes on Water Mobility Correlates with Their Stabilizing Effect on Proteins’, *The Journal of Physical Chemistry B*, 126(13), pp. 2466–2475. doi: 10.1021/acs.jpcc.1c10634.

Homouz, D. *et al.* (2009) ‘Modulation of Calmodulin Plasticity by the Effect of Macromolecular Crowding’, *Journal of Molecular Biology*, 391(5), pp. 933–943. doi: 10.1016/j.jmb.2009.06.073.

Horvath, I., Kumar, R. and Wittung-Stafshede, P. (2021) ‘Macromolecular crowding modulates α -synuclein amyloid fiber growth’, *Biophysical Journal*, 120(16), pp. 3374–3381. doi: 10.1016/j.bpj.2021.06.032.

Ikura, M., Kay, L. E. and Bax, A. (1990) ‘A novel approach for sequential assignment of proton, carbon-13, and nitrogen-15 spectra of larger proteins: heteronuclear triple-resonance three-dimensional NMR spectroscopy. Application to calmodulin’, *Biochemistry*, 29(19), pp. 4659–4667. doi: 10.1021/bi00471a022.

Irukuvajjula, S. S., Reddy, J. G. and Vadrevu, R. (2022) ‘Crowding by Poly(ethylene glycol) Destabilizes Chemotaxis Protein Y (CheY)’, *Biochemistry*, 61(14), pp. 1431–1443. doi:

10.1021/acs.biochem.2c00030.

Jackson, S. E. and Fersht, A. R. (1991) 'Folding of chymotrypsin inhibitor 2. 1. Evidence for a two-state transition', *Biochemistry*, 30(43), pp. 10428–10435. doi: 10.1021/bi00107a010.

Jeener, J. *et al.* (1979) 'Investigation of exchange processes by two-dimensional NMR spectroscopy', *The Journal of Chemical Physics*, 71(11), pp. 4546–4553. doi: 10.1063/1.438208.

Johnson, L. N. and Barford, D. (1993) 'The effects of phosphorylation on the structure and function of proteins', *Annual Review of Biophysics and Biomolecular Structure*, pp. 199–232. doi: 10.1146/annurev.bb.22.060193.001215.

Joshi, A. and Kishore, N. (2022) 'Macromolecular crowding and preferential exclusion counteract the effect of protein denaturant: Biophysical aspects', *Journal of Molecular Liquids*, 360, p. 119429. doi: 10.1016/j.molliq.2022.119429.

Kadumuri, R. V. *et al.* (2016) 'Crowding interactions perturb structure and stability by destabilizing the stable core of the α -subunit of tryptophan synthase', *FEBS Letters*, 590(14), pp. 2096–2105. doi: 10.1002/1873-3468.12259.

Kalač, P. and Krausová, P. (2005) 'A review of dietary polyamines: Formation, implications for growth and health and occurrence in foods', *Food Chemistry*, 90(1), pp. 219–230. doi: <https://doi.org/10.1016/j.foodchem.2004.03.044>.

Kathuria, S. V. *et al.* (2008) 'Kinetic Traps in the Folding of $\beta\alpha$ -Repeat Proteins: CheY Initially Misfolds before Accessing the Native Conformation', *Journal of Molecular Biology*, 382(2), pp. 467–484. doi: 10.1016/j.jmb.2008.06.054.

Kay, L. E. *et al.* (1990) 'Three-dimensional triple-resonance NMR spectroscopy of isotopically enriched proteins', *Journal of Magnetic Resonance (1969)*, 89(3), pp. 496–514. doi:

[https://doi.org/10.1016/0022-2364\(90\)90333-5](https://doi.org/10.1016/0022-2364(90)90333-5).

Keller, R. (2004) *The computer aided resonance assignment tutorial, Goldau, Switzerland: Cantina Verlag*. Cantina. Available at: <http://cara.nmr.ch>.

Kelly, S. M., Jess, T. J. and Price, N. C. (2005) ‘How to study proteins by circular dichroism’, *Biochimica et Biophysica Acta - Proteins and Proteomics*, 1751(2), pp. 119–139. doi: 10.1016/j.bbapap.2005.06.005.

Kelly, S. and Price, N. (2005) ‘The Use of Circular Dichroism in the Investigation of Protein Structure and Function’, *Current Protein & Peptide Science*, 1(4), pp. 349–384. doi: 10.2174/1389203003381315.

Kim, Y.-S. *et al.* (2003) ‘Effects of sucrose on conformational equilibria and fluctuations within the native-state ensemble of proteins’, *Protein Science*, 12(6), pp. 1252–1261. doi: 10.1110/ps.0242603.

Knowles, D. B. *et al.* (2015) ‘Chemical Interactions of Polyethylene Glycols (PEGs) and Glycerol with Protein Functional Groups: Applications to Effects of PEG and Glycerol on Protein Processes’, *Biochemistry*, 54(22), pp. 3528–3542. doi: 10.1021/acs.biochem.5b00246.

Köhn, B. and Kovermann, M. (2019) ‘Macromolecular Crowding Tunes Protein Stability by Manipulating Solvent Accessibility’, *ChemBioChem*, 20(6), pp. 759–763. doi: 10.1002/cbic.201800679.

Köhn, B. and Kovermann, M. (2020) ‘All atom insights into the impact of crowded environments on protein stability by NMR spectroscopy’, *Nature Communications*, 11(1), p. 5760. doi: 10.1038/s41467-020-19616-w.

Koshland, D. E. (1995) ‘The Key–Lock Theory and the Induced Fit Theory’, *Angewandte Chemie International Edition in English*, 33(23–24), pp. 2375–2378. doi:

10.1002/anie.199423751.

Kudou, M. *et al.* (2003) 'Prevention of thermal inactivation and aggregation of lysozyme by polyamines', *European Journal of Biochemistry*, 270(22), pp. 4547–4554. doi: 10.1046/j.1432-1033.2003.03850.x.

Kumar Panigrahi, S. and Kumar Mishra, A. (2019) 'Inner filter effect in fluorescence spectroscopy: As a problem and as a solution', *Journal of Photochemistry and Photobiology C: Photochemistry Reviews*, 41, p. 100318. doi: 10.1016/j.jphotochemrev.2019.100318.

Kumar, R. *et al.* (2018) 'Macromolecular crowding-induced molten globule states of the alkali pH-denatured proteins', *Biochimica et Biophysica Acta - Proteins and Proteomics*, 1866(11), pp. 1102–1114. doi: 10.1016/j.bbapap.2018.08.012.

Kundu, J. *et al.* (2015) 'Unusual effects of crowders on heme retention in myoglobin', *FEBS Letters*, 589(24), pp. 3807–3815. doi: 10.1016/j.febslet.2015.11.015.

Kuznetsova, I. M. *et al.* (2015) 'Beyond the excluded volume effects: Mechanistic complexity of the crowded milieu', *Molecules*, 20(1), pp. 1377–1409. doi: 10.3390/molecules20011377.

Kuznetsova, I. M., Turoverov, K. K. and Uversky, V. N. (2014) 'What macromolecular crowding can do to a protein', *International Journal of Molecular Sciences*, 15(12), pp. 23090–23140. doi: 10.3390/ijms151223090.

Lai, J. jing *et al.* (2015) 'Effects of PEG molecular weight on its interaction with albumin', *Chinese Journal of Polymer Science (English Edition)*, 33(10), pp. 1373–1379. doi: 10.1007/s10118-015-1687-y.

Lakowicz, J.R (2006) 'Instrumentation for Fluorescence Spectroscopy', in Lakowicz, Joseph R (ed.) *Principles of Fluorescence Spectroscopy*. Boston, MA: Springer US, pp. 27–61. doi: 10.1007/978-0-387-46312-4_2.

Lee, L. L. Y. and Lee, J. C. (1987) 'Thermal Stability of Proteins in the Presence of Poly(ethylene glycols)', *Biochemistry*, 26(24), pp. 7813–7819. doi: 10.1021/bi00398a042.

Lukat, G. S., Stock, A. M. and Stock, J. B. (1990) 'Divalent Metal Ion Binding to the CheY Protein and Its Significance to Phosphotransfer in Bacterial Chemotaxis', *Biochemistry*, 29(23), pp. 5436–5442. doi: 10.1021/bi00475a004.

Majumder, S. *et al.* (2015) 'Probing protein quinary interactions by in-cell nuclear magnetic resonance spectroscopy', *Biochemistry*, 54(17), pp. 2727–2738. doi: 10.1021/acs.biochem.5b00036.

Malik, A. *et al.* (2012) 'Myoglobin unfolding in crowding and confinement', *Journal of Physical Chemistry B*, 116(43), pp. 12895–12904. doi: 10.1021/jp306873v.

Marion, D. *et al.* (1989) 'Overcoming the overlap problem in the assignment of proton NMR spectra of larger proteins by use of three-dimensional heteronuclear proton-nitrogen-15 Hartmann-Hahn-multiple quantum coherence and nuclear Overhauser-multiple quantum coherence spectroscopy', *Biochemistry*, 28(15), pp. 6150–6156. doi: 10.1021/bi00441a004.

Masino, L., Martin, S. R. and Bayley, P. M. (2000) 'Ligand binding and thermodynamic stability of a multidomain protein, calmodulin', pp. 1519–1529.

Matilla, M. A. and Krell, T. (2018) 'The effect of bacterial chemotaxis on host infection and pathogenicity', *FEMS Microbiology Reviews*, 42(1), pp. 40–67. doi: 10.1093/femsre/fux052.

Mazurenko, S. *et al.* (2018) 'CalFitter: A web server for analysis of protein thermal denaturation data', *Nucleic Acids Research*, 46(W1), pp. W344–W349. doi: 10.1093/nar/gky358.

Messerle, B. A. *et al.* (1989) 'Solvent suppression using a spin lock in 2D and 3D NMR spectroscopy with H₂O solutions', *Journal of Magnetic Resonance (1969)*, 85(3), pp. 608–

613. doi: 10.1016/0022-2364(89)90252-7.

Michael, A. J. (2016) 'Polyamines in Eukaryotes, Bacteria, and Archaea *', *Journal of Biological Chemistry*, 291(29), pp. 14896–14903. doi: 10.1074/jbc.R116.734780.

Mikaelsson, T. *et al.* (2014) 'Macromolecular crowding effects on two homologs of ribosomal protein S16: Protein-dependent structural changes and local interactions', *Biophysical Journal*, 107(2), pp. 401–410. doi: 10.1016/j.bpj.2014.05.038.

Miklos, A. C. *et al.* (2010) 'Volume exclusion and soft interaction effects on protein stability under crowded conditions', *Biochemistry*, 49(33), pp. 6984–6991. doi: 10.1021/bi100727y.

Miklos, A. C. *et al.* (2011) 'Protein crowding tunes protein stability', *Journal of the American Chemical Society*, 133(18), pp. 7116–7120. doi: 10.1021/ja200067p.

Minh, D. D. L. *et al.* (2006) 'The influence of macromolecular crowding on HIV-1 protease internal dynamics', *Journal of the American Chemical Society*, 128(18), pp. 6006–6007. doi: 10.1021/ja060483s.

Minton, A. P. (1981) 'Excluded volume as a determinant of macromolecular structure and reactivity', *Biopolymers*, 20(10), pp. 2093–2120. doi: 10.1002/bip.1981.360201006.

Minton, A. P. (2000) 'Effect of a concentrated "inert" macromolecular cosolute on the stability of a globular protein with respect to denaturation by heat and by chaotropes: a statistical-thermodynamic model.', *Biophysical journal*, 78(1), pp. 101–9. doi: 10.1016/S0006-3495(00)76576-3.

Minton, A. P. (2001) 'The Influence of Macromolecular Crowding and Macromolecular Confinement on Biochemical Reactions in Physiological Media', *Journal of Biological Chemistry*, 276(14), pp. 10577–10580. doi: 10.1074/jbc.R100005200.

Minton, A. P. (2015) 'Correction to How can biochemical reactions within cells differ from

those in test tubes? [J. Cell Sci., 119, (2006) 2863-2869]', *Journal of Cell Science*, 128(6), p. 1254. doi: 10.1242/jcs.170183.

Mittal, S. and Singh, L. R. (2013) 'Denatured state structural property determines protein stabilization by macromolecular crowding: A thermodynamic and structural approach', *PLoS ONE*, 8(11). doi: 10.1371/journal.pone.0078936.

Mittal, S. and Singh, L. R. (2014) 'Macromolecular crowding induces holo α -lactalbumin aggregation by converting to its apo form', *PLoS ONE*, 9(12), pp. 1–20. doi: 10.1371/journal.pone.0114029.

Momeni, L. *et al.* (2016) 'The effect of spermine on the structure, thermal stability and activity of bovine pancreatic trypsin', *RSC Advances*, 6(65), pp. 60633–60642. doi: 10.1039/c6ra10549a.

Monteitha, W. B. and Pielak, G. J. (2014) 'Residue level quantification of protein stability in living cells', *Proceedings of the National Academy of Sciences of the United States of America*, 111(31), pp. 11335–11340. doi: 10.1073/pnas.1406845111.

Moy, F. J. *et al.* (1994) 'Assignments, Secondary Structure, Global Fold, and Dynamics of Chemotaxis Y Protein Using Three- and Four-Dimensional Heteronuclear (^{13}C , ^{15}N) NMR Spectroscopy', *Biochemistry*, 33(35), pp. 10731–10742. doi: 10.1021/bi00201a022.

Muhandiram, D. R. and Kay, L. E. (1994) 'Gradient-Enhanced Triple-Resonance Three-Dimensional NMR Experiments with Improved Sensitivity', *Journal of Magnetic Resonance, Series B*, 103(3), pp. 203–216. doi: <https://doi.org/10.1006/jmrb.1994.1032>.

Müller, C. W. *et al.* (1996) 'Adenylate kinase motions during catalysis: An energetic counterweight balancing substrate binding', *Structure*, 4(2), pp. 147–156. doi: 10.1016/S0969-2126(96)00018-4.

- Müller, C. W. and Schulz, G. E. (1992) 'Structure of the complex between adenylate kinase from *Escherichia coli* and the inhibitor Ap5A refined at 1.9 Å resolution. A model for a catalytic transition state', *Journal of Molecular Biology*, 224(1), pp. 159–177. doi: 10.1016/0022-2836(92)90582-5.
- Munoz, V. *et al.* (1994) 'Kinetic Characterization of the Chemotactic Protein from *Escherichia coli*, CheY. Kinetic Analysis of the Inverse Hydrophobic Effect', *Biochemistry*, 33(19), pp. 5858–5866. doi: 10.1021/bi00185a025.
- Nasreen, K. *et al.* (2018) 'Macromolecular crowding induces molten globule state in the native myoglobin at physiological pH', *International Journal of Biological Macromolecules*, 106, pp. 130–139. doi: 10.1016/j.ijbiomac.2017.08.014.
- Nasreen, K. *et al.* (2020) 'Interactions under crowding milieu: Chemical-induced denaturation of myoglobin is determined by the extent of heme dissociation on interaction with crowders', *Biomolecules*, 10(3), pp. 1–2. doi: 10.3390/biom10030490.
- Nicholson, E. M. and Scholtz, J. M. (1996) 'Conformational stability of the *Escherichia coli* HPr protein: Test of the linear extrapolation method and a thermodynamic characterization of cold denaturation', *Biochemistry*, 35(35), pp. 11369–11378. doi: 10.1021/bi960863y.
- Nolan, V. *et al.* (2020) 'Effect of Polyethylene Glycol-Induced Molecular Crowding on the Enzymatic Activity and Thermal Stability of β -Galactosidase from *Kluyveromyces lactis*', *Journal of Agricultural and Food Chemistry*, pp. 8875–8882. doi: 10.1021/acs.jafc.0c02316.
- Nolan, V., Sánchez, J. M. and Perillo, M. A. (2015) 'PEG-induced molecular crowding leads to a relaxed conformation, higher thermal stability and lower catalytic efficiency of *Escherichia coli* β -galactosidase', *Colloids and Surfaces B: Biointerfaces*, 136, pp. 1202–1206. doi: 10.1016/j.colsurfb.2015.11.003.

Ogunmoyole, T., Fodeke, A. A. and Adewale, I. O. (2019) 'Denaturation studies of *Clarias gariepinus* glutathione transferase in dilute and crowded solutions', *European Biophysics Journal*, 48(8), pp. 789–801. doi: 10.1007/s00249-019-01405-z.

Okanojo, M. *et al.* (2005) 'Diamines prevent thermal aggregation and inactivation of lysozyme', *Journal of Bioscience and Bioengineering*, 100(5), pp. 556–561. doi: <https://doi.org/10.1263/jbb.100.556>.

Paik, S. P. *et al.* (2012) 'Poly(ethylene glycol) vesicles: Self-assembled site for luminescence generation', *Analytical Chemistry*, 84(17), pp. 7555–7561. doi: 10.1021/ac301731x.

Parray, Z. A. *et al.* (2019) 'First evidence of formation of pre-molten globule state in myoglobin: A macromolecular crowding approach towards protein folding in vivo', *International Journal of Biological Macromolecules*, 126, pp. 1288–1294. doi: 10.1016/j.ijbiomac.2018.12.170.

Parray, Z. A., Hassan, M. I., *et al.* (2020) 'Amphiphilic nature of polyethylene glycols and their role in medical research', *Polymer Testing*, 82(December 2019), p. 106316. doi: 10.1016/j.polymertesting.2019.106316.

Parray, Z. A., Ahmad, F., *et al.* (2020) 'Formation of molten globule state in horse heart cytochrome c under physiological conditions: Importance of soft interactions and spectroscopic approach in crowded milieu', *International Journal of Biological Macromolecules*, 148, pp. 192–200. doi: 10.1016/j.ijbiomac.2020.01.119.

Parray, Z. A. *et al.* (2022) 'Size-Dependent Interplay of Volume Exclusion Versus Soft Interactions: Cytochrome c in Macromolecular Crowded Environment', *Frontiers in Molecular Biosciences*, 9(May), pp. 1–18. doi: 10.3389/fmolb.2022.849683.

Paudel, B. P. *et al.* (2018) 'Optimal molecular crowding accelerates group II intron folding and

maximizes catalysis’, *Proceedings of the National Academy of Sciences of the United States of America*, 115(47), pp. 11917–11922. doi: 10.1073/pnas.1806685115.

Perham, M., Stagg, L. and Wittung-Stafshede, P. (2007) ‘Macromolecular crowding increases structural content of folded proteins’, *FEBS Letters*, 581(26), pp. 5065–5069. doi: 10.1016/j.febslet.2007.09.049.

Poddar, N. K. *et al.* (2008) ‘Effect of monomeric and oligomeric sugar osmolytes on ΔG_D , the Gibbs energy of stabilization of the protein at different pH values: Is the sum effect of monosaccharide individually additive in a mixture?’, *Biophysical Chemistry*, 138(3), pp. 120–129. doi: 10.1016/j.bpc.2008.09.013.

Politi, R. and Harries, D. (2010) ‘Enthalpically driven peptide stabilization by protective osmolytes’, *Chemical Communications*, 46(35), pp. 6449–6451. doi: 10.1039/c0cc01763a.

Popielec, A. *et al.* (2020) ‘Crowded environment affects the activity and inhibition of the NS3/4A protease’, *Biochimie*, 176, pp. 169–180. doi: 10.1016/j.biochi.2020.07.009.

Powroznik, B. *et al.* (2004) ‘Enhancement of lysozyme stability and activity by polyamines’, *Biochimie*, 86(9–10), pp. 651–656. doi: 10.1016/j.biochi.2004.09.009.

Ptitsyn, O. B. (1995) ‘Molten globule and protein folding’, *Advances in Protein Chemistry*, 47, pp. 83–229. doi: 10.1016/s0065-3233(08)60546-x.

Qi, H. W. *et al.* (2014) ‘The effect of macromolecular crowding on the electrostatic component of barnase-barstar binding: A computational, implicit solvent-based study’, *PLoS ONE*. Edited by C. M. Soares, 9(6), p. e98618. doi: 10.1371/journal.pone.0098618.

Rezaei-Ghaleh, N. *et al.* (2007) ‘Effect of polyamines on the structure, thermal stability and 2,2,2-trifluoroethanol-induced aggregation of α -chymotrypsin’, *International Journal of Biological Macromolecules*, 41(5), pp. 597–604. doi: 10.1016/j.ijbiomac.2007.07.018.

- Rivas, G. and Minton, A. P. (2018) 'Toward an understanding of biochemical equilibria within living cells', *Biophysical Reviews*, 10(2), pp. 241–253. doi: 10.1007/s12551-017-0347-6.
- Rubin, C. S. and Rosen, O. M. (1975) 'Protein phosphorylation.', *Annual review of biochemistry*, pp. 831–887. doi: 10.1146/annurev.bi.44.070175.004151.
- Sada, K. *et al.* (2001) 'Structure and Function of Syk Protein-Tyrosine Kinase', *Journal of Biochemistry*, 130(2), pp. 177–186. doi: 10.1093/oxfordjournals.jbchem.a002970.
- Santoro, M. M. and Bolen, D. W. (1988) 'Unfolding Free Energy Changes Determined by the Linear Extrapolation Method. 1. Unfolding of Phenylmethanesulfonyl a-Chymotrypsin Using Different Denaturants', *Biochemistry*, 27(21), pp. 8063–8068. doi: 10.1021/bi00421a014.
- Sapir, L. and Harries, D. (2014) 'Origin of enthalpic depletion forces', *Journal of Physical Chemistry Letters*, 5(7), pp. 1061–1065. doi: 10.1021/jz5002715.
- Sarkar, M., Li, C. and Pielak, G. J. (2013) 'Soft interactions and crowding', *Biophysical Reviews*, 5(2), pp. 187–194. doi: 10.1007/s12551-013-0104-4.
- Sasahara, K., McPhie, P. and Minton, A. P. (2003) 'Effect of dextran on protein stability and conformation attributed to macromolecular crowding', *Journal of Molecular Biology*, 326(4), pp. 1227–1237. doi: 10.1016/S0022-2836(02)01443-2.
- Schrödinger, LLC (2015) *The {PyMOL} Molecular Graphics System, Version~1.8.*
- Schumann, F. H. *et al.* (2007) 'Combined chemical shift changes and amino acid specific chemical shift mapping of protein-protein interactions', *Journal of Biomolecular NMR*, 39(4), pp. 275–289. doi: 10.1007/s10858-007-9197-z.
- Schuster, M., Silversmith, R. E. and Bourret, R. B. (2001) 'Conformational coupling in the chemotaxis response regulator CheY', *Proceedings of the National Academy of Sciences of the United States of America*, 98(11), pp. 6003–6008. doi: 10.1073/pnas.101571298.

Senske, M. *et al.* (2014) 'Protein Stabilization by Macromolecular Crowding through Enthalpy Rather Than Entropy', *Journal of the American Chemical Society*, 136(25), pp. 9036–9041. doi: 10.1021/ja503205y.

Sharma, G. S., Mittal, S. and Singh, L. R. (2015) 'Effect of Dextran 70 on the thermodynamic and structural properties of proteins', *International Journal of Biological Macromolecules*, 79, pp. 86–94. doi: 10.1016/j.ijbiomac.2015.04.051.

Shinde, R. A. *et al.* (2020) 'Unraveling thermodynamic and conformational correlations in action of osmolytes on hen egg white lysozyme', *Journal of Molecular Liquids*, 317, p. 113996. doi: 10.1016/j.molliq.2020.113996.

Shirdel, S. A. and Khalifeh, K. (2019) 'Thermodynamics of protein folding: methodology, data analysis and interpretation of data', *European Biophysics Journal*, 48(4), pp. 305–316. doi: 10.1007/s00249-019-01362-7.

Siemiarczuk, A. *et al.* (2004) 'Analysis of tryptophan fluorescence lifetimes in a series of human serum albumin mutants with substitutions in subdomain 2A', *Cell Biochemistry and Biophysics*, 40(2), pp. 115–122. doi: 10.1385/CBB:40:2:115.

Simonovic, M. and Volz, K. (2001) 'A Distinct Meta-active Conformation in the 1.1-Å Resolution Structure of Wild-type ApoCheY', *Journal of Biological Chemistry*, 276(31), pp. 28637–28640. doi: 10.1074/jbc.C100295200.

Smith, A. E. *et al.* (2015) 'NMR studies of protein folding and binding in cells and cell-like environments', *Current Opinion in Structural Biology*, 30, pp. 7–16. doi: 10.1016/j.sbi.2014.10.004.

Sola-Penna, M. *et al.* (1997) 'Carbohydrate protection of enzyme structure and function against guanidinium chloride treatment depends on the nature of carbohydrate and enzyme', *European*

Journal of Biochemistry, 248(1), pp. 24–29. doi: 10.1111/j.1432-1033.1997.00024.x.

Somero, G. N. (1986) ‘Protons, osmolytes, and fitness of internal milieu for protein function.’, *The American journal of physiology*, 251(2 Pt 2). doi: 10.1152/ajpregu.1986.251.2.r197.

Somkuti, J. *et al.* (2017) ‘Low crowding agent concentration destabilizes against pressure unfolding’, *Biophysical Chemistry*, 231(January), pp. 125–134. doi: 10.1016/j.bpc.2017.04.013.

Song, X. *et al.* (2021) ‘Osmolytes Can Destabilize Proteins in Cells by Modulating Electrostatics and Quinary Interactions’, *ACS Chemical Biology*, 16(5), pp. 864–871. doi: 10.1021/acscchembio.1c00024.

Sotomayor-Pérez, A. C. *et al.* (2013) ‘Molecular crowding stabilizes both the intrinsically disordered calcium-free state and the folded calcium-bound state of a repeat in toxin (RTX) protein’, *Journal of the American Chemical Society*, 135(32), pp. 11929–11934. doi: 10.1021/ja404790f.

Speer, S. L. *et al.* (2022) ‘Macromolecular Crowding Is More than Hard-Core Repulsions’, *Annual Review of Biophysics*, 51(1), pp. 267–300. doi: 10.1146/annurev-biophys-091321-071829.

Stadmler, S. S. *et al.* (2020) ‘Protein-Peptide Binding Energetics under Crowded Conditions’, *Journal of Physical Chemistry B*, 124(42), pp. 9297–9309. doi: 10.1021/acs.jpcc.0c05578.

Stagg, L. *et al.* (2007) ‘Molecular crowding enhances native structure and stability of α/β protein flavodoxin’, *Proceedings of the National Academy of Sciences of the United States of America*, 104(48), pp. 18976–18981. doi: 10.1073/pnas.0705127104.

Stepanenko, Olesya V. *et al.* (2019) ‘Open access the unfolding of irfp713 in a crowded milieu’, *PeerJ*, 2019(4), p. e6707. doi: 10.7717/peerj.6707.

Stock, A. M. *et al.* (1989) ‘Three-dimensional structure of CheY, the response regulator of bacterial chemotaxis’, *Nature*, 337(6209), pp. 745–749. doi: 10.1038/337745a0.

Stock, A. M. *et al.* (1993) ‘Structure of the Mg²⁺-Bound Form of CheY and Mechanism of Phosphoryl Transfer in Bacterial Chemotaxis’, *Biochemistry*, 32(49), pp. 13375–13380. doi: 10.1021/bi00212a001.

Stock, A. M., Robinson, V. L. and Goudreau, P. N. (2000) ‘Two-Component Signal Transduction’, *Annual Review of Biochemistry*, 69(1), pp. 183–215. doi: 10.1146/annurev.biochem.69.1.183.

Subadini, S. *et al.* (2021) ‘Polyethylene glycol perturbs the unfolding of CRABP I: A correlation between experimental and theoretical approach’, *Colloids and Surfaces B: Biointerfaces*, 202(January), p. 111696. doi: 10.1016/j.colsurfb.2021.111696.

Sukenik, S. *et al.* (2013) ‘Diversity in the mechanisms of cosolute action on biomolecular processes’, *Faraday Discussions*, 160, pp. 225–237. doi: 10.1039/c2fd20101a.

Sulmann, S. *et al.* (2014) ‘Conformational changes in calcium-sensor proteins under molecular crowding conditions’, *Chemistry - A European Journal*, 20(22), pp. 6756–6762. doi: 10.1002/chem.201402146.

Suthar, M. K. *et al.* (2013) ‘Behavior of Plasmodium falciparum purine nucleoside phosphorylase in macromolecular crowded environment’, *International Journal of Biological Macromolecules*, 62, pp. 657–662. doi: 10.1016/j.ijbiomac.2013.09.036.

Tajmir-Riahi, H. A. (2006) ‘An overview of protein-DNA and protein-RNA interactions’, *Journal of the Iranian Chemical Society*, 3(4), pp. 297–304. doi: 10.1007/BF03245950.

Tate, C. G. and Schertler, G. F. (2009) ‘Engineering G protein-coupled receptors to facilitate their structure determination’, *Current Opinion in Structural Biology*, 19(4), pp. 386–395. doi:

10.1016/j.sbi.2009.07.004.

Taylor, L. S. *et al.* (1995) ‘Sucrose reduces the efficiency of protein denaturation by a chaotropic agent’, *Biochimica et Biophysica Acta (BBA)/Protein Structure and Molecular*, 1253(1), pp. 39–46. doi: 10.1016/0167-4838(95)00142-H.

Tsao, D. and Dokholyan, N. V. (2010) ‘Macromolecular crowding induces polypeptide compaction and decreases folding cooperativity’, *Physical Chemistry Chemical Physics*, 12(14), pp. 3491–3500. doi: 10.1039/b924236h.

Verma, S. and Mishra, S. N. (2005) ‘Putrescine alleviation of growth in salt stressed Brassica juncea by inducing antioxidative defense system’, *Journal of Plant Physiology*, 162(6), pp. 669–677. doi: <https://doi.org/10.1016/j.jplph.2004.08.008>.

Wang, Q. *et al.* (2011) ‘The effect of macromolecular crowding, ionic strength and calcium binding on calmodulin dynamics’, *PLoS Computational Biology*, 7(7). doi: 10.1371/journal.pcbi.1002114.

Wang, Y. *et al.* (2012) ‘Macromolecular crowding and protein stability’, *Journal of the American Chemical Society*, 134(40), pp. 16614–16618. doi: 10.1021/ja305300m.

Wang, Y., He, H. and Li, S. (2010) ‘Effect of Ficoll 70 on thermal stability and structure of creatine kinase’, *Biochemistry (Moscow)*, 75(5), pp. 648–654. doi: 10.1134/S0006297910050160.

Weiger, T. M. and Hermann, A. (2014) ‘Cell proliferation, potassium channels, polyamines and their interactions: a mini review’, *Amino Acids*, 46(3), pp. 681–688. doi: 10.1007/s00726-013-1536-7.

Williamson, M. P. (2013) ‘Using chemical shift perturbation to characterise ligand binding’, *Progress in Nuclear Magnetic Resonance Spectroscopy*, 73, pp. 1–16. doi:

10.1016/j.pnmrs.2013.02.001.

Williamson, M. P. (2018) 'Chemical shift perturbation', in Webb, G. A. (ed.) *Modern Magnetic Resonance*. Cham: Springer International Publishing, pp. 995–1012. doi: 10.1007/978-3-319-28388-3_76.

Wu, J. *et al.* (2014) 'Binding characteristics between polyethylene glycol (PEG) and proteins in aqueous solution', *Journal of Materials Chemistry B*, 2(20), pp. 2983–2992. doi: 10.1039/c4tb00253a.

Wüthrich, K. *et al.* (1982) 'Sequential resonance assignments as a basis for determination of spatial protein structures by high resolution proton nuclear magnetic resonance', *Journal of Molecular Biology*, 155(3), pp. 311–319. doi: [https://doi.org/10.1016/0022-2836\(82\)90007-9](https://doi.org/10.1016/0022-2836(82)90007-9).

Wüthrich, K. (1986) 'NMR with Proteins and Nucleic Acids', *Europhysics News*, 17(1), pp. 11–13. doi: 10.1051/e pn/19861701011.

Xie, G. and Timasheff, S. N. (1997) 'Mechanism of the stabilization of ribonuclease A by sorbitol: Preferential hydration is greater for the denatured than for the native protein', *Protein Science*, 6(1), pp. 211–221. doi: 10.1002/pro.5560060123.

Xu, G. *et al.* (2017) 'The Effects of Macromolecular Crowding on Calmodulin Structure and Function', *Chemistry - A European Journal*, 23(28), pp. 6736–6740. doi: 10.1002/chem.201700367.

Zhai, Y. and Winter, R. (2013) 'Effect of Molecular Crowding on the Temperature–Pressure Stability Diagram of Ribonuclease A', *ChemPhysChem*, 14(2), pp. 386–393. doi: <https://doi.org/10.1002/cphc.201200767>.

Zhang, D. L. *et al.* (2012) 'Effects of macromolecular crowding on the structural stability of human α -lactalbumin', *Acta Biochimica et Biophysica Sinica*, 44(8), pp. 703–711. doi:

10.1093/abbs/gms052.

Zhu, Y. *et al.* (2001) 'A Method for the Quantitation of Charge by Size Exclusion Chromatography Demonstrated with Components of Ficoll 400', *Macromolecular Chemistry and Physics*, 202(1), pp. 61–72. doi: 10.1002/1521-3935(20010101)202:1<61::AID-MACP61>3.0.CO;2-H.

Ziaee, E. *et al.* (2021) 'The effect of putrescine on stability and structural properties of bovine serum albumin', *Journal of Biomolecular Structure and Dynamics*, 39(1), pp. 254–262. doi: 10.1080/07391102.2020.1719199.

Zimmerman, S. B. and Harrison, B. (1987) 'Macromolecular crowding increases binding of DNA polymerase to DNA: An adaptive effect', *Proceedings of the National Academy of Sciences of the United States of America*, 84(7), pp. 1871–1875. doi: 10.1073/pnas.84.7.1871.

Zimmerman, S. B. and Minton, A. P. (1993) 'Macromolecular Crowding: Biochemical, Biophysical, and Physiological Consequences', *Annual Review of Biophysics and Biomolecular Structure*, 22(1), pp. 27–65. doi: 10.1146/annurev.bb.22.060193.000331.

Zimmerman, S. B. and Trach, S. O. (1991a) 'Estimation of macromolecule concentrations and excluded volume effects for the cytoplasm of *Escherichia coli*', *Journal of Molecular Biology*, 222(3), pp. 599–620. doi: 10.1016/0022-2836(91)90499-V.

Zimmerman, S. B. and Trach, S. O. (1991b) 'Estimation of macromolecule concentrations and excluded volume effects for the cytoplasm of *Escherichia coli*', *Journal of Molecular Biology*, 222(3), pp. 599–620. doi: 10.1016/0022-2836(91)90499-V.

Appendices

Table 1 lists the chemical shift values for each nucleus of approximately 80% residues of CheY.

Residue number	^1H	^{15}N	$^{13}\text{C}\alpha$	$^{13}\text{C}\beta$	$^{13}\text{C}\alpha\text{-1}$	$^{13}\text{C}\beta\text{-1}$
5	7.4445	124.2013	53.8325	40.5306	53.0509	26.1977
6	8.4234	126.133	53.5185	30.9081	53.8169	40.5302
7	9.1299	128.6271	54.5039	40.7932	53.4918	30.7999
8	8.7207	121.9539	50.3696		54.5109	40.6554
9	8.9074	127.3447	58.7392	30.5905	50.3862	41.3764
10	9.1899	127.4455	57.5122	29.587	58.7685	30.5801
17	7.536	117.2837	57.8965		53.6416	28.3776
18	7.5781	116.9513	53.6473			
20	8.2386	119.4957	65.0179	28.4843	62.6469	
21	8.5657	119.6524	57.8922		65.0182	28.3282
23	8.3684	123.344	55.4815	39.7193	53.2539	34.7214
24	8.2666	118.144	55.5413		55.3403	39.4941
27	7.361	117.229	51.9414	39.4665	56.7634	26.2757
28	7.6706	106.2225	42.0077		51.933	39.3941
29	8.102	121.0509	54.6555	35.885	42.008	16.426
30	8.2377	118.3368	51.013	38.0018	54.633	35.8264
31	9.7883	124.498	49.5335	33.8389	51.0257	37.8458
32	7.4512	122.0955	58.2207	34.9919	49.4046	33.7945
33	9.0408	126.9349	51.0902	31.1267	58.2308	33.4846
34	8.8724	120.994	52.1475		51.0918	31.2744
35	8.8221	120.7315	47.5612	20.1215	52.2162	31.2982
36	9.4035	117.5134	54.1406	29.1043	47.5438	20.022
37	7.3863	109.691	50.8826	38.8463	54.1535	28.9068
39	7.864	122.6653	63.7624	28.6902	45.7605	16.9076
40	8.4748	121.1455	53.884	39.812	63.721	28.6389
41	8.2629	117.0386	52.5	16.9814	53.8873	39.7193
42	8.0472	118.3069	55.5279	38.624	52.4997	16.9187
44	7.8618	120.6566	57.1431	29.0945	55.5897	
45	8.6678	118.6266	54.71	39.4306	57.506	29.0727

47	7.5312	120.5625	50.757	16.4379	55.1362	25.3589
48	7.5044	104.3075	41.8827		50.6719	16.3336
49	8.2949	103.7865	42.6366		41.852	
50	8.0467	118.7379	58.1382	36.3287	42.6351	
51	9.4706	106.9607	41.7068		58.1466	36.2582
52	7.4736	121.4505	55.5022	40.7647	41.7015	
53	8.14	127.106	58.3905	31.9737	55.3589	40.5784
54	9.2044	128.2965	58.1387	37.7405	58.3212	31.8913
56	8.2642	127.3263	52.2942		59.403	29.7217
66	8.1066	120.026	56.3909	26.1587	55.7562	38.217
67	8.2433	123.8036		30.0853	56.2843	26.2713
69	8.3165	116.3068	57.2229	29.7957	55.7565	38.4702
70	7.9371	117.4551	64.6413	65.4756	57.3181	29.8083
72	8.0698	113.4873	54.5216	26.5053	63.5251	35.9435
73	7.2187	119.0288	49.2011	16.5168	54.5203	26.3504
74	7.3175	121.8642	51.3842	41.0501	49.2477	16.4849
78	7.3714	112.9119	59.0834	60.7326	53.1591	31.3974
79	8.1735	123.1884	48.3781	16.1317	59.0183	60.6312
80	7.7673	124.2099	51.0154	40.2435	48.317	15.972
82	7.6273	118.9232	57.6921	33.3293	59.8607	28.5983
83	9.088	130.4709	49.9043	42.6948	57.6778	33.1593
84	7.9687	124.5939	50.0102	29.0812	49.8959	42.5127
85	9.0494	124.1443	58.0397		50.0399	
86	8.4268	116.1823	53.1519	67.8332	50.766	16.812
90	7.3457	121.0785	52.4875	30.4777	48.6019	14.7186
92	9.5823	116.5145	57.2078	25.8311	57.2204	29.057
93	7.1854	118.2921	52.1341	34.3304	57.1392	25.9122
94	7.3911	121.6769	62.2738		52.1371	34.307
95	7.8592	119.8569	61.5578		62.2782	34.7105
96	7.5834	122.0349	52.4047	15.5749	61.5566	35.0349
97	8.3672	119.2151	53.2426	34.8683	52.2621	15.4385
100	7.4812	118.4195	49.1397	16.561	55.882	25.3333
101	7.515	102.6449	43.0106		49.1833	16.5815
102	8.6705	124.9643	50.8922	15.7392	43.0093	

103	8.9905	118.3365	57.3926	58.3661	50.9404	15.6766
104	7.5777	102.8743	42.1326		57.2076	58.3587
105	8.3627	118.8935	53.262			
106	8.8718	120.1247	56.7167	32.6014	53.2602	38.7687
107	8.0847	126.9362	57.7904	29.8793	56.5946	32.5239
108	8.3585	123.9739	50.5728		57.7604	29.7284
110	7.7079	116.0847	50.8866	37.8984	59.6376	31.8856
111	7.8127	108.7709	56.7605	69.1155	50.8823	37.8894
112	9.1553	123.0547	53.2299	14.5611	56.7804	69.1622
115	8.1881	122.2117	55.4258	38.3651	63.1956	65.6807
116	8.8186	119.1041	57.1977	26.8253	55.3965	38.1844
117	7.5814	118.0355	56.7752		57.2076	26.8811
119	8.4915	118.4005	55.1359	37.7678	54.6243	28.6804
120	8.5175	116.0259	53.3856	34.653	55.0264	37.8339
121	7.6985	119.2989	56.014	29.3023	53.3637	34.5688
127	7.8769	110.0846	44.0101		52.1367	39.7134

List of Publications and Presentations

Publications

Irukuvajjula, S. S. et al. (2023) ‘Contrasting effect of Ficoll on apo and holo forms of bacterial chemotaxis protein Y: Selective destabilization of the conformationally altered holo form’, *International Journal of Biological Macromolecules*, 232(November 2022), p. 123505. doi: 10.1016/j.ijbiomac.2023.123505.

Irukuvajjula, S. S., Reddy, J. G. and Vadrevu, R. (2022) ‘Crowding by Poly(ethylene glycol) Destabilizes Chemotaxis Protein Y (CheY)’, *Biochemistry*, 61(14), pp. 1431–1443. doi: 10.1021/acs.biochem.2c00030.

Kadamuri, Rajshekhar Varma; **Shivkumar Sharma, Irukuvajjula** ;Vadrevu, R. (2018) ‘Beta-alpha-beta super secondary motifs: Sequences, Structural overview, and pursuit of potential autonomously folding beta-alpha-beta sequences from (Beta/Alpha)₈ tim barrels’, in Kister, A. E. (ed.) *Protein Supersecondary structures: Methods and protocols*. Second. Springer Protocols.

Mulukala SKN, **Irukuvajjula SS**, Kumar K, Garai K, Venkatesu P, Vadrevu R, Pasupulati AK. Structural features and oligomeric nature of human podocin domain. *Biochem Biophys Rep.* 2020 Jun 25;23:100774.

Presentations/Conferences

Irukuvajjula, S.S., Reddy, J. and Vadrevu, R., 2021, October. Protein-Crowder interactions: Biophysical studies and NMR spectroscopy reveal an interplay of enthalpic and entropic effects on the structure and thermal stability. In *PROTEIN SCIENCE* (Vol. 30, pp. 160-160). 111 RIVER ST, HOBOKEN 07030-5774, NJ USA: WILEY.

Brief Biography of the Candidate

Mr. I Shivkumar Sharma is a PhD student in the Department of Biological Sciences. He obtained BTech. in Biotechnology from a Jawaharlal Nehru Technological University affiliated college, Sreenidhi Institute of Science and Technology, Hyderabad, in 2017. He then briefly worked at Biocon Research Limited, in the downstream processing lab, with the goal of gaining hands-on experience in peptide and protein purification. Mr. Shivkumar was selected as a doctoral student in January 2018, at BITS-Pilani, Hyderabad Campus, under the guidance of Prof. Ramakrishna Vadrevu.

He is well trained in experimental lab work. During his Ph.D., he gained hands-on experience in protein expression and purification in *E. coli*-based systems using AKTA FLPC for processes such as size-exclusion chromatography and affinity chromatography. He also gained a good amount of experience in determining protein thermodynamic parameters, as well as static and dynamic fluorescence studies. He was also trained to analyze the data from 2D and 3D NMR spectroscopy. Currently, his research interests are focused on protein structure, stability, and thermodynamics under crowded, small-molecule/metabolite-induced crowding conditions, peptide design, and the functionalization of self-assembling amyloid-based peptides.

Brief Biography of the Supervisor

Prof. Ramakrishna Vadrevu, was a Professor in the Department of Biological Sciences. After obtaining a Ph.D. from the Indian Institute of Technology, Bombay, India, he joined as a Post-Doctoral Fellow at Pennsylvania State University and later as a faculty member at the University of Massachusetts Medical School, Boston, USA. He joined the BITS Pilani-Hyderabad Campus in 2008 and served until his demise in December 2022. His research interests include protein design and engineering; self-assembly and bionanomaterials; NMR spectroscopy/biophysical approaches to understand protein folding and dynamics in vitro and in vivo; and drug discovery. He was a member of the Protein Society, authored more than 20 publications in peer-reviewed international journals, and chaired in some seminal international conferences. He has been a reviewer for research proposals submitted to funding agencies, and manuscripts submitted to journals and theses. His administrative contributions include serving as the Head of the Department of Biology, Chairperson DRC-Departmental Research Committee, and General Secretary Technology Business Incubator Society.

Brief Biography of the Co-Supervisor

Prof. Sridev Mohapatra, Associate Professor in the Department of Biological Sciences, joined BITS-Pilani, Hyderabad Campus, India, in 2012. He obtained his Ph.D. degree from the University of New Hampshire in 2008 and M.Sc. from Utkal University, Bhubaneswar, India, in 2001. He served as a post-doctoral research associate at Texas Tech. University, Lubbock, Texas, U.S.A.; and University of Texas at Arlington, Arlington, Texas, USA.

Prof. Sridev Mohapatra's research focus is on plant biotechnology, plant-microbial interactions under abiotic and biotic stress conditions, molecular signalling mechanisms underlying PGPR-mediated amelioration of stresses, and their biotechnological applications. Beginning with his professional career in 2008, Prof. Sridev Mohapatra has almost 15 years of academic experience in the field of Plant Biotechnology. He has published over 15 research papers, with good citations, in reputed international journals and conferences. He has served as a reviewer for many international journals. Currently, his group is engaged in elucidating the precise signalling mechanisms and regulatory patterns involved in PGPR-mediated abiotic stress tolerance in plants. He has successfully completed/currently investigating research projects sponsored by SERB, DBT, CSIR, and BITS-Pilani. Till date Prof. Mohapatra has graduated two PhD students.